AIR FORCE REPORT

SAMSO TR 78-57

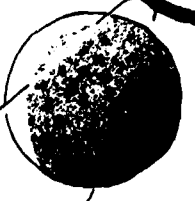

GLOBAL POSITIONING SYSTEM NAVIGATION ALGORITHMS

BY
LEONARD R. KRUCZYSKI

AMRL 1079 MAY 1977

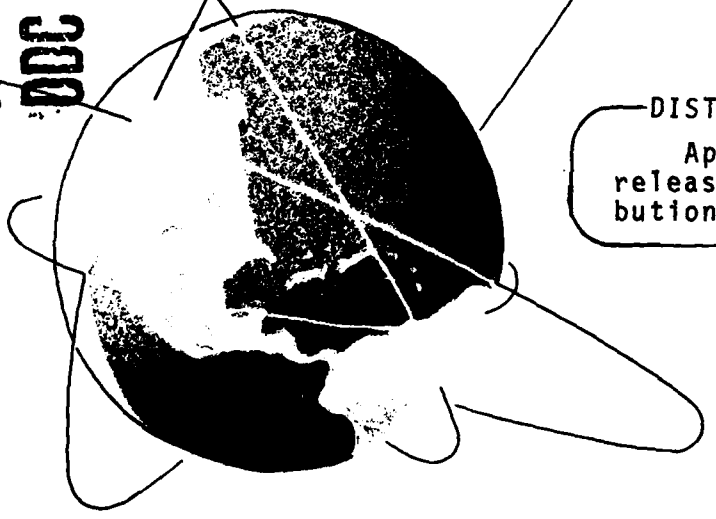

APPLIED MECHANICS RESEARCH LABORATORY
THE UNIVERSITY OF TEXAS AT AUSTIN AUSTIN, TEXAS

This final report was submitted by the Applied Mechanics Research Laboratory, University of Texas at Austin, Austin TX under contract F04701-76-C-0090 with the SPACE NAVIGATION SYSTEM Program Office at Space and Missile Systems Organization (AFSC), Los Angeles Air Force Station, CA 90009.

This technical report has been reviewed and is approved for publication and public release with unlimited distribution.

Brock T. Strom

BROCK T. STROM, Lt Col, USAF
Director of Nav Equip & Avionics

UNCLASSIFIED

SECURITY CLASSIFICATION OF THIS PAGE (When Data Entered)

REPORT DOCUMENTATION PAGE	READ INSTRUCTIONS BEFORE COMPLETING FORM
1. REPORT NUMBER: SAMSO TR-78-57	2. GOVT ACCESSION NO.
	3. RECIPIENT'S CATALOG NUMBER
4. TITLE (and Subtitle): GLOBAL POSITIONING SYSTEM NAVIGATION ALGORITHMS.	5. TYPE OF REPORT & PERIOD COVERED: Final Report. 1 April 76-31 August 77
	6. PERFORMING ORG. REPORT NUMBER: AMRL-1079
7. AUTHOR(s): Leonard Richard Kruczynski	8. CONTRACT OR GRANT NUMBER(s): F04701-76-C-0090
9. PERFORMING ORGANIZATION NAME AND ADDRESS: Applied Mechanics Research Laboratory, University of Texas at Austin, Austin TX 78712	10. PROGRAM ELEMENT, PROJECT, TASK AREA & WORK UNIT NUMBERS: 63421F, 632075, 00
11. CONTROLLING OFFICE NAME AND ADDRESS: HQ SAMSO/YEU, PO BOX 92960, WORLDWAY POSTAL CENTER, Los Angeles CA 90009	12. REPORT DATE: May 77
	13. NUMBER OF PAGES: 310 pages
14. MONITORING AGENCY NAME & ADDRESS (if different from Controlling Office)	15. SECURITY CLASS. (of this report): Unclassified
	15a. DECLASSIFICATION/DOWNGRADING SCHEDULE: N/A

16. DISTRIBUTION STATEMENT (of this Report)

This technical report has been reviewed and is approved for publication and public release with unlimited distribution.

17. DISTRIBUTION STATEMENT (of the abstract entered in Block 20, if different from Report)

18. SUPPLEMENTARY NOTES

19. KEY WORDS (Continue on reverse side if necessary and identify by block number)

Global Positioning System (GPS), Kalman Filter, Low Cost User, Limited Operational Capability, Navigation Algorithms

20. ABSTRACT (Continue on reverse side if necessary and identify by block number)

The Global Positioning System (GPS) will be a constellation of 24 satellites placed in 12-hour, 63 degree inclination, circular orbits. The satellite configuration is designed to provide accurate three-dimensional position, velocity, and time information by transmitting signals from which users can extract range and range-rate measurements. This investigation describes the passive-ranging concept of the system and the various hardware, software, and environmental factors which determine system accuracy. The simulation of a

DD FORM 1 JAN 73 1473 EDITION OF 1 NOV 65 IS OBSOLETE

405 333

UNCLASSIFIED

SECURITY CLASSIFICATION OF THIS PAGE (When Data Entered)

New York-to-Chicago aircraft flight with satellite range and range-rate measurements and with barometric altimeter measurements is used to numerically evaluate navigation algorithms. The satellite configuration used in the simulation is the limited operational configuration which consists of only nine satellites. For 95 percent of the simulated flight, only three satellites are visible to the user.

The search for acceptable navigation algorithms begins with a review of a linear filtering and prediction theory. A filter model for the aircraft is developed based on the assumption of an exponentially correlated random acceleration. The resulting model, combined with measurement bias models, is incorporated into an extended Kalman filter. Numerical results show that, for the basic filter model, filters which maintain good accuracy during the maneuvering phases of flight have poor performance during cruising flight, and conversely, filters which perform well during cruise, have degraded accuracy during maneuvers.

Finally, several adaptive algorithms are evaluated. Numerical results show that a simple adaptive index can be used to enhance the performance of the basic filter model without a substantial increase in the navigation algorithm program complexity.

Using the simulated flight adopted for this study, root-sum-square position errors generally less than 100 meters were achieved. The results show that accuracy is strongly dependent on user-satellite geometry. Maximum position errors equal to at least 700 meters occurred at a time of poor geometry in all algorithms which were considered.

GLOBAL POSITIONING SYSTEM NAVIGATION ALGORITHMS

by

LEONARD RICHARD KRUCZYNSKI, B.S., M.S.
The University of Texas at Austin
Austin, Texas

AMRL 1079
May 1977

Applied Mechanics Research Laboratory
The University of Texas at Austin
Austin, Texas

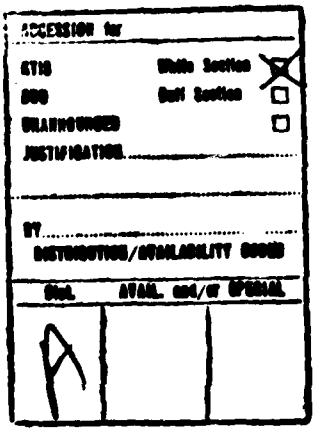

This report was prepared under

Grant No. F 04701-76-C0090

for the

Space and Missile Systems Organization

by the

Applied Mechanics Research Laboratory
The University of Texas at Austin
Austin, Texas

under the direction of

Byron D. Tapley
Professor and Chairman

TABLE OF CONTENTS

GLOBAL POSITIONING SYSTEM NAVIGATION ALGORITHMS

Publication No.

Leonard Richard Kruczynski, Ph.D.
The University of Texas at Austin, 1976

Supervising Professor: Byron D. Tapley

The Global Positioning System (GPS) will be a constellation of 24 satellites placed in 12-hour, 63 degree inclination, circular orbits. The satellite configuration is designed to provide accurate three-dimensional position, velocity, and time information by transmitting signals from which users can extract range and range-rate measurements. This investigation describes the passive-ranging concept of the system and the various hardware, software, and environmental factors which determine system accuracy. The simulation of a New York-to-Chicago aircraft flight with satellite range and range-rate measurements and with barometric altimeter measurements is used to numerically evaluate navigation algorithms. The satellite configuration used in the simulation is the limited operational configuration which consists of only nine satellites. For 95 per cent of the simulated flight, only three satellites are visible to the user.

The search for acceptable navigation algorithms begins with a review of a linear filtering and prediction theory. A filter model for

the aircraft is developed based on the assumption of an exponentially correlated random acceleration. The resulting model, combined with measurement bias models, is incorporated into an extended Kalman filter. Numerical results show that, for the basic filter model, filters which maintain good accuracy during the maneuvering phases of flight have poor performance during cruising flight and, conversely, filters which perform well during cruise, have degraded accuracy during maneuvers.

Finally, several adaptive algorithms are evaluated. Numerical results show that a simple adaptive index can be used to enhance the performance of the basic filter model without a substantial increase in the navigation algorithm program complexity.

Using the simulated flight adopted for this study, root-sum-square position errors generally less than 100 meters were achieved. The results show that accuracy is strongly dependent on user-satellite geometry. Maximum position errors equal to at least 700 meters occurred at a time of poor geometry in all algorithms which were considered.

LIST OF FIGURES

LIST OF TABLES

CHAPTER 1

INTRODUCTION

1.1 Some Historical Remarks on Navigation

In Greek mythology, Odysseus sailed safely by the Sirens only to encounter the monsters Scylla and Charybdis, traditionally located in the Straits of Messina between Italy and Sicily. Scylla was a squid-like monster with six long necks, each with a head on it with three rows of teeth. Charybdis was a whirlpool which sucked in water and belched it out three times a day. Odysseus steered between the two monsters with limited success. He survived to continue on to Ithaca but Scylla was able to catch and devour six of his men [1:133-134]*. Although no mention is made of Odysseus' navigation technique in the Straits of Messina, the episode may be one of the earliest references to the requirement for accurate navigation.

Methods for the determination of latitude from direct observations of the sun and stars had been known since Hipparchus, Menelaus, and Ptolemy created and refined trigonometry to aid in the telling of time, calendar-reckoning, and navigation [2:119]. Determination of longitude, however, remained a difficult problem. After 1514, the direction of the moon relative to the stars was used to calculate

---

*Bracketed numbers indicate references as enumerated in the Bibliography section. Unless noted otherwise, numbers following the colon are page numbers.

longitude. An error of one minute of angle, an accuracy beyond the capabilities of Sixteenth Century equipment, resulted in an approximately 1/2-degree (60 km) longitude error. This limitation, attenuated by the difficulties in taking measurements from heaving ships, resulted in longitude errors on the order of 150 km. In the absence of other longitude determination techniques, considerable effort was expended to improve the prediction of lunar motion in order to improve longitude determination accuracy [2:336].

In 1712, recognizing that other methods had to be developed, the British government established the Commission for the Discovery of Longitude which offered rewards up to 20,000 pounds sterling for ideas on how to compute longitude. The Flemish cartographer Gemma Frisius (1508-1555) had suggested in 1522 the use of time to determine longitude [3:245]. To be competitive with the 1/2-degree accuracy of the lunar methods, however, time on board the ship had to be accurate to two minutes for the duration of the voyage. Clocks with such accuracy did not exist until John Harrison (1693-1776) invented the chronometer in 1761 [2:337]. With chronometers, celestial navigation techniques could be used to determine latitude and longitude on the open seas to accuracies on the order of a few kilometers.

1.2 Classification of Navigation Techniques

Navigation techniques can be placed into four broad categories: celestial navigation, pilotage, dead-reckoning, and radio navigation. Pilotage is simply the use of maps to determine position. When a user

is in uncharted areas or is away from known shorelines, this method is inapplicable. It is interesting to note that currently there is considerable interest in the use of landmark tracking, a form of pilotage, for cruise missiles and space satellites.

Dead-reckoning, or "deduced reckoning," is based on the propagation of a user's position using knowledge of the velocity and a previously known location. Inertial navigation systems, which sense acceleration, can be referred to as acceleration dead-reckoning systems. When used without other navigation aids, such as periodic position updates, dead-reckoning methods are subject to long-term drift errors caused by errors in the sensed velocity (or acceleration).

Celestial navigation is the use of angular measurements of the sun, moon, and stars to determine latitude and longitude on the earth. As discussed previously, accurate longitude determination also requires accurate knowledge of time. Prior to the introduction of radio navigation systems, celestial navigation was the only method for open seas navigation which provided acceptable accuracy.

Radio navigation techniques have been in widespread use since World War II. Perhaps the simplest position determination method, based on radio signals, is radio direction finding to determine lines-of-position on the Earth's surface. The intersection of two lines-of-position determine the position of the user. Current ground-based radio navigation systems include: LORAN-C (LOng-RAnge Navigation); OMEGA a global version of LORAN: and VOR/DME, a line-of-sight high-frequency system. Up to 80 radio navigation systems or system variants have been

identified [4]. Accuracy and range capabilities of selected systems are summarized in Figure 1.1.

For ground-based radio navigation systems, low frequencies are needed to increase coverage because, for the lower frequencies, the signal follows the curvature of the Earth for longer distances. Most radio navigation concepts require accurate tracking of the signal waveform, however, and, as frequency decreases, errors in tracking the signals increase.

In 1958, the use of a satellite-based radio navigation system was proposed [5]. The concept called for the measurement of the Doppler shift in satellite transmitted signals and was eventually incorporated into the TRANSIT navigation satellite system. A primary advantage of a satellite-based system is the increased coverage without decreased signal tracking accuracy.

The TRANSIT system requires the use of a Doppler curve for the entire satellite pass and, therefore, is limited to slow moving users, such as ships, or to use as an auxiliary navigation aid for other systems such as inertial navigation systems. In December 1973, the Department of Defense approved the first phase of a new navigation satellite program which combined elements of the Air Force Program 621B and the Navy TIMATION program. The system, designated the NAVSTAR Global Positioning System, is scheduled to be fully operational in 1984. The fully operational system is expected to have horizontal and vertical position accuracy on the order of 10 meters for 90 percent of the time and will provide nearly continuous navigation fixes (after

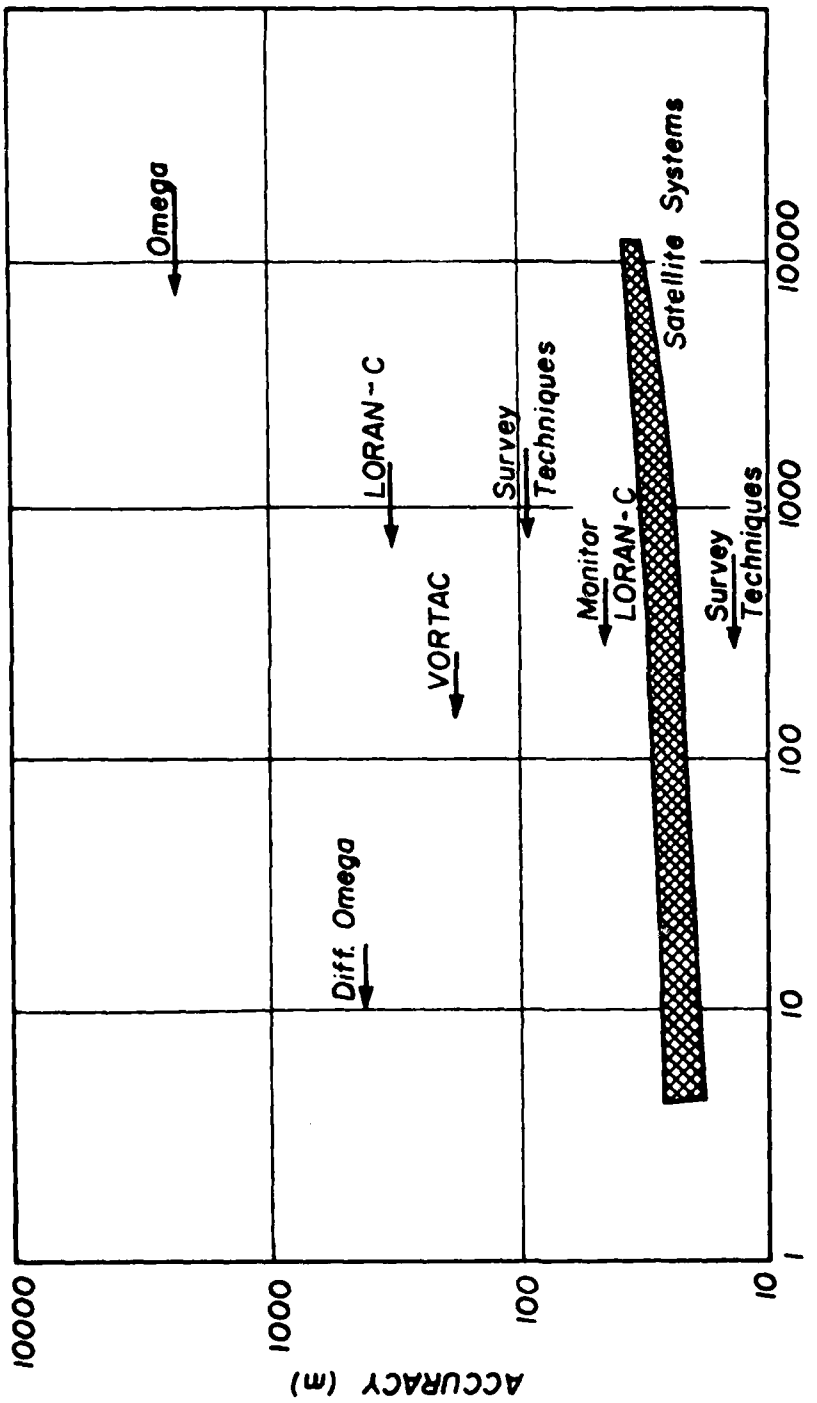

Figure 1.1 Navigation System Capabilities

establishing an initial fix). The key element of the NAVSTAR system is the atomic frequency standard to be on board each of 24 high-altitude satellites. Transmission of accurate time signals from the satellites will permit a user to determine accurate ranges or range-differences from a number of satellites. These measurements can be used to determine the user's three-dimensional position and time [6].

If a NAVSTAR user has four simultaneous independent satellite measurements, then three-dimensional position and time can be calculated using deterministic solutions. If the measurements are not perfect, however, then algorithms based on deterministic solutions can result in non-optimal state estimates. Also, if the observations are available sequentially, then sequential estimation techniques should be used.

If other navigational aids such as a barometric altimeter are used, then the navigation algorithm must integrate the auxiliary sensor measurement into the solution. Any a priori knowledge of the user's state should also be considered in the algorithm. It is fortunate that a wealth of information exists from which a NAVSTAR user can derive an algorithm which minimizes the effects of observation errors, operates sequentially, optimally combines different measurements sources, and considers the a priori information. Such information is to be found in recent advances in estimation theory, a theory with beginnings in the early Nineteenth Century.

1.3 Historical Background of Estimation Theory

At the age of eighteen, Karl Friedrich Gauss (1777-1855)

invented the method of least squares [2:870]. He used his new method to derive a set of orbital elements for the minor planet Pallas. The development of the least squares technique was the beginning of estimation theory.

The Wiener-Kolmogorov theory of filtering and prediction was described in detail by Norbert Wiener (1894-1964) in 1949 [7]. This theory centered on the derivation of the Wiener-Hopf Equation, an integral equation which specified the construction for the gain of an optimal*estimator. The work of Wiener and Kolmogorov was the first major contribution to estimation theory since Gauss' least squares.

Much effort in the 1950's was devoted to the application of the computer in estimation theory. The Wiener-Hopf Equation, an integral equation, was not appropriate for computer use unless an explicit solution could be obtained. Since explicit solutions were available only in certain restricted cases, most computer applications used least squares or recursive least squares methods. In 1960 and 1961, Kalman and Bucy [8] [9] transformed the Wiener-Hopf Equation into an equivalent set of differential equations. Although this did not make explicit solutions for the optimal gain easier to derive, it did place the gain computation into a form well adapted to the digital computer. The resulting formulation has tremendous practical utility.

---

*"Optimal," in this case, means "unbiased, linear, minimum variance."

1.4 Purpose and Scope of the Dissertation

Since its appearance in 1961, Kalman filtering has been applied to countless aerospace systems. It is the purpose of this dissertation to apply the Kalman filter to another aerospace problem, i.e., aircraft navigation using the NAVSTAR Global Positioning System navigation satellites. The problem specified has one outstanding challenge - the lack of any reasonable (computationally tractable) model, stochastic or deterministic, that will describe the behavior of an aircraft.

The scope of this paper is limited to the use of an extended sequential Kalman filter after acquisition of the GPS navigation signal. In addition, applicability to a low-cost user further restricts the scope, especially in the use of auxiliary sensors (i.e., no inertial navigation systems) and receiver capabilities (no simultaneous reception). A discussion of all factors to be considered in actual implementation of a navigation algorithm is beyond the scope of this study. The characteristics of specific hardware items, which would be influential in determining the exact implementation method, were not integrated into the analyses. The accuracies of available equipment, such as altimeters, were approximated in the study.

This dissertation evaluates several adaptive and non-adaptive methods for implementing sequential estimation techniques into GPS user navigation algorithms. Although the analyses are based on the limited operational phase of the GPS and low-cost user equipment, the algorithms are expected to be applicable for many user categories in both the limited operational and fully operational phases of GPS. Each estimation

technique is described in general terms. The specific formulation for the user navigation algorithm is then derived. The algorithms are tested using a simulated New York-to-Chicago flight with satellite and altimeter measurements. Using many different values for the filter parameters, the performance of each algorithm during the takeoff and departure portions of flight is analyzed. Based on these initial evaluations, selected algorithms are tested using the entire 111-minute simulated flight. The results are presented using plots and tabular summaries of errors in the estimated position, velocity, and measurement bias states.

1.5 Results of the Dissertation

It will be shown that comparatively simple filter models can be used to successfully estimate the state of a maneuvering aircraft. In addition, the analysis of adaptive techniques will show that measurement residuals can be used to modify the parameters of the filter model to improve overall performance of the navigation algorithm. Because the numerical tests are based on a single Monte Carlo trial, the conclusions of the study can be interpreted as an elimination process, i.e., based on the numerical results, certain filter algorithms should be eliminated as candidates for implementation. Those algorithms which "survived" the tests must be tested further.

1.6 Overview of the Dissertation

Chapter 2 is a description of the Global Positioning System.

Included in Chapter 2 are brief descriptions of current navigation systems that the GPS is designed to replace. Also discussed are those elements of the GPS and its environment that are critical to navigation algorithm testing. The limited operational capability phase of GPS and the low-cost user, two restrictions of this study, are described also. Chapter 3 specifies the methods used to develop the simulated user trajectory and the measurements which were used in the analyses. The methods used are adequate for initial testing of navigation algorithms. In more detailed tests, the simple models described in Chapter 3 may be replaced by the more accurate and more detailed models which are reviewed in Chapter 2.

Chapter 4 is a review of linear estimation theory. A specific formulation of the general results is derived. Algorithms for three basic estimation philosophies are outlined.

Chapter 5 derives the basic twelve-state acceleration dead-reckoning (ADR) model. Also described are the parameters which will be used throughout the study to evaluate the navigation algorithms. The twelve-state ADR model test results are given in Chapter 5. Chapter 6 examines a nine-state velocity dead-reckoning (VDR) model and expands the analysis of the twelve-state ADR model. Chapter 6 also derives and examines an algorithm which estimates the inverse correlation time parameter of the ADR model. Chapter 7 derives and examines an algorithm which estimates the spectral level process noise parameter of the ADR model. Three easily-implemented adaptive indices are discussed also. The implementation method and results for each of the adaptive indices

are described. Chapter 8 summarizes the results of the study and makes recommendations for follow-on analyses.

CHAPTER 2

DESCRIPTION OF THE NAVSTAR GLOBAL POSITIONING SYSTEM

2.1 Current Navigation System

The NAVSTAR Global Positioning System (GPS) is a navigation satellite program which is scheduled to be operational in 1984. The system is designed to replace the ground-based navigation systems LORAN-C and OMEGA, and the navigation satellite system, TRANSIT.

The LORAN-C system is a ground-based radio navigation system operating between 90 and 100 khz. A LORAN-C network consists of a master station and at least two slave stations. The master station radiates a pulsed transmission which is received by the slave stations. After precise, fixed time delays from reception of the master station signal, the slave stations transmit groups of pulses similar to that transmitted by the master station. Each group of pulses is coded to identify the transmitting station. Two independent range-difference measurements are obtained by measuring the differences in the times-of-arrival of the signals from two transmitters relative to the time-of-arrival of the signal from a third transmitter. Each range-difference places the user on a hyperbola on the Earth's surface. Recall that a hyperbola is defined as a curve for which the difference of the distances of any point on the curve from two fixed points is constant. The fixed points are the foci of the hyperbola and, in LORAN-C, are

located at the transmitting stations. The intersection of the two hyperbolas, determined from two independent range differences, defines the user's position on the Earth's surface. Altitude of the user cannot be determined using LORAN-C because the transmitting stations are all in the plane of the Earth's surface [10:1-7][11:35-41].

The accuracy of a LORAN-C navigation fix is a function of instrumentation accuracy and knowledge of radio wave propagation and also varies with user-transmitting station geometry* and range. Within the service region of a LORAN-C network (2000-3000 km) accuracies are typically on the order of 25 to 100 meters [4:Table 2-7][11:54].

The OMEGA system is also a ground-based hyperbolic system which uses time difference measurements. However, it operates between 10 and 14 khz. In this frequency range, OMEGA can provide worldwide coverage with only eight transmitting stations. With these eight stations, there is sufficient redundancy in the selection of transmitting stations that good user-transmitting station geometry can usually be assured. OMEGA does not provide altitude information. Because of the long signal propagation distance over land and sea surfaces, the accuracy of OMEGA is a function of the predictability of radio wave propagation. Typical accuracies for OMEGA are on the order of two to five kilometers [4:Table 2-7][11:41-47].

Satellites have inherent characteristics that make them

---

*As will be evident in later discussions, user-transmitting station geometry is a basic factor in maximizing the accuracy of any navigation concept that depends on a geometric solution. For example, poor selection of stars can result in a poor celestrial navigation fix.

attractive as navigation signal transmitting stations. A proper choice of the orbits and the number of satellites will insure global coverage with good user-satellite geometry. Also, the propagation of satellite signals is more predictable than the ground-wave propagation of LORAN and OMEGA. Furthermore, three-dimensional position determination is also possible using satellites. The TRANSIT system attempted to take advantage of some of the desirable characteristics of satellites as navigation signal transmitters.

The TRANSIT system, operational since 1964, consists of five satellites in 1100 km polar orbits. The satellites transmit stable frequency signals at 150 mhz and 400 mhz. Position fixes are obtained by taking precise measurements of the Doppler frequency shifts from a satellite. Because the determination of a single navigation fix requires about 15 minutes [12], the TRANSIT system does not provide real-time position determination and is restricted to users with low dynamics such as ships. During the observation time interval, the user must either remain stationary or he must predict his position by dead-reckoning or other means.

In addition, TRANSIT satellites are not visible continuously. The system can, however, provide periodic position resets to an inertial navigation system (INS) and thereby limit the divergence of the INS solutions. Also, a single Doppler observation from a TRANSIT satellite pass can be used to improve the performance of systems such as an INS.

To achieve 200 meter navigation accuracy, the TRANSIT satellites must maintain transmission frequency stability to within one part in 10^9 for an observation interval of about 15 minutes [13] [14:84]. The quartz crystal clocks used on the TRANSIT satellites have demonstrated short term stabilities better than one part in 10^{10} [14:101][15]. Whereas Doppler navigation satellites require accurate frequency over the observation interval, satellites in a passive-ranging system require accurate time. Accurate time requires good long-term frequency stability which can be achieved using atomic frequency standards. The development of atomic frequency standards capable of operation in a space environment has made a passive-ranging navigation satellite system possible. A primary advantage of a passive-ranging system is its ability to provide a measurement within fractions of a second. With a sufficient number of satellites visible, a real-time position fix can be made on a near-instantaneous basis. Hence, the system need not be restricted to slow moving or stationary users.

The Global Positioning System is such a passive-ranging system. This chapter describes the purpose of the GPS, its characteristics, and its operation. The three primary segments of the GPS are discussed. These segments are referred to as the Control System Segment, the Space System Segment, and the User System Segment.

The GPS navigation signals are based on pseudo-random-noise (PRN) sequences. This chapter describes how the PRN sequence is generated by the satellite and how the user equipment can detect the signal. Atmospheric and relativistic effects are described also. In addition,

the limited operational phase of GPS (Phase II) and the application for a low-cost user are discussed since the primary objective of the dissertation is to evaluate navigation algorithms under these two restrictions.

2.2 Role and Characteristics of GPS

The role of the GPS will be to provide accurate three-dimensional position, velocity, and time information to its users. The satellite signals, when processed, will give the position, velocity, and time in the GPS coordinate frame. All GPS information will be referenced to a common coordinate system. The navigation signals, available continuously, will provide the navigation information on a near-instantaneous basis in all weather conditions. Since the GPS users will be passive with respect to the satellites (the users will only receive the satellite signals), they will not require transmitting equipment and the system can support an unlimited number of users.

2.3 The GPS Concept

Given the range measurements from three satellites whose positions are known, a user can determine his location at the intersection of three spheres whose centers coincide with the locations of the satellites.* A GPS user with a synchronized clock and knowledge of all clock biases and signal delays can compute range by using the time difference between the satellite clock time at signal transmission and

*It is assumed that the user can resolve any ambiguities in the solution and that the satellite geometry does not cause any singularities.

the user's clock time at the time-of-arrival of the satellite signal.

To eliminate the requirement that the user have an expensive clock, a fourth satellite can be used to enable the user to compute his clock bias. This is similar to processing three independent range-differences which also requires four satellites. When four satellites are used to determine three-dimensional position and clock bias, the user is located at the intersection of three hyperboloids of revolution.

In the above description, it is assumed that the user can take pseudo-range* measurements simultaneously from the required number of satellites. A user equipped with a receiver that takes the measurements sequentially, one satellite at a time, must use techniques that account for his motion and his clock drift. A moving user with a sequentially-tracking receiver can improve his navigation fixes by estimating his velocity and clock drift using pseudo-range-rate measurements which directly sense the components of velocity along the line-of-sight vector and the clock drifts. Recursive filter algorithms are available for the case where the measurements are to be processed sequentially.

A range-rate measurement can be obtained by differencing range measurements and dividing by the time interval between measurements. However, since a carrier tracking loop will be required in the user receiver, a more accurate measurement of range-rate is available using the difference between the carrier tracking loop oscillator frequency and the user oscillator frequency. If the user oscillator and the

---

*The measured time displacement is defined as pseudo-range since it includes the clock bias.

satellite oscillators are operating at the nominal frequency and other effects (atmospheric and relativistic) have been eliminated, then the difference between the carrier tracking loop oscillator frequency and the user oscillator frequency is a function of range-rate (velocity along the line-of-sight) only. The user oscillator, however, will be offset from the nominal frequency because perfect oscillator adjustment is impossible to achieve and maintain. The measurement of the difference between the carrier tracking loop oscillator frequency and the user oscillator frequency, which includes the effect of the user oscillator frequency offset, will be called a pseudo-range-rate measurement. It is assumed that the user oscillator drives the user's clock. The deviation of the user oscillator frequency from the nominal frequency will, therefore, be referred to as clock drift since the frequency deviation causes the user's clock to drift with respect to a nominal clock.

2.4 Control System Segment

The Control System Segment of the GPS will track the GPS satellites, determine the satellite ephemerides and clock parameters, and transmit this information to the satellites. The satellites will retransmit this data to the users. Orbit corrections and satellite clock frequency adjustments can be made also via the Air Force Satellite Control Facility, Sunnyvale, California.

Satellite tracking will be accomplished using four monitor stations (MS) located at Vandenburg AFB, California; Elmendorf AFB,

Alaska; Wahiawa, Hawaii; and Guam. Each monitor station will receive and process the satellite navigation signals. Each station will edit the satellite data and transmit the edited data along with meteorological and other pertinent information to the Master Control Station.

Satellite ephemerides and clock data will be determined by the Control System Segment. The Master Control Station (MCS), located at Vandenburg AFB, will receive data from the monitor stations every 15 minutes. The MCS will correct the data for known biases such as atmospheric delays, antenna lever arms, and relativistic effects. The data will be smoothed and placed on a file for transmission to the Naval Surface Weapons Center (NSWC), Dahlgren, Virginia.

Using the smoothed data, the NSWC will perform a batch estimate for the satellite state at a specified epoch and for the monitor station locations. The NSWC batch estimate will be performed approximately weekly. An ephemeris epoch will be defined at the end of the estimation period and the NSWC will then integrate the state forward from the estimation epoch to the ephemeris epoch. Then the state and state transition matrix will be integrated forward to predict satellite ephemerides for approximately two weeks. (See Figure 2.1.) The frequency and time span of the batch estimate may vary depending on satellite anomalies and confidence levels. Furthermore, the NSWC will have the capability to process the uncorrected data during diagnostic studies.

The NSWC will provide the MCS with the ephemeris epoch conditions, the predicted satellite ephemerides, and partial derivatives to

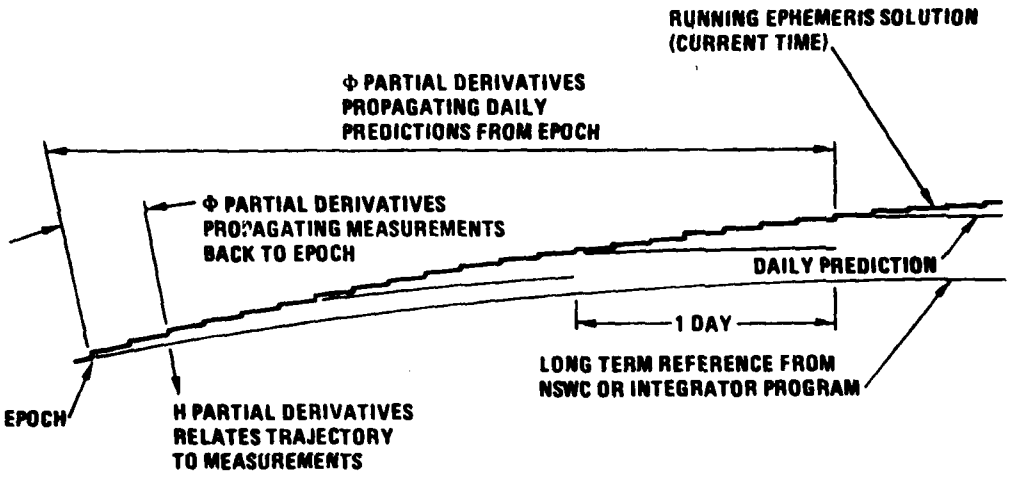

Figure 2.1 Ephemeris Determination About a Predicted Reference Solved at an Epoch

propagate corrections to epoch conditions forward to a future time (the state transition matrix). In addition, the NSWC will provide revised monitor station locations and the measurement partials for the monitor stations. The partials will be determined during the integration of the predicted trajectory.

The MCS will use the NSWC trajectory and partial derivatives in conjunction with the smoothed 15-minute data to determine current ephemeris and clock data for the satellites. This will be a near-real-time estimation using a Kalman estimator. Finally, the MCS will make daily predictions of the satellite ephemerides and clock behavior. The accuracy goal of the daily ephemeris generation is 1.5 meters (one

sigma) line-of-sight error [16]. The daily prediction will be broken down into nominal hourly periods. A set of Keplerian elements and seven correction terms will be used to fit the hour-long periods of the daily ephemeris prediction for each satellite. The fit to the daily prediction is expected to be within 0.01 meters [17:49]. The MCS will then format a daily group of ephemeris data sets and provide it to the upload station, also located at Vandenburg AFB, for transmission to the satellites. Each satellite will store a daily group of ephemeris data sets and will update the transmitted ephemeris data nominally every hour. After truncation into the satellite data stream, the fit to the hourly predicted ephemeris is expected to be within 0.10 meters [17:45].

2.5 Space System Segment

The Space System Segment includes the satellites, the launch equipment, and the associated hardware/software required to provide space-based radio navigation signals. In the following paragraphs, the satellite constellations for both the limited operational capability phase and the fully operational phase of the GPS will be described. Accurate frequency standards, which are the key hardware elements in the GPS satellites, will be analyzed. The navigation signal format will be described and the atmospheric and relativistic effects on the generation and propagation of the signal will be discussed.

2.5.1 Satellite constellations.

2.5.1.1 Phase III constellation. The fully operational (Phase III) Space System Segment will consist of twenty-four satellites in

one-half-sidereal-day orbits (20,183 km altitude). Nominal inclination will be 63 degrees. Eight satellites will be in each of three orbital planes with the ascending nodes of the planes separated by 120 degrees. Within each plane, the satellites will be equally spaced. (See Figure 2.2.)

2.5.1.2 Phase II constellation. This dissertation evaluates navigation algorithms for the Phase II GPS, a limited operational capability phase scheduled for 1979. The Phase II constellation will consist of nine satellites equally spaced in three orbit planes with the ascending nodes of the orbit planes separated by 120 degrees. Table 2.1 specifies the planned orbit for the Phase II satellites.

Table 2.1 Phase II Orbital Elements

Satellite	Longitude of Ascending Node (deg)	Time to Ascending Node (sec)
1	-130.	0.
2	-130.	-14400.
3	-130.	14400.
4	110.	0.
5	110.	-14400.
6	110.	14400.
7	-10.	0.
8	-10.	-14400.
9	-10.	14400.

Note: All satellites have Period = 43082.049456 sec; Semi-major axis = 26561.820982 km; Inclination = 63 deg; Eccentricity = 0; and Epoch of Elements = 0 sec.

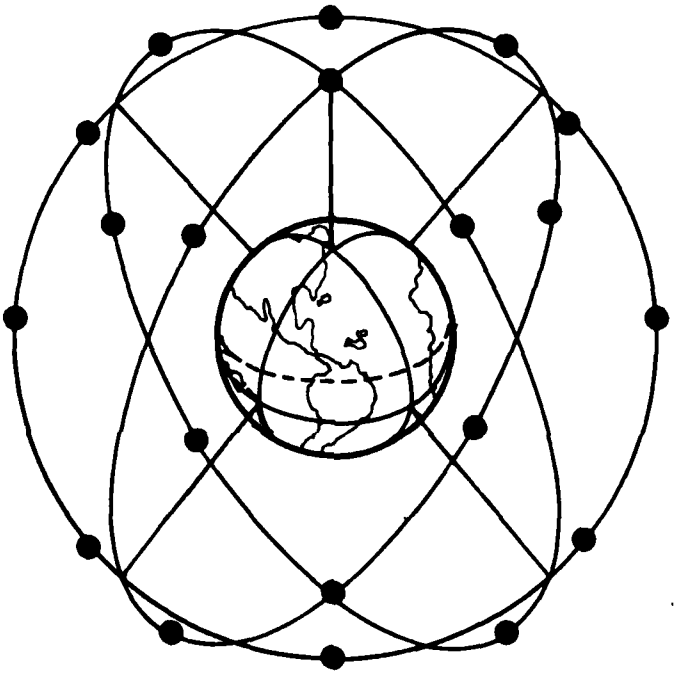

Figure 2.2 Orbital Configuration

The primary impact of Phase II with respect to the fully operational phase is the reduced number of satellites visible to a user. Whereas Phase III will provide six to eleven visible satellites, Phase II will provide only two to six visible satellites. Figure 2.3 shows the expected number of satellites visible to users at various latitudes for Phase II and Phase III.

2.5.2 Satellite clocks.

2.5.2.1 Atomic frequency standards. Clocks count the number of occurrences of a periodic phenomenon. The gears in an ordinary clock count the swings of a pendulum and move the hands on a clock face. In an electronic clock, an electronic counter counts the cycles of an oscillator and updates the display. In an atomic clock, the oscillator frequency is controlled by the frequency of an atomic transition. In an atomic transition, electrons move between specific energy levels and either absorb or emit energy at a frequency which is proportional to the difference between the energy levels. Since the allowable energy levels have precisely known quantum values, the frequency of the energy associated with the transition is very stable. The high stability of an atomic transition distinguishes the atomic clock from clocks whose periodic phenomenon is dynamical. It should be noted that most atomic frequency standards use an atomic transition to control a quartz oscillator. The vibration of the quartz crystal oscillator is the periodic phenomenon which is counted [19].

Quartz clocks, without synchronization by atomic transitions, were used in the TRANSIT navigation satellites [13]. Quartz clocks have

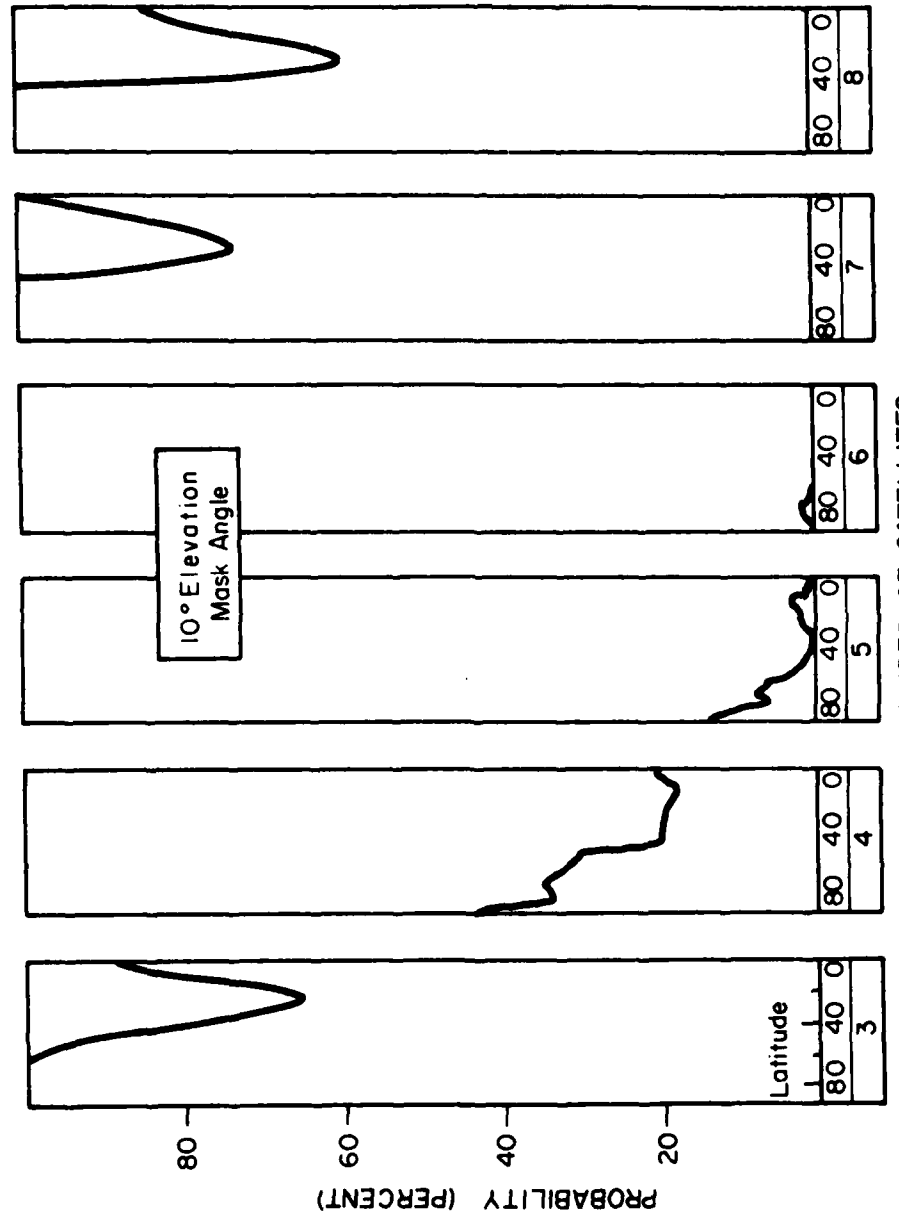

Figure 2.3 Probability Distribution of Global Satellite Visibility [32]

proven portability and recent manufacturing methods have improved considerably their stability [20]. In the following discussions, quartz clocks will be included for comparison with their more complex atomic counterparts.

Atomic sources, commonly used in current frequency standards, include (1) cesium beam resonators; (2) hydrogen masers, and (3) rubidium vapor cells. Descriptions of the operation of these clocks and other possible atomic standards are available in [21] and [22]. Atomic clocks can be compared with respect to cost, stability, reliability, and production experience. Relative figures of merit f have been assigned to the common clock types by Kartaschoff and Barnes [22]. (See Table 2.2.)

Table 2.2 Relative Comparisons of Standard Frequency Generators [22]

Parameter (code)	Cesium Standard	Rubidium Vapor Cell	Hydrogen Maser	Quartz Crystal
Initial Cost (a)	1	.5	5.0	.1
Support (b)	1	.5	10.0	.1
Stability (c)	1	.1	10.0	.01
Reliability (d)	1	1.0	.2	10.
Production Experience (e)	1	.5	.1	10.
Figure of Merit (f)	1	0.2	0.004	100.0

$$f = \frac{c \cdot d \cdot e}{a \cdot b}$$

2.5.2.2 Clock stability measures. Oscillators have an output of the form

$$V(t) = [V_0 + \varepsilon(t)] \sin[2\pi f_0 t + \phi(t)] \quad (2.1)$$

where: V_0 is the nominal amplitude;

f_0 is the nominal frequency;

$\varepsilon(t)$ is the amplitude deviation; and

$\phi(t)$ is the phase deviation.

The instantaneous fractional frequency deviation is defined as

$$y(t) = \frac{\dot{\phi}(t)}{2\pi f_0} \quad (2.2)$$

An important measure of a clock is its frequency stability. Several methods have been proposed to characterize frequency stability. In the frequency domain, the one-sided spectral density is defined as [23:116]

$$S_y(f) = 4\int_0^\infty R_y(\tau)\cos(2\pi f\tau)\, d\tau \quad (2.3)$$

where: $R_y(\tau)$ is the auto-correlation of $y(\tau)$.

In the time domain, stability can be characterized by the N-sample variance. The time average of the fractional frequency deviation over a sample duration τ is defined by

$$\bar{y}_k = \frac{1}{\tau}\int_{t_k}^{t_k+\tau} y(t)dt = \frac{\phi(t_k+\tau) - \phi(t_k)}{2\pi f_o \tau} \tag{2.4}$$

If N samples are taken at a repetition period $T = t_{k+1} - t_k$, then the N-sample variance is given by

$$\sigma_y^2(N,T,\tau) = \frac{1}{N-1}\sum_{i=1}^{N}\left(\bar{y}_i - \frac{1}{N}\sum_{k=1}^{N}\bar{y}_k\right)^2 \tag{2.5}$$

The Allan variance is the most commonly used stability measure for atomic frequency standards. Allan variance is obtained using Eq. 2.5 with a sample size of two, N = 2, and no dead time, $T = \tau$.

$$\sigma_y^2(2,\tau) = \left\langle\left(\frac{\bar{y} - \bar{y}}{2}\right)^2\right\rangle \tag{2.6}$$

where: $\langle\cdot\rangle$ denotes the infinite time average.

The Allan variance may be estimated for a set of M data points as follows [24]:

$$\phi_y^2(2,\tau) \approx \frac{1}{2M}\sum_{i=1}^{M}(\Delta y_i)^2 \tag{2.7}$$

where: Δy is the difference between adjacent frequency measurements over a nominal sample time.

Barnes [23] and Allan [25] provide comprehensive discussions of stability measures and show the relationship between spectral density in the frequency domain and the Allan variance in the time domain. Other forms of stability measures are discussed by Lindsey and Lewis [26]. For more details on frequency stability measurement see Allan [27].

Figure 2.4 [13] depicts the range of stabilities, expressed as Allan variance, available in commercial clocks. The GPS specification for developmental satellite clocks [28: Par. 3.7.2.4.3] has been included on Figure 2.4 for reference.

The variance of a time interval measurement is related to the Allan variance by

$$\sigma^2_{\Delta\tau} = \tau^2 \sigma^2_y (2,\tau) \qquad (2.8)$$

Using the specification for the GPS satellite clock, the standard deviation of a time interval of 10,000 seconds (2.78 hours) is ten nanoseconds. For a one week interval, the standard deviation is 604.8 nsec.

Current GPS plans call for the testing of a cesium beam atomic clock on the first satellite, Navigation Technology Satellite No. 2 (NTS-II), scheduled for launch in 1976. Rubidium vapor atomic clocks are planned for the five Navigation Development Satellites (NDS). If flight proven, later GPS satellites may use cesium clocks.

Additional information on the design and capabilities of atomic clocks is available in References 29 through 33.

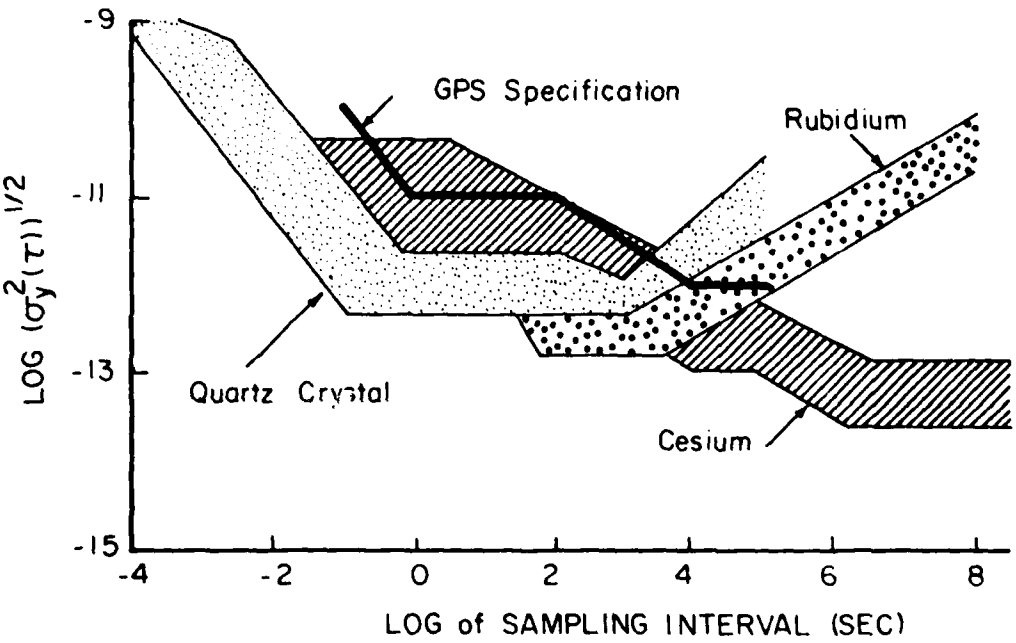

Figure 2.4 Stability Ranges of Commercial Frequency Standards [20]

2.5.2.3 Satellite clock timing data. Satellite clock time will be expressed as "Z-count" which is the number of seconds from a weekly epoch divided by 1.5. Using this transmitted Z-count, the user will be able to time-tag any bit in the received signal by counting bits from an epoch associated with the transmitted Z-count. This will provide a nominal time-tag θ_s.

The capability to adjust the frequency of the satellite clock, via the Air Force Satellite Control Facility, will exist. The precision of the frequency adjustments will be four parts in 10^{12} over a range of plus/minus two parts in 10^9. Also, the Master Control Station will have the capability to adjust the phase of the satellite clocks.

To increase timing accuracy, the satellite data stream will contain clock correction data. In addition to an "age of data" word, the clock data will include:

Epoch for the clock correction polynomial, t_{oc};
Clock bias at epoch, Δt_o;
Clock drift at epoch, $\Delta f/f$; and
Clock drift rate, D/2

The clock data, transmitted by the satellite, will be changed by the satellite nominally every hour. The clock parameters will be chosen to best fit the expected clock error over the hourly period using the polynomial

$$\Delta t_s(T_s) = \Delta t_o + \frac{\Delta f}{f}(T_s - t_{oc}) + \frac{D}{2}(T_s - t_{oc})^2 \qquad (2.9)$$

where: T_s is the GPS time at signal transmission.

The user will correct the nominal time tag θ_s to determine the estimate of the satellite transmission time $\hat{t}_s$.

$$\hat{t}_s = \theta_s - \Delta t_s(\theta_s) \tag{2.10}$$

Note that the argument of the user's clock correction polynomial is the nominal time-tag θ_s because the true system time at transmission T_s is not available. Even if the fit in Eq. 2.9 is perfect, Eq. 2.10 will not, in general, provide the exact answer. If more accuracy is needed, the user can repeat the computation of Eq. 2.10 using $\hat{t}_s$ as the argument of the clock correction polynomial. This is a successive approximation technique. After applying the clock correction information, satellite clock time accuracy is expected to be on the order of a few nanoseconds over a one hour period.

2.5.2.4 Relativistic effects. Cretcher [34] has shown that the only relativistic effects of concern for GPS are clock corrections. Relativistic effects on signal propagation and on satellite dynamics are negligible. A clock in a twelve-hour circular orbit will have a relativistic drift of +38 μsec/day with respect to a clock at mean sea level on the earth. This is the primary relativistic effect. Second order effects and orbit eccentricity effects are negligible. For the one-hour period between changes in the transmitted clock correction parameter set, the relativistic effects can be included in the correction parameters. Furthermore, satellite clock frequency can be adjusted to account for the relativistic effects. Prior to launch, the P-code of

a GPS satellite clock could be adjusted to have a code rate of $10.22999999545 \times 10^6$ bits-per-second. Then, assuming that only the bias effect of the general relativity term affects the clock, an Earth-bound user would see a code rate of 10.23×10^6 bits-per-second.

If relativistic effects are accounted for by the GPS using satellite clock adjustments or by modifying the downlink clock parameters, most users will not have to concern themselves with relativistic effects. If the GPS is used by earth satellites for autonomous tracking, however, relativity may have to be considered because the satellite velocities and the gravitational potential at the user satellite may cause relativistic effects to be non-negligible. The extent of the required corrections depends on the accuracy requirements and the user satellite orbit. A detailed analysis would have to be performed for the specific mission of concern to determine the magnitude of these effects.

2.5.3 Satellite signal structure.

2.5.3.1 Pseudo-random-noise sequences. The navigation signals are pseudo-random-noise (PRN) sequences transmitted on two frequencies in the L-band. The primary frequency L_1 is 1575.42 mhz and the secondary frequency L_2 is 1227.6 mhz. The PRN sequences will be produced by linear feedback shift-register generators.

A linear feedback shift-register generator (SRG) shifts the contents of each stage of the generator toward the output stage and modulo-2 adds the contents of the specified stages for feedback to the

initial stage. The SRG shown in Figure 2.5 will produce the 31-bit sequence

1111100011011101010000100101100

when the stages are initially loaded with ones. For a five-stage SRG this is a maximal sequence, i.e., it is the longest sequence possible for the specified number of stages in the SRG that will yield sequences of 31 bits. All other connections produce sequences shorter than 31 bits. The length of the PRN sequence produced by a non-maximal SRG depends on the initial contents of the SRG states.

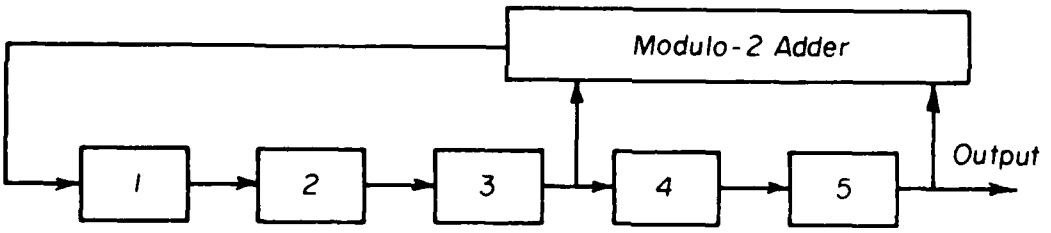

Figure 2.5 A Five-Stage Maximal Linear Shift-Register Generator

Ristenbatt [35] provides a good discussion of shift-register-generators. He shows that the length of a maximal sequence is

$$L = 2^n - 1 \qquad (2.11)$$

where: L is the length of the maximal sequence; and

n is the number of stages in the SRG.

The number of maximal sequences possible for an n-stage SRG is given by

$$\frac{\phi(2^n - 1)}{n} \tag{2.12}$$

where: ϕ is Euler's phi-function evaluated as $\phi(k) = k - 1$ if k is prime, otherwise, $\phi(k) = k \prod (P_i - 1)/P_i$ and P_i are the prime factors of k.

Table 2.3 gives the number of maximal sequences possible for n-stage SRGs.

Table 2.3 Number of Maximal Sequences

Number of Stages	Maximal Sequence Length	Number of Maximal Length Sequences
2	3	1
3	7	2
4	15	2
5	31	6
6	63	6
7	127	18
8	255	16
9	511	48
10	1023	60
11	2047	176
12	4095	144
13	8191	630
14	16383	756

Ristenbatt further states that the tap selections required for a maximal n-stage SRG can be determined from the primitive irreducible polynomials of degree n. Such polynomials will have an odd number of terms and will include the n^{th} power term and the constant term. Table 2.4 lists the polynomials corresponding to maximal SRGs with up to six stages.

Table 2.4 Polynomials for Maximal Length Sequences

Number of Stages	Maximal Sequence Length	
2	3	$x^2 + x^1 + 1$
3	7	$x^3 + x^1 + 1$
		$x^3 + x^2 + 1$
4	15	$x^4 + x^1 + 1$
		$x^4 + x^3 + 1$
5	31	$x^5 + x^2 + 1$
		$x^5 + x^3 + 1$
		$x^5 + x^3 + x^2 + x^1 + 1$
		$x^5 + x^4 + x^3 + x^2 + 1$
		$x^5 + x^4 + x^2 + x^1 + 1$
		$x^5 + x^4 + x^3 + x^1 + 1$
6	63	$x^6 + x^1 + 1$
		$x^6 + x^5 + 1$
		$x^6 + x^5 + x^2 + x^1 + 1$
		$x^6 + x^5 + x^4 + x^1 + 1$
		$x^6 + x^4 + x^3 + x^1 + 1$
		$x^6 + x^5 + x^3 + x^2 + 1$

The auto-correlation function of a PRN sequency of length N is shown in Figure 2.6.

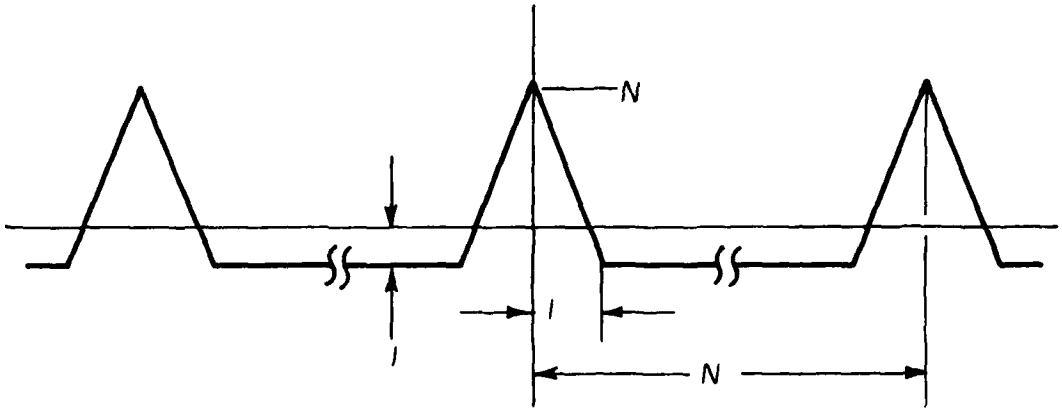

Figure 2.6 Ideal Auto-Correlation Function for an N-Bit PRN Sequence

Unfortunately, the cross-correlation between two maximal sequences may be undesirably high as the period becomes shorter. This is detrimental to the mutiplexing of twenty-four satellites on the same frequency. Gold [36] has developed a method of determining families of SRG-generated PRN sequences that have low cross-correlations. He shows that any two polynomials corresponding to maximal n-stage SRGs can be multiplied to give the polynomial corresponding to a non-maximal 2n-stage SRG. The number of members in each family is $2^n + 1$ and the length is $2^n - 1$. The cross correlation θ among the family members will satisfy the inequality

$$\theta \leq t = \begin{cases} 2^{(n+1)/2} + 1 & \text{for } n \text{ odd} \\ 2^{(n+2)/2} + 1 & \text{for } n \text{ even, } n \neq \text{mod } 4 \end{cases} \qquad (2.13)$$

Thus, if a specified auto-correlation characteristic requires an n-stage SRG, Gold's procedures will specify non-maximal 2n-stage SRGs with significantly lower cross-correlations.

2.5.3.2 GPS navigation signals. Two PRN sequences are transmitted by each satellite: a Precision (P) code and a Clear/Acquisition (C/A) code. The P-code bit rate is 10.23×10^6 bits-per-second (10.23 mbps). The bit width is 97.75 nsec. The P-code is generated by combining an X1 code and an X2 code. Two twelve-stage SRGs are used to generate the X1 code and two twelve-stage SRGs generate the X2-code. A combination of four twelve-stage SRGs can be connected to give a P-code sequence lasting up to 318 days. However, the SRGs are implemented so that the X1-code component period is 1.5 seconds* and the P-code sequence for each satellite repeats every seven days. This method allows a user to quickly shift his local code for signal acquisition.

The C/A-code is a 1023-bit sequence with a bit rate of 1.023 mbps. The sequence repeats every millisecond. Bit width is 977.5 nsec. The sequences are from the 1023-bit Gold family and require two ten-stage SRGs whose tap connections correspond to the product of polynomials for maximal ten-stage SRGs. Although there are 1025 members in this family, only 36 will be selected for GPS use, thus improving on the maximum cross-correlation of 65 for the entire 1023-bit Gold family.

---

*The X1-code epoch provides basic synchronization for satellite signal generation. The number of X1 epochs from midnight Saturday night/Sunday morning is referred to as Z-count. (See Par. 2.5.2.5.)

The P-code sequence is so long that very accurate position and time information for both the user and the satellite is required to lock on to the P-code. The C/A sequence, however, is only one millisecond long and requires much less shifting of the user generated code to correlate the received code. The disadvantage of a short code is ambiguity. The user can correlate a received C/A code in steps of one millisecond, each time changing his pseudo-range measurement by approximately 300 km (i.e., the speed of light multiplied by one millisecond). A pseudo-range measurement residual of 300 km can be accounted for by changing the user's assumed position by 300 km along the line-of-sight between the user and the satellite, or by changing the user's clock bias by one millisecond, or by a combination of a change in the user's estimated position and estimated clock bias. The details of the acquisition methods and ambiguity resolution are beyond the scope of this dissertation. For further information, see [37] and [38].

2.5.3.3 Data modulation. Data is modulated onto the PRN sequence by modulo-2 addition of a 50 bps data stream to the P-code and to the C/A-code. The resulting P-signal and C/A-signal are used to biphase-modulate a continuous carrier. In biphase modulation, if a "zero" code state is indicated by $s_0 = \cos(\omega t - 90°)$, then the "one" code state is indicated by $s_1 = \cos(\omega t + 90°)$. The secondary frequency (L_2) contains either the P-signal or the C/A-signal. The primary frequency (L_1) carries both the P-signal and the C/A-signal in phase quadrature. (See Table 2.5.)

Table 2.5 Signal Phase for Composite P- and C/A-Codes

Code State		Composite Signal Phase
P	C/A	
0	0	0.0°
1	0	-70.5°
0	1	109.5°
1	1	180.0°

2.5.3.4 Signal detection. The preceding information is based on current specifications of the satellite navigation signals. Though details may change, the structure of the signal is expected to conform closely to the signal described in the previous paragraph. User equipment for a given signal structure can be designed in many ways. It is impossible to describe "the" user receiver. Certain similarities, however, must exist among all users. These similarities and basic user equipment functions will be discussed briefly.

The following are some general remarks about variations in the user receivers:

1. In a simultaneous receiver, certain portions of the equipment are duplicated and additional equipment is needed for switching.

2. A user of both the L_1 and L_2 frequencies must have equipment to multiplex the data.

3. Code switching between the P- and C/A-codes must be incorporated for the precision user.

Given frequency, code, and satellite identifier, Figure 2.7 is a basic functional diagram of a user receiver, called a correlation receiver.

In addition to the usual radio frequency (RF) and intermediate frequency (IF) functions, the correlation receiver includes a correlator, a code tracking loop, and a carrier tracking loop. A Costas loop will probably be used in the carrier tracking loop since modulation is biphase. A Costas loop for biphase modulation consists of two branches. One branch detects the "zero" state (s_0) and the second branch detects the "one" state (s_1). The Costas loop will extract the data and provide Doppler information. The carrier tracking loop recovers the code tracking loop error signal which is then fed back to the code tracking loop. The code tracking loop adjusts the local code generator in response to the code tracking loop error signal. The correlator multiplies the received signal by the locally generated code signal. A perfect receiver would have the correlator output appear as shown in Figure 2.6 and would maintain lock at the peak of the auto-correlation function.

The Doppler information from the carrier tracking loop provides a pseudo-range-rate measurement because the offset of the carrier tracking loop oscillator from the local oscillator is determined by the relative velocity between the user and the satellite and by the frequency offset of the local oscillator. The pseudo-range measurement is obtained by differencing the phase of the local code, which is correlated to the incoming code, and the phase of a local reference. This

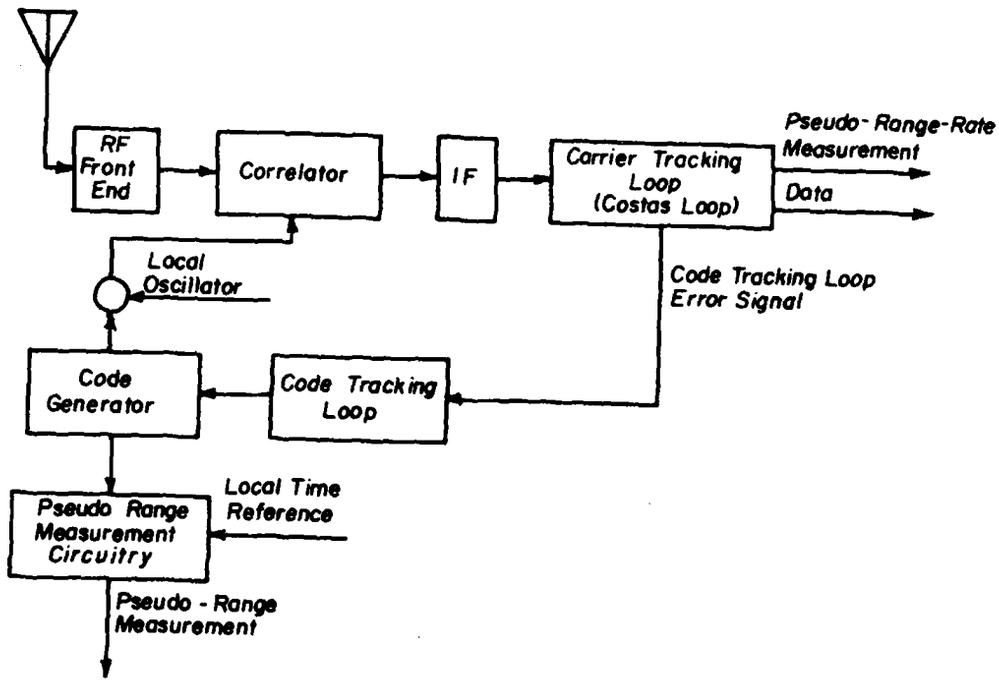

Figure 2.7 Correlation Receiver Functional Diagram

phase difference, equivalent to a time displacement, is a measure of transit time (range) and the phase bias of the local reference.

2.5.4 Atmospheric excess time delay. The velocity of propagation of radio waves in the atmosphere is not equal to the vacuum speed of light. In the ionosphere, radio wave velocity is affected by free electron density. In the lower atmosphere, radio wave velocity is affected by pressure, temperature, and humidity. The result is a transit time that is greater than the time predicted by using the vacuum speed of light. The excess time delays due to atmospheric effects are described in more detail in the following paragraphs.

2.5.4.1 Ionospheric delay. The one-way transmission time for an RF pulse from a satellite to a user is given by [39:19]

$$t = \frac{1}{c} \int_{R_u}^{R_{sv}} n'(s)ds \qquad (2.14)$$

where: c is the vacuum speed of light;
n' is the group refractive index; and
the integral is taken over the ray path.

The group refractive index for frequencies above VHF can be evaluated using

$$n' = n + f \frac{dn}{df} \qquad (2.15)$$

$$n = \frac{c}{v} = \left[1 - \frac{f_p^2}{f^2} \right]^{1/2} \tag{2.16}$$

$$f_p^2 = \frac{e^2 N_e}{4 \pi^2 \varepsilon_o m} \tag{2.17}$$

where: f is the frequency of interest;

f_p is the plasma frequency;

n is the ionospheric refractive index;

v is the velocity of propagation;

e is the electron charge;

ε_o is the permittivity of free space;

m is the electron mass; and

N_e is the free electron density.

Equation 2.14 can be used to obtain an expression for ionospheric excess time delay.

$$\delta_{ion} = \frac{1}{c} \int_{R_u}^{R_{sv}} n' \, ds - \frac{R}{c} \tag{2.18}$$

where: R is the line-of-sight range.

Neglecting ray bending, the ionospheric delay is

$$\delta_{ion} = \frac{e^2}{8\pi^2 \varepsilon_o m f^2} \int_{\underline{R}_u}^{\underline{R}_{sv}} N_e \, ds \qquad (2.19)$$

The integral requires that ionospheric electron density be known along the ray path.

The primary effects on an electron density profile are diurnal (day/night), seasonal (winter/summer), latitudinal (polar/equatorial), and solar (sunspot cycle). Ionospheric models generally include parameters whose values are based on the above effects. A static model of the ionosphere will be developed for GPS users. The values of the parameters for the GPS model will be transmitted in the satellite data stream.

Many models of ionospheric electron density have been developed and evaluated. One of the most popular is the Chapman model which can be defined as follows [39:11]:

$$N_e(h) = N_m \exp\left[\frac{1}{2}(1 - z - e^{-z})\right] \qquad (2.20)$$

$$z = \frac{h - h_m}{h_s}$$

where: h_s is the scale height;

N_m is the peak electron density; and

h_m is the altitude of peak electron density.

Ray-tracing methods perform a numerical integration of Eq. 2.19. Many ray-tracing methods model the electron density as a series of Chapman layers. For GPS user implementation and for purposes of basic navigation algorithm evaluation, ray-tracing methods are too complicated and time consuming.

Rao, Youakim, and Yeh [40] evaluated the capabilities of empirical ionospheric delay models of varying complexity. In all cases, the model parameters were adjusted to fit the data available for selected time periods. The resulting root-mean-square residuals in ionospheric vertical group delay were on the order of 1 nsec to 7 nsec. The vertical group delay is the excess one-way transit time for a satellite directly overhead. For a satellite at ten degrees elevation, the obliquity factor is approximately 5.8. An error of 1 nsec in vertical group delay corresponds to a 5.8 nsec error for a satellite at ten degrees elevation.

It must be noted that the models evaluated by Rao, et al, were used to fit periods of available data after the data had been obtained. If a model with parameters fitted to a period of time is used to predict the delays in another time period, it is reasonable to expect larger errors. However, it must be noted that the models evaluated were fitted to time periods ranging from four months to one year. Using the GPS data stream, a model can have its parameters adjusted frequently based on the best available information. This more frequent updating will result in smaller errors.

The Bent ionospheric model [41] is a complicated empirical model which was evaluated also against a large volume of available data. The Bent model had RMS errors ranging from 12% to 30% of the vertical group delay.

Pisacane, Feen, and Sturmanis [42] evaluated algorithms for long-term ionospheric prediction and algorithms for near-real-time prediction. For vertical group delays ranging from 5.6 nsec to 28.3 nsec, the RMS of the residuals ranged from 18% to 55% of the vertical group delay [42:68].

Wand [39] combined sets of ray-tracing results to obtain an empirical expression for ionospheric delay which is a function of user-satellite geometry, scale height of the ionosphere, height of peak electron density, and plasma frequency at peak electron density.

The ionospheric delay model to be evaluated using the NTS-II satellite is as follows [17:43-45]:

$$\delta_{ion} = \begin{cases} F\left[5.\times10^{-9}+\left(\sum_{i=0}^{3}\alpha_i\,\phi_m{}^i\right)\left(1-\frac{x^2}{2}+\frac{x^4}{24}\right)\right] & \text{sec}, |x|<1.57 \\ F\,(5.\times10^{-9}) & \text{sec}, |x|\geq 1.57 \end{cases} \tag{2.21}$$

$$x = (t - 50{,}400)/\left(\sum_{i=0}^{3}\beta_i\,\phi_m{}^i\right) \tag{2.21a}$$

$$F = 1. + 16.\,(.53 - el)^3 \tag{2.21b}$$

$$t = (43{,}200\,\lambda_{ion} + T) \bmod 86{,}400 \quad \text{sec} \tag{2.21c}$$

$$\phi_m = \phi_{ion} + .064 \cos (\lambda_{ion} - 1.617) \text{ semi-circles} \quad (2.21d)$$

$$\lambda_{ion} = \lambda + \frac{\psi \sin az}{\cos \phi_{ion}} \text{ semi-circles} \quad (2.21e)$$

$$\phi_{ion} = \begin{cases} \phi + \Psi \cos az \text{ semi-circles}, & \phi < .416 \text{ semi-circles} \\ \phi \text{ semi-circles}, & \phi \geq .416 \text{ semi-circles} \end{cases} \quad (2.21f)$$

$$\Psi = \frac{0.0137}{el + 0.11} - 0.022 \text{ semi-circles} \quad (2.21g)$$

The satellite transmitted terms are:

α_i - coefficients of a cubic equation representing the amplitude of the vertical group delay as a function of ϕ_m;

β_i - coefficients of a cubic equation representing the normalized period of the model (true period divided by 2π) as a function of ϕ_m.

The user supplied terms are:

el - elevation angle between the user and the satellite (semi-circles);

az - azimuth between the user and the satellite, measured clockwise positive from true North (semi-circles);

ϕ - user geodetic latitude (semi-circles);

λ - user longitude (semi-circles);

T - GPS time of signal reception (sec);

Intermediate calculations to be performed by the user include:

F - obliquity factor (dimensionless);

t - local time (sec);

ϕ_m - geometric latitude of the earth projection of the ionospheric intersection point (semi-circles);

λ_{ion} - longitude of the earth projection of the ionospheric intersection point (semi-circles);

ϕ_{ion} - geodetic latitude of the earth projection of the ionospheric intersection point (semi-circles);

Ψ - earth central angle between user position and earth projection of ionospheric intersection point (semi-circles).

The result of Eqs. 2.21 is applicable to the ionospheric excess time delay for the primary frequency L_1. For the secondary frequency L_2, the correction term must be multiplied by $(L_1/L_2)^2$, which, for the designated frequencies, is 1.647. The satellite transmitted terms are expected to be valid for ten-day periods.

Other models for ionospheric delay include a truncated Appleton-Hartree equation evaluated by Rohde [43], and a model suggested for use in the NASA Deep Space Tracking Network [44:22-23].

2.5.4.2 Tropospheric delay. Equation 2.14 also applies to a neutral atmosphere. The neutral atmosphere of importance to GPS consists of the troposphere, which extends to about 10 km, and the stratosphere, which extends to about 50 km [45]. In these regions, the index of refraction n varies with pressure, temperature and humidity. The

index of refraction is used to define the parameter called refractivity N_r as follows:

$$N_r = (n - 1)10^6 \tag{2.22}$$

Using Eq. 2.22, the tropospheric excess time delay is given by

$$\delta_{trop} = \frac{10^{-6}}{c} \int_{\underline{R}}^{R} N_r \, ds \tag{2.23}$$

The refractivity can be partitioned into a dry component N_d and a wet component N_w.

$$N_r = N_d + N_w \tag{2.24}$$

The two components can be evaluated using

$$N_d = 77.6 \, P/T \tag{2.25}$$

$$N_w = 3.73 \times 10^5 \, e/T^2 \tag{2.26}$$

where: P is total pressure (mb);

T is temperature (°K); and

e is the partial pressure of the water vapar (mb).

Hopfield used the partitioned refractivity expressions in quartic equations to model a refractivity profile [46]. The CRPL Reference Atmosphere, 1958, used a refractivity model for three altitude ranges based on a sea level refractivity [47].

Altschuler [48] evaluated a model for tropospheric excess time delay from an aircraft to a satellite as a function of the delay for a sea level user, the aircraft altitude, and the sea level refractivity. The standard deviation of the errors in the model was 1.3 nsec for satellites at 5 deg elevation. Using an average value for sea level refractivity of 324.8, the expected error for 5 deg elevation increased to 6.7 nsec. At higher elevation angles, the delay and the expected error in the calculated delay decrease.

Altschuler and Kalagher [49] have developed tropospheric delay models more suited to GPS users because they avoid transcendental and trigonometric expressions. The Jet Propulsion model suggested for use by the NASA Deep Space Tracing Network [44:22-23] was adapted for use in the simulation. (See Par. 3.5.2)

Most models examined assumed a profile which was based on sea level refractivity. An aircraft may be above much of the troposphere and could reduce the error in the delay computation by using readily available pressure and temperature information at aircraft altitude to estimate the refractivity.

2.6 User System Segment

2.6.1 Classes of users. The User System Segment includes all the hardware and software needed to determine the user's position, velocity, clock behavior, and other parameters as required. Various classes of users have been defined based on user requirements and characteristics such as desired accuracy, user motion, jamming immunity, and

cost [50]. Navigation algorithms evaluated in this dissertation are to be applicable to a low-cost user.

2.6.2 The low-cost user. The low-cost user will have a sequential receiver that operates on a single frequency, and will have a minimum of auxiliary sensors. A sequential receiver is cheaper than a simultaneous receiver because the simultaneous receiver is effectively four receivers. A sequential receiver eliminates the additional hardware required by the simultaneous receiver. The disadvantage is the requirement for a more complex navigation algorithm to account for user motion and clock drift.

The low-cost user will have a single-frequency receiver and will save the cost of the additional hardware required by a dual-frequency user. The disadvantage for the single-frequency user is the lack of accurate real-time ionospheric delay computation.

Ionospheric delay is inversely proportional to the square of the frequency. A dual-frequency user can process the phase difference between the code received on L_1 and the code received on L_2 to calculate the ionospheric delays [51]. The single-frequency user must use a static model for ionospheric delay. Satellite data will include parameters for an ionospheric delay model. The specific structure of the ionospheric delay model will be evaluated in the GPS developmental tests. (See Par. 2.5.4.1.)

It is assumed that the low-cost user has a barometric altimeter. This is a basic item of aircraft equipment. The low-cost restriction is not violated by requiring a digitized signal from the

altimeter. Analog-to-digital converters are available in microcircuits for costs which are negligible when compared to other items of required equipment.

CHAPTER 3

SIMULATION OF THE GLOBAL POSITIONING SYSTEM

3.1 Simulation Philosophy

Since one of the goals of this dissertation is the evaluation of the behavior of several proposed Global Positioning System (GPS) user navigation algorithms, the procedure for simulating the GPS is of critical importance. To accomplish this goal, portions of the GPS Space System Segment and an approximate model which describes the user's dynamics were used to generate simulated observations. Selected navigation algorithms were tested by varying the parameters of the filter and examining the filter performance. All navigation filters were tested using a single set of observations. Extensive tests were made using a small portion of the generated data, i.e., that portion which corresponded to the first ten minutes of flight. Selected filters, which appeared to have good performance, were tested also for the entire simulated trajectory.

The simulation philosophy was designed to produce a physically realizable set of data points against which the filter could be tested and evaluated. The simulation used simplified models of the GPS system which was described in Chapter 2 because the use of simple models reduces the computer time requirements and increases the programmer's control of the error behavior. With a reasonable choice of parameters,

a set of realizable trajectory and measurement data points can be generated.

The simulation program can be separated into five parts:

1. Simulation of the satellite dynamics;
2. Simulation of the user dynamics;
3. Simulation of system instruments, especially the clocks;
4. Simulation of the environment, i.e., atmospheric delays; and
5. Generation of the measurements.

Figure 3.1 depicts the role of the simulation in the generation of the measurements, the filter processing, and the filter evaluation. This chapter will describe each part of the simulation in more detail.

3.2 Simulation of Phase II GPS Constellation

For simplicity, the simulated GPS satellites are assumed to be in circular orbits about a point-mass Earth. Table 2.1 lists the orbital elements for the simulated satellites. The simulated GPS user assumed the same model. Satellite position can thus be determined using a closed form solution and a set of Keplerian elements at an epoch. For basic navigation algorithm evaluation, it is unnecessary to include higher order geopotential terms or other perturbing forces because errors in the user calculated satellite positions can be simulated more easily and more predictably by corrupting the users orbital elements.

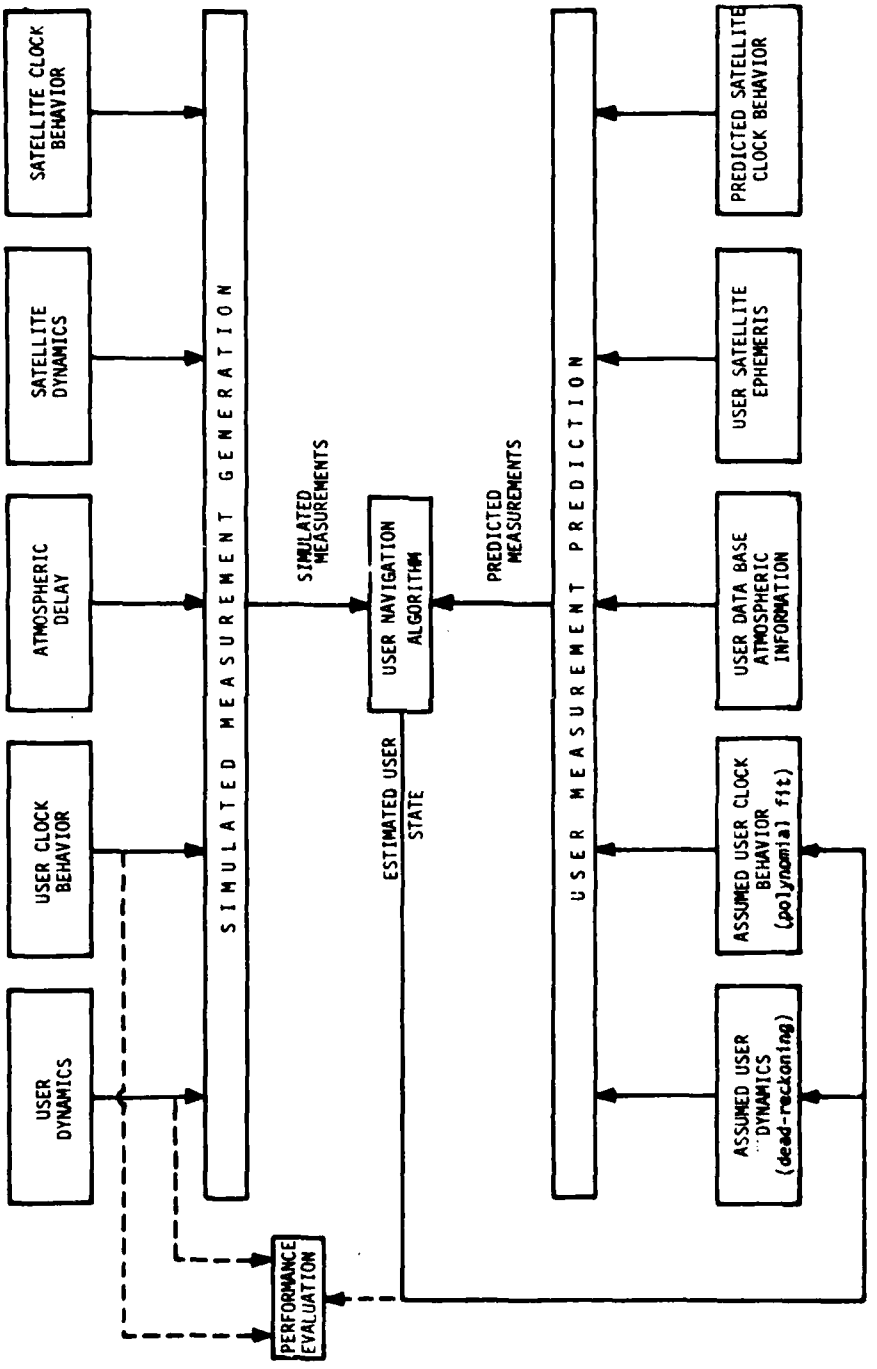

Figure 3.1 Functional Relationships Between the Simulation Computer Program and the Navigation Filter Processing and Evaluation Computer Program

Table 3.1 lists the user data base almanac for the satellites which are visible in the basic simulation.

Table 3.1 User Data Base Orbital Elements

Satellite	Longitude of Ascending Node (deg)	Time to Ascending Node (sec)	Period (sec)	Inclination (deg)
1	-130.	0.	43082.051000	63.
2	-130.	0.	43082.049456	63.00002292
5	110.00002292	0.	43082.049456	63.
7	-10.	0.0025	43082.049456	63.

Note: All satellites were assumed to have zero eccentricity. The time associated with these elements is T = 0.

3.3 Aircraft Trajectory Simulation

3.3.1 Aircraft simulation philosophy. The goal of the simulation is to determine a sequence of position and velocity vectors which represents possible aircraft motion. The aircraft simulation does not attempt a rigorous definition of the airplane trajectory. Differences between the computed numerical values and the values that would result from a more rigorous solution to the differential equations of motion can be attributed to wind gusts. In fact, the basic simulation provided a trajectory that was unreasonably smooth. To "bounce" the aircraft, a perturbation to the position and velocity is applied at the end of each 1.25 second interval. (See Par. 3.3.3.)

3.3.2 Aircraft model. The aircraft model is similar to that used in [51]. The aircraft is modeled as a point mass. The aircraft is described by the heading angle θ, horizontal speed V, altitude rate $\dot{h}$, altitude above the reference ellipsoid h, geodetic latitude ϕ, and longitude λ.

A series of waypoints consisting of latitude, longitude, altitude, and horizontal speed must be specified. The simulated aircraft attempts to pass through each waypoint. The waypoints used in the simulation represent a flight from New York to Chicago. (See Table 3.2.)

At the beginning of each integration step, the aircraft state is compared to the current waypoint requirements. If the distance to go to the current waypoint is small, the next waypoint is selected. Distance-to-go in radians of arc is calculated using

$$\alpha = \cos^{-1} [\sin \phi_i \sin \phi + \cos \phi_i \cos \phi \cos(\lambda_i - \lambda)] \qquad (3.1)$$

where: ϕ_i and λ_i are the geodetic latitude and longitude of the waypoint.

Figure 3.2 depicts the aircraft model simulation. Table 3.3 lists the aircraft response model parameters. The waypoint altitude is used as a command to a second-order response model. Waypoint speed is used as a command to a first-order response model. The user's latitude and longitude are compared to the latitude and longitude of the waypoint and a desired heading angle is commanded. The commanded heading angle θ_c is computed using:

Table 3.2 New York to Chicago Waypoints

Geodetic Latitude (deg N)	Longitude (deg E)	Horizontal Speed (m/sec)	Altitude (m)	Time Reached (sec)
40.400	-74.000	0.	0.	0.00
40.415	-73.992	75.	0.	50.00
40.534	-73.933	160.	600.	155.00
40.534	-73.716	180.	1800.	270.00
40.420	-87.467	240.	11300.	5228.75
41.350	-87.467	180.	4900.	5832.50
41.370	-87.650	165.	3000.	5948.75
41.259	-87.767	75.	2100.	6123.75
41.250	-87.609	75.	900.	6323.75
41.387	-87.600	65.	0.	6567.50
41.420	-87.600	25.	0.	6687.50

Table 3.3 Aircraft Trajectory Simulation Parameters

Velocity rate gain	.2	sec^{-1}
Velocity rate limit	1.5	m/sec^2
Turn rate gain	.2	sec^{-1}
Lateral acceleration limit	5.67	m/sec^2
Altitude rate gain	.025	sec^{-2}
Altitude rate limit	12.	m/sec
Altitude time constant	3.	sec

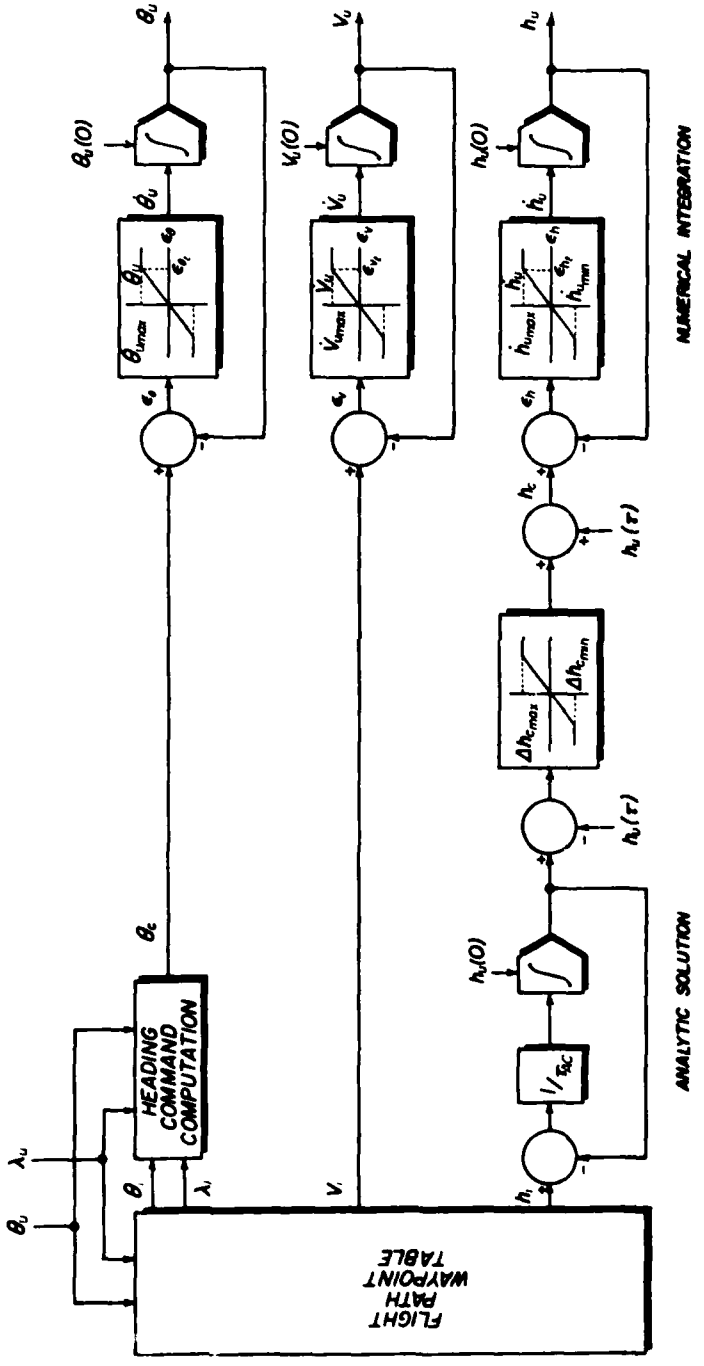

Figure 3.2 Aircraft Response Model

$$\sin \theta_c = \frac{\cos \theta_i \sin(\lambda_i - \lambda)}{\sin \alpha} \tag{3.2}$$

Equations 3.1 and 3.2 are solutions for great circle paths on a spherical earth [52:45-46].

The numerical integrator is a fixed-step fifth-order Runge-Kutta method. Commanded heading angle, speed, and altitude are not allowed to change at the intermediate derivative evaluations. Rate limits, however, are enforced at all derivative evaluations. The integration step size is equal to the interval between measurements of 1.25 sec.

The rate of change of horizontal speed and the vertical speed have limits fixed by the programmer. Maximum turn rate is a function of horizontal speed and a programmer-supplied maximum lateral acceleration a_{lat}.

$$\left| \dot{\theta}_{max} \right| = \left| \frac{a_{lat}}{V} \right| \tag{3.3}$$

The first-order loop that forms the input to the numerical altitude integrator is solved analytically at the start of each time step. To prevent the appearance of large vertical accelerations caused by large changes in vertical velocity, the input to the numerical altitude integrator is limited to a range about the user's altitude at the beginning of each time step.

A fixed-step integrator is used because high accuracy is not required and the discontinuities in the acceleration limits cause a

variable-step method to take excessive time. In numerical tests, the variable-step integration required many iterations to converge to the time of the acceleration discontinuity. From that point, the variable-step integration quickly completed the integration step. The results of the fixed-step integration differed from the variable-step integration on the order of a few centimeters if a limit occurred during the integration step. If a limit did not occur, the fixed-step integration and the variable-step integration provided nearly identical results.

The numerical integrator also solves the differential equations for user geodetic latitude and longitude.

$$\dot{\phi} = \frac{V}{\nu + h} \cos \theta \tag{3.4}$$

$$\dot{\lambda} = \frac{V}{(\nu + h) \cos \phi} \sin \theta \tag{3.5}$$

$$\nu = \frac{a_e}{(1 - e^2 \sin^2 \phi)^{1/2}} \tag{3.6}$$

where: a_e is mean equatorial radius of the Earth, and

e is eccentricity of the reference ellipsoid.

3.3.3 Gust model. The results of the integration were unrealistically smooth. To "bounce" the airplane, a gust model was added to the simulation. For one dimension, the gust model is represented by the following differential equations:

$$\Delta\dot{x} = \Delta v, \qquad \Delta x(t_o) = 0$$

$$\Delta\dot{v} = \Delta a, \qquad \Delta v(t_o) = 0$$

$$\Delta\dot{a} = -\beta_a \Delta a + w_a, \qquad \Delta a(t_o) = 0$$

$$\dot{\beta}_a = w_\beta, \qquad \beta(t_o) = 0 \tag{3.7}$$

where: w_a and w_β are random processes.

The *a priori* statistics for w_a and w_β are given by

$$E[w_a] = 0, \quad E[w_a(t)w_a(\tau)] = q_a\delta(t-\tau) \tag{3.8}$$

$$E[w_\beta] = 0, \quad E[w_\beta(t)w_\beta(\tau)] = q_\beta\delta(t-\tau) \tag{3.9}$$

where: $\delta(t)$ is the Dirac delta function.

Assuming that w_a and β_a are constant over the integration step, the position and velocity are determined by integrating Eqs. 3.7. The results of the integration from T to $T+\Delta T$ are as follows:

$$\Delta x(T+\Delta T) = \frac{1}{\beta_a^3}\left[\beta_a\Delta T^2 - \beta_a\Delta T + 1 - \exp(-\beta_a\Delta T)\right]w_a(T) \tag{3.10}$$

$$\Delta v(T+\Delta T) = \frac{1}{\beta_a^2}\left[\exp(-\beta_a\Delta T) + \beta_a\Delta T - 1\right]w_a(T) \tag{3.11}$$

The user trajectory simulation incorporates three sets of gust equations for each of the three user coordinates. As implemented, the forcing terms w_a are obtained from a Gaussian random number generator.

Position and velocity perturbations are calculated using Eqs. 3.10 and 3.11. The perturbations are added to the results of the numerical integrator at the end of each integration step. The horizontal position perturbations are added to the latitude and longitude as follows:

$$\phi(T+\Delta T) = \phi'(T+\Delta T) + \frac{\Delta x_N(T+\Delta T)}{\partial x_N/\partial \phi} \tag{3.12}$$

$$\lambda(T+\Delta T) = \lambda'(T+\Delta T) + \frac{x_E(T+\Delta T)}{\partial x_E/\partial \lambda} \tag{3.13}$$

where: The primes indicate the no-gust integrator results; and the partial derivatives are given in Appendix A.

The vertical position gust term and the three gust velocities are added directly to the corresponding user states.

Inverse correlation time is modified at each time step according to the relations:

$$\beta_a(T+\Delta T) = \beta_a(T) + \sigma_\beta \, w_\beta(T) \tag{3.14}$$

$$\beta_{a_{min}} \leq \beta_a \leq \beta_{a_{max}} \tag{3.15}$$

where: σ_β is the standard deviation of the inverse correlation time;

$\beta_{a_{min}}$ and $\beta_{a_{max}}$ are limits on β_a, and

w_β is a random number, N(0,1).

For the adopted simulation, the gust model parameters were identical for all aircraft directions. The initial inverse correlation time was 1 sec^{-1} and the standard deviation σ_β was 0.001 sec^{-2}. Inverse correlation time was limited between 0.25 sec^{-1} and 10. sec^{-1}. The standard deviation of the forcing terms w_a was 0.01 m/sec^3. The forcing functions are obtained from a Gaussian random number generator. (See Appendix B.)

The profile of the simulated trajectory is shown in Figures 3.3 through 3.6.

3.4 Clock Simulation

The basic signal transmitted to the user will be the satellite's indicated time of transmission. If the satellite were manned, the astronaut would say, "At the tone, the time will be 144,000 Z - - - beep." The user would then determine the time he received the tone and would process the difference between the user's time of reception and the time of the tone as given by the "astronaut." As previously discussed (Par. 2.5.2.3), the "astronaut" will also provide the epoch for the Z-count and the clock correction data. The following describes how the uncorrected "tone" is simulated and how the clock correction parameters are determined for the simulation.

Three independent clock error sources were simulated: a noise free error with a polynomial form ε_1; an error caused by exponentially correlated frequency noise ε_2; and a random walk bias error ε_3. The noise free error term is simulated using the polynomial

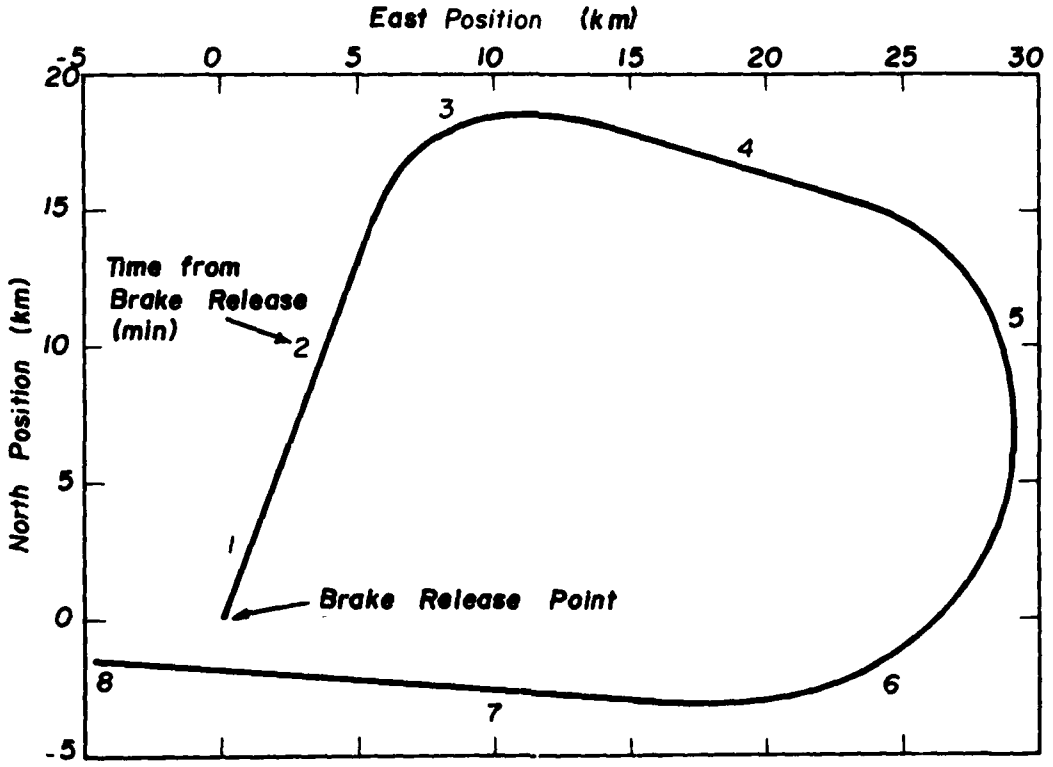

Figure 3.3 Departure Ground Track

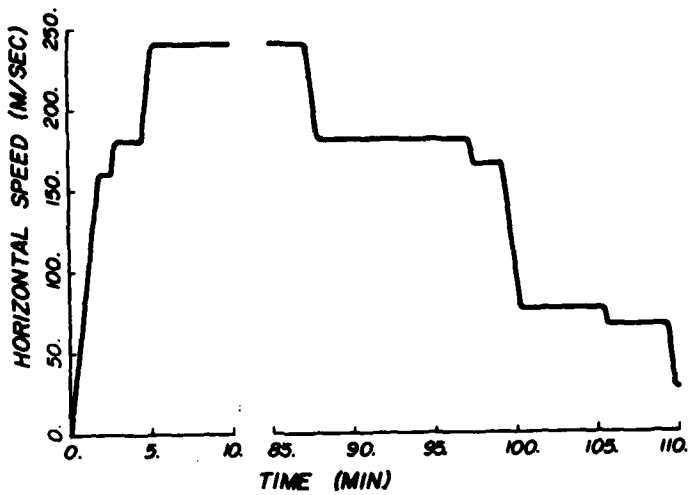

Figure 3.4 Horizontal Speed Profile

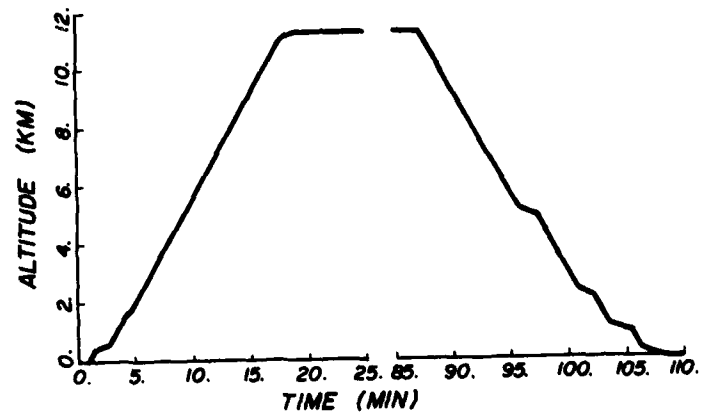

Figure 3.5 Altitude Profile

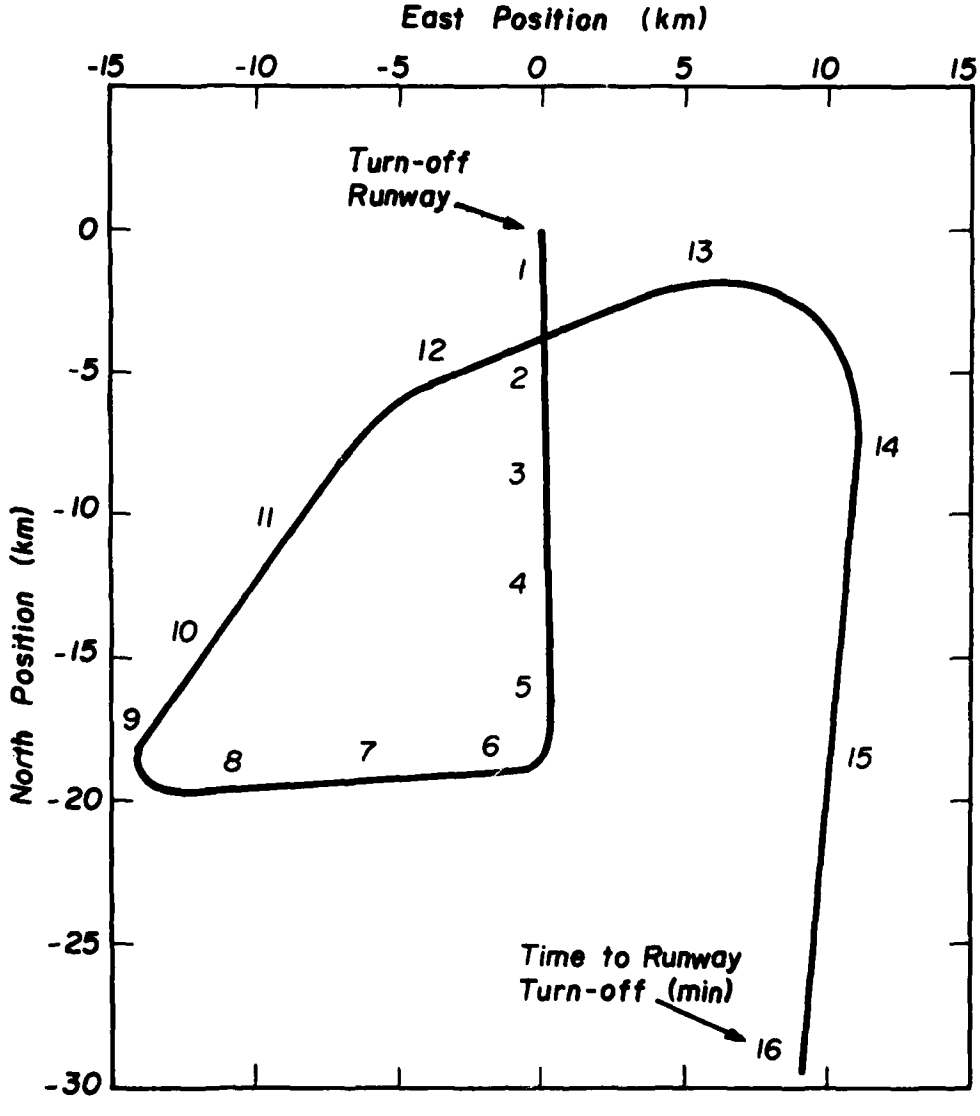

Figure 3.6 Approach Ground Track

$$\varepsilon_1(T) = a_2 + a_3 (T - a_1) + \frac{1}{2} a_4 (T - a_1)^2 \qquad (3.16)$$

where: T is system time; and

a_i, i = 1,2,3,4 are similar to t_{oc}, Δt_o, $\Delta f/f$, and D/2 in in the satellite data stream. (See para. 2.5.2.3.)

The time derivative of Eq. 3.16 gives the clock drift required for the pseudo-range-rate measurements.

$$\dot{\varepsilon}_1(T) = a_3 + a_4 (T - a_1) \qquad (3.17)$$

In the simulation, the clock frequency noise is assumed to be exponentially correlated in time with zero mean and standard deviation σ_f. The following discrete time equation is used to generate this term:

$$\dot{\varepsilon}_2(T+\Delta T) = \dot{\varepsilon}_2(T) \exp(-\Delta T/T_c) + \sigma_f[1 - \exp(-2\Delta T/T_c)]^{1/2} w_2(T) \qquad (3.18)$$

where: T is a discrete step size;

T_c is the correlation time; and

w_2 is a normally distributed random number with zero mean and unit variance, N(0,1).

The corresponding phase error is generated by "integrating" Eq. 3.18.

$$\varepsilon_2(T+\Delta T) = \varepsilon_2(T) + \frac{1}{2} [\dot{\varepsilon}_2(T+\Delta T) + \dot{\varepsilon}_2(T)]\Delta T \qquad (3.19)$$

An additional phase noise is generated by a simulated random walk.

$$\varepsilon_3(T+\Delta T) = \varepsilon_3(T) + \sigma_p\, w_3(T) \tag{3.20}$$

where: σ_p is the standard deviation of the random walk; and

w_3 is a random number, N(0,1).

The clock error propagation for the three error sources is summarized as follows:

$$\begin{aligned}\dot{\theta}(T) - 1 = \dot{\varepsilon}(T) &= a_3 + a_4\,(T-a_1) \\ &+ \dot{\varepsilon}_2(T-\Delta T)\,\exp(-\Delta T/T_c) \\ &+ \sigma_f[1 - \exp(-2\Delta T/T_c)]^{1/2}\, w_2(T-\Delta T)\end{aligned} \tag{3.21}$$

$$\begin{aligned}\theta(T) - T = \varepsilon(T) &= a_2 + a_3\,(T-a_1) + \tfrac{1}{2}\, a_4\,(T-a_1)^2 \\ &+ \varepsilon_2(T-\Delta T) + \tfrac{1}{2}\,[\dot{\varepsilon}_2(T) + \dot{\varepsilon}_2(T-\Delta T)]\,\Delta T \\ &+ \varepsilon_3(T-\Delta T) + \sigma_p w_3(T-\Delta T)\end{aligned} \tag{3.22}$$

Figure 3.7 shows the results of the simulation of the clock errors using the parameters of Table 3.4. Only those satellites visible to the user in the basic simulation are shown.

The clock correction polynomial for the user data base is obtained using least squares fits to the curves of Figure 3.7. One linear fit for each satellite is used for the 1.86 hour flight time. The parameters of the least-squares fits are given in Table 3.5. Note that the RMS errors after correction were on the order of the errors expected for the GPS satellites. (See Par. 2.5.2.3.)

Table 3.4 Clock Simulation Parameters

Satellite	Epoch (sec)	Initial Bias (nsec)	Initial Drift (nsec/sec)	Drift Rate (1/day)	Exponentially Correlated Frequency Noise Std Deviation (nsec/sec)	Exponentially Correlated Frequency Noise Correlation Time (sec)	Random Walk Bias Noise Std Deviation (nsec)
1	0.	0.	0.	0.	0.015	3600.	0.01
2	0.	0.	0.	0.	0.015	3600.	0.01
3	0.	0.	0.	0.	0.015	3600.	0.01
4	0.	0.	0.	0.	0.015	3600.	0.01
5	0.	0.	0.	0.	0.015	3600.	0.01
6	0.	0.	0.	0.	0.015	3600.	0.01
7	0.	0.	0.	0.	0.015	3600.	0.01
8	0.	0.	0.	0.	0.015	3600.	0.01
9	0.	0.	0.	0.	0.015	3600.	0.01
User	0.	100.	2.	0.	1.000	1800.	0.10

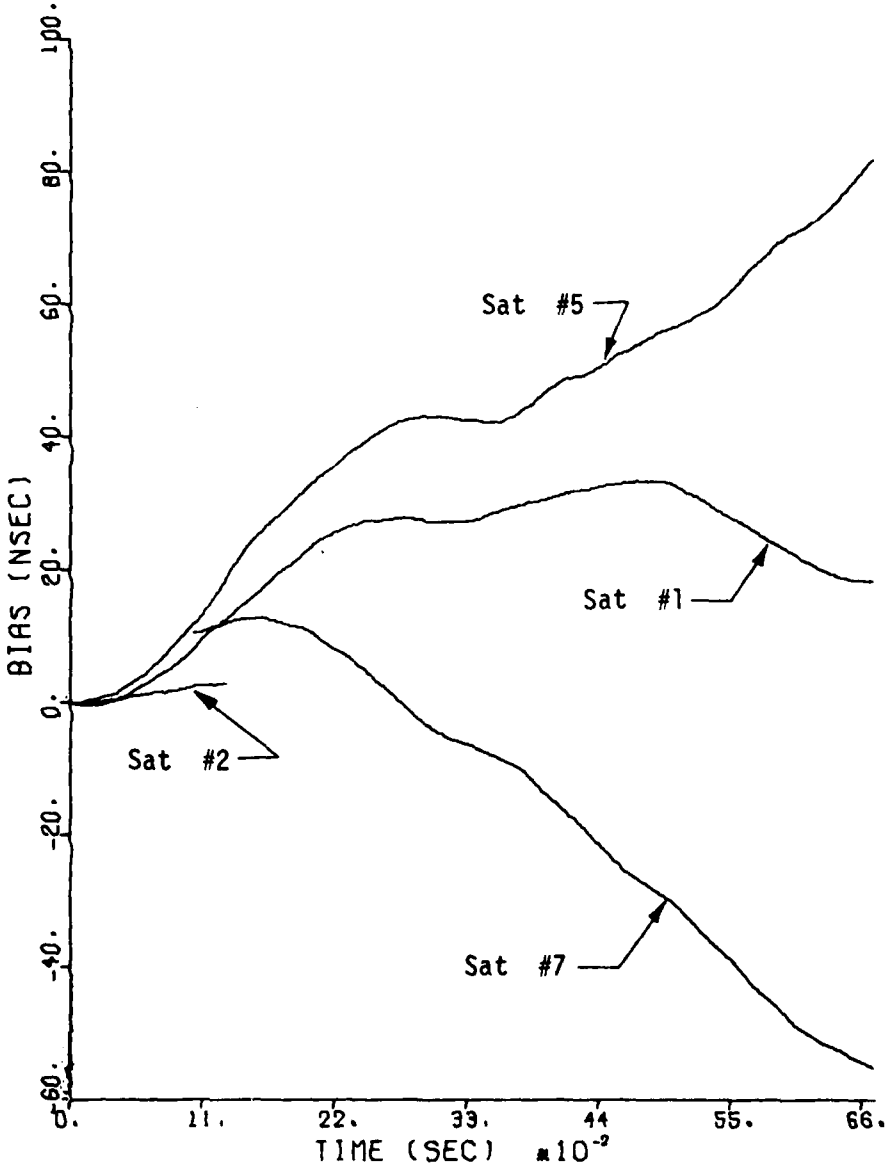

Figure 3.7 Satellite Clock Bias

Table 3.5 Results of Linear Fits to Satellite Clock Biases

Satellite	1	2	5	7
Number of Samples	1327	248	1327	1124
Minimum bias (nsec)	-.06	-.36	-.13	-55.15
Maximum bias (nsec)	33.61	2.93	82.33	12.95
RSS error after least-squares fit (nsec)	7.62	.18	4.38	2.99

There are various approaches that can be used for the clock simulation including a method suggested by Meditch that more accurately represents an Allan variance curve [53]. The approach used in this study was chosen because it is quickly implemented, the error behavior is easily understood, and, with a proper choice of parameters, it will result in a root-sum-square (RSS) error close to that expected for the GPS satellite clocks. This latter requirement is critical. Early algorithm tests yielded results which were interpreted first as classical filter divergence. On closer inspection, it was determined that the measurement residuals were low and that the gains had not decreased. This suggested that filter divergence was not the problem. The difficulty was actually caused by large satellite clock errors. During the first half of the flight, two satellites with large clock errors of identical sign were oriented so that the errors counteracted each other. The estimate of the user position was determined to minimize the squares of the residuals from the satellite range measurements. During flight,

one satellite reached its zenith and passed into the same half-plane as the other satellite. At that point, the clock errors reinforced each other and the user estimated position moved to decrease the measurement residuals. The result was an increase in actual user position error and a decrease in the observation residuals. Unpredictable clock errors will vary in sign and no guarantee can be made that the positions of the satellites will be such that the clock errors counteract, rather than reinforce, each other. Accordingly, the satellite clock errors are a critical factor for navigation accuracy.

3.5 Atmospheric Delay Simulation

3.5.1 Ionospheric delay simulation. The simulation program assumes that the ionosphere is a constant electron density layer. Three parameters describe this ionosphere model: altitude above the reference ellipsoid for the bottom of the ionosphere h_{min}; altitude above the reference ellipsoid for the top of the ionosphere h_{max}; and the vertical group delay δ_{vg}. The ionospheric delay resulting from the model is a function of the obliquity factor which is the ratio of the length of the path through the ionosphere at an elevation angle el, to the length of the path at 90 deg elevation. The vertical path length is $h_{max} - h_{min}$. At L-band frequencies, ray-bending causes an elevation error less than 0.003 deg for a satellite at ten degrees elevation [39]. Therefore, ray bending is neglected in the simulation.

Ionospheric delay is calculated as follows:

$$\delta_{ion} = \frac{\ell}{\ell_{vert}} \delta_{vg} \tag{3.23}$$

$$\ell_{vert} = h_{max} - h_{min} \tag{3.24}$$

$$\ell = \frac{R_{min} R_{max} \sin[\sin^{-1}(R \cos el / R_{min}) - \sin^{-1}(R \cos el / R_{max})]}{R \cos el}, \quad 0° \leq el < 90° \tag{3.25}$$

where: R is the geocentric radius of the user;

$R_{min} = (R - h) + h_{min}$;

$R_{max} = (R - h) + h_{max}$; and

h is the user's altitude above the reference ellipsoid.

Equation 3.25 is an approximation to the path length based on an assumption that the ionospheric layer is spherical in the vicinity of the user.

Wand [39] states that typical values of the height parameters in the model he evaluated can be used somewhat arbitrarily since the plasma frequency is more important in determining the delay. Accordingly, the height parameters h_{min} and h_{max} in Equation 3.25 are kept constant for the simulation. The vertical group delay, which can be considered similar to Wand's plasma frequency term, is simulated as an exponentially correlated random variable as follows:

$$\delta_{vg}(T+\Delta T) = \overline{\delta_{vg}} + \epsilon_{vg}(T+\Delta T) \tag{3.27}$$

$$\varepsilon_{vg}(T+\Delta T) = \varepsilon_{vg}(T)\exp(-\beta_{vg}\Delta T) + \sigma_{vg}[1 - \exp(-2\beta_{vg}\Delta T)]^{1/2} w_{vg}(T) \quad (3.28)$$

$$\delta_{vg_{min}} \leq \delta_{vg} \leq \delta_{vg_{max}} \quad (3.29)$$

where: $\overline{\delta_{vg}}$ is the mean vertical group delay;

β_{vg} is the inverse correlation time for the vertical group delay;

σ_{vg} is the standard deviation of the vertical group delay;

w_{vg} is a random number, N(0,1); and

$\delta_{vg_{min}}$ and $\delta_{vg_{max}}$ are limits on the vertical group delay.

Small scale irregularities in the ionosphere cause fluctuations in propagation time called scintillations. Scintillations are larger in the equatorial and polar regions than in the middle latitudes and the scintillations are larger for low elevation angles. Ionospheric scintillations have been examined by Wand [39] and in [54:133-144].

A small amount of scintillation is included in the simulation as an uncorrelated, Gaussian random variable.

$$S_{ion}(T+\Delta T) = \frac{\sigma_{S_{ion}} w_{S_{ion}}(T)}{\sin\left[(el^2 + .315^2)^{1/2}\right]} \quad (3.30)$$

where: $\sigma_{S_{ion}}$ is the standard deviation of the scintillation; and

$w_{S_{ion}}$ is a random number N(0,1).

The ionospheric delay parameters used in the basic simulation are given in Table 3.6 and the realization for the vertical group delay of Eq. 3.27 is shown in Figure 3.8.

Table 3.6 Ionospheric Delay Simulation Parameters

Layer Limits Base (km)	Top (km)	Mean Delay (nsec)	Std. Deviation (nsec)	Vertical Group Delay Correlation Time (sec)	Min/Max (nsec)	Initial Delay (nsec)
50.0	500.0	40.0	5.0	1000.	0/100.	40.

Scintillation Model: $\sigma_{S_{ion}}$ = 1.0 nsec

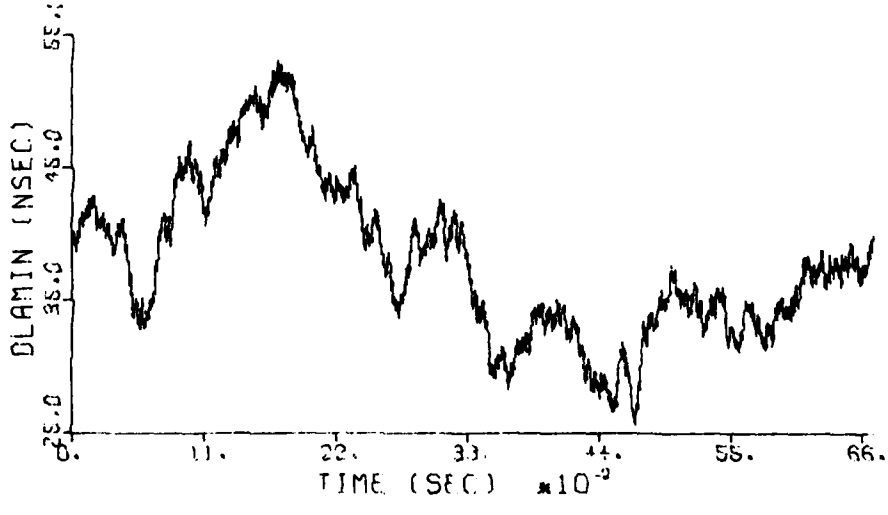

Figure 3.8 Ionospheric Vertical Group Delay

3.5.2 Tropospheric delay simulation. The tropospheric delay model used in the simulation is the JPL model [44:22-23].

$$\delta_{trop} = \frac{6.3237}{(\sin el + .06483)^{1.4}} \frac{N_{SL}\exp(-h/H_{trop})}{338.0} \quad (3.31)$$

where: δ_{trop} is the excess time delay in nsec;

H_{trop} is the scale height; and

N_{SL} is sea level refractivity.

Sea level refractivity is simulated as an exponentially correlated random variable as follows:

$$N_{SL}(T+\Delta T) = \overline{N_{SL}} + \varepsilon_N(T+\Delta T) \quad (3.32)$$

$$\varepsilon_N(T+\Delta T) = \varepsilon_N(T)\exp(-\beta_N\Delta t) + \sigma_N[1 - \exp(-2\beta_N\Delta T)]^{1/2} w_N(T) \quad (3.33)$$

$$N_{SL_{min}} \leq N_{SL} \leq N_{SL_{max}} \quad (3.34)$$

where: $\overline{N_{SL}}$ is the mean sea level refractivity;

β_N is the inverse correlation time for the sea-level refractivity;

σ_N is the standard deviation of sea level refractivity;

w_N is a random number, N(0,1); and

$N_{SL_{min}}$ and $N_{SL_{max}}$ are limits on the refractivity.

Tropospheric scintillation is simulated as follows:

$$S_{trop}(T+\Delta T) = \frac{\sigma_{S_{trop}} w_{S_{trop}}(T)}{\sin el} \qquad (3.35)$$

where: $\sigma_{S_{trop}}$ is the standard deviation of tropospheric scintillation; and

$w_{S_{trop}}$ is a random number, N(0,1).

In this investigation, the tropospheric simulation used the parameters given in Table 3.7. The realization of the sea level refractivity is shown in Figure 3.9.

Table 3.7. Tropospheric Delay Simulation Parameters

Sea Level Refractivity Model

Mean Refractivity	Std. Deviation	Correlation Time (sec)	Min/Max	Scale Height (km)
325.	30.	1000.	262./338.	7.62

Scintillation Model: $\sigma_{S_{trop}}$ = 0.9 nsec

3.6 Measurement Generation

3.6.1 Range-time algorithm. The user trajectory simulation provides a sequence of position and velocity vectors which represent

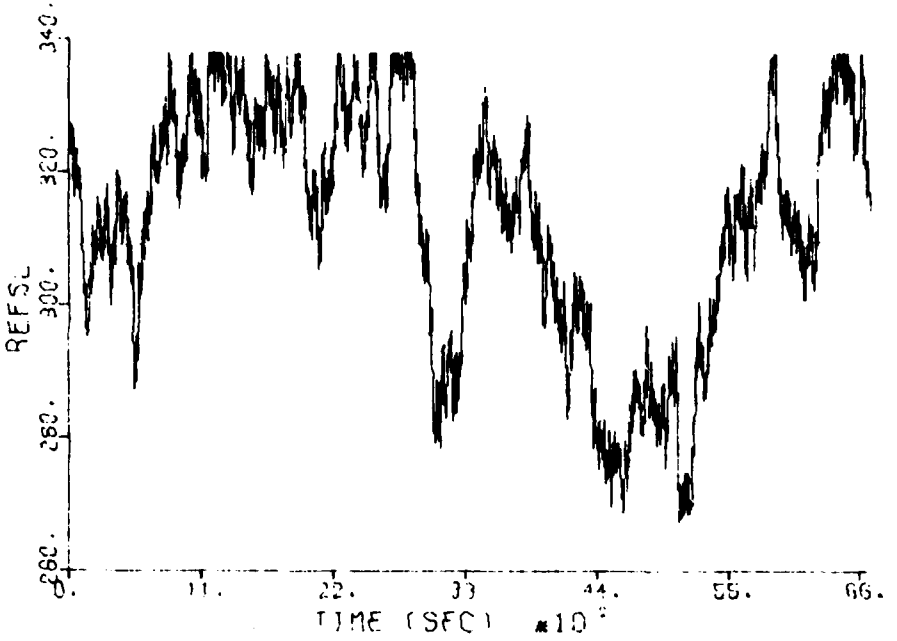

Figure 3.9 Sea-Level Refractivity

aircraft motion. Each user state vector applies at a time T the true GPS time when a measurement is taken. To calculate the measurement, the simulation must determine the true time the satellite sent the signal.

The range-time equation is defined as follows:

$$\frac{1}{c}\left|\underline{R}_S(T_S) - \underline{R}(T)\right| + \delta_{atm}(T, \underline{R}(T), \underline{R}_S(T_S)) = T - T_S \qquad (3.36)$$

where: T_S is the true GPS time when the satellite sent the signal which is received by the user at T;

$\underline{R}_s(T_s)$ is the position vector of the satellite at the time of signal transmission, T_s;

$\underline{R}(T)$ is the position vector of the user at the signal time-of-arrival, T; and

δ_{atm} is the total atmospheric delay.

Equation 3.36 is solved recursively for T_s using a false-position method [55:45-47]. The position of the satellite is propagated from the ephemeris data. User position remains constant based on the user trajectory simulation. Vertical group delay and sea level refractivity remain constant during the range-time recursion but the total atmospheric delay will change because of changes in elevation angle during the recursion. In the simulation, the range-time equation converged within 0.033 nsec (1 cm).

3.6.2 Pseudo-range measurement generation. After solution of the range-time algorithm, the measurements are generated. A pseudo-range measurement consists of the time of signal transmission, as indicated by the satellite, and the user's indicated time of reception.

The behavior of the user's clock is simulated identically to the satellite clock simulation. (See Par. 3.4.) Table 3.4 includes the user clock simulation parameters and Figure 3.10 shows the realization of the user clock errors. The clock errors are added to the true times to give the indicated received time $\theta(T)$ and the indicated transmission time $\theta_s(T_s)$. To attempt to account for miscellaneous receiver errors, quantization errors, and multipath effects, an additional

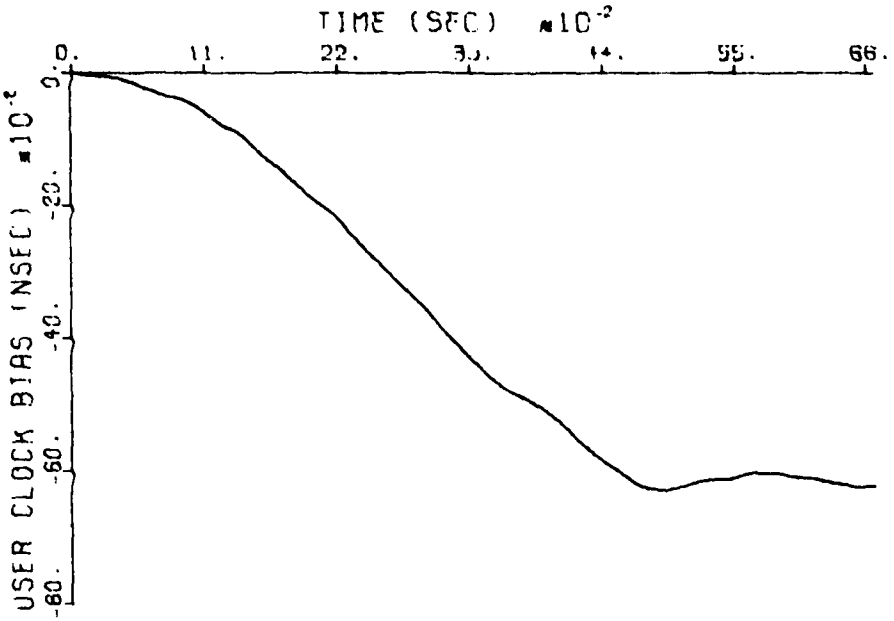

Figure 3.10a User Clock Bias

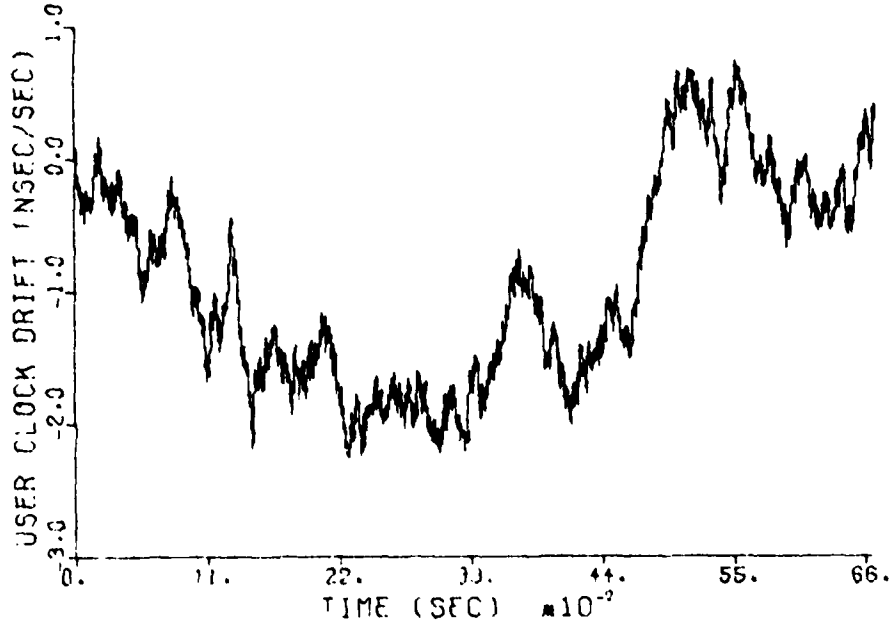

Figure 3.10b User Clock Drift

Gaussian noise is added to the indicated satellite time. For programmer convenience, this additional noise term is added in the algorithm testing program. It can be assumed that this noise term is imbedded in the satellite phase error term, as simulated using Eq. 3.21.

3.6.3 Pseudo-range-rate measurement generation. A pseudo-range-rate measurement that is obtained from the carrier tracking loop is relatively free of atmospheric effects. In the simulation procedure, the pseudo-range-rate measurements are generated by combining range-rate, relative drift between the user clock and the satellite clock, and a Gaussian noise.

Range-rate is given by:

$$\dot{\rho} = \underline{l}_{ui} \cdot (\underline{V}_s^{(I)} - \underline{v}^{(I)}) \qquad (3.37)$$

where: $\dot{\rho}$ is the range-rate;

$\underline{V}_s^{(I)}$ is the inertial velocity vector of the satellite;

$\underline{v}^{(I)}$ is the inertial velocity vector of the user; and

$\cdot$ indicates the vector dot product.

The computer programs used in this study normally maintain the components of the inertial satellite velocity vector rotated into the Geocentric Earth-Fixed (GEF) frame and the components of the relative user velocity vector rotated into the GEF frame. If the unit vectors $\underline{i}$, $\underline{j}$, and $\underline{k}$ represent the basis vectors of the GEF coordinate system, then the following position and velocity vectors are defined:

1. Position vector of the satellite:

$$\underline{R} = X\underline{i} + Y\underline{j} + Z\underline{k}$$

2. Inertial velocity vector of the satellite rotated into the GEF frame:

$$\underline{V}_s^{(I)} = V_X\underline{i} + V_Y\underline{j} + V_Z\underline{k}$$

3. Position vector of the user:

$$\underline{r} = x\underline{i} + y\underline{j} + z\underline{k}$$

4. Relative velocity vector of the user rotated into the GEF frame:

$$\underline{v}^{(rel)} = v_x\underline{i} + v_y\underline{j} + v_z\underline{k}$$

Using these definitions, the range-rate can be calculated as

$$\dot{\rho} = \frac{[(X-x)(V_X-v_x+\omega_e y) + (Y-y)(V_Y-v_y-\omega_e x) + (Z-z)(V_Z-v_z)]}{[(X-x)^2 + (Y-y)^2 + (Z-z)^2]^{1/2}} \tag{3.38}$$

where: ω_e is the Earth's angular velocity.

The pseudo-range-rate measurement is formed using

$$Y_{\dot{\rho}}(T) = \dot{\rho}(T) + c[\dot{\theta}(T) - \dot{\theta}_s(T_s)] + \sigma_{\dot{\rho}}\, w_{\dot{\rho}}(T)$$

where: $Y_{\dot{\rho}}$ is the pseudo-range-rate;

$\dot{\theta}$ and $\dot{\theta}_s$ are the user and the satellite clock drifts;

$\sigma_{\dot{\rho}}$ is the standard deviation of pseudo-range-rate; and

$w_{\dot{\rho}}$ is a random number, N(0,1).

3.6.4 Altimeter measurement generation. In the simulation, the altimeter measurement is formed by adding to the true user altitude above the reference ellipsoid, a bias term (which the user may attempt to estimate), and an uncorrelated zero-mean noise term. The true altitude is computed by the user trajectory simulation. The simulated bias is selected to represent two error sources: an initial sea level bias which propagates to the user's altitude assuming an exponential pressure profile, and a distance-correlated random variable which represents aircraft motion through the air mass and motion of the air mass itself.

The initial sea level bias results in a bias error at altitude as follows:

$$\delta y_{h_1}(T) = \delta y_{h_{SL}} \exp(h(T)/H_{alt}) \tag{3.39}$$

where: H_{alt} is the altimeter scale height; and

$\delta y_{h_{SL}}$ is the sea level bias.

The distance-correlated bias is simulated using

$$\delta y_{h_2}(T+\Delta T) = \delta y_{h_2}(T) \exp(-V\Delta T/D_{alt}) + \sigma_{h_2} [1 - \exp(-2V\Delta T/D_{alt})]^{1/2} w_h(T) \tag{3.40}$$

where: V is the user's horizontal speed; and

D_{alt} is the correlation distance.

The uncorrelated noise term is simulated using

$$\delta y_{h_3}(T+\Delta T) = \sigma_{h_3} w_{h_3}(T) \tag{3.41}$$

where: σ_{h_3} is the standard deviation of the uncorrelated noise.

The mean deviations σ_{h_2} and σ_{h_3} are simulated as functions of altitude similar to Lear's recommendations [56].

$$\sigma^2_{h_2} = \sigma^2_{h_{2_{SL}}} + (\alpha_{h_2} h)^2 \tag{3.42}$$

$$\sigma^2_{h_3} = \sigma^2_{h_{3_{SL}}} + [\alpha_{h_3} \exp(h/H_{h_3})]^2 \tag{3.43}$$

where: $\sigma_{h_{2_{SL}}}$ and $\sigma_{h_{3_{SL}}}$ are the standard deviations at sea level; and

α_{h_2}, α_{h_3}, and H_{h_3} are arbitrary parameters.

The altimeter measurement is generated as follows:

$$Y_h(T) = h(T) + \delta y_{h_1}(T) + \delta y_{h_2}(T) + \delta y_{h_3}(T) \tag{3.44}$$

Table 3.8 specifies the parameters used in the basic simulation. Figure 3.11 shows the correlated bias term, $\delta y_{h_1} + \delta y_{h_2}$.

Table 3.8 Altimeter Bias Simulation Parameters

Exponentially Correlated Std. Deviation	Correlation Distance	Uncorrelated Std. Deviation	Sea Level Bias
$\sigma^2_{h_2}(h)$	100.00 km	$\sigma^2_{h_3}(h)$	10.0 m

$$\sigma^2_{h_2}(h) = 2.7^2 + (.0035h)^2 \text{ m}^2$$

$$\sigma^2_{h_3}(h) = [.70 \exp(h/7110.)]^2 \text{ m}^2$$

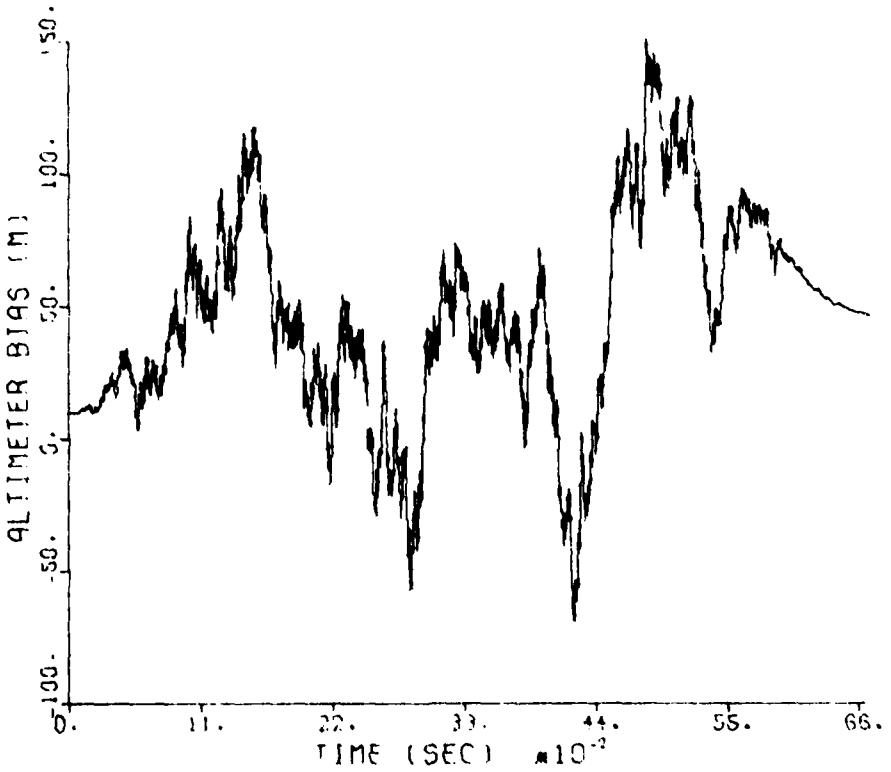

Figure 3.11 Correlated Altimeter Bias

3.7 User-Satellite Geometry of the Simulation

The navigation accuracy attainable in a satellite ranging system is strongly affected by the user-satellite geometry. Bogen [18] has analyzed this geometric effect for the GPS using a performance index called geometric dilution of precision (GDOP). It will be shown in Chapter 4 that the linear minimum variance unbiased estimate of a state is given by

$$\hat{\underline{x}} = (H^T R^{-1} H)^{-1} H^T R^{-1} \underline{y} \tag{3.45}$$

where: R is the covariance matrix of the measurements;

H is the observation-state relationship

$$\underline{y} = H\underline{x} + \underline{\varepsilon} \tag{3.46}$$

$\underline{y}$ is the observation vector.

The covariance of the a posteriori estimate is given by

$$P = (H^T R^{-1} H)^{-1} \tag{3.47}$$

A GDOP analysis was performed using the user-satellite geometry of the adopted simulation. The analysis was accomplished by setting the R matrix in Eq. 3.47 equal to the identity matrix and by using an H matrix whose rows corresponded to simultaneous pseudo-range measurements from each visible satellite and to an altimeter measurement. Appendix C describes the form of the individual rows of the H matrix. Since a minimum of three satellites is visible in the simulated profile, then up to four state parameters can be considered in the GDOP analysis. If only

three-dimensional position of the user is to be estimated, then $(H^T R^{-1} H)^{-1}$ is a 3x3 matrix whose diagonal elements represent the variances of the position component estimates that result from processing simultaneous pseudo-range measurements and an altimeter measurement.

The user-satellite geometry of the adopted simulation is shown in Figure 3.12 and the GDOP analysis yields the position component standard deviations as shown in Figure 3.13. If the user clock bias is added to the state vector, then Figure 3.14 represents the results of the GDOP analysis. Figure 3.14 is limited to values of standard deviation of twelve or less. A continuous solution of the four-state estimate with the three satellites and altimeter would have a singularity in the vicinity of 2770 sec.

Figures 3.13 and 3.14 represent the standard deviations of the estimated state parameters that result if simultaneous pseudo-range observations of all visible satellites and an altimeter measurement are used in a least-squares solution with no a priori information from any previous estimates and with identical weighting of all measurements. It was assumed that all measurements have uncorrelated noise with standard deviation one meter for the figures shown.

The benefit of the GDOP analysis is that it depicts the information content on the measurements at any given time. The analysis does not account for dynamics or larger state vectors that may be included in actual navigation algorithm implementation. Nor are the results of the analysis quantitatively exact for algorithms that differ from the assumptions of the GDOP analysis. In navigation algorithm

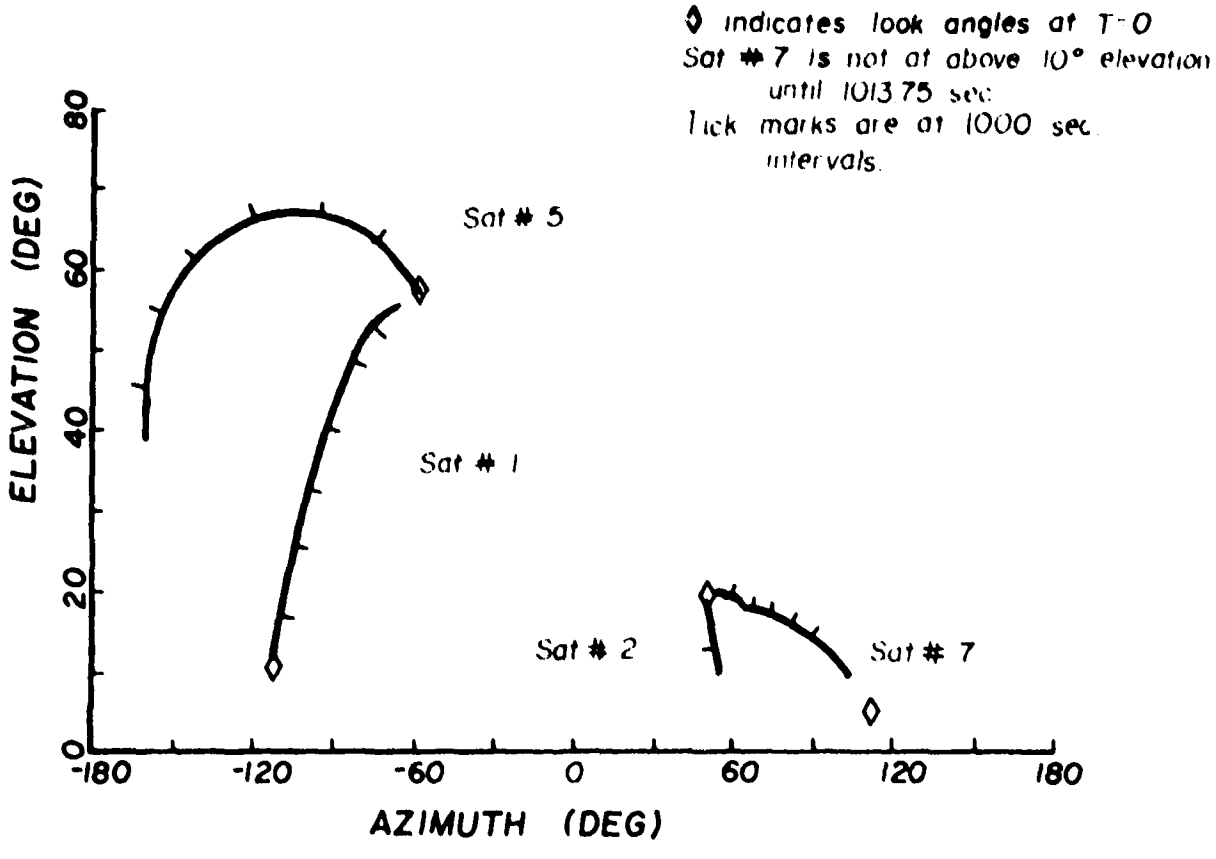

Figure 3.12 Satellite Visibility

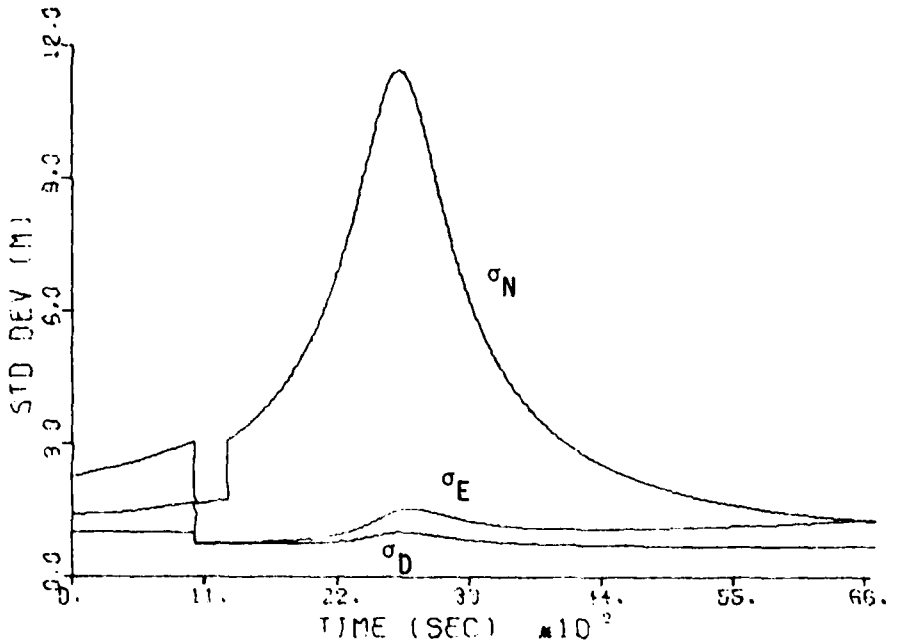

Figure 3.13 Geometric Dilution of Precision
(North, East, and Down state)

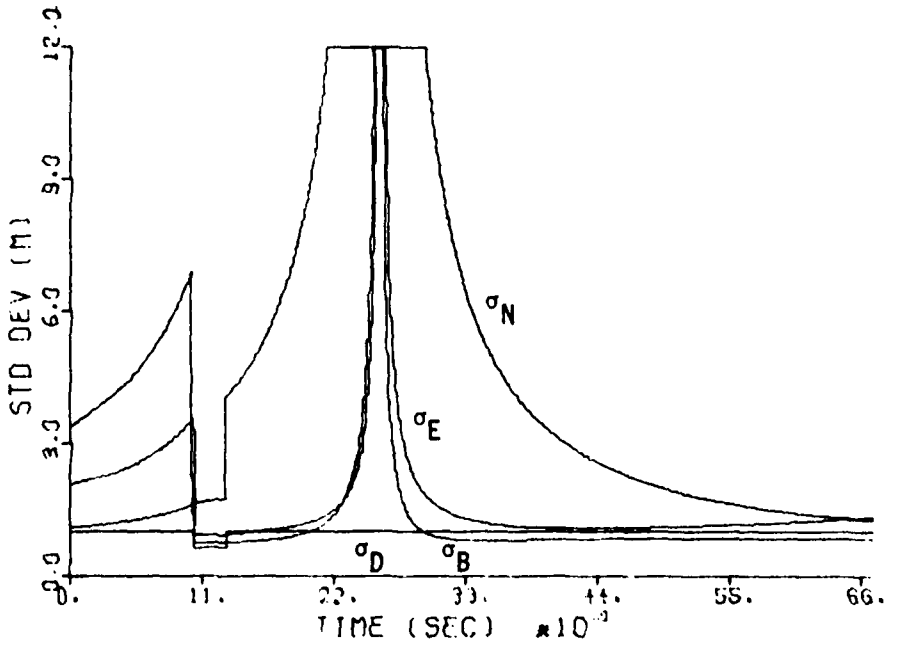

Figure 3.14 Geometric Dilution of Precision
(North, East, Down, and Clock Bias state)

tests performed for this dissertation, the behavior of the standard deviations closely paralleled the character of the GDOP curves. The errors in the estimated state vector components also had a remarkable similarity to the GDOP analysis results.

CHAPTER 4

LINEAR ESTIMATION THEORY

AND

THE KALMAN-BUCY FILTER

4.1 Background of Linear Estimation Theory

4.1.1 Description of the linear system. Linear estimation theory concerns itself with the problem of estimating the values of a random process $\underline{x}(t)$ that is governed by a linear differential equation.

$$\dot{\underline{x}} = A(t)\underline{x} + B(t)\underline{u}(t), \quad \underline{x}(t_o) = \underline{x}_o \tag{4.1}$$

where: $\underline{x}$ is the state vector;

$A(t)$ is the plant matrix;

$B(t)$ is the noise matrix; and

$\underline{u}(t)$ is the process noise vector.

In the following discussion, the state vector will always be assumed to be a random process since dynamical systems, such as aircraft and clocks, can generally be represented using differential equations such as Eq. 4.1.

The plant noise vector $\underline{u}(t)$ is a random process with statistics given by

$$E[\underline{u}(t)] = 0, \quad E[\underline{u}(t)\underline{u}^T(\tau)] = Q(t)\delta(t-\tau) \tag{4.2}$$

where: $\delta(t-\tau)$ is the Dirac delta function;

$Q(t)$ is the spectral level process noise covariance matrix and is non-negative definite.

Observations of the system can be assumed to be available continuously. A linear observation will be described by

$$\underline{y}(t) = H(t)\underline{x}(t) + \underline{\varepsilon}(t) \tag{4.3}$$

where: $H(t)$ is the observation matrix;

$\underline{\varepsilon}(t)$ is the observation noise vector; and

$\underline{y}(t)$ is the observation vector.

The measurement noise vector $\underline{\varepsilon}(t)$ is a random process with statistics given by

$$E[\underline{\varepsilon}(t)] = 0, \quad E[\underline{\varepsilon}(t)\underline{\varepsilon}^T(\tau)] = R(t)\delta(t-\tau) \tag{4.4}$$

where: $R(t)$ is the continuous measurement noise covariance matrix.

When the observations are available at discrete times, they will be described by

$$\underline{y}_j = H(t_j)\underline{x}(t_j) + \underline{\varepsilon}_j \tag{4.5}$$

The statistics of the random sequence $\underline{\varepsilon}_j$ are given by

$$E[\underline{\varepsilon}_j] = 0, \quad E[\underline{\varepsilon}_j\underline{\varepsilon}_k^T] = R_j\delta_{jk} \text{ for all } j \text{ and } k \tag{4.6}$$

where: δ_{jk} is the Kronecker delta; and

R_j is the discrete measurement noise covariance matrix.

In the following discussions, all cross-correlations among the terms used in Eq. 4.1 and Eq. 4.3 or Eq. 4.5 will be assumed equal to zero.

4.1.2 The Wiener-Hopf equation. Until 1949, the major tool in linear estimation theory was Gauss' method of least squares. This method is still in widespread use for many problems but it is not easily adapted for sequential estimation. The method of least squares can also be very inefficient, especially for real-time computer implementation.

The Wiener-Hopf equation [7] specifies the requirement for the *gain of an optimal estimator using continuous measurements*. The linear optimal estimate has the form

$$\hat{x}(t_1|t) = \int_{t_o}^{t} W(t_1,\tau)\underline{y}(\tau)d\tau \qquad (4.7)$$

where: $\hat{x}(t_1|t)$ is the estimate of the state at time t_1 after processing all measurement up to time t; and

$W(t_1,\tau)$ is the filter gain.

The Wiener-Hopf equation is

$$E[\underline{\hat{x}}(t_1)y^T(s)] - \int_{t_o}^{t} W(t_1,\tau)E(\underline{y}(\tau)\underline{y}^T(s)]d\tau = 0 \qquad (4.8)$$

If the matrix $W(t_1,\tau)$ satisfies the Wiener-Hopf equation, then Eq. 4.7 is the optimal estimate. Meditch [57:292-294] shows that this is a necessary and sufficient condition for the estimate to be optimal in a minimum variance sense.

By taking the partial derivative of Eq. 4.7 with respect to t, the filter differential equation can be derived.

$$\dot{\underline{\hat{x}}} = A(t)\underline{\hat{x}} + K(t)\ (\underline{y}(t) - H(t)\underline{\hat{x}}) \tag{4.9}$$

where: $K(t)$ is defined to be $W(t,t)$.

Meditch [57:Chap. 8] shows that the gain term required in Eq. 4.9 can be related to the covariance matrix P as follows:

$$K(t) = P(t|t)H^T(t)R^{-1}(t) \tag{4.10}$$

where: $P(t|t) = E[(x(t)-\hat{x}(t|t))(x(t)-\hat{x}(t|t))^T]$

Equation 4.10 can be used to replace the integral equation for $W(t,t)$ by an integral equation for $P(t|t)$. The practical difficulty of developing a solution to the integral equation remains.

4.1.3 Kalman-Bucy filtering. In 1961, Kalman [8] derived an expression for the optimal estimate when the measurements are available at discrete times. This derivation emphasized the concepts of system state, state transition matrix, and white noise processes. The optimal estimate was derived to be a conditional expectation. Kalman showed that the optimal estimate is the orthogonal projection of the state

onto the space generated by the measurements. Kalman also described the duality between the estimation problem and optimal control theory.

Kalman and Bucy [9] derived the differential equation for the covariance matrix. This can be accomplished by taking the partial derivative of the integral equation for $P(t|t)$ with respect to t. The result is given by

$$\dot{P}(t|t) = A(t)P + PA^T(t) + B(t)Q(t)B^T(t) - PH^T(t)R^{-1}(t)H(t)P \qquad (4.11)$$

For the calculation of the optimal gain, the differential equation of Eq. 4.11 replaces the Wiener-Hopf integral equation. For computer applications, the differential equation is considerably easier to implement.

The algorithm resulting from the works of Kalman and Bucy is frequently referred to as the Kalman-Bucy filter, (or, more simply, the Kalman filter) and the gain is often called the Kalman gain. The equations that constitute the Kalman-Bucy filter can be derived in many ways. This chapter will derive the filter equations by first showing that, under certain fairly general conditions, the conditional mean is the optimal estimate, and then by deriving an explicit expression for the conditional mean assuming Gaussian statistics.

An excellent introduction to Kalman filtering is given by duPlessis [58]. A report by the Mitre Corp. [59] also provides a good intuitive derivation of the Kalman filter equations. Several texts that describe the Kalman filter are available. Jazwinski [60] emphasizes

stochastic calculus in the derivation of the Kalman filter Jazwinski also described many options to the basic algorithm. Meditch [57] derives the Kalman filter and provides good example problems for exercising the filter. Applications are emphasized in a text published by The Analytical Sciences Corporation [61] and in a report edited by Leondes [62].

4.2 Criterion for the Optimal Estimate

4.2.1 The loss function. Consider x the parameter to be estimated, to be a scalar. The estimate of x will be denoted $\hat{x}$. A good estimate is one which minimizes $|x-\hat{x}|$, the absolute error of the estimate. To eliminate the absolute value operation, this can be restated to say that a good estimate is one which minimizes $(x-\hat{x})^2$. The term $(x-\hat{x})^2$ will be called the penalty or loss function.

$$L = (x - \hat{x})^2 \tag{4.12}$$

The loss function of Eq. 4.12 is continuous and differentiable to the same extent that x is continuous and differentiable. Equation 4.12 is a quantitive expression of the failure of $\hat{x}$ to estimate x. The loss function of Eq. 4.12 has the following properties:

1. it is a scalar;
2. if $\hat{x} = x$, the loss is zero;
3. the amount of loss is a monotonically increasing function of the departure of the estimate from the true state; and
4. it is symmetric.

The absolute minimum of the loss function is zero, implying that the estimate should be

$$\hat{x} = x \tag{4.13}$$

If x is random, there is no way to calculate the right hand side of Eq. 4.13. The criterion that the estimate minimize L can be restated to require that the estimate minimize the expected value of L conditioned on the realization of the measurements y.

$$E[L|y] = E[(x - \hat{x})^2|y] \tag{4.14}$$

Under some general restrictions, an expression for $\hat{x}$ which minimizes the expected loss can be derived. The estimate which minimizes Eq. 4.14 will be called the "optimal" or "best" estimate.

4.2.2 Minimization of the loss function. To minimize the expected loss, set the first derivative of Eq. 4.14 with respect to $\hat{x}$ to zero.

$$\frac{\partial}{\partial \hat{x}} E[L|y] = 2\,E[x|y] - 2\,E[\hat{x}|y] = 0 \tag{4.15}$$

In Eq. 4.15, $\hat{x}$ is an independent variable. Therefore,

$$E[\hat{x}|y] = \hat{x} \tag{4.16}$$

Substituting Eq. 4.16 into Eq. 4.15 and solving yields

$$\hat{x} = E[x|y] \tag{4.17}$$

Equation 4.17 is the desired expression for the optimal estimate. The result is intuitively pleasing - it states that the best estimate of x is the expected value of x conditioned on the measurements.

For an n-dimensional state vector $\underline{x}$, the loss function will be defined as follows:

$$L(\underline{x} - \hat{\underline{x}}) = (\underline{x} - \hat{\underline{x}})^T (\underline{x} - \hat{\underline{x}}) \tag{4.18}$$

If $\underline{x}$ is one-dimensional, Eq. 4.18 reduces to Eq. 4.12. Equation 4.18 has the four properties of Eq. 4.12 discussed in Par. 4.2.1. The minimization of the conditional expectation of Eq. 4.18 is accomplished by setting the first derivative of the conditional expectation with respect to the estimate to zero.

$$\frac{\partial}{\partial \hat{\underline{x}}} E[(\underline{x} - \hat{x})^T (\underline{x} - \hat{\underline{x}}) | \underline{y}] = 2 E[\underline{x}^T | \underline{y}]$$

$$- 2 E[\hat{\underline{x}}^T | \underline{y}] = 0 \tag{4.19}$$

The solution to Eq. 4.19 is the conditional mean,

$$\hat{\underline{x}} = E[\underline{x} | \underline{y}] \tag{4.20}$$

which reduces to the result for the scalar case if $\underline{x}$ is one-dimensional.

Jazwinski [60:Chap. 5] and Meditch [57:Chap. 5] discuss loss functions in more detail. In particular, loss functions with the four properties of Par. 4.2.1 are examined without reference to a specific expression for the loss function. It can be shown that the conditional mean is the optimal estimate if the loss function has the four

properties listed in Par. 4.2.1 and if the probability density function of $\underline{x}$ is symmetric and unimodal [37:160-161]. For the loss function of Eq. 4.18, the conditional mean is the optimal estimate without restrictions on the probability density function. The estimate which minimimizes the loss function of Eq. 4.18 is called the minimum variance or minimum mean square estimate.

4.3 Evaluation of the Conditional Mean.

4.3.1 An expression of the conditional mean.

The conditional density function, for a scalar x, will be evaluated using Bayes Rule:

$$p(x|y) = p(y|x)\, p(x) / p(y) \tag{4.21}$$

Bayes Rule is derived using the following statement:

> The probability that two events jointly occur is equal to the probability that the first event occurs times the probability that the second event occurs given that the first event occurred.

Since "first event" and "second event" can apply to x and y in either order, this statement can be written:

$$p(x \text{ and } y) = p(x)\, p(y|x) = p(y)\, p(x|y) \tag{4.22}$$

from which Bayes Rule follows directly.

For a scalar x and Gaussian statistics, the mean and variance are easily identified from the probability density function:

$$p(x) = \frac{1}{\sqrt{2\pi}\ \sigma_x} \exp\left[-(x - \mu_x)^2 / 2\sigma_x^2\right] \tag{4.23}$$

where: x is the random variable;

μ_x is the mean; and

σ_x is the standard deviation about the mean.

At this point, a linear relationship between the state and the observation will be assumed:

$$y = Hx + \varepsilon \tag{4.24}$$

where: H is a scale factor for the scalar case; and

ε is the random measurement error, $N(0,\sigma_\varepsilon)$.

The variance of the measurement can be obtained as follows:

$$\sigma_y^2 = E[(y - \mu_y)^2] = E[(Hx + \varepsilon - H\mu_x)^2]$$

$$= H^2\sigma_x^2 + 2H\sigma_{x\varepsilon} + \sigma_\varepsilon^2 \tag{4.25}$$

If x and ε are uncorrelated, Eq. 4.25 becomes:

$$\sigma_y^2 = H^2\sigma_x^2 + \sigma_\varepsilon^2 \tag{4.26}$$

Equation 4.26 is used to describe the probability density of the measurement y.

$$p(y) = \frac{1}{\sqrt{2\pi}\ \sigma_y} \exp\left[-(y - H\mu_x)^2/2\sigma_y^2\right] \tag{4.27}$$

Following duPlessis' argument [58], the conditional probability density $p(y|x)$ is equivalent to the probability density for the specific value of ϵ given by

$$\epsilon = y - Hx \tag{4.28}$$

Substituting Eq. 4.28 into the Gaussian form for the probability density function of ϵ gives

$$p(\epsilon = y - Hx) = p(y|x)$$

$$= \frac{1}{\sqrt{2\pi}\,\sigma_\epsilon} \exp\left[-(y - Hx)^2/2\sigma_\epsilon^2\right] \tag{4.29}$$

Substituting Eqs. 4.23, 4.27, and 4.29 into Bayes' Rule, Eq. 4.21, gives

$$p(x|y) = \frac{1}{\sqrt{2\pi}} \left(\frac{\sigma_y}{\sigma_\epsilon \sigma_x}\right) \exp\left\{ -\frac{1}{2}\left(\frac{\sigma_y}{\sigma_\epsilon \sigma_x}\right)^2 \left(x - \left[\mu_x + \frac{H\sigma_x^2}{\sigma_y^2}(y - H\mu_x)\right]\right)^2\right\} \tag{4.30}$$

By comparison with the Gaussian form, the conditional expectation is:

$$E[x|y] = \mu_x + \frac{H\sigma_x^2}{\sigma_y^2}(y - H\mu_x) \tag{4.31}$$

Substituting Eq. 4.26 into Eq. 4.31 gives the expression for the optimal estimate in the scalar case.

$$E[x|y] = \mu_x + \frac{H\sigma_x^2}{H^2\sigma_x^2 + \sigma_\varepsilon^2}(y - H\mu_x) \tag{4.32}$$

If the state and the measurement noise are correlated, the optimal estimate can be formed by substituting Eq. 4.25 into Eq. 4.31.

An expression for the conditional expectation in the vector case will now be developed. The n-dimensional state vector and the ℓ-dimensional observation vector are combined into a single vector $\underline{z}$ of dimension $\ell + n$.

$$\underline{z}^T = [\underline{x}^T, \underline{y}^T] \tag{4.33}$$

The joint density function, if Gaussian statistics are assumed, is given by

$$p(x,y) = p(\underline{z}) = \frac{1}{\sqrt{(2\pi)^{n+\ell}\,|P|}}$$

$$\exp\left[-\frac{1}{2}(\underline{z} - E[\underline{z}])^T P^{-1} (\underline{z} - E[\underline{z}])\right] \tag{4.34}$$

$$P = \begin{bmatrix} P_{xx} & P_{xy} \\ P_{yx} & P_{yy} \end{bmatrix}$$

$$P_{xx} = E\left[(\underline{x} - E[x])(\underline{x} - E[x])^T\right] \tag{4.35}$$

$$P_{xy} = E\left[(\underline{x} - E[x])(\underline{y} - E[y])^T\right] \tag{4.36}$$

$$P_{yx} = P_{xy}^T \tag{4.37}$$

$$P_{yy} = E\left[(\underline{y} - E[y])(\underline{y} - E[\underline{y}])^T\right] \tag{4.38}$$

The inverse of P is

$$P^{-1} = \begin{bmatrix} A & B \\ B^T & C \end{bmatrix}$$

$$\begin{bmatrix} (P_{xx} - P_{xy}P_{yy}^{-1} P_{yx})^{-1} & -P_{xx}P_{xy}(P_{yy} - P_{yx}P_{xx}^{-1} P_{xy})^{-1} \\ -P_{yy}^{-1} P_{yx} (P_{xx} - P_{xy}P_{yy}^{-1} P_{yx})^{-1} & (P_{yy} - P_{yx}P_{xx}^{-1} P_{xy})^{-1} \end{bmatrix} \tag{4.39}$$

Using an alternate form of Bayes' Rule given by

$$p(x|y) = p(x,y)/p(y) \tag{4.40}$$

and

$$p(y) = \frac{1}{\sqrt{(2\pi)^{\ell} |P_{yy}|}} \exp\left[-\frac{1}{2}(\underline{y} - E[\underline{y}])^T P_{yy}^{-1} (\underline{y} - E[\underline{y}])\right] \tag{4.41}$$

Equations 4.34 through 4.41 can be combined to give

$$p(\underline{x}|\underline{y}) = \frac{1}{\sqrt{(2\pi)^n \left|\frac{|P|}{P_{yy}}\right|}} \exp\left\{-\frac{1}{2}\begin{pmatrix} \underline{x} - E[\underline{x}] \\ \underline{y} - E(\underline{y}) \end{pmatrix}^T \begin{bmatrix} A & B \\ B^T & C - P_{yy}^{-1} \end{bmatrix} \begin{pmatrix} \underline{x} - E[\underline{x}] \\ \underline{y} - E[\underline{y}] \end{pmatrix}\right\} \tag{4.42}$$

If $\underline{m}$ is defined as

$$\underline{m} = E[\underline{x}] + P_{xy}P_{yy}^{-1} (\underline{y} - E[\underline{y}]) \tag{4.44}$$

and using

$$A = (P_{xx} - P_{xy}P_{yy}^{-1} P_{yx})^{-1} \tag{4.45}$$

the exponent can be reduced to

$$(\underline{x} - \underline{m})^T (P_{xx} - P_{xy}P_{yy}^{-1} P_{yx})^{-1} (\underline{x} - \underline{m}) \tag{4.46}$$

The covariance matrix, P can be written

$$P = \begin{vmatrix} P_{xx} - P_{xy} P^{-1} P_{yx} & P_{xy} \\ 0 & P_{yy} \end{vmatrix} \begin{vmatrix} I & 0 \\ P_{yy}^{-1} P_{xy} & I \end{vmatrix} \tag{4.47}$$

The determinant of the covariance matrix is

$$|P| = |P_{xx} - P_{xy}P_{yy}^{-1} P_{yx}||P_{yy}| \tag{4.48}$$

Substituting Eq. 4.46 and Eq. 4.48 into Eq. 4.42 yields

$$p(\underline{x}|\underline{y}) = \frac{1}{\sqrt{(2\pi)^n | P_{xx} - P_{xy} P_{yy}^{-1} P_{yx}|}}$$

$$\exp \left| -\frac{1}{2} (\underline{x} - \underline{m})^T (P_{xx} - P_{xy} P_{yy}^{-1} P_{yx})^{-1} (\underline{x} - \underline{m}) \right| \tag{4.49}$$

By comparing Eq. 4.49 with the Gaussian form, the conditional mean is given by

$$E[\underline{x}|\underline{y}] = \underline{m} = E[\underline{x}] + P_{xy}P_{yy}^{-1}(\underline{y} - E[\underline{y}]) \quad (4.50)$$

and has covariance

$$P_{x|y} = P_{xx} - P_{xy}P_{yy}^{-1}P_{yx} \quad (4.51)$$

For the optimality conditions discussed in Par. 4.2.1, $\underline{m}$, as determined by Eq. 4.50, is the optimal estimate.

Assuming the following linear observation-state relationship for vector measurements*

$$\underline{y} = H\underline{x} + \underline{\varepsilon} \quad (4.52)$$

where: $$E[\underline{\varepsilon}] = 0 \quad (4.53)$$

$$E[\underline{\varepsilon\varepsilon}^T] = R \quad (4.54)$$

then Eq. 4.36 becomes

$$P_{xy} = P_{xx}H^T + E[\underline{x\varepsilon}^T] \quad (4.55)$$

If there is no correlation between the state and the measurement noise, Eq. 4.55 becomes

$$P_{xy} = P_{xx}H^T \quad (4.56)$$

The covariance of the measurements is defined by

$$P_{yy} = E[(\underline{y} - E[\underline{y}])(\underline{y} - E[\underline{y}])^T] \quad (4.57)$$

---

*Equations 4.52 through 4.54 are identical to Eqs. 4.5 and 4.6 for a single measurement.

Substituting Eq. 4.52 into Eq. 4.57, applying the expectation operator, and assuming no correlation between the state and the measurement noise, Eq. 4.57 becomes

$$P_{yy} = HP_{xx}H^T + R \tag{4.58}$$

Substituting Eq. 4.56 and Eq. 4.58 into Eq. 4.50 gives

$$E[\underline{x}|\underline{y}] = E[\underline{x}] + P_{xx}H^T(HP_{xx}H^T + R)^{-1}\,(\underline{y} - E[\underline{y}])$$

$$= \underline{\mu}_x + K(\underline{y} - H\underline{\mu}_x) \tag{4.59}$$

where: $$K = P_{xx}H^T(HP_{xx}H^T + R)^{-1} \tag{4.60}$$

As used in Eq. 4.59, K is the filter gain.

The expression for the covariance matrix, Eq. 4.51, becomes

$$P_{x|y} = P_{xx} - P_{xx}H^T(HP_{xx}H^T + R)^{-1}\,HP_{xx} = (I - KH)P_{xx} \tag{4.61}$$

4.3.2 Time propagation of the conditional mean and its covariance. Equations 4.59 and 4.61 represent the measurement update. If the state is a dynamical system and measurements are available at discrete times, then the mean μ_x and its covariance P_{xx} will propagate with time. The mean and covariance terms in Eqs. 4.59 and 4.61 must be the values propagated to the time of the measurement.

A linear differential equation will be used to describe the state dynamics.

$$\dot{\underline{x}} = A(t)\underline{x} + B(t)\underline{u}(t), \quad \underline{x}(t_0) = \underline{x}_0 \tag{4.1}$$

The solution to Eq. 4.1 is given by Liebelt [63:40-48].

$$\underline{x}(t) = \Phi(t,t_0)\hat{\underline{x}}_0 + \int_{t_0}^{t} \Phi(t,s)B(s)\underline{u}(s)\, ds \qquad (4.62)$$

where: Φ is the state transition matrix which satisfies the differential equation

$$\dot{\Phi}(t,t_0) = A(t)\Phi(t,t_0), \quad \Phi(t_0,t_0) = I \qquad (4.63)$$

The integral expression in Eq. 4.62 is a stochastic integral. The ability to actually evaluate the integral depends on the character of the random process $\underline{u}(t)$. For purposes of further discussion, evaluation of the integral is not required. For further information on stochastic integrals, see Jazwinski [60].

The conditional expectation is applied to Eq. 4.62. If the process noise $\underline{u}(t)$ is independent of the measurements, then the propagated conditional mean is given by

$$E[\underline{x}(t)|\underline{y}(t_0)] = \Phi(t,t_0)\hat{\underline{x}}_0 \qquad (4.64)$$

It will be assumed that all measurements up to and including any measurements taken at t_0 were processed to obtain $\hat{\underline{x}}_0$. This does not require that a measurement be available at t_0.

The propagated covariance matrix is determined by using Eqs. 4.62 and 4.64 to form

$$\underline{x}(t) - E[\underline{x}(t)|\underline{y}(t_0)] = \Phi(t,t_0)(\underline{x}_0 - \hat{\underline{x}}_0) + \int_{t_0}^{t} \Phi(t,s)B(s)\underline{u}(s)\, ds \qquad (4.65)$$

Substituting Eq. 4.65 into

$$P(t|t_o) = \bar{P}(t)$$

$$= E[(\underline{x}(t) - E[\underline{x}(t)|\underline{y}(t_o)])(\underline{x}(t) - E[\underline{x}(t)|\underline{y}(t_o)])^T] \tag{4.66}$$

yields

$$\bar{P}(t) = \Phi(t,t_o)P_{x_o|y_o}\Phi^T(t,t_o)$$

$$+ \int_{t_o}^{t} \Phi(t,t_o)\, E[(\underline{x}_o - \hat{\underline{x}}_o)\underline{u}^T(s)|\underline{y}(t_o)]\, B^T(s)\, \Phi^T(t,s)\, ds$$

$$+ \int_{t_o}^{t} \Phi(t,s)\, B(s)\, E[\underline{u}(s)(\underline{x}_o - \hat{\underline{x}}_o)^T|\underline{y}(t_o)]\, \Phi^T(t,t_o)\, ds$$

$$+ \int_{t_o}^{t}\int_{t_o}^{t} \Phi(t,s)\, B(s)\, E[\underline{u}(s)\underline{u}^T(r)|\underline{y}(t_o)]\, B^T(r)\, \Phi^T(t,r)\, dr\, ds \tag{4.67}$$

If the process noise and the state are uncorrelated, the middle integrals of Eq. 4.67 are zero. If the process noise is independent of the measurements and is uncorrelated in time, then

$$E[u(s)u^T(r)] = Q(s)\delta(r - s) \tag{4.68}$$

Substituting Eq. 4.68 into Eq. 4.67 and evaluating one integral based on the properties of the Dirac delta function, the propagated covariance matrix is given by

$$\bar{P}(t) = \Phi(t,t_o)P_{x_o|y_o}\Phi^T(t,t_o)$$

$$+ \int_{t_o}^{t} \Phi(t,s)B(s)Q(s)B^T(s)\Phi^T(t,s)\, ds \tag{4.69}$$

Equations 4.64 and 4.69 represent the time propagation of the estimate and its covariance.

4.3.3 Unbiased property of the linear estimate. The linear estimate of Eq. 4.59 is repeated here for convenience.

$$\underline{\hat{x}} = \underline{\mu}_x + K(\underline{y} - H\underline{\mu}_x) \tag{4.59}$$

According to Liebelt [63:137] and Tapley [64], an estimate is defined to be unbiased if, given a value for the state, the following equality is satisfied:

$$E[\underline{\hat{x}}] = \underline{x} \tag{4.70}$$

Equation 4.70 implies that the state $\underline{x}$ is the independent variable. Therefore, the expectation of $\underline{x}$ is $\underline{x}$ itself.

$$\underline{\mu}_x = E[\underline{x}] = \underline{x} \tag{4.71}$$

Substituting Eq. 4.71 into Eq. 4.59 and applying the expectation operator gives

$$E[\underline{\hat{x}}] = \underline{x} + KE[\underline{y}] - KH\underline{x} \tag{4.72}$$

Substituting Eq. 4.52 into Eq. 4.72 gives the sequence

$$\begin{aligned} E[\underline{\hat{x}}] &= \underline{x} + KE[H\underline{x} + \underline{\epsilon}] - KH\underline{x} \\ &= \underline{x} + KH\underline{x} - KH\underline{x} \\ &= \underline{x} \end{aligned}$$

Thus, the linear estimate of Eq. 4.59 has been shown to be an unbiased estimate where Eq. 4.70 defines the unbiased property. Jazwinski [60:150] and Sorenson [65:5] used an alternate definition of an unbiased estimate given by

$$E[\hat{\underline{x}}] = E[\underline{x}] \tag{4.73}$$

Jazwinski and Sorenson show that the estimate of Eq. 4.59 is unbiased using the definition of Eq. 4.73.

The choice between Eq. 4.70 and Eq. 4.73 as the requirement for an unbiased estimate is a function of the definition for the ensemble of the estimates and the definition for the ensemble of the random variables. Equation 4.73 states that the ensemble average of the estimates for the ensemble of the random variables must be equal to the ensemble average of the random variables. Equation 4.70 states, however, that the ensemble average of the estimates for a realization of the random variable must be equal to the realization of the random variable. This distinction can be illustrated by the following example. Given a bucket of resistors and a bucket of ohmmeters, a user will measure the resistance of the resistors. Equation 4.70 states that if one resistor is pulled from the bucket and its resistance is measured using all the ohmmeters, then the average of the measurements will equal the resistance of the resistor. Equation 4.73 states that if all the resistors are measured using all the ohmmeters on each resistor, then the average of the measurements will equal the average resistance of the resistors. Thus, Eq. 4.70 and Eq. 4.73 are complementary requirements rather than conflicting requirements.

4.4 Linearization

The results of linear filtering theory can be easily applied to non-linear systems by assuming the existence of a nominal trajectory and a perturbation to the nominal trajectory. The linear estimation equations are then used to estimate the perturbation state.

Assume the following non-linear differential equation:

$$\dot{\underline{X}} = \underline{F}(\underline{X},t), \quad \underline{X}(t_0) = \underline{X}_0 \tag{4.74}$$

Expand Eq. 4.74 about a nominal trajectory, $\underline{X}^*$.

$$\begin{aligned} \dot{\underline{X}} &= \dot{\underline{X}}^* + \dot{\underline{x}} \\ &= \underline{F}(\underline{X}^*,t) + \left[\frac{\partial \underline{F}}{\partial \underline{X}}\right]^* \underline{x} + \text{H.O.T.} \end{aligned} \tag{4.75}$$

where: $[\ ]^*$ indicates that the partial derivative is evaluated on the nominal trajectory.

Equation 4.75 is separated into a nominal part and a perturbation part.

$$\dot{\underline{X}} = \underline{F}(\underline{X}^*,t), \quad \underline{X}^*(t_0) = \underline{X}_0^* \tag{4.76}$$

$$\dot{\underline{x}} = \left[\frac{\partial \underline{F}}{\partial \underline{X}}\right]^* \underline{x} + \text{H.O.T.}, \quad \underline{x}(t_0) = \underline{x}_0 \tag{4.77}$$

Deterministic control inputs, if present, can be added to the nominal system, Eq. 4.76. Random inputs can be added to Eq. 4.77.

If higher order terms are deleted and a linear process noise term is included, then Eq. 4.77,takes the form

$$\dot{\underline{x}} = \left[\frac{\partial \underline{F}}{\partial \underline{X}}\right]^{*} \underline{x} + B\underline{u} \ , \quad \underline{x}(t_o) = \underline{x}_o \tag{4.78}$$

Similarly, a non-linear observation-state relationship can be linearized.

$$\begin{aligned} \underline{G}(\underline{X},t) &= \underline{G}(\underline{X}^{*} + \underline{x},t) = \underline{G}(\underline{X}^{*},t) \\ &= \underline{G}(\underline{X}^{*},t) + \left[\frac{\partial \underline{G}}{\partial \underline{X}}\right]^{*} \underline{x} + \text{H.O.T.} \end{aligned} \tag{4.79}$$

If $\underline{Y}$ is the actual measurement given by

$$\underline{Y} = \underline{G}(\underline{X},t) + \underline{\varepsilon} \tag{4.80}$$

then the residual is given by

$$\underline{y} = \underline{Y} - \underline{G}(\underline{X}^{*},t) = \left[\frac{\partial \underline{G}}{\partial \underline{X}}\right]^{*} \underline{x} + \underline{\varepsilon} + \text{H.O.T.} \tag{4.81}$$

Deleting the higher order terms,

$$\underline{y} = \left[\frac{\partial \underline{G}}{\partial \underline{X}}\right]^{*} \underline{x} + \underline{\varepsilon} \tag{4.82}$$

Equations 4.78 and 4.82 are the linearized equations corresponding to Eqs. 4.1 and 4.52 respectively with the following equivalences:

$$A(t) = \left[\frac{\partial \underline{F}}{\partial \underline{X}}\right]^{*} \tag{4.83}$$

$$H = \left[\frac{\partial \underline{G}}{\partial \underline{X}}\right]^{*} \tag{4.84}$$

4.5 Differential Equations for the Covariance Matrix

The propagated covariance matrix was given by Eq. 4.69.

$$\bar{P}(t) = \Phi(t,t_o)P(t_o)\Phi^T(t,t_o) + \int_{t_o}^{t} \Phi(t,s)B(s)Q(s)B^T(s)\Phi^T(t,s)ds \qquad (4.69)$$

The covariance matrix required in the measurement update, Eqs. 4.59, 4.60, and 4.61, is the result of Eq. 4.69 at $t = t_k$.

$$P_{xx}(t_k) = P(t_k|t_{k-1}) = \bar{P}(t_k) \qquad (4.85)$$

where: t_{k-1} is the time of the previous measurement.

For purposes of the following discussions $t_{k-1} = t_o$.

Evaluation of Eq. 4.69 must be accomplished numerically in many applications. To derive a differential equation for the covariance matrix, Leibnitz's Rule is applied to Eq. 4.69. Using the differential equation for the state transition matrix, Eq. 4.63,

$$\dot{\Phi}(t,t_o) = A(t)\Phi(t,t_o), \quad \Phi(t_o,t_o) = I \qquad (4.63)$$

the differential equation is given by

$$\dot{\bar{P}}(t) = A(t)\bar{P}(t) + \bar{P}(t)A^T(t) + B(t)Q(t)B^T(t), \quad \bar{P}(t_o) = P_{x_o|y_o} \qquad (4.86)$$

The solution to the linear differential equation, Eq. 4.86, as given in Eq. 4.69, can be separated into a homogeneous solution and a

particular solution. The particular solution will be designated Γ and will be referred to as the discrete process noise matrix. The integral of Eq. 4.69 can be replaced with a quadrature relation which will lead directly to the differential equation

$$\dot{\Gamma}(t_k,t) = \Phi(t_k,t)B(t)Q(t)B^T(t)\Phi^T(t_k,t),$$
$$\Gamma(t_k,t_k) = 0 \qquad (4.87)$$

The covariance matrix update equation is then

$$\bar{P}(t_k) = \Phi(t_k,t_o)P(t_o)\Phi^T(t_k,t_o) + \Gamma(t_k,t_o) \qquad (4.88)$$

Covariance matrix propagation using Eq. 4.88 requires the integration of Eq. 4.63 forward in time and the integration of Eq. 4.87 backward in time. The requirement to store or recompute the state transition matrix for the backward integration of Eq. 4.87 reduces the attractiveness of the method.

The particular solution of Eq. 4.69 has been defined as

$$\Gamma(t) = \int_{t_o}^{t} \Phi(t,s)B(s)Q(s)B^T(s)\Phi^T(t,s)ds \qquad (4.89)$$

Leibnitz's Rule can be applied to Eq. 4.89.

$$\dot{\Gamma}(t) = B(t)Q(t)B^T(t) + \int_{t_o}^{t} \dot{\Phi}(t,s)B(s)Q(s)B^T(s)\Phi^T(t,s)ds$$
$$\int_{t_o}^{t} \Phi(t,s)B(s)Q(s)B^T(s)\dot{\Phi}^T(t,s)ds \qquad (4.90)$$

Substituting Eq. 4.63 into Eq. 4.90 yields

$$\dot{r}(t) = B(t)Q(t)B^T(t) + \int_{t_0}^{t} A(t)\Phi(t,s)B(s)Q(s)B^T(s)\Phi^T(t,s)ds + \int_{t_0}^{t} \Phi(t,s)B(s)Q(s)B^T(s)\Phi^T(t,s)A^T(t)ds \quad (4.91)$$

Since the plant matrix $A(t)$ is not a function of the parameter of integration, it can be moved outside the integrals.

$$\dot{r}(t) = B(t)Q(t)B^T(t) + A(t)\left[\int_{t_0}^{t} \Phi(t,s)B(s)Q(s)B^T(s)\Phi^T(t,s)ds\right] + \left[\int_{t_0}^{t} \Phi(t,s)B(s)Q(s)B^T(s)\Phi^T(t,s)ds\right] A^T(t) \quad (4.92)$$

Substituting Eq. 4.89 into Eq. 4.92 yields

$$\dot{r}(t) = A(t)r(t) + r(t)A^T(t) + B(t)Q(t)B^T(t), \quad r(t_0) = 0 \quad (4.93)$$

where: $r(t_0)=0$, the initial condition is obtained from Eq. 4.89.

Thus, the covariance matrix can be propagated by integrating Eqs. 4.63 and 4.93 forward in time and substituting the results into

$$\bar{P}(t_k) = \Phi(t_k,t_o)P(t_o)\Phi^T(t_k,t_o) + \Gamma(t_k) \qquad (4.94)$$

The selection of a covariance matrix propagation method must be based on an analysis of the efficiency and stability of the various methods for each specific application. Such an analysis must consider the system model and parameters and the user's requirements and capabilities.

Each covariance matrix propagation technique can be shown to have a maximum number of equations that must be integrated. Equation 4.86 requires the integration of a maximum of $n(n+1)/2$ equations for an n-dimensional state. Equations 4.88 nd 4.94 require the integration of a maximum of $n^2+n(n+1)/2$ equations because the state transition matrix must also be integrated. Selection of Eq. 4.86 as the covariance matrix propagation method cannot, however, be based solely on the analysis of a theoretical maximum number of equations to be integrated. The system model must be considered also. Frequently, the differential equations of the individual elements of the matrices may be solved analytically, thereby avoiding the requirement to numerically integrate these elements. This is especially true for the elements of the state transition matrix.

A count of the equations to be integrated after removing the analytic solutions is still an incomplete criterion. The user's accuracy requirement and his capabilities must be considered. A user with loose accuracy requirements can expand the state transition matrix in a power series as follows:

$$\Phi(t,t_0) = I + A(t_0)(t-t_0) + \frac{1}{2}[A^2(t_0)+\dot{A}(t_0)](t-t_0)^2+... \quad (4.95)$$

Typically, the power series is not expanded beyond the quadratic term. The low accuracy user can also replace the discrete process noise matrix of Eq. 4.88 and 4.94 with an approximation.

$$\Gamma(t) \approx B(t_0)Q(t_0)B^T(t_0)\ (t-t_0) \quad (4.96)$$

The implementation of Eqs. 4.95 and 4.96 with Eq. 4.94 effectively eliminates the need for numerical integration.

A user who requires an accurate covariance matrix must concern himself with the numerical stability and the computer time requirements of the methods. Numerical integration of Eq. 4.86 is often time-consuming when high accuracy is specified. Applications of Eq. 4.86 with variable step integrators usually specify tolerances on the integration of the covariance matrix which are less stringent than the tolerances specified for integration of the state. This will reduce the time requirement for the numerical integrations but it will also reduce confidence in the resulting covariance matrix.

In general, the state transition matrix can be integrated with accuracies on the order of the accuracy of the state integration. With an accurate state transition matrix, the propagated initial covariance matrix $\Phi P \Phi^T$ will be accurate. The discrete process noise matrix Γ generally contributes terms to the covariance matrix $\bar{P}$ which are orders of magnitude less than the contribution of the $\Phi P \Phi^T$ term.

Consequently, errors in the discrete process noise matrix are less influential in causing errors in the $\bar{P}$ matrix. This is a fortunate situation because the spectral level process noise matrix Q is often of dubious accuracy. Frequently, Eq. 4.96 is used to generate the discrete process noise matrix for Eq. 4.94.

Equation 4.96, however is incomplete. It does not describe the correct propagation of a spectral level noise among the elements of the discrete process noise matrix. For example, it can be argued that the only spectral level noises which influence an aircraft are random forces or, equivalently, accelerations. Accordingly, the only non-zero elements of BQB^T should be in the acceleration terms. Equation 4.96 will not propagate spectral level acceleration noise into the position or velocity states although, intuitively, a result of acceleration noise is an uncertainty in the position and velocity of the aircraft as well as an acceleration uncertainty.

Integration of Eq. 4.87 or Eq. 4.93 will produce non-zero values in all elements of the covariance matrix that are affected by spectral level noise terms. Because of the relative magnitude of the discrete process noise matrix compared to the covariance matrix itself, integrating the discrete process noise matrix separately allows the use of a relaxed tolerance on that part of the system which is least known. When the result is added to an accurate $\Phi P \Phi^T$ terms, the covariance matrix $\bar{P}$ can maintain accuracy on the order of that specified for the integration of the state transition matrix.

The numerical advantages of separate integration of the discrete process noise matrix can be overshadowed by the requirement for the backward integration of Eq. 4.87. Equation 4.94, is a forward integration and eliminates this disadvantage. Also, some high-order variable step numerical integration techniques such as a Runge-Kutta (7)8 [88] will not operate properly for quadratures such as Eq. 4.87. The form of Eq. 4.94, however, can be integrated successfully using the variable-step Runge-Kutta (7)8 algorithm.

The navigation algorithms evaluated in this study are examples of the dangers inherent in selecting a method without examination of the system model. For all algorithms studied, the state transition matrix and the discrete process noise matrix are solved analytically.

The techniques discussed herein are the basic covariance matrix propagation techniques. Many variations have been developed, and other alternate approaches should be considered prior to selection of a specific method for the covariance matrix propagation.

4.6 Linear Estimation Algorithms

The estimation equations developed in this chapter will be implemented into three basic algorithms. In each case, a comprehensive set of equations is shown. Specific applications of the algorithms must determine the precise form of the equations to be evaluated, otherwise the computation will be inefficient and may have numerical difficulties.

4.6.1 The standard sequential filter. The equations developed for the minimum variance estimate are used in a sequential filtering algorithm for a non-linear system.

1. Propagate the nominal state vector, the state transition matrix, and the covariance matrix to t_k, the time of the measurement.

$$\dot{\underline{X}}^*(t) = \underline{F}(\underline{X}^*, t), \qquad \underline{X}^*(t_{k-1}) = \underline{X}^*_{k-1}$$

$$\dot{\Phi}(t, t_{k-1}) = A(t)\,\Phi(t, t_{k-1}), \qquad \Phi(t_{k-1}, t_{k-1}) = I$$

$$\dot{\bar{P}}(t) = A\bar{P} + \bar{P}A^T + BQB^T, \qquad \bar{P}(t_{k-1}) = P_{k-1}$$

where: $$A = \left[\frac{\partial \underline{F}}{\partial \underline{X}}\right]^*$$

2. Compute the gain at t_k.

$$K_k = \bar{P}_k H_k^T (H_k \bar{P}_k H_k^T + R_k)^{-1}$$

3. Propagate the estimated perturbation state.

$$\bar{\underline{x}}_k = \Phi(t_k, t_{k-1})\hat{x}_{k-1}$$

or $$\dot{\bar{\underline{x}}} = A(t)\bar{\underline{x}}, \quad \bar{\underline{x}}(t_{k-1}) = \hat{x}_{k-1}$$

4. Calculate the observation residual.

$$\underline{y}_k = \underline{Y}_k - G(\underline{X}^*_k, t_k)$$

5. Estimate the state correction.

$$\hat{\underline{x}}_k = \bar{\underline{x}}_k + K_k(y_k - H_k\bar{\underline{x}}_k)$$

6. Update the covariance matrix.

$$P_k = (I - K_kH_k)\bar{P}_k$$

7. Replace k with k-1 and go to 1.

4.6.2 The extended sequential algorithm. An examination of the standard sequential algorithm shows that the propagation of the nominal trajectory is based solely on $\underline{X}_0^*$ the initial estimate of the state, despite knowledge that the best estimate of the state at a time t_{k-1} is $\underline{X}_{k-1} + \hat{\underline{x}}_{k-1}$. This results in errors that depend on the nonlinearity of the system and the departure of the nominal state from the true state.

The difference between the nominal and the true states can be made smaller by assuming that the estimate is closer to the true state and rectifying the nominal accordingly. After rectification, the estimated perturbation is zero. The extended sequential algorithm can be summarized as follows:

1. Integrate to t_k the nominal state $\underline{X}$ and the covariance matrix.

$$\dot{\underline{X}} = F(\underline{X},t), \qquad \underline{X}(t_{k-1}) = \hat{\underline{X}}_{k-1}$$

$$\dot{P} = AP + PA^T + BQB^T, \quad P(t_{k-1}) = P_{k-1}$$

2. Compute the gain.

$$K_k = \bar{P}_k H_k^T (H_k \bar{P}_k H_k^T + R_k)^{-1}$$

3. Determine the observation residual.

$$\underline{y}_k = \underline{Y}_k - \underline{G}(\bar{\underline{X}}_k, t_k)$$

4. Estimate the perturbation state.

$$\hat{\underline{x}}_k = K_k \underline{y}_k$$

5. Update the covariance matrix.

$$P_k = (I - K_k H_k)\bar{P}_k$$

6. Rectify the nominal trajectory.

$$\hat{\underline{X}}_k = \bar{\underline{X}}_k + \hat{\underline{x}}_k$$

7. Replace k with k-1 and go to 1.

For a linear system, the standard sequential filter and the extended sequential filter will provide identical results.

4.6.3 The batch filter. The batch filter is designed to take many observations and estimate the state at a specific epoch. If all the measurements are taken at the epoch, a single step of the sequential estimator defines the estimate. If, however, measurements are available at times t_ℓ and the epoch for the estimate is t_k, then the observation-state relationship must be modified.

$$y_\ell = H_\ell(\underline{X}_\ell, t_\ell)\Phi(t_\ell, t_k)\underline{x}_k + \underline{\varepsilon}_\ell$$

If a vector $\underline{y}_k$ is to represent ℓ measurement vectors, then a new observation-state relationship can be defined.

$$\underline{y}_k = \begin{bmatrix} y_1 \\ y_2 \\ y_3 \\ \vdots \\ y_\ell \end{bmatrix} = \begin{bmatrix} H_1(\underline{X}_1, t_1)\Phi(t_1, t_k) \\ H_2(\underline{X}_2, t_2)\Phi(t_2, t_k) \\ H_3(\underline{X}_3, t_3)\Phi(t_3, t_k) \\ \vdots \\ H_\ell(X_\ell, t_\ell)\Phi(t_\ell, t_k) \end{bmatrix} \underline{x}_k + \begin{bmatrix} \underline{\varepsilon}_1 \\ \underline{\varepsilon}_2 \\ \underline{\varepsilon}_3 \\ \vdots \\ \underline{\varepsilon}_\ell \end{bmatrix} \tag{4.97}$$

Equation 4.97 can be rewritten.

$$\underline{y}_k = H_k\underline{x}_k + \underline{\varepsilon}_k \tag{4.98}$$

The correspondence between Eq. 4.97 and Eq. 4.98 is obvious. Equation 4.98 can be interpreted as an expanded observation-state relation and is equivalent to Eq. 4.52.

If each measurement is a p-dimensional vector, then H_k in Eq. 4.98 is dimensioned $(\ell p \times n)$ and the $\underline{y}_k$ and $\underline{\varepsilon}_k$ vectors are ℓp-dimensional. The gain term as expressed in Eq. 4.60 is repeated here.

$$K_k = \overline{P}_k H_k^T (H_k \overline{P}_k H_k^T + R_k)^{-1} \tag{4.60}$$

To account for an augmented $\underline{\varepsilon}_k$, the term R_k is changed to an $(\ell p \times \ell p)$ matrix as follows:

$$R_k = \begin{bmatrix} R_1 & 0 & 0 & \cdots & 0 \\ 0 & R_2 & 0 & & 0 \\ 0 & 0 & R_3 & & 0 \\ \vdots & & & \ddots & \vdots \\ 0 & 0 & 0 & \cdots & R_1 \end{bmatrix}$$

The gain term as expressed in Eq. 4.60 requires the inversion of an $(\ell p \times \ell p)$ matrix. Using matrix identities, an alternate expression for the gain can be obtained.

$$K_k = (\bar{P}_k^{-1} + H_k^T R_k^{-1} H_k)^{-1} H_k^T R_k^{-1} \tag{4.100}$$

Equation 4.100 requires the inverse of an $(n \times n)$ matrix.

Though it is possible to execute the batch algorithm using a $(p \times n)$ H_k matrix and a $(p \times p)$ R_k matrix, there is a considerable penalty in storage. If the measurement noise matrix is as shown in Eq. 4.99, the term $H_k^T R_k^{-1} H_K$ in Eq. 4.100 can be evaluated using the summation

$$H_k^T R_k^{-1} H_k = \sum_{i=1}^{\ell} \Phi^T(t_i, t_k) H_i^T(\underline{X}_i, t_i) R_i \, H_i(\underline{X}_i, t_i) \Phi(t_i, t_k) \tag{4.101}$$

Similarly, the term $H_k^T R_k^{-1} \underline{y}_k$ can be evaluated using

$$H_k^T R_k^{-1} \underline{y}_k = \sum_{i=1}^{\ell} \Phi^T(t_i,t_k) H_i(X_i,t_i) R_i^{-1} y_i \qquad (4.102)$$

If t_k, the desired time for the estimate is equal to t_o, the initial time, then an appropriate algorithm for the batch filter is as follows:

1. Set: $i = 1$

   $L = \overline{P}_0^{-1}$

   $M = L\underline{\overline{x}}_o$

2. Integrate from t_{i-1} to t_i .

   $\dot{\underline{\overline{X}}} = \underline{F}(\underline{\overline{X}},t), \quad \underline{\overline{X}}(t_o) = \underline{\overline{X}}_o$

   $\dot{\Phi} = A\Phi, \qquad \Phi(t_o,t_o) = I$

3. Increment L.

   $$L = L + \Phi^T(t_i,t_o) H_i(\underline{\overline{X}}_i,t_i) R_i^{-1} H_i(\underline{\overline{X}}_i,t_i) \Phi(t_i,t_o)$$

4. Compute the observation residual.

   $$\underline{y}_i = \underline{Y}_i - \underline{G}_i(\underline{\overline{X}}_i,t_i)$$

5. Increment M.

   $$M = M + \Phi^T(t_i,t_o) H_i(\underline{\overline{X}}_i,t_i) R_i^{-1} \underline{y}_i$$

6. If more measurements, i=i+1 and go to 2.

7. Estimate the initial conditions.

$$\hat{\underline{x}}_0 = L^{-1}M$$

$$\hat{\underline{X}}_0 = \overline{\underline{X}}_0 + \hat{\underline{x}}_0$$

8. Update the covariance matrix.

$$P_0 = L^{-1}$$

4.7 Summary

The conditional mean was shown to be an unbiased estimate, optimal in a minimum variance sense. The conditional mean is also the maximum likelihood estimate in the case of symmetric, unimodal probability density functions.* Assuming Gaussian statistics, a linear state equation, and a linear observation state relationship, expressions for measurement updates and time updates of the conditional mean and its covariance were developed. A method for linearizing a non-linear problem was shown and the results of linear estimation theory were applied to the linearized problem. Three basic filtering algorithms were described: the standard sequential filter (Kalman filter); the extended sequential filter (the extended Kalman filter); and the batch filter.

---

*If the probability density function is not symmetric and unimodal, the maximum likelihood estimate is of questionable value.

CHAPTER 5

DEVELOPMENT OF A BASIC FILTER MODEL

5.1 Navigation Applications of the Sequential Filter

A sequential filter, as derived in the original works of Kalman [8] and Kalman and Bucy [9], will provide the optimal estimate if:

1. The dynamic system model and the observation model are linear;

2. The dynamic system model and the observation model are correct;

3. The a priori statistics for the initial conditions of the state and for the noise models are Gaussian with zero mean and known covariance.

In real-world filter applications, precise knowledge of the system model and the noise statistics is not available. Nishimura [66] has analyzed the behavior of the sequential filter with incorrect system models, noise statistics, or initial condition statistics. Assuming the correct linear system model, Nishimura shows that, if the statistics are chosen conservatively (i.e., the filter assumes a magnitude of the covariance of the noise which is larger than the actual noise covariance magnitude), then the actual errors will be within the range specified by the suboptimal covariance matrix. As would be

expected, the statistics should not be excessively conservative or the filter may become ill-conditioned.

The application of sequential filters to orbit determination problems has been successful since system models are available which will adequately predict the state of a spacecraft for long periods of time. For example, using Keplerian elements and a set of seven correction parameters, the line-of-sight position error for a GPS satellite is expected to be less than 1.5 meters (one sigma) for a one-hour prediction [16].

Unfortunately, the dynamic models for a maneuvering aircraft cannot predict adequately the behavior for more than a few seconds. Sequential filters, however, have been applied successfully to aircraft navigation systems especially when an inertial navigation system (INS) is used [62]. With an INS, the ability of onboard computers to integrate accelerometer data at high sampling rates compensates for the prediction errors of an assumed aircraft dynamic model. The sequential filter is especially useful when an INS is augmented with additional equipment such as an altimeter or a LORAN receiver. The sequential filter for the augmented INS can be used to determine measurement errors in the INS, to optimally combine the measurements with the INS measurements, and, using the additional measurements, to automatically damp the 84-minute and the 24-hour oscillations of an INS [67]. Errors in system models frequently will not cause large errors over short estimation time spans. For example, air-to-air missiles, with short flight times, have used approximate models in sequential filters to obtain an effective guidance solution.

The low-cost GPS user faces a challenging filter implementation problem - he does not have the ability to accurately model aircraft motion; he does not have sampling rates as high as INS users; and he must maintain an accurate estimate of the state for long time intervals. No general remarks can be made about the effects of incorrect system models on filter performance. The development of an adequate model for a specific implementation is the engineering challenge facing the filter designer.

Brock and Schmidt [67] state that, because of the lack of a good model, the results obtained with a sequential filter in aircraft applications may not be much better than the results obtained with deterministic solutions. Using the parameters that optimized a selected model (Par. 5.5.2), Singer [68] states that the filter is operating almost as a least-squares filter with no a priori information. Counter to these discouraging remarks are some factors which motivate the use of a sequential filter.

1. A sequential filter (Par. 4.6.2) is not difficult to implement. Measurements can be processed as scalars, further simplifying the filter coding. A simple sequential filter will require only a limited amount of data storage.

2. The sequential filter easily combines different measurement sources.

3. Non-stationary noise can be accomodated easily.

4. With appropriate choices of a system model and statistics, the sequential filter should perform as well as deterministic solutions or least squares methods.

In this chapter, a basic aircraft model will be developed for the extended sequential filter. Initially, the system equations will be specified arbitrarily but with intuitively pleasing characteristics. The equations will be modified so that the resulting system model can be accommodated by the Kalman filter. Then it will be shown that, with certain restrictions, the equations specified originally are satisfied by the resulting filter model. The aircraft model is referred to as an acceleration dead-reckoning (ADR) model with exponentially correlated random acceleration. The state transition matrix and the discrete process noise matrix for the basic model will be determined analytically.

The measurement bias states and their statistics as assumed by the filter will be discussed. The simulated measurement rejections, the additional noise terms, and the testing philosophy for the basic filter will be described. The quantitative parameters that will be used to evaluate filter performance throughout this study will be described. Finally, the basic filter model will be evaluated.

5.2 Components of the State Vector.

5.2.1 Aircraft states. The basic state vector consists of the parameters listed in Table 5.1. Position states are an obvious requirement for navigation purposes. Velocity is included because the

Table 5.1 Filter Parameters for the Twelve-State Acceleration Dead-Reckoning Model

State	Initial Error	Initial Standard Deviation	Correlation Time	Process Noise Spectral Density
North Position Error, δx_N	49.96 m	60.0 m	-	0.
East Position Error, δx_E	-42.43 m	60.0 m	-	0.
Vertical Position Error, δx_D	10.00 m	20.0 m	-	0.
North Velocity Error, δv_N	0. m/sec	0. m/sec	-	0.
East Velocity Error, δv_E	0. m/sec	0. m/sec	-	0.
Vertical Velocity Error, δv_D	0. m/sec	0. m/sec	-	0.
North Acceleration Error, δa_N	-1.39 m/sec	2.5 m/sec^2	* sec	* m^2/sec^5
East Acceleration Error, δa_E	-.56 m/sec	2.5 m/sec^2	* sec	* m^2/sec^5
Vertical Acceleration Error, δa_D	0. m/sec	2.5 m/sec^2	* sec	* m^2/sec^5
Altimeter Bias Error, δy_h	-10.00 m	20.0 m	500. sec	*** m^2/sec^5
Clock Bias Error, δa_1	29.98 m	60.0 m	∞**	7.2×10^{-4} m^2/sec
Clock Drift Error, δa_2	-.30 m/sec	6.0 m/sec	1800. sec	1.0×10^{-4} m^2/sec^3

*Parameters to be varied.

**Clock bias includes a random walk term. This is equivalent to an infinite correlation time.

***Altimeter noise is evaluated as a function of estimated altitude (See Eq. 5.47)

measurements are taken sequentially. Over the 1.25 second measurement interval, the aircraft can move 300 meters. Acceleration states were included also. If accelerations are not included, only an uncorrelated* random acceleration can be modeled in a Kalman filter. Aircraft accelerations are assumed to be correlated in time with correlation times ranging from one second to one minute depending on the flight profile [51] [68]. The shorter correlation times apply to atmospheric turbulence while the longer correlation times are appropriate for slow turns. Evasive maneuvers are modeled typically with correlation times from ten to thirty seconds. Inclusion of the acceleration states permits modeling the acceleration as a correlated random variable. In addition, the estimated accelerations can be used to improve the aircraft state prediction.

As implemented, the actual filter states represent the errors in the assumed position, velocity, and acceleration. The aircraft state is expressed in the Topocentric-North-East-Down (TNED) coordinate system where the origin of the coordinate system is located at the user's a priori position. (See App. A.) The a priori user position vector in the TNED system is identically zero. The precise formulation of the filter model follows.

5.2.2 Aircraft model. The model for the aircraft will be developed for one dimension. Identical models are implemented for all

*Unless specified otherwise, correlation will imply correlation in time.

aircraft directions although specific values of the model parameters need not be identical. For the one-dimensional case, the states will include position r or position error δr; velocity v or velocity error δv; and acceleration a or acceleration error δa. A nominal state is defined to include the nominal position $\bar{r}$, the nominal velocity $\bar{v}$, and the nominal acceleration $\bar{a}$. The relationship between the true state vector $\underline{x}$, the nominal state vector $\underline{\bar{x}}$, and the perturbation state vector $\underline{\delta x}$ is as follows:

$$\underline{x} = \begin{bmatrix} r \\ v \\ a \end{bmatrix} = \underline{\bar{x}} + \underline{\delta x} = \begin{bmatrix} \bar{r} + \delta r \\ \bar{v} + \delta v \\ \bar{a} + \delta a \end{bmatrix} \tag{5.1}$$

The goal of the following development is to determine a linear system model suitable for Kalman filter application. In matrix-vector notation, a linear model has the form

$$\dot{\underline{x}} = A(t)\underline{x} + B(t)\underline{u} \tag{5.2}$$

where: $\underline{x}$ is the state vector which, for navigation algorithms, usually includes a position error, a velocity error, and an acceleration error, and
$B(t)\underline{u}$ is a random forcing function.

There are many assumptions that can be made in the development of the basic system model. Changing any of the assumptions may result in a different system model or different expressions for the parameters of the model. In the following, a specific sequence of assumptions,

intuitive approximations, and engineering decisions will be outlined. The result is a system model that has been numerically tested with good results. In addition, the model has some characteristics that make it desirable for sequential filter applications. Perhaps the most desirable characteristic of the model is that the gain terms have non-zero steady-state values. Other intuitively pleasing characteristics include:

1. The model approximates exponentially correlated acceleration;

2. There is a finite upper limit on acceleration uncertainty;

3. The exponentially correlated model has a finite power spectrum.

For the one-dimensional case, the prescribed system model will consist of position r, velocity v, and acceleration a. The governing equations for the prescribed model are as follows:

$$\dot{r} = v, \quad r(t_k) = r_k$$

$$\dot{v} = a, \quad v(t_k) = v_k \tag{5.3}$$

where: a is a random variable with statistics

$$E[a(t)] = a(t_k) = a_k \tag{5.4a}$$

$$E[(a(t) - E[a(t)])(a(\tau) - E[a(\tau)])]$$

$$= \sigma_m^2 \exp(-\beta|t - \tau|) \tag{5.4b}$$

Some remarks on Eqs. 5.3 and 5.4 are in order. If one considers the set of all possible realizations of a system, then at $t = t_k$ the state can only be specified in terms of the mean and covariance of the entire set. A subset can be defined, however, which consists of all members of the set whose state at $t = t_k$ has the realization r_k, v_k, and a_k. It is this subset which constitutes the ensemble described by Eqs. 5.3 and 5.4.

The filter model to be developed from Eqs. 5.3 and 5.4 is used for each of the three aircraft directions. No correlation between the directions is assumed. The model will be referred to as an acceleration dead-reckoning model with exponentially correlated random acceleration. A random variable with the a oriori statistics described by Eq. 5.4b will be referred to as an exponentially correlated random variable (ECRV).

The solutions to Eqs. 5.3 are given by [5:Par. 2-3]:

$$r(t) = r_k + v_k(t - t_k) + \int_{t_k}^{t} a(s)\,(t - s)\,ds \qquad (5.5)$$

$$v(t) = v_k + \int_{t_k}^{t} a(s)\,ds \qquad (5.6)$$

where: the integrals are stochastic integrals.

If the nominal state is defined to be the mean solution to Eq. 5.3, then taking the expectation of Eqs. 5.5 and 5.6 yields

$$\bar{r}(t) = E[r(t)]$$

$$= r_k + v_k(t - t_k) + \frac{a_k(t - t_k)^2}{2} \qquad (5.7)$$

$$\bar{v}(t) = E[v(t)] = v_k + a_k(t - t_k) \qquad (5.8)$$

Unfortunately, the statistics of Eqs. 5.4 cannot be accommodated by a Kalman filter. The system models of Eqs. 5.3 and 5.4 can, however, be transformed into a model that satisfies the uncorrelated noise restriction of the Kalman filter. This transformation is accomplished by adding to Eq. 5.3 an acceleration state which is driven by a white noise forcing function. This "augmented state" method is referred to as Wiener-Kolmogorov whitening in Singer [68]. Bucy and Joseph [69:147] refer to the method as the Bode-Shannon technique of approximating the spectral density. The method is an application of a theorem quoted by Kalman [8:45] that "Given any random process with mean $E[x(t)]$ and covariance $E[x(t)x(\tau)]$, there exists a unique Gaussian random process with the same mean and covariance."

The transformation of the random process of Eqs. 5.4 can be accomplished by using the Wiener-Khintchine theorem which states that the autocorrelation function and the power spectrum form a Fourier transform pair [70:431]. The power spectrum of white noise is given by

$$F_w(j\omega) = \int_{-\infty}^{\infty} \exp(-j\omega z) q_a \delta(z)\, dz = q_a \qquad (5.9)$$

where: q_a is the spectral density of the white noise; and

δ is the Dirac delta function.

The power spectrum of the ECRV of Eqs. 5.4 is derived as follows:

$$F_o(j\omega) = \int_{-\infty}^{\infty} \exp(-j\omega z)\sigma_m^2 \exp(-\beta|z|)\, dz$$

$$= \frac{2\beta\sigma_m^2}{(\beta - j\omega)(\beta + j\omega)} \tag{5.10}$$

The transfer function of the shaping filter can be derived from Eqs. 5.9 and 5.10 as follows [67] [69:271]:

$$F_o(j\omega) = \frac{2\beta\sigma_m^2}{(\beta - j\omega)(\beta + j\omega)}$$

$$= \frac{1}{\beta + j\omega} \frac{1}{\beta - j\omega} q_a \tag{5.11}$$

$$= F_s(j\omega) F_s(-j\omega) F_w(j\omega) \tag{5.12}$$

The transfer function of the shaping filter is obtained by setting $j\omega = s$ to obtain the Laplace transform.

$$F_s(s) = \frac{1}{s + \beta} \tag{5.13}$$

The time domain representation of the shaping filter is given by

$$\delta\dot{a} = -\beta\delta a + w_a, \quad \delta a(t_k) = 0 \tag{5.14}$$

$$\dot{\bar{a}} = 0, \quad \bar{a}(t_k) = a_k \tag{5.15}$$

where: w_a is a white noise forcing function with statistics

$$E[w_a] = 0$$

$$E[w_a(t)w_a(\tau)] = 2\beta\sigma_m^2\delta(t - \tau) = q_a\delta(t - \tau) \quad (5.16)$$

The mean of Eq. 5.4a is satisfied by $\bar{a}$ using Eq. 5.15. The mean of δa must therefore be zero. By specifying zero initial condition and zero mean white noise, the mean of δa is zero and the mean of the shaping filter satisfies Eq. 5.4a. Note that if the acceleration a were modeled in Eq. 5.14 instead of δa, then the mean of Eq. 5.4a would not be satisfied. It will be shown (Par. 5.2.4) that the correlation function of Eq. 5.4b is satisfied under certain conditions.

Equations 5.14 and 5.15 describe the random variable $a = \bar{a} + \delta a$ as a constant with a region of uncertainty given by

$$\sigma_a^2(t) = \sigma_a^2(t_k)\exp(-2\beta(t - t_k)) + \frac{q_a}{2\beta}[1 - \exp(-2\beta(t - t_k))] \quad (5.17)$$

where: $q_a = 2\beta\sigma_m^2$.

Equation 5.17 will be derived later in this chapter.

Figure 5.1 illustrates the random variable a with regions of uncertainty based on a value of σ_m^2 and two values of correlation time. Initial uncertainty $\sigma_a^2(t_k)$ is assumed to be zero. Figure 5.1 also illustrates the result of an estimation of acceleration at a time t_{k+1} which results in an estimate $\hat{a}_{k+1}$ and an a posteriori

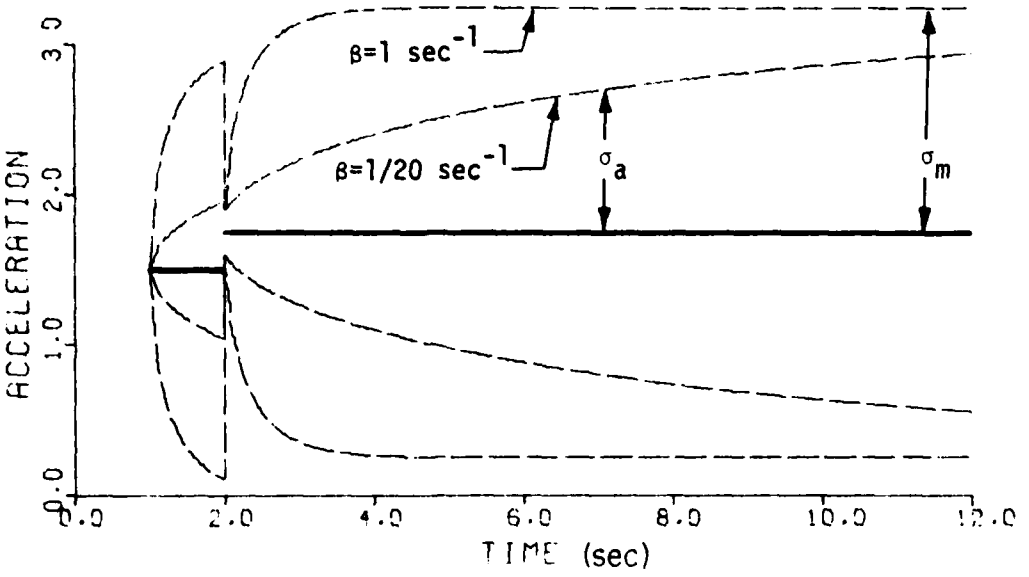

Figure 5.1 Exponentially Correlated Random Acceleration Covariance Propagation.

variance of $\sigma_a^2(t_{k+1})$. Note that the region of uncertainty has a finite steady state value equal to σ_m .

More details on shaping filters are available in Sorenson and Stubberud [65:15-20], Kochenburger [71:434-439], Wiener [7:Chap. 2], and Laning and Battin [72:217-218].

If the random variable $a = \bar{a} + \delta a$ is substituted into Eqs. 5.5 and 5.6, and the expectation operator applied, then Eqs. 5.7 and 5.8 will remain valid. If the state vector is to consist of δr and δv, the error quantities, then Eqs. 5.3 become

$$\dot{\bar{r}} + \delta\dot{r} = \bar{v} + \delta v, \quad \bar{r}(t_k) + \delta r(t_k) = r_k \qquad (5.18)$$

$$\dot{\bar{v}} + \delta\dot{v} = \bar{a} + \delta a, \quad \bar{v}(t_k) + \delta v(t_k) = v_k \qquad (5.19)$$

Equations 5.18 and 5.19 can be separated as follows:

$$\dot{\bar{r}} = \bar{v}, \quad \bar{r}(t_k) = r_k \tag{5.20}$$

$$\dot{\bar{v}} = \bar{a}, \quad \bar{v}(t_k) = v_k \tag{5.21}$$

$$\delta\dot{r} = \delta v, \quad \delta r(t_k) = 0 \tag{5.22}$$

$$\delta\dot{v} = \delta a, \quad \delta v(t_k) = 0 \tag{5.23}$$

The system defined by Eqs. 5.15, 5.20, and 5.21 has the mean solution of Eqs. 5.4, 5.7, and 5.8. The filter model is given by Eqs. 5.14, 5.16, 5.22, and 5.23. Note that the statistics of the filter model, Eq. 5.16, are consistent with the restrictions of the Kalman filter.

5.2.3 Summary of the aircraft model equations. In summary, the specified aircraft model of Eqs. 5.3 and 5.4

$$\dot{r} = v, \quad r(t_k) = r_k \tag{5.3}$$

$$\dot{v} = a, \quad v(t_k) = v_k \tag{5.4a}$$

where:

$$E[a(t)] = a(t_k) = a_k$$

$$E[(a(t) - E[a(t)])(a(\tau) - E[a(\tau)])]$$

$$= \sigma_m^2 \exp(-\beta|t-\tau|) \tag{5.4b}$$

is whitened to determine a form compatible with the Kalman-Bucy filter. The mean state propagates according to Eqs. 5.4a, 5.7, and 5.8.

$$\bar{r}(t) = r_k + v_k(t-t_k) + a_k(t-t_k)^2/2 \qquad (5.7)$$

$$\bar{v}(t) = v_k + a_k(t-t_k) \qquad (5.8)$$

$$\bar{a}(t) = a_k \qquad (5.4a)$$

The state used by the filter is governed by Eqs. 5.14, 5.16, 5.22, and 5.23.

$$\delta\dot{r} = \delta v, \qquad \delta r(t_k) = 0 \qquad (5.22)$$

$$\delta\dot{v} = \delta a, \qquad \delta v(t_k) = 0 \qquad (5.23)$$

$$\delta\dot{a} = -\beta\,\delta a + w_a, \qquad \delta a(t_k) = 0 \qquad (5.14)$$

where: $E[w_a] = 0$

$$E[w_a(t)w_a(\tau)] = 2\beta\,\sigma_m^2\delta(t-\tau) \qquad (5.16)$$

In matrix form, the filter model is

$$\dot{\underline{x}} = A\underline{x} + B\underline{u} \qquad (5.2)$$

$$\underline{x}^T = [\delta v,\ \delta r,\ \delta a] \qquad (5.24)$$

$$A = \begin{bmatrix} 0 & 1 & 0 \\ 0 & 0 & 1 \\ 0 & 0 & -\beta \end{bmatrix} \qquad (5.25)$$

$$B\underline{u} = \begin{bmatrix} 0 \\ 0 \\ w_a \end{bmatrix} \qquad (5.26)$$

5.2.4 Proof of the shaping filter. It will now be shown that the random process which is the solution to the shaping filter of Eqs. 5.14, 5.15, and 5.16 duplicates the mean and covariance of Eq. 5.4. The solution to Eq. 5.14 for arbitrary $\delta a(t_k)$ is

$$\delta a(t) = \delta a(t_k)\exp[-\beta(t-t_k)] + \int_{t_k}^{t} w_a(s)\exp[-\beta\ (t-s)]ds \qquad (5.27)$$

where: the integral is a stochastic integral.

The solution of the random process $a = \bar{a} + \delta a$ is given by

$$a(t) = a_k + \delta a(t_k)\exp[-\beta(t-t_k)] + \int_{t_k}^{t} w_a(s)\exp[-\beta(t-s)]ds \qquad (5.28)$$

Taking the expectation of Eq. 5.28 yields

$$E[a(t)] = E[a_k] + E[\delta a(t_k)]\exp[-\beta(t-t_k)] \qquad (5.29)$$

If at each time t_i the estimate of the acceleration perturbation is set equal to zero and Eq. 5.15 is initialized with an unbiased estimate of acceleration, then Eq. 5.29 yields

$$E[a(t)] = a_k$$

The mean statistic of Eq. 5.4a is therefore satisfied.

The covariance kernel is determined by

$$P(t,\tau) = E[(a(t)-E[a(t)])(a(\tau)-E[a(\tau)])] \tag{5.30}$$

Using Eqs. 5.28 and 5.29 gives

$$P(t,\tau) = \int_{t_k}^{t}\int_{t_k}^{\tau} E[w_a(s)w_a(r)]\exp(-\beta(t-s))\exp(-\beta(t-r))drds \tag{5.31}$$

Substituting Eq. 5.16 into Eq. 5.31

$$P(t,\tau) = \int_{t_k}^{t}\int_{t_k}^{\tau} 2\beta\sigma_m^2\delta(r-s)\exp(-\beta(t-s))\exp(-\beta(t-r))drds \tag{5.32}$$

Note that the Dirac delta function is zero if $r \neq s$. Assuming that $t \geq \tau \geq t_k$, the upper limit of the outer integral of Eq. 5.32 can be changed to τ since $s > \tau$, $\delta(r-s)$ is equal to zero.

$$P(t,\tau) = \int_{t_k}^{\tau}\int_{t_k}^{\tau} 2\beta\sigma_m^2\delta(r-s)\exp(-\beta(t-s))\exp(-\beta(\tau-r))drds \tag{5.33}$$

At this point, the integral property of the Dirac delta function

$$\int_{t_k}^{\tau} \delta(r-s)g(r)dr = g(s), \quad \text{if } t_k \leq s \leq \tau \tag{5.34}$$

is applied to Eq. 5.33 giving

$$P(t,\tau) = \int_{t_k}^{\tau} 2\beta\sigma_m^2\exp(-\beta(t-s))\exp(-\beta(\tau-s))ds \tag{5.35}$$

Evaluating the integral in Eq. 5.35 yields

$$P(t,\tau) = \sigma_m^2\exp[-\beta(t-\tau)] - \sigma_m^2\exp[-\beta(t-t_k)]\exp[-\beta(\tau-t_k)] \tag{5.36}$$

Equation 5.36 immediately provides the solution to the propagation of the covariance of the acceleration.

$$\sigma_a^2(t_k+\Delta t) = \sigma_m^2[1 - \exp(-2\beta\Delta t)] \qquad (5.37)$$

Unfortunately, Eq. 5.36 does not satisfy the variance statistic of Eq. 5.4b unless $t_k = -\infty$. Satisfaction of this requirement implies that the shaping filter has reached steady state. Accordingly, the initial covariance term for the exponentially correlated acceleration state must be specified as σ_m^2 the steady state variance.

Jazwinski [60:123] also showed that the random process of Eqs. 5.14 *and* 5.16 resulted in an ECRV. He avoided any requirement on $t < 0$ by specifying that the initial condition δa_k was a random variable with mean zero and variance σ_m^2.

This steady state requirement is of greatest concern when an ECRV is to be simulated. In a simulation, either the initial condition must be a random variable with zero mean and variance σ_m^2 or the process should be run for several time constants (correlation times) before exponential correlation is required. In filter model applications, the initial time is the time of the last measurement and almost never has a variance equal to σ_m^2 nor is the time between measurements likely to be several time constants. Despite this discrepancy in the rigorous sense, the state augmentation method will be used because it is easily implemented. It should be noted that the assumption of exponential correlation is itself an approximation.

5.2.5 State transition matrix and covariance matrix propagation. As implemented in the filter, the covariance matrix is propagated using the concepts of Par. 4.5.

$$\dot{\Phi}(t,t_k) = A(t)\Phi(t,t_k), \quad \Phi(t_k,t_k) = I \tag{5.38}$$

$$\dot{\Gamma}(t) = A(t)\Gamma + \Gamma A^T(t) + B(t)Q(t)B^T(t), \; \Gamma(t_k) = 0 \tag{5.39}$$

$$\bar{P}(t_{k+1}) = \Phi(t_{k+1},t_k)P(t_k)\Phi^T(t_{k+1},t_k) + \Gamma(t_{k+1}) \tag{5.40}$$

If the correlation times and the measurement interval Δt are fixed, Eqs. 5.38 and 5.39 can be solved analytically. The results, with $t_{k+1} = t_k + \Delta t$, are:

$$\Phi(t_k+\Delta t,t_k) = \begin{bmatrix} 1 & t & \phi_{ra}(\beta) \\ 0 & 1 & \phi_{va}(\beta) \\ 0 & 0 & \phi_{aa}(\beta) \end{bmatrix} = \begin{bmatrix} 1 & t & [1 + \beta\Delta t + \exp(-\beta\Delta t)]/\beta^2 \\ 0 & 1 & [1 - \exp(-\beta\Delta t)]/\beta \\ 0 & 0 & \exp(-\beta\Delta t) \end{bmatrix} \tag{5.41}$$

$$\Gamma(t_k+\Delta t) = \begin{bmatrix} q_r\Delta t + q_v\frac{\Delta t^3}{3} + q_a\gamma_{rr}(\beta) & q_v\frac{\Delta t^2}{2} + q_a\gamma_{rv}(\beta) & q_a\gamma_{ra}(\beta) \\ q_v\frac{\Delta t^2}{2} + q_a\gamma_{rv}(\beta) & q_v\Delta t + q_a\gamma_{vv}(\beta) & q_a\gamma_{va}(\beta) \\ q_a\gamma_{ra}(\beta) & q_a\gamma_{va}(\beta) & q_a\gamma_{aa}(\beta) \end{bmatrix} \tag{5.42}$$

where: q_r, q_v, and q_a are the diagonal elements of the spectral level process noise covariance matrix, BQB^T; and

γ elements are as follows:

$$\gamma_{rr} = [-\exp(-2\beta\Delta t) - 4\beta\Delta t \exp(-\beta\Delta t) + 2(\beta\Delta t)^3/3 - 2(\beta\Delta t)^2 + 2\beta\Delta t + 1]/(2\beta^5)$$

$$= \Delta t^5[1/20 - \beta\Delta t/36 + 5(\beta\Delta t)^2/504 - (\beta\Delta t)^3/360 + 17(\beta\Delta t)^4/25920 - 41(\beta\Delta t)^5/302400 + \ldots]$$

$$\gamma_{rv} = [\exp(-2\beta\Delta t) + (2\beta\Delta t-2)\exp(-\beta\Delta t) + (\beta\Delta t)^2 - 2\beta\Delta t + 1]/(2\beta^4)$$

$$= \Delta t^4[1/8 - \beta\Delta t/12 + 5(\beta\Delta t)^2/144 - (\beta\Delta t)^3/90 + 17(\beta\Delta t)^4/5760 - 41(\beta\Delta t)^5/60480 + \ldots]$$

$$\gamma_{ra} = [-\exp(-2\beta\Delta t) - 2\beta\Delta t \exp(-\beta\Delta t) + 1]/(2\beta^3)$$

$$= \Delta t^3[1/6 - \beta\Delta t/6 + 11(\beta\Delta t)^2/120 - 13(\beta\Delta t)^3/360 + 19(\beta\Delta t)^4/1680 - (\beta\Delta t)^5/336 + \ldots]$$

$$\gamma_{vv} = [-\exp(-2\beta\Delta t) + 4\exp(-\beta\Delta t) + 2\beta\Delta t - 3]/(2\beta^3)$$

$$= \Delta t^3[1/3 - \beta\Delta t/4 + 7(\beta\Delta t)^2/60 - (\beta\Delta t)^3/24 + 31(\beta\Delta t)^4/2520 - (\beta\Delta t)^5/320 + \ldots]$$

$$\gamma_{va} = [\exp(-2\beta\Delta t) - 2\exp(-\beta\Delta t) + 1]/(2\beta^2)$$

$$= \Delta t^2[1/2 - \beta\Delta t/2 + 7(\beta\Delta t)^2/24 - (\beta\Delta t)^3/8 + 31(\beta\Delta t)^4/720 - (\beta\Delta t)^5/80 + \ldots]$$

$$\gamma_{aa} = [1 - \exp(-2\beta\Delta t)]/(2\beta)$$

$$= \Delta t[1 - \beta\Delta t + 2(\beta\Delta t)^2/3 - (\beta\Delta t)^3/3 + 2(\beta\Delta t)^4/15 - 2(\beta\Delta t)^5/45 + \ldots]$$

For convenience, Δt will not be incorporated into the argument list of of the γ elements or the elements ϕ_{ra}, ϕ_{va}, and ϕ_{aa}.

For the discrete process noise matrix Γ the solutions are given both in a closed form and in a power series form. The power series are shown because the analytical expressions are numerically ill-conditioned if $\beta\Delta t$ is small. The state transition matrix can also be numerically ill-conditioned for small $\beta\Delta t$. The power series expressions for the state transition matrix elements are easily formed from Eq. 5.41.

Use of Eqs. 5.41 and 5.42 eliminates the need for numerical integration in the filter implementation. State propagation is accomplished using Eqs. 5.7, 5.8, and 5.4a. Covariance matrix propagation is accomplished using Eq. 5.40 where the state transition matrix and the discrete process noise matrix are pre-calculated.

The GPS filter mechanization includes three independent dimensions, each modeled in accordance with the one-dimensional analysis outlined here. Obviously, the parameters for the three dimensions need not be identical.

5.2.6 Measurement bias state. The measurement bias errors included in the state vector were selected based on the possible magnitudes of the bias errors and their effects on the measurements. The user clock bias and clock drift errors can become unacceptably large unless the user has a calibrated atomic standard. The user clock bias and clock drift errors will cause one-for-one errors in the pseudo-range and pseudo-range-rate measurements respectively. For example, a user with a

flat frequency stability of one part in 10^8 on an Allen variance curve will have a clock bias uncertainty equivalent to 10 km after one hour. This implies that the uncertainty of the pseudo-range measurements will be at least 10 km. The pseudo-range-rate measurement will have an uncertainty of 3 m/sec.

Altimeter bias errors can also become large although they do not take on the unbounded character that the clock errors can have. Cole [73] provided an analysis of a 300 millibar pressure surface which is near the 9 km level. Standard deviations of the distance-correlated data ranged from 90 meters to 180 meters. Standard deviations for time-correlated data ranged from 40 meters for one-half hour to 60 meters for four hours. Lear [56] analyzed atmospheric data and, for a 9 km level, determined a standard deviation of 315 meters with sea level pressure updates and a standard deviation of 340 meters if no sea level pressure updates are used.

The altimeter bias error was included as a state because:

1. Expected errors are on the order of the ambiquity in the C/A PRN code;
2. The altimeter bias error is a correlated error;
3. The effect on the altimeter measurement is one-for-one, i.e., a one meter bias error leads to a one meter altimeter error in the altimeter measurement.

The state vector could include the various noise sources that contribute to the measurement errors. Since the forcing functions of the simulated error sources are uncorrelated random variables (within

the capabilities of the random number generator), a filter that includes all the simulated error sources could be designed within the restrictions of a Kalman filter. For simplicity, however, a single state for each of the measurement biases was assumed adequate.

5.2.7 Measurement bias error models and statistics. To properly evaluate the performance of the aircraft model, the measurement bias models and statistics used in the filter should closely match the models and statistics used in the simulation within the constraints of the filter. To corrupt the measurement bias model statistics would cause non-optimal filter performance even if a perfect aircraft model is available. Using the best information for the measurement bias models places the burden of performance on the aircraft model.

The simulated clock drift used only an exponentially correlated noise term. The filter model for the clock drift used the correlation time that was used in the simulation and a state model identical to the aircraft acceleration model. The spectral level process noise was adjusted so that the discrete process noise resulted in a value equal to the variance of the simulated forcing function. The clock drift forcing function of Eq. 3.21 has the form

$$\sigma_f[1 - \exp(-2\beta_f \Delta t)]^{1/2} w_f$$

where: σ_f is the standard deviation of the clock drift;

β_f is the inverse correlation time of the clock drift;

Δt is the time interval (1.25 sec); and

w_f is a random number, N(0,1).

The discrete process noise for an ECRV from Eq. 5.37 is

$$\gamma_f = \frac{q_f}{2\beta_f} \left(1 - \exp(-2\beta_f \Delta t)\right)$$

The spectral noise q_f required to match the simulated ECRV is therefore

$$q_f = 2\,\beta_f \sigma_f^2 \tag{5.43}$$

which is the result for an ECRV at steady state.

The formulation of the filter model automatically accounts for the effect of clock drift errors on clock bias errors. The simulation, however, also included a random walk term as an additional clock bias error source. For a random walk, the relationship between the discrete process noise and the spectral level process noise is represented by

$$\gamma = q\Delta t \tag{5.44}$$

Since the simulation used the forcing function $\sigma_b\,\omega_b$ (see Eq. 3.20) the requirement to match the simulation of the random walk is

$$q_b = \sigma_b^2/\Delta t \tag{5.45}$$

The simulated altimeter bias included errors from two sources: a sea level bias error and a distance correlated term. In the filter, the altimeter bias error is modeled as an ECRV with a constant correlation time of 500 seconds. The correlation time associated with the

simulated correlation distance of 100 km and the maximum aircraft speed of 240 m/sec is 417 seconds. As in the clock drift term, the relation between the spectral level noise and the standard deviation used in the simulation is

$$q_h = 2\beta_h\sigma_{h_2}^2$$

where: $\sigma_{h_2}^2$ is defined in Eqs. 3.40 and 3.42.

For the altimeter, the variance of the correlated error was specified as a function of altitude in the simulation. The filter model used the same function to determine the variance of the altimeter bias noise magnitude. It should be noted that this violates the assumption of stationarity implied in the development of the state augmentation method since the statistics are a function of altitude. Again, this failure of the method in the rigorous sense will be overruled based on engineering judgement.

The portion of the model that is associated with the measurement bias states can be described independently of the aircraft model. In the following, a summary of the measurement bias model is given which includes the values of the parameters selected to match the simulated biases. The differential equation for the measurement biases is:

$$\frac{d}{dt}\begin{bmatrix}\delta y_h\\ \delta a_1\\ \delta a_2\end{bmatrix} = \begin{bmatrix}-\beta_h & 0 & 0\\ 0 & 0 & 1\\ 0 & 0 & -\beta_f\end{bmatrix}\begin{bmatrix}\delta y_h\\ \delta a_1\\ \delta a_2\end{bmatrix} + \begin{bmatrix}u_h\\ u_b\\ u_f\end{bmatrix}$$

$$= \begin{bmatrix}-1/500 & 0 & 0\\ 0 & 0 & 1\\ 0 & 0 & -1/1800\end{bmatrix}\begin{bmatrix}\delta y_h\\ \delta a_1\\ \delta a_2\end{bmatrix} + \begin{bmatrix}u_h\\ u_b\\ u_f\end{bmatrix} \qquad (5.46)$$

The statistics for the filter assumed process noise terms are given by:

$$E[u_h] = 0$$

$$E[u_h(t)u_h(\tau)] = q_h\delta(t-\tau)$$

$$= 2(1/500)(2.7^2 + (.0035\ h(t))^2)\delta(t-\tau)$$

$$= .002916\ \delta(t-\tau)\ m^2/sec^2 \qquad (5.47)$$

where: the altimeter statistic is evaluated at zero altitude.

The clock bias noise term for the simulated random walk has statistics:

$$E[u_b] = 0$$

$$E[u_b(t)u_b(\tau)] = q_b\delta(t-\tau) = .0072\ \delta(t-\tau)\ m^2/sec^2 \qquad (5.48)$$

The clock drift filter statistics are given by

$$E[u_f] = 0$$

$$E[u_f(t)u_f(\tau)] = q_f\delta(t-\tau) = .0001\ \delta(t-\tau)\ m^2/sec^4 \quad (5.49)$$

The state transition matrix for the measurement bias portion of the model is

$$\Phi(t+\Delta t,t) = \begin{bmatrix} \phi_{aa}(\beta_h) & 0 & 0 \\ 0 & 1 & \phi_{va}(\beta_f) \\ 0 & 0 & \phi_{aa}(\beta_f) \end{bmatrix}$$

$$= \begin{bmatrix} .9975 & 0 & 0 \\ 0 & 1 & 1.24956 \\ 0 & 0 & .99931 \end{bmatrix} \quad (5.50)$$

where: the terms ϕ_{aa} and ϕ_{va} refer to the results described in Eq. 5.41.

The discrete process noise matrix for the measurement bias model is

$$\Gamma = \begin{bmatrix} q_h\gamma_{aa}(\beta_h) & 0 & 0 \\ 0 & q_b\Delta t + q_f\gamma_{vv}(\beta_f) & q_f\gamma_{va}(\beta_f) \\ 0 & q_f\gamma_{va}(\beta_f) & q_f\gamma_{aa}(\beta_f) \end{bmatrix}$$

$$= \begin{bmatrix} .0364 & 0 & 0 \\ 0 & 9.651\times10^{-4} & 7.807\times10^{-5} \\ 0 & 7.807\times10^{-5} & 1.249\times10^{-4} \end{bmatrix} \quad (5.51)$$

The initial errors and the initial covariance matrix are given in Table 5.1.

5.3 Measurement Rejections

To simulate signal dropouts and measurement rejections, the measurements are randomly rejected. Satellite measurements are rejected five percent of the time and altimeter measurements are rejected two percent of the time. When a measurement is rejected, the covariance matrix is propagated and the state is predicted based on the *a priori* information. Therefore, the contributions to the performance measures listed below are due solely to *a priori* data when a measurement is rejected.

5.4 Uncorrelated Measurement Noise

To simulate uncorrelated measurement noises, the filter test program adds Gaussian noise to the satellite indicated clock time, the pseudo-range-rate measurement, and the altimeter measurement. The standard deviations of these uncorrelated noises are as in Table 5.2.

Table 5.2 Additional Gaussian Measurment Noise

	Standard Deviation
Indicated Satellite Time	1. meters (∿3.33 nsec)
Pseudo-Range-Rate	.02 m/sec (.0667 nsec/sec)
Altimeter	20. meters

The filter assumed the measurements to have uncorrelated noise with the standard deviations of Table 5.3. The assumed noise magnitudes of Table 5.3 should bound the values in Table 5.2.

Table 5.3 Measurement Noise Assumed by the Filter

	Standard Deviation
Pseudo-Range	$(25. + 6.25\ \csc^2 el)^{1/2}$ meters
Psuedo-Range-Rate	.1 m/sec
Altimeter	$(400 + h^2 \times 10^{-6})^{1/2}$ meters

5.5 Testing the Selected Model

5.5.1 *Independent variables for sensitivity studies*. The model has been selected and must be tested using the simulation of Chapter 3. Values have been assigned to most of the model parameters. The measurement bias model parameters are specified to match the simulated biases. (See Para. 5.2.7.) The initial condition statistics for both the aircraft and the measurement states are chosen to be consistent with the errors in the initial state. The aircraft inverse correlation times β and the maneuver variances σ_m^2 (or the spectral level aircraft noise $q_a = 2\beta\sigma_m^2$) remain to be specified. Values of correlation time and maneuver variance will be identical for all aircraft dimensions. This will decrease the number of variables considered in the sensitivity analysis.

Prior to proceeding with the sensitivity study, limits on the values of maneuver variance and correlation time were selected.

Correlation time limits were one second to 50 seconds based on suggestions in Singer [68], Hampton [74], and Kanyuck [75]. Singer used a probability density function as in Figure 5.2a and arrived at the variance

$$\sigma_m^2 = a_{max}^2[1 + 4\,P(a_{max}) - P(0)]/3 \qquad (5.52)$$

Asher [76] suggested the use of a double triangular density as in Figure 5.2b to arrive at

$$\sigma_m^2 = (a_{max}^2 + a_{max}\,a_m + a_m^2)/6 \qquad (5.53)$$

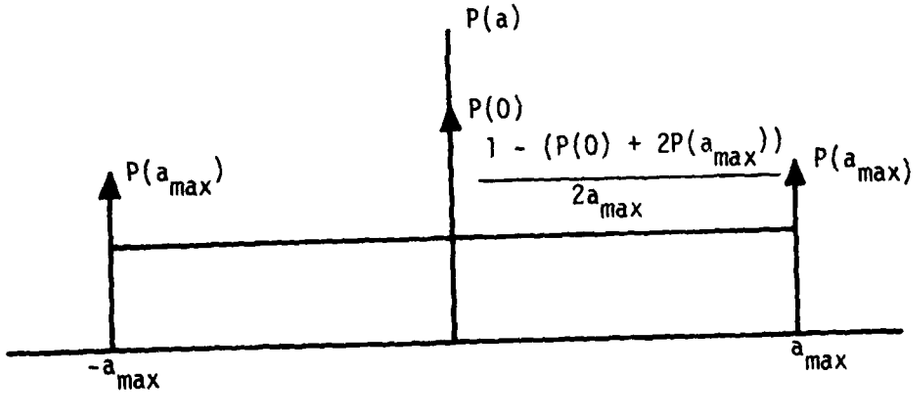

Figure 5.2a Acceleration Probability Density (Singer [68])

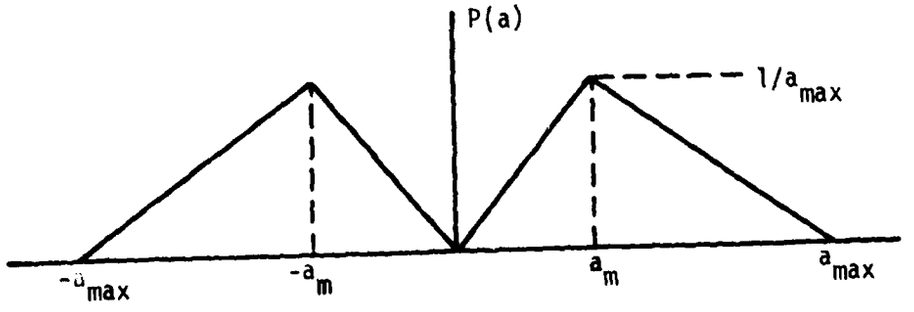

Figure 5.2b Acceleration Probability Density (Asher [76])

The possibilities are limitless. An upper limit on maneuver variance was chosen by assuming a density function as follows:

$$P(a) = \frac{1}{2}, \quad a = \pm 1.5 \text{ m/sec}^2$$

$$= 0, \quad a \neq \pm 1.5 \text{ m/sec}^2 \qquad (5.54)$$

The maximum longitudinal acceleration* allowed in the simulation is 1.5 m/sec^2. Knowing this basic fact about the aircraft, the maximum uncertainty for any acceleration estimate should be 1.5 m/sec^2. This can be assumed to be the steady state value for the variance though additional information on flight conditions would change the value. The manuever variance upper limit was chosen, therefore, as 2.25 m^2/sec^4. The lower limit was selected during the optimization process as that value which did not yield acceptable filter performance.

5.5.2 Optimization baseline. The independent variables for optimization of the filter are the correlation time β and the maneuver variance σ_m^2. These parameters will be identical for each aircraft direction. The optimization effort involved analyzing the performance of the filter for the first 600 seconds of flight. This portion of flight is characterized by a maneuvering aircraft trajectory (takeoff and departure) and a worse than average geometry with three satellites visible. A difficulty encountered in the study was the choice of performance

*In the simulation, this acceleration limit applies to longitudinal accelerations but does not necessarily bound the lateral and vertical accelerations.

indicator. No single quantitative value is adequate to rank the performance of the filter with varying parameters. Table 5.4 summarizes the results of the optimization effort using the following performance measures:

1. RSS position error in meters (RSS POS ERR)*: Effectively, the North, East, and Down components are combined for n measurement intervals using

$$\left[\frac{1}{n}\sum_{i=1}^{n}\left[(\hat{x}_N(t_i)-x_N(t_i))^2+(\hat{x}_E(t_i)-x_E(t_i))^2+(\hat{x}_D(t_i)-x_D(t_i))^2\right]\right]^{1/2} \tag{5.55}$$

2. RSS velocity error in m/sec (RSS VEL ERR): Similar to RSS position error except the velocity states and covariances were used.

3. Maximum position component error in meters (MAX POS ERR): This term is the maximum position error that occurs in any component direction. Because of the satellite geometry the North component usually was the source for this term. The value is suffixed with an "E" if the maximum error is in the East direction or with a "D" if the maximum error is in the Down direction.

---

*The parenthetical mnemonics will be used later in this report to represent the corresponding performance indicator.

4. Maximum velocity component error in m/sec (MAX VEL ERR): Similar to maximum position component error except the velocity errors were used.

5. Position RSS error/standard deviation (POS ERR/SIG): The ratio of the RSS position error to RSS position standard deviation. In an ideal situation, this term should be approximately unity indicating that the filter estimates its error accurately, i.e., it is not too conservative nor too optimistic.

6. Velocity RSS error/standard deviation (VEL ERR/SIG): Similar to position RSS error/standard deviation except using the velocity terms.

7. RSS final cycle position error in meters (FIN POS ERR): Similar to RSS position error except the summation applies only for the last cycle of measurements.*

8. RSS final cycle velocity error in m/sec (FIN VEL ERR): Similar to RSS final cycle position error except velocity terms were used.

9. RSS position standard deviation in meters: Similar to RSS position error except the position terms of the covariance matrix were used.

$$\left[\frac{1}{n}\sum_{i=1}^{n}\left(P_{x_N x_N}(t_i) + P_{x_E x_E}(t_i) + P_{x_D x_D}(t_i)\right)\right]^{1/2} \qquad (5.56)$$

*A cycle of measurements includes a pseudo-range and pseudo-range-rate measurement from each satellite and an altimeter measurement.

Table 5.4 Initial Evaluation of Exponentially Correlated Random Acceleration Filter

Maneuver Variance (m^2/sec^4)	Correlation Time (sec)							
	1.00	3.33	5.00	6.25	10.00	20.00	33.33	50.00
RSS Position Error (m)								
2.25	107.20	69.37	63.99	62.11	59.83	58.75	58.75	59.04
.75	163.92	94.03	80.70	75.55	68.60	64.65	64.41	65.40
.375	220.33	122.63	101.57	93.05	81.07	73.86	73.57	75.70
.1875	299.32	165.98	135.01	121.97	103.11	91.38	91.13	94.94
.0225	786.26	455.53	379.77	343.94	285.01	241.35	235.94	243.92
RSS Velocity Error (m/sec)								
2.25	19.18	12.77	11.18	10.55	9.68	9.19	9.17	9.30
.75	24.98	17.19	14.90	13.88	12.31	11.24	11.15	11.40
.375	29.45	20.81	18.06	16.78	14.76	13.32	13.21	13.58
.1875	34.59	25.07	21.89	20.37	17.92	16.17	16.07	16.60
.0225	55.06	43.13	39.38	37.38	33.76	30.90	30.72	31.52
Maximum Position Component Error (m)								
2.25	301.31	183.37	157.20	149.77	147.33	149.19	153.36	157.68
.75	442.08	254.11	214.77	196.33	183.18	180.71	188.04	197.88
.375	575.59	314.87	264.53	241.57	225.84	219.26	224.46	232.84
.1875	760.01	418.98	329.33	298.14	270.84	258.47	260.80	267.47
.0225	1805.84	1081.83	896.48	805.01	659.65	549.08	532.32	548.54
Maximum Velocity Component Error (m/sec)								
2.25	43.44	32.82	30.72	30.13	30.33	30.57	30.48	30.20
.75	54.24	41.66	37.72	35.84	33.00	31.55	31.62	32.78
.375	63.45	47.45	43.82	41.94	38.82	36.74	36.94	37.88
.1875	74.44	52.93	49.32	47.52	44.29	41.87	41.82	42.54
.0225	121.64	91.40	80.82	75.55	67.23	60.14	58.09	58.34
Position RSS Error/Standard Deviation								
2.25	2.06	1.22	1.11	1.07	1.03	1.04	1.07	1.11
.75	3.51	1.86	1.57	1.46	1.33	1.27	1.29	1.34
.375	5.01	2.58	2.10	1.92	1.66	1.53	1.55	1.61
.1875	7.18	3.70	2.96	2.66	2.23	1.98	1.99	2.10
.0225	21.59	11.66	9.53	8.54	6.96	5.81	5.67	5.88

Table 5.4 Initial Evaluation of Exponentially Correlated Random Acceleration Filter (Continued)

Maneuver Variance (m^2/sec^4)	Correlation Time (sec)							
	1.00	3.33	5.00	6.25	10.00	20.00	33.33	50.00
Velocity RSS Error/Standard Deviation								
2.25	2.83	1.39	1.16	1.08	1.02	1.00	1.09	1.20
.75	5.64	2.81	2.28	2.08	1.87	1.73	1.84	2.01
.375	8.67	4.38	3.53	3.19	2.72	2.51	2.63	2.86
.1875	13.24	6.75	5.43	4.88	4.10	3.70	3.82	4.12
.0225	44.76	23.12	18.72	16.78	13.76	11.67	11.46	11.88
RSS Final Cycle Position Error (m)								
2.25	43.01	60.06	59.71	58.95	56.28	50.64	46.01	42.32
.75	24.97	44.96	56.49	44.54	42.62	38.44	34.94	32.25
.375	16.85	32.88	34.82	34.90	34.18	31.53	29.17	27.50
.1875	22.51	18.71	23.61	24.87	26.06	25.66	24.84	24.36
.0225	21.01	80.68	40.40	23.38	12.02	18.48	22.69	26.30
RSS Final Cycle Velocity Error (m/sec)								
2.25	1.11	4.88	5.13	5.17	4.96	4.12	3.39	2.87
.75	2.23	2.59	2.85	2.89	2.81	2.41	2.08	1.86
.375	3.33	1.52	1.91	1.98	2.00	1.82	1.66	1.55
.1875	4.28	.71	1.27	1.37	1.47	1.46	1.40	1.35
.0225	6.97	4.53	1.68	.71	.52	.79	.87	.90
RSS Position Standard Deviation (m)								
2.25	52.03	56.93	57.84	58.07	57.92	56.39	54.70	53.25
.75	46.73	50.70	51.50	51.74	51.78	50.88	49.83	48.92
.375	44.01	47.54	48.30	48.56	48.74	48.24	47.55	46.91
.1875	41.66	44.88	45.63	45.93	46.26	46.14	45.73	45.30
.0225	36.43	39.06	39.87	40.26	40.96	41.53	41.61	41.51
RSS Velocity Standard Deviation (m/sec)								
2.25	6.79	9.17	9.67	9.81	9.82	9.17	8.41	7.74
.75	4.43	6.12	6.54	6.69	6.80	6.51	6.07	5.67
.375	3.40	4.76	5.12	5.27	5.43	5.30	5.02	4.74
.1875	2.61	3.71	4.04	4.18	4.37	4.37	4.21	4.03
.0225	1.23	1.87	2.10	2.23	2.45	2.65	2.68	2.65

10. RSS velocity standard deviation in m/sec: Similar to RSS position standard deviation except the velocity terms of the covariance matrix were used.

The data in Table 5.4 were generated with the approximation $\phi_{12,12} = 1$ whereas the correct value should be $\phi_{12,12} = \exp(-1.25/1800) = .9933$. This discrepancy was corrected for the full flight test runs. In all cases, the differences in performance did not affect the tendencies illustrated in Table 5.4. It was therefore decided that the optimization runs yielded an adequate indication of the sensitivity of the performance to the values specified for σ_m and β. This approximation to $\phi_{12,12}$ was corrected for subsequent tests.

5.5.3 Full flight tests. Based on a qualitative analysis of Tables 5.4, four pairs of maneuver variance and correlation time were chosen for further analysis. The choices are:

Case 1. $\sigma_m^2 = 2.25\ m^2/sec^4$, $1/\beta = 20$ sec; This pair of parameters resulted in low RSS errors and low maximum errors. Also, the ratio of RSS error to standard deviation was near unity. The parameters are representative of a turning aircraft.

Case 2. $\sigma_m^2 = 0.1875\ m^2/sec^4$, $1/\beta = 1$ sec; This pair of parameters provided a good final state estimate. At the final time, the aircraft is climbing to altitude and no turns have been initiated for about 200 seconds. The parameters are representative of cruising flight with some turbulence.

Case 3. $\sigma_m^2 = 0.1875\ m^2/sec^4$, $1/\beta = 20$ sec: This pair of parameters was selected because it has the same maneuver variance as Case 2 and the same correlation time as Case 1.

Case 4. $\sigma_m^2 = 2.25\ m^2/sec^4$, $1/\beta = 1$ sec: This pair of parameters was chosen because it has the same maneuver variance as Case 1 and the same correlation time as Case 2.

Tables 5.5 through 5.8 summarize the performance of Cases 1 through 4. The performance measures for each flight phase are as described in Par. 5.5.2. Figures 5.3 through 5.6 are plots of the estimator errors and the estimator standard deviations for Cases 1 through 4. The errors plotted are the RSS of the errors for an integral number of measurement cycles except for the first 18.75 seconds of Phase 1 when the absolute value of the error is plotted after each measurement interval. The standard deviations are the square roots of the appropriate diagonal elements of the covariance matrix. The plotted standard deviations (dashed lines) are calculated in the same manner as the plotted error curves (solid lines). This plotting method was chosen to reduce storage and computer time. Because of the use of RSS values, two cautions should be observed in the interpretation of the error curves:

1. The plotting method gives a smoother curve than that which would result if the errors after each measurement were plotted.

2. Sign changes are not shown. An important example of a sign change occurs when satellite number 5 crosses its zenith.

At this point, the East position error and the user clock errors change signs. The error curves, however, show only a sudden dip in error.

The entire flight is analyzed using parameters identical to those in Table 5.4 except that the summations are applied only for selected flight phases. The time limits and characteristics of the flight phases are as follows:

Phase 1. $0 \leq T \leq 598.75$ sec; During this portion of flight, the aircraft executes the departure trajectory and begins a cruise to altitude. Three satellites are visible with a poor geometry.

Phase 2. $598.75 < T \leq 1013.75$ sec; Climb to altitude continues. Three satellites are visible and the geometry is poor.

Phase 3. $1013.75 < T \leq 1295.00$ sec; Cruising altitude is reached near the end of this phase of flight. Four satellites are visible. The geometry is very good.

Phase 4. $1295.00 < T \leq 2760.00$ sec; The aircraft is at cruising altitude. Three satellites are visible with an extremely bad geometry near the end of this flight phase.

Phase 5. $2760.00 < T \leq 5100.00$ sec; The aircraft continues its cruise. Three satellites are visible and the geometry improves through this flight phase.

Phase 6. $5100.00 < T \leq 6687.00$ sec; This flight phase includes approach and landing. Three satellites are visible and the geometry is good.

Table 5.5 Case No. 1 Performance ($\sigma_m^2 = 2.25\ m^2/sec^4$, $\beta = 1/20\ sec^{-1}$)

	Flight Phase Final Times (sec)					
	598.75	1013.75	1295.00	2760.00	5100.00	6687.50
RSS POS ERR	58.66	139.66	18.98	236.35	101.07	52.62
RSS VEL ERR	9.18	2.64	.52	2.11	1.81	2.50
MAX POS ERR	149.36	227.49	128.45	672.41	312.17	110.60D
MAX VEL ERR	30.58	6.27	1.85	10.92	13.27	18.62
POS ERR/SIG	1.04	1.75	1.02	.86	1.13	1.65
VEL ERR/SIG	1.00	.36	.14	.30	.31	.66

Table 5.6 Case No. 2 Performance ($\sigma_m^2 = .1875\ m^2/sec^4$, $\beta = 1\ sec^{-1}$)

	Flight Phase Final Times (sec)					
	598.75	1013.75	1295.00	2760.00	5100.00	6687.50
RSS POS ERR	298.96	125.35	18.15	211.17	97.20	50.08
RSS VEL ERR	34.57	2.18	.32	1.08	2.79	3.40
MAX POS ERR	758.56	221.41	122.41	708.81	273.36	105.98
MAX VEL ERR	74.39	4.58	1.30	5.13	2.79	19.98
POS ERR/SIG	7.18	1.66	1.08	.81	1.14	1.66
VEL ERR/SIG	13.24	.85	.22	.40	.31	2.47

Table 5.7 Case No. 3 Performance (σ_m^2 = .1875 m^2/sec^4, β = 1/20 sec^{-1})

	Flight Phase Final Times (sec)					
	598.75	1013.75	1295.00	2760.00	5100.00	6687.50
RSS POS ERR	91.25	133.40	20.00	205.63	100.63	46.02
RSS VEL ERR	16.16	1.45	.32	1.70	.81	2.78
MAX POS ERR	258.69	222.93	133.78	801.10	236.74	168.05
MAX VEL ERR	41.88	2.71	1.48	8.15	5.41	27.41
POS ERR/SIG	1.98	1.79	1.33	.81	1.21	1.54
VEL ERR/SIG	3.70	.48	.26	.51	.36	2.28

Table 5.8 Case No. 4 Performance (σ_m^2 = 2.25 m^2/sec^4, β = 1 sec^{-1})

	Flight Phase Final Times (sec)					
	598.75	1013.75	1295.00	2760.00	5100.00	6687.50
RSS POS ERR	107.12	142.58	18.21	238.38	97.96	56.90
RSS VEL ERR	19.18	3.15	.72	1.75	1.31	3.21
MAX POS ERR	300.99	242.22	123.80	811.31	370.02	107.80D
MAX VEL ERR	43.44	5.77	2.33	8.18	8.80	18.87
POS ERR/SIG	2.06	1.72	.78	.81	1.96	1.73
VEL ERR/SIG	2.83	.46	.15	.26	.23	.70

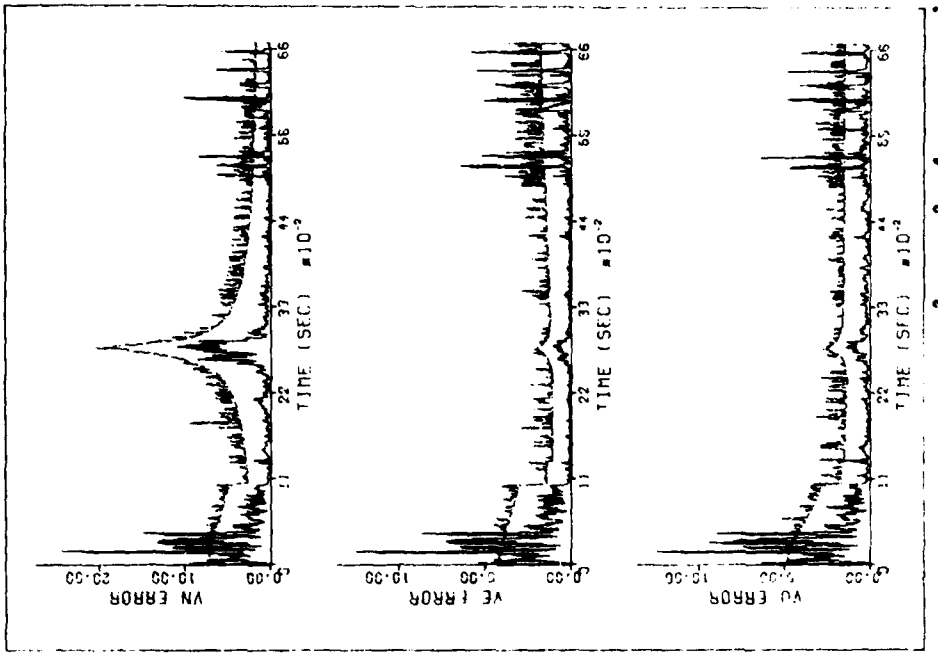

Figure 5.3 Case No. 1 Performance (σ_n^2 = 2.25 m²/sec⁴, β = 1/20 sec⁻¹) (Continued)

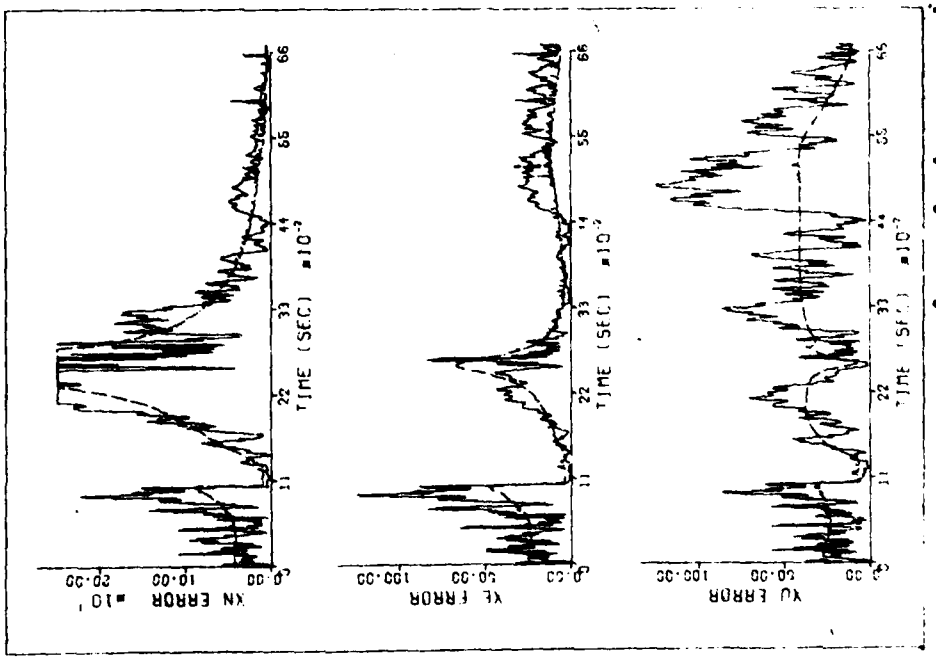

Figure 5.2 Case No. 1 Performance (σ_n^2 = 2.25 m²/sec⁴, β = 1/20 sec⁻¹)

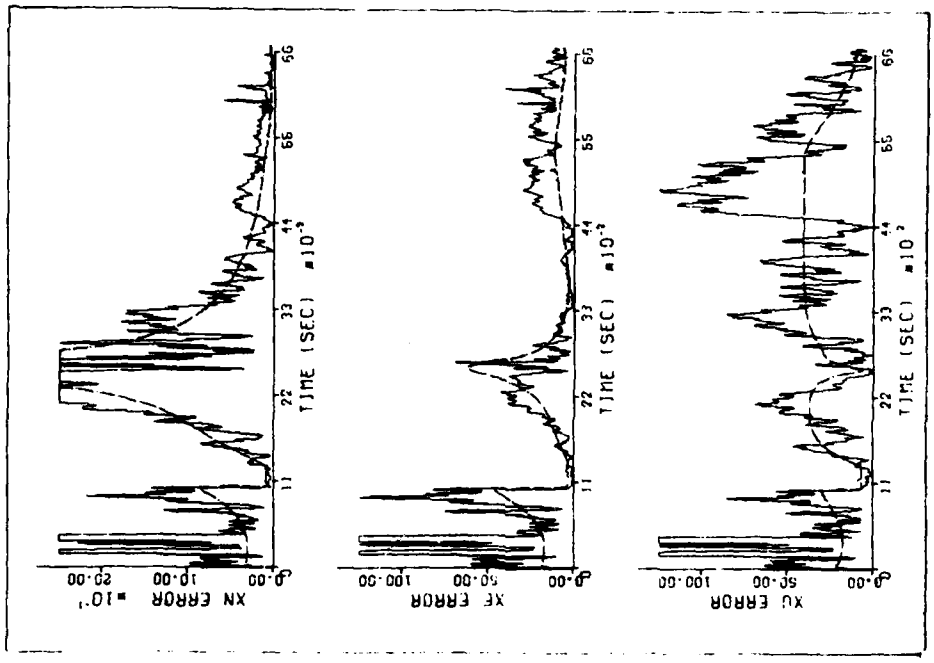

Figure 5.4 Case No. 2 Performance (σ_m^2 = .1875 ft^2/sec^4, β = 1 sec^{-1})

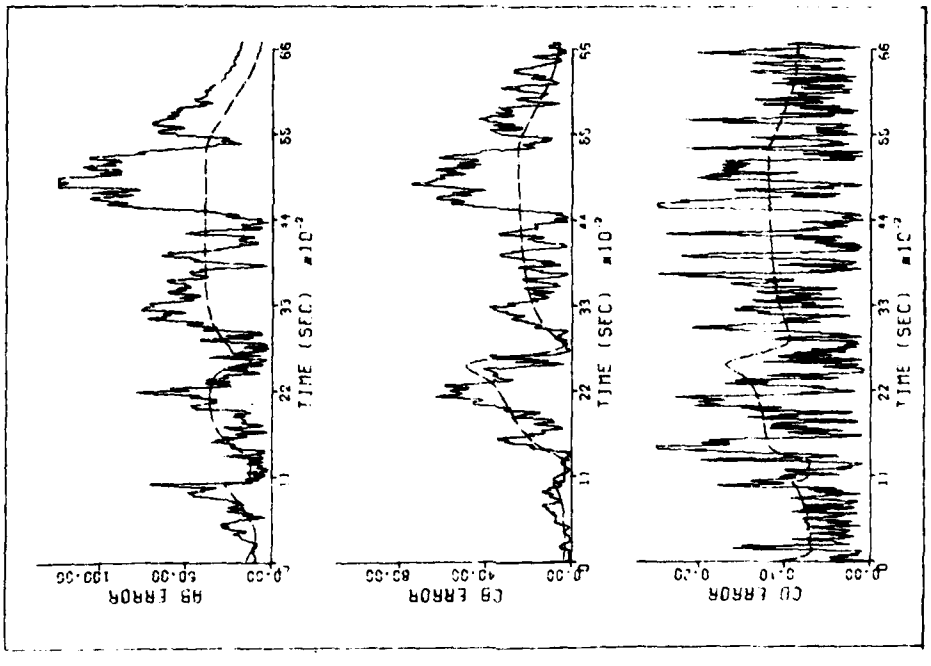

Figure 5.3 Case No. 1 Performance (σ_m^2 = 2.25 ft^2/sec^4, β = 1/20 sec^{-1}) (Continued)

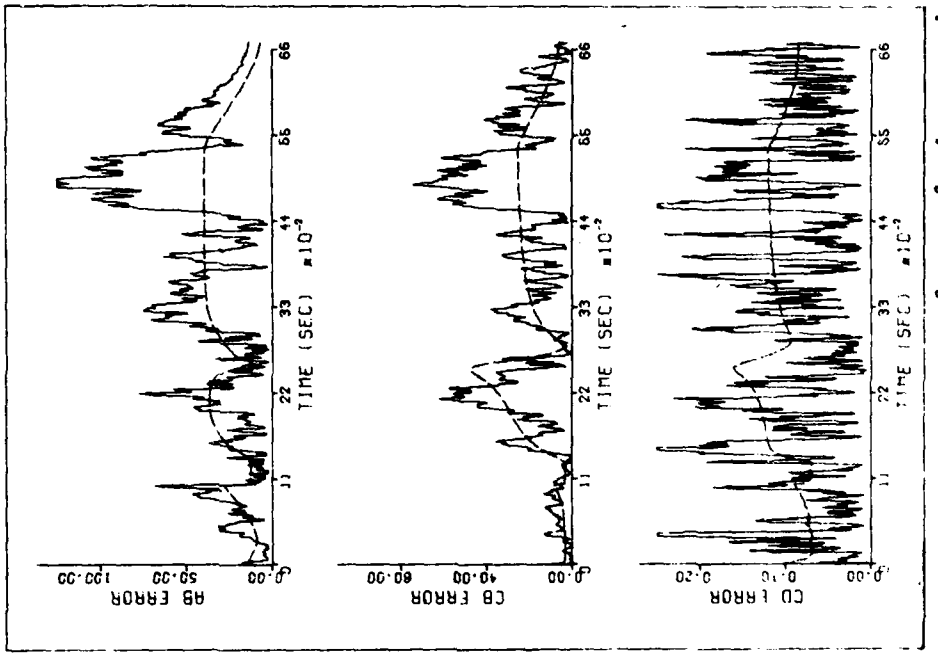

Figure 5.4 Case No. 2 Performance (σ_w^2 = .1875 ft^2/sec^4, β = 1 sec^{-1}) (Continued)

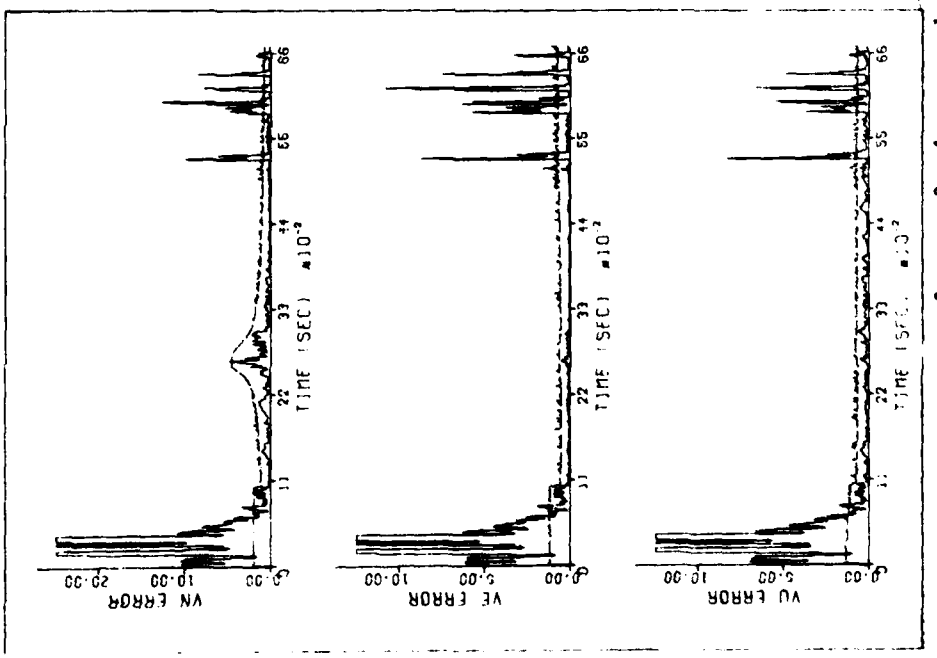

Figure 5.4 Case No. 2 Performance (σ_w^2 = .1875 ft^2/sec^4, β = 1 sec^{-1}) (Continued)

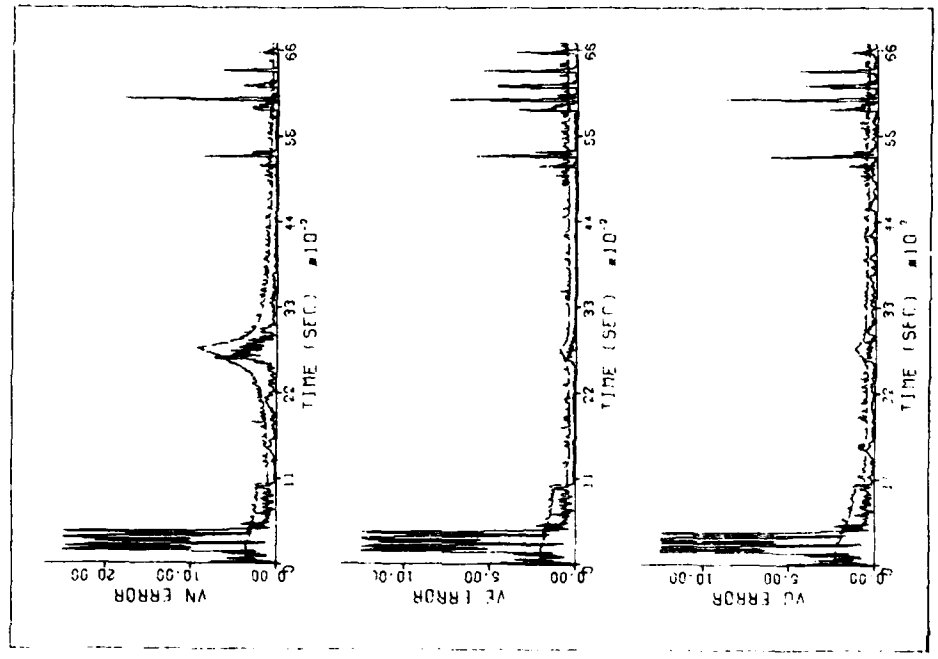

Figure 5.5 Case No. 3 Performance (σ_m^2 = .1875 m^2/sec^4, β = 1/20 sec^{-1}) (Continued)

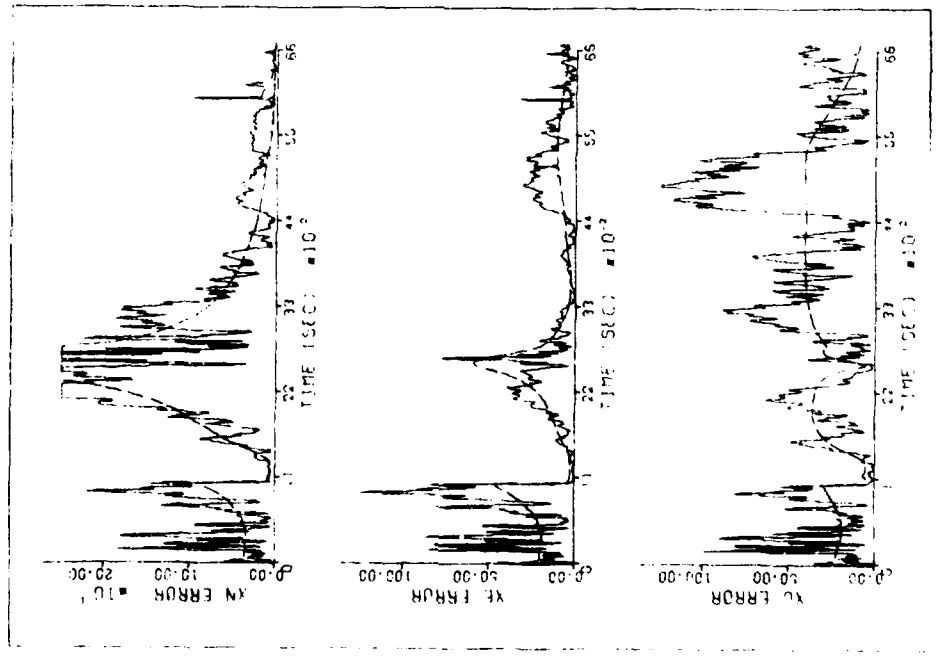

Figure 5.5 Case No. 3 Performance (σ_m^2 = .1875 m^2/sec^4, β = 1/20 sec^{-1})

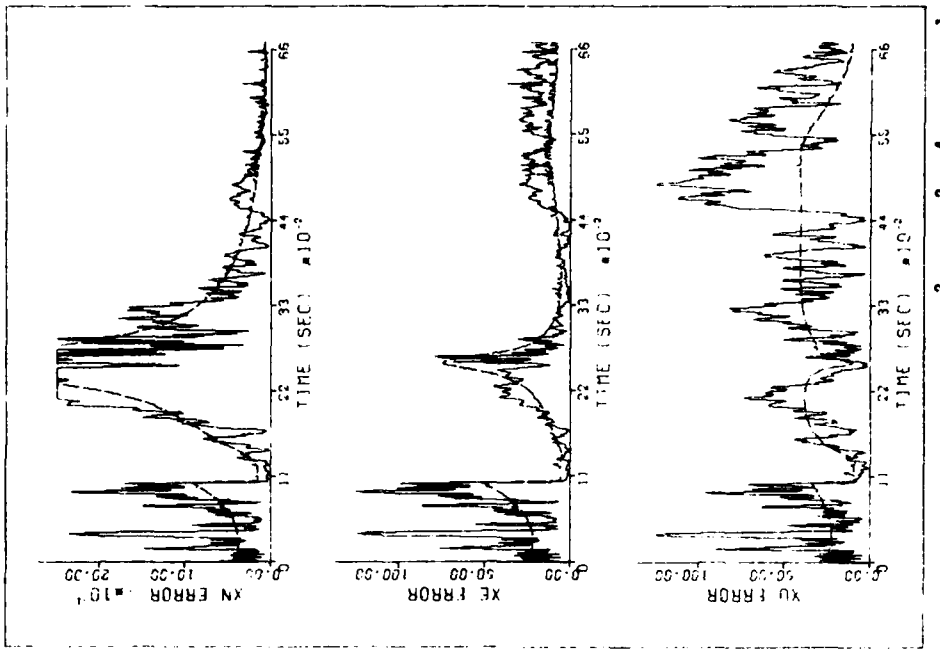

Figure 5.5 Case No. 3 Performance ($\sigma_m^2 = .1875$ m^2/sec^4, $\beta = 1/20$ sec^{-1}) (Continued)

Figure 5.6 Case No. 4 Performance ($\sigma_m^2 = 2.25$ m^2/sec^4, $\beta = 1$ sec^{-1})

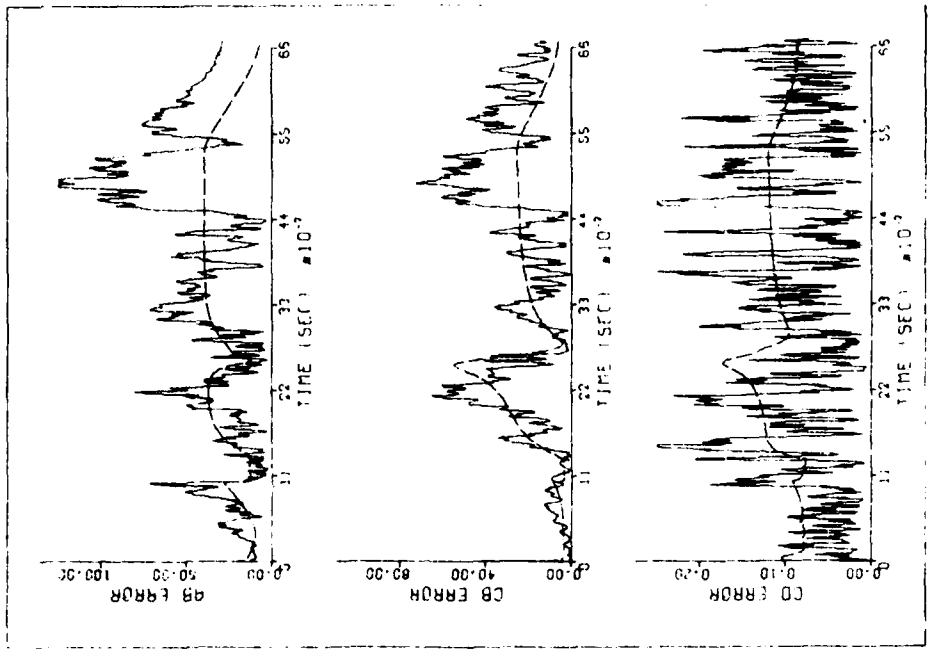

Figure 5.6 Case No. 4 Performance ($\sigma_m^2 = 2.25$ m^2/sec^4, $\beta = 1$ sec^{-1}) (Continued)

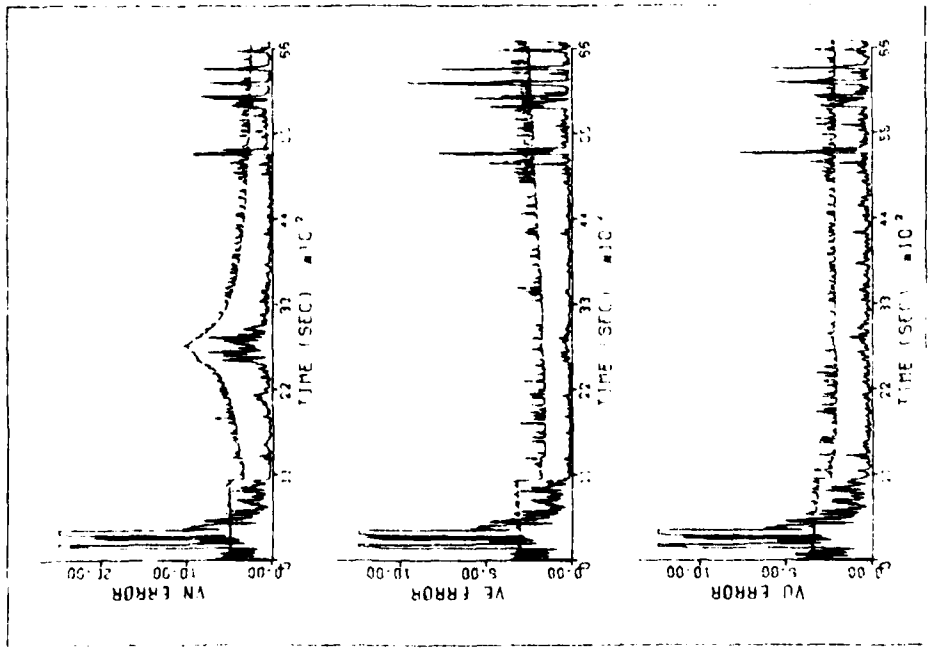

Figure 5.6 Case No. 4 Performance ($\sigma_m^2 = 2.25$ m^2/sec^4, $\beta = 1$ sec^{-1}) (Continued)

5.5.4 Summary of flight tests. This chapter was concerned with the acceleration dead-reckoning navigation algorithm which was based on the assumption that acceleration is an exponentially correlated random variable. The statistical basis of the model was described and its modification into a form suitable for sequential filter implementation was detailed. Following a discussion of measurement bias models, the performance evaluation technique, used throughout this study, was described. These techniques were applied to an evaluation of the ADR filter. The results of this evaluation show that the navigation algorithm had satisfactory performance for a wide range of parameters. A single set of parameters which optimizes all performance indicators for the entire flight cannot be determined. In the following chapters, other algorithms will be tested and their performance will be compared to the performance of the ADR navigation algorithm.

CHAPTER 6

NON-ADAPTIVE MODIFICATIONS

6.1 Discussion of System Model Development

In Chapter 5, a basic system model for the navigation filter was defined. The system model consisted of an assumed aircraft model and an assumed measurement model. The state vector for the aircraft model included the components of the aircraft position vector and the components of the aircraft velocity vector. The components of the aircraft acceleration vector were added to the aircraft state vector under the assumption that the aircraft acceleration could be approximated as an exponentially correlated random process.

A dynamical system, such as an airplane, can be modeled exactly by including the position vector components and the velocity vector components in the system state vector. The accelerations (forces), however, must be completely known and described in the appropriate coordinate system.* In many examples, such as satellite orbit determination, the forces may be known to a high degree of accuracy. Perfect knowledge of the forces, however, never exists in real-world applications.

---

*At this point in the discussion, filter restrictions on the form of the acceleration model are immaterial.

If the unknown and unmodeled forces* are random and uncorrelated, the Kalman filter can be used with a basic position/velocity model by including velocity process noise to represent an uncorrelated random acceleration. In such cases, the filter requires the correct statistics for the random acceleration. Incorrect and possibly catastrophic filter operation can be caused by either an erroneous acceleration model or by incorrect a priori statistics for the random acceleration.

Frequently, the unknown forces may have a known structure with unknown parameters. In other cases, a structure for the unknown forces can be derived based on their statistics. This latter procedure was followed in Chapter 5 for the case of an exponentially correlated random acceleration. If the assigned structure correctly represents the unknown forces, then the filter will perform optimally**. For example, if the acceleration is exponentially correlated, then the basic filter defined in Chapter 5 is the optimal filter. As another example, if a constant acceleration structure is modeled by the filter and if the true acceleration is a constant, then the filter is the optimal filter. Note that there is no process noise matrix in this latter example. If a constant acceleration assumption is modeled with acceleration process

---

*The unmodeled forces include non-linea terms from the expansion of the forces where a linearized model is used.

**At this point, it must be assumed that the structure assigned to the forces satisfies any filter restrictions.

noise, then the model is a random walk model. In this case, the filter is optimal if the true acceleration is a random walk.

For purposes of this study, the terminology "model compensation" will be applied to any technique that involves modification of the system model only, i.e., the filter equations are not modified. If the model is correct, then the filter is the optimal filter. Model compensation techniques will be classified as non-adaptive techniques where "adaptive" implies a modification of the filter equations.

It can be argued easily that all real-world filters use model compensation techniques since perfect knowledge of a system and its statistics is never available. In general, however, the term is usually applied to the assignment of structure to small, random, unmodeled forces. In the case of the algorithms evaluated in this dissertation, the primary emphasis is on model compensation for acceleration.

6.2 Uncorrelated Random Acceleration Model

Numerical tests were performed using a model in which the acceleration was assumed to be a zero mean, uncorrelated random variable. If this model can be made to operate adequately compared to the exponentially correlated acceleration model, then the dimension of the state vector can be reduced by eliminating the three acceleration states. Computer run-time and storage will be reduced accordingly. This model can be referred to as a velocity dead-reckoning (VDR) model. A one-dimensional example of the VDR model is summarized as follows:

$$\delta\dot{r} = \delta v, \quad \delta r(t_o) = \delta r_o$$
$$\delta\dot{v} = u_a, \quad \delta v(t_o) = \delta v_o \tag{6.1}$$

where: δr is the position error;

δv is the velocity error; and

u_a is random velocity noise with statistics

$$E[u_a] = 0$$
$$E[u_a(t)u_a(\tau)] = q_v\delta(t-\tau) \tag{6.2}$$

Identical VDR models were implemented for each aircraft direction.

Initial testing of the VDR model was accomplished using the first ten minutes of flight in a manner similar to the evaluation runs of Par. 5.5.2. Table 6.1 summarizes the performance of the VDR filter with varying velocity noise magnitude q_v.

Table 6.1 Uncorrelated Acceleration (VDR) Filter Performance

	Velocity Noise Magnitude (m^2/sec^3)					
	.9375	2.8125	11.25	28.125	100.00	281.25
RSS POS ERR	203.78	131.14	85.51	71.30	62.30	59.58
RSS VEL ERR	27.88	21.64	16.19	13.87	12.02	11.40
MAX POS ERR	526.85	347.71	229.00	183.24	152.28	146.64
MAX VEL ERR	61.48	48.12	36.94	33.49	30.65	29.11
POS ERR/SIG	4.50	2.60	1.45	1.06	.72	.52
VEL ERR/SIG	7.08	3.54	1.50	.88	.44	.26
FIN POS ERR	50.22	52.83	64.00	73.26	85.66	92.63
FIN VEL ERR	1.41	2.79	5.55	7.83	11.20	13.08

For the cases which were considered in developing Table 5.4, an intuitive value for maximum maneuver variance of 2.25 m^2/sec^4 was arrived at using the maximum longitudinal acceleration of 1.5 m/sec^2. Similarly, an intuitive value of velocity noise can be arrived at by considering that a maximum acceleration of 1.5 m/sec^2 for the 1.25 second measurement interval results in a velocity change of 1.875 m/sec. Using the square of 1.875 m/sec as the desired discrete velocity process noise, the spectral level velocity noise should be 2.8125 m^2/sec^3.

Table 6.1 indicates that, as the noise magnitude increases, the RSS errors and the maximum errors decrease but the errors at the end of the 600 seconds of flight increase.

6.3 Additional Exponentially Correlated Acceleration Tests

To further analyze filter behavior with increasing noise magnitude, the exponentially correlated acceleration (ADR) filter of Chapter 5 was implemented using a wider choice of maneuver variances for the 20-second correlation time and also by examining filter behavior with infinite correlation time. The 20-second correlation time results are shown in Table 6.2. The infinite correlation time results are summarized in Table 6.3. A value for acceleration noise magnitude q_a equal to 1.8 m^2/sec^5 and an infinite correlation time $\beta = 0$ results in a discrete acceleration process noise term of 2.25 m^2/sec^4 for a 1.25 second measurement interval.

The behavior of the 20-second correlation time and the infinite correlation time filters is similar to the uncorrelated acceleration

Table 6.2 Twenty-Second Correlation Time ADR Filter Performance

	Acceleration Noise Magnitude (m^2/sec^5)					
	.0225	.225	2.25	4.50	10.00	22.50
RSS POS ERR	85.62	58.66	55.94	55.84	55.89	56.20
RSS VEL ERR	15.33	9.18	8.39	8.75	9.36	10.17
MAX POS ERR	248.24	149.36	141.80	141.34	139.23	139.78
MAX VEL ERR	40.56	30.58	29.43	28.40	27.62	27.83
POS ERR/SIG	1.84	1.04	.75	.67	.58	.49
VEL ERR/SIG	3.34	1.00	.44	.36	.29	.24
FIN POS ERR	26.35	50.01	80.46	88.12	94.10	97.48
FIN VEL ERR	1.52	4.11	11.11	13.18	14.99	16.34

Table 6.3 Infinite Correlation Time ADR Filter Performance

	Acceleration Noise Magnitude (m^2/sec^5)					
	.018	.03	.18	1.80	18.00	180.00
RSS POS ERR	63.70	60.40	56.95	55.80	56.50	60.15
RSS VEL ERR	10.95	9.91	8.28	8.67	10.79	14.92
MAX POS ERR	198.48	173.72	147.92	139.95	138.81	144.16
MAX VEL ERR	32.30	28.96	31.37	28.73	28.08	43.57
POS ERR/SIG	1.32	1.21	.98	.72	.48	.26
VEL ERR/SIG	2.00	1.59	.80	.42	.24	.14
FIN POS ERR	29.58	32.96	50.11	80.52	97.78	100.91
FIN VEL ERR	1.68	1.93	4.25	11.51	16.81	24.16

filter. That is, as the magnitude of the noise increased, the RSS errors and the maximum errors decreased while, at the end of the 600 seconds of flight, the errors increased. Within the noise ranges considered, the errors appeared to have limiting values. The maximum errors, however, were significantly larger for the low noise cases. An intuitive explanation for filter behavior with increasing aircraft noise magnitudes can be given. If the filter aircraft noise is low, then the filter changes the values of the predicted aircraft state at a slow rate. Consequently, the filter will be unable to track a rapid turn. During such a maneuver, the errors can become quite large. If the filter aircraft noise is high, then the errors in the navigation fix are bounded by the measurement bias errors and measurement noise.

Tables 6.4 and 6.5 summarize the performance of uncorrelated acceleration filters for the entire flight. Table 6.4 is based on a velocity noise of 2.8125 m^2/sec^3 (Case 5) and Table 6.5 is based on a velocity noise of 281.25 m^2/sec^3 (Case 6). Figures 6.1 and 6.2 depict the filter performance of Cases 5 and 6 respectively.

The infinite correlation time ADR filter was tested for the entire flight using an acceleration noise of .18 m^2/sec^5 (Case 7) and an acceleration noise of 18. m^2/sec^5 (Case 8). Case 7 performance is summarized in Table 6.6 and is shown in Figure 6.3. Case 8 performance is summarized in Table 6.7 and is shown in Figure 6.4.

Table 6.4 Case No. 5 Performance (q_v = 2.8125 m^2/sec^3)

	Flight Phase Final Times (sec)					
	598.75	1013.75	1295.00	2760.00	5100.00	6687.50
RSS POS ERR	131.14	147.46	18.66	238.81	97.48	57.75
RSS VEL ERR	21.64	3.02	.65	1.59	1.17	5.48
MAX POS ERR	347.71	253.01	127.52	819.03	368.41	131.75
MAX VEL ERR	48.12	6.57	2.64	7.28	7.51	37.56
POS ERR/SIG	2.60	1.79	.76	.81	1.05	1.74
VEL ERR/SIG	3.54	.48	.14	.25	.21	1.23

Table 6.5 Case No. 6 Performance (q_v = 281.25 m^2/sec^3)

	Flight Phase Final Times (sec)					
	598.75	1013.75	1295.00	2760.00	5100.00	6687.50
RSS POS ERR	59.58	145.00	29.76	231.72	106.58	63.48
RSS VEL ERR	11.40	7.59	6.48	7.76	7.45	9.31
MAX POS ERR	146.64	292.46	133.65	736.25	529.09	145.57
MAX VEL ERR	29.11	18.24	21.07D	25.78	37.08	30.23E
POS ERR/SIG	.52	1.09	.32	.68	.67	.72
VEL ERR/SIG	.26	.17	.16	.17	.17	.23

Table 6.6 Case No. 7 Performance (q_a = .18 m^2/sec^5, β = 0)

	Flight Phase Final Times (sec)					
	598.75	1013.75	1295.00	2760.00	5100.00	6687.50
RSS POS ERR	56.95	140.40	19.35	235.70	101.81	51.71
RSS VEL ERR	8.28	2.67	.52	2.44	2.31	2.43
MAX POS ERR	147.92	228.55	131.01	872.11	302.03	111.06D
MAX VEL ERR	31.37	7.02	1.95D	15.98	18.61	18.81
POS ERR/SIG	.98	1.76	1.05	.86	1.13	1.62
VEL ERR/SIG	.80	.34	.14	.32	.36	.63

Table 6.7 Case No. 8 Performance (q_a = 18. m^2/sec^5, β = 0)

	Flight Phase Final Times (sec)					
	598.75	1013.75	1295.00	2760.00	5100.00	6687.50
RSS POS ERR	56.50	144.07	23.38	246.02	104.64	61.64
RSS VEL ERR	10.79	10.82	5.45	10.32	9.70	8.60
MAX POS ERR	138.81	278.69	141.66	821.83	466.69	173.92E
MAX VEL ERR	28.08	28.56	15.50	57.43	73.95	41.56
POS ERR/SIG	.48	1.14	.41	.76	.77	.96
VEL ERR/SIG	.24	.26	.19	.23	.26	.31

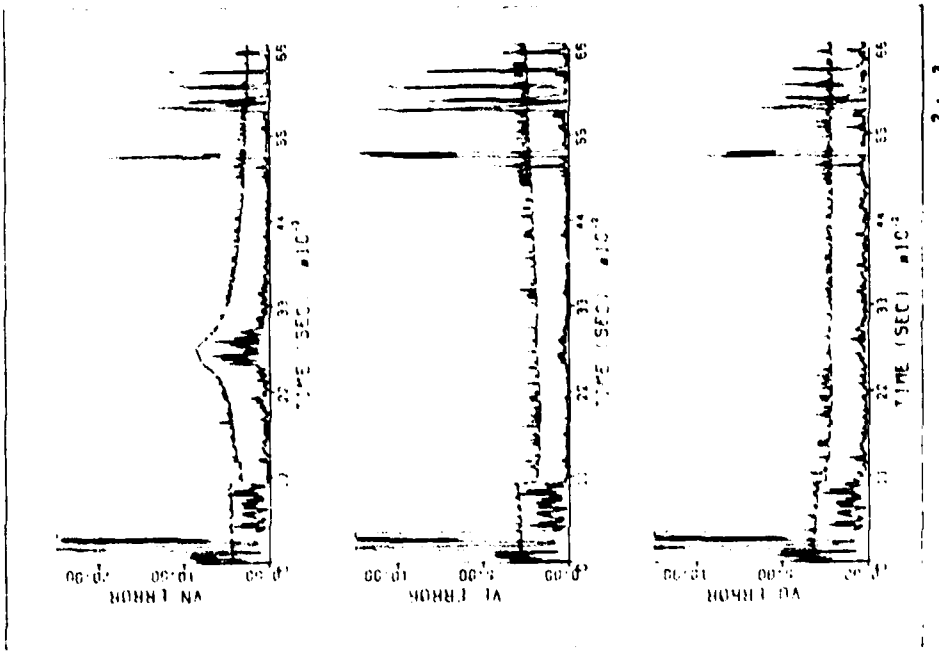

Figure 6.1 Case No. 5 Performance (q_v = 2.8125 ft^2/sec^3) (Continued)

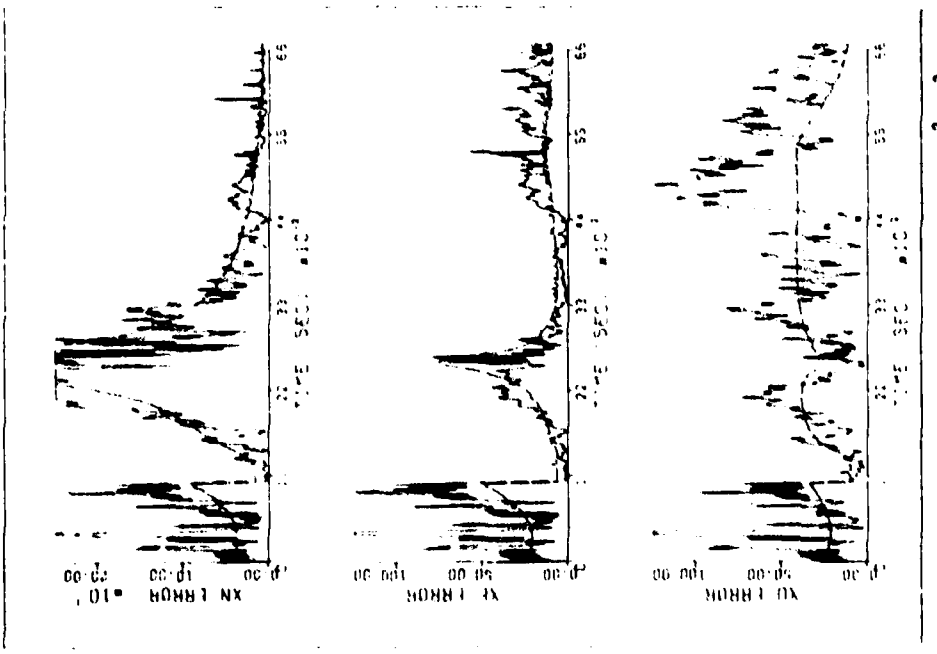

Figure 6.1 Case No. 5 Performance (q_v = 2.8125 ft^2/sec^3)

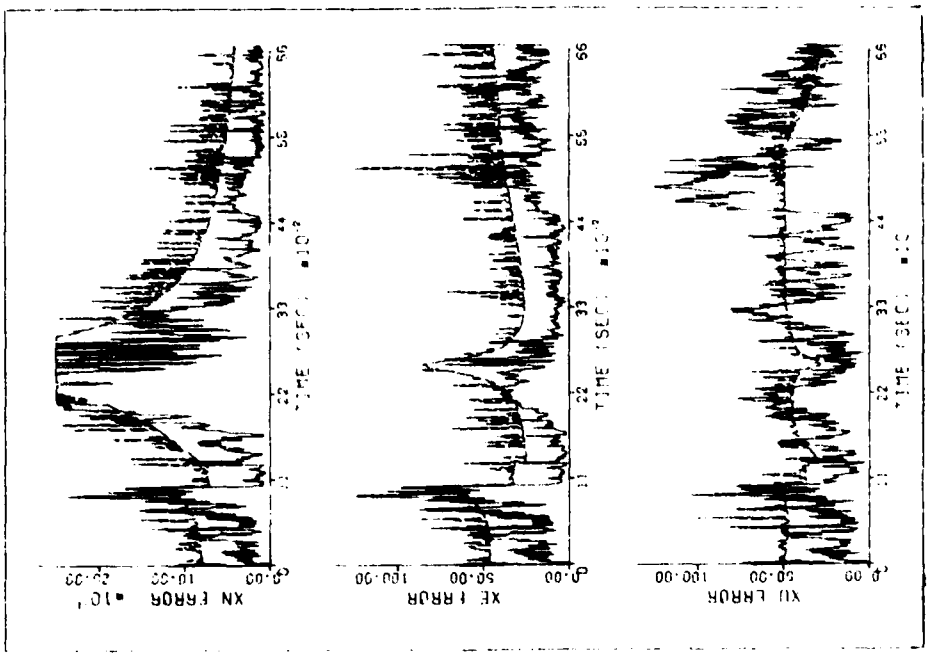

Figure 6.2 Case No. 6 Performance (q_v = 281.25 m^2/sec^3)

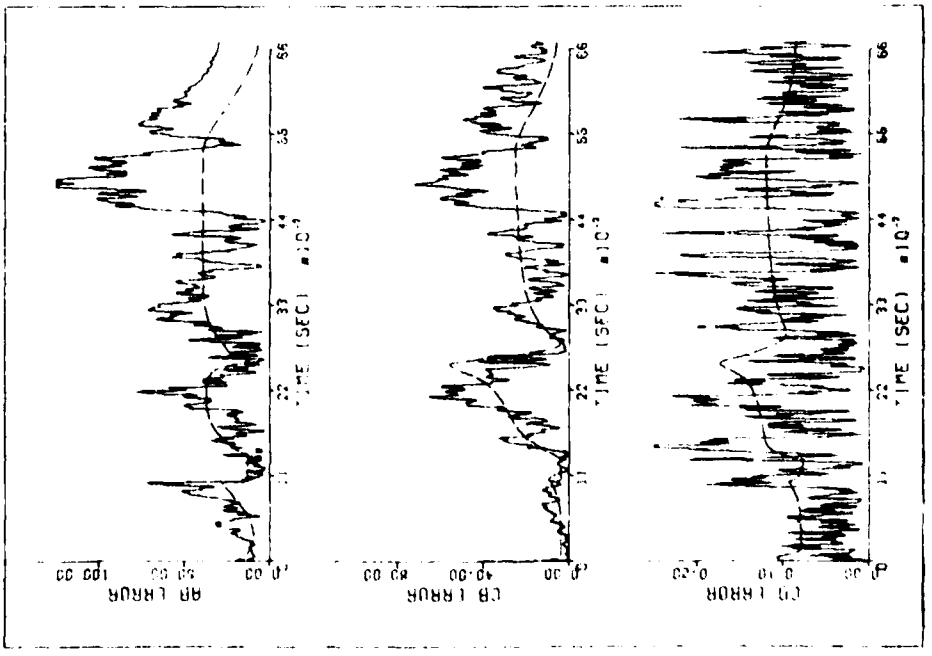

Figure 6.1 Case No. 5 Performance (q_v = 2.8125 m^2/sec^3)
(Continued)

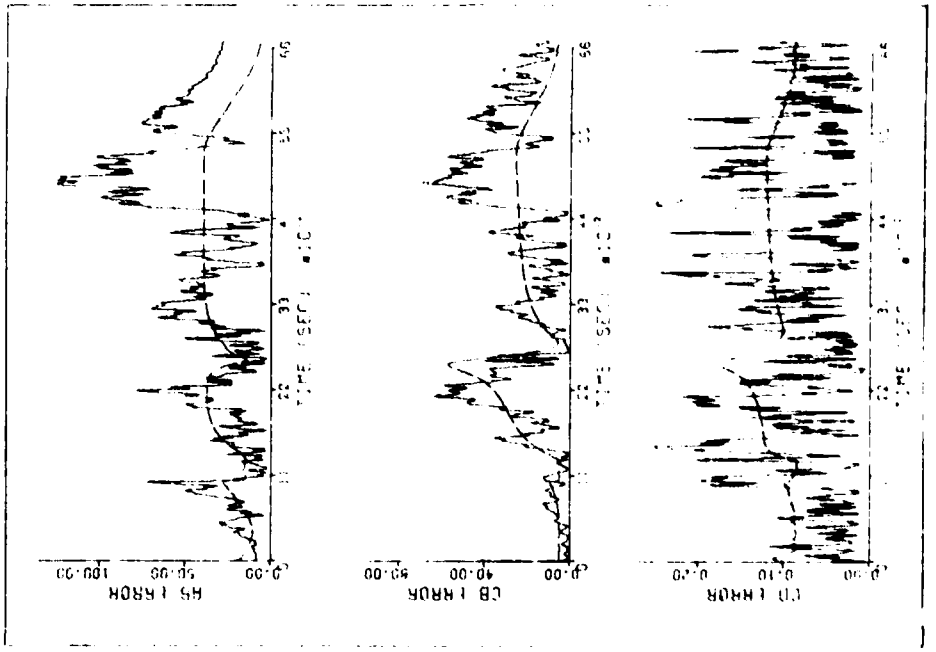

Figure 6.2 Case No. 6 Performance (q_v = 281.25 ft^2/sec^3) (Continued)

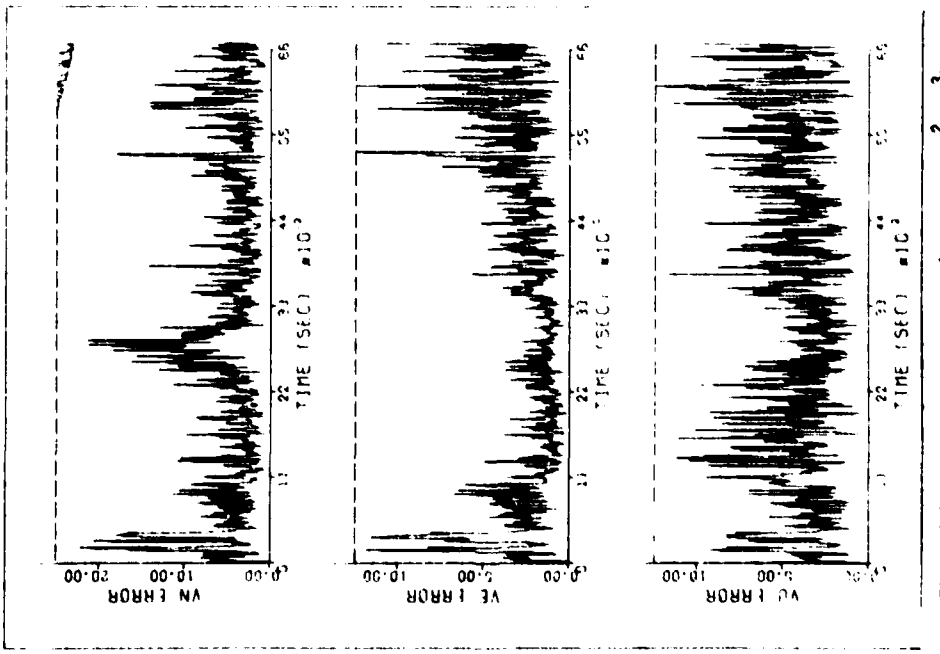

Figure 6.2 Case No. 6 Performance (q_v = 281.25 ft^2/sec^3) (Continued)

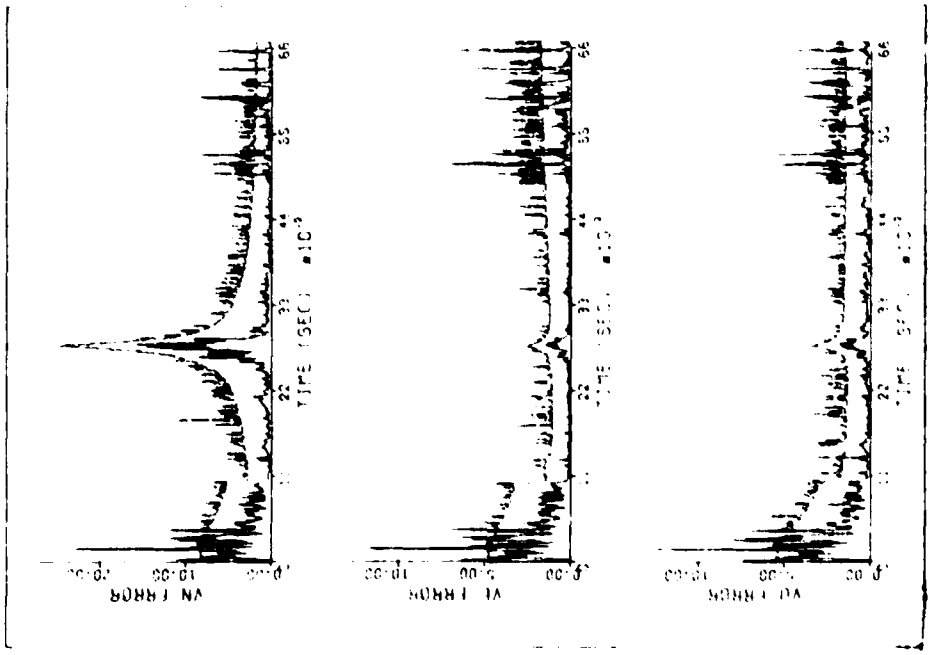

Figure 6.3 Case No. 7 Performance (q_B = .18 m^2/sec^5, s = 0) (Continued)

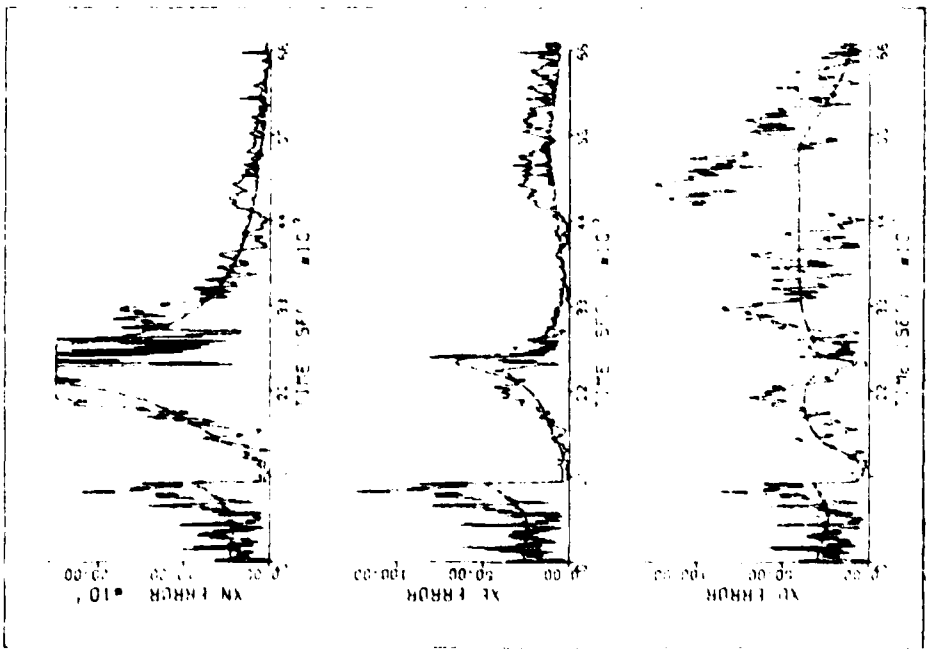

Figure 6.3 Case No. 7 Performance (q_B = .18 m^2/sec^5, s = 0)

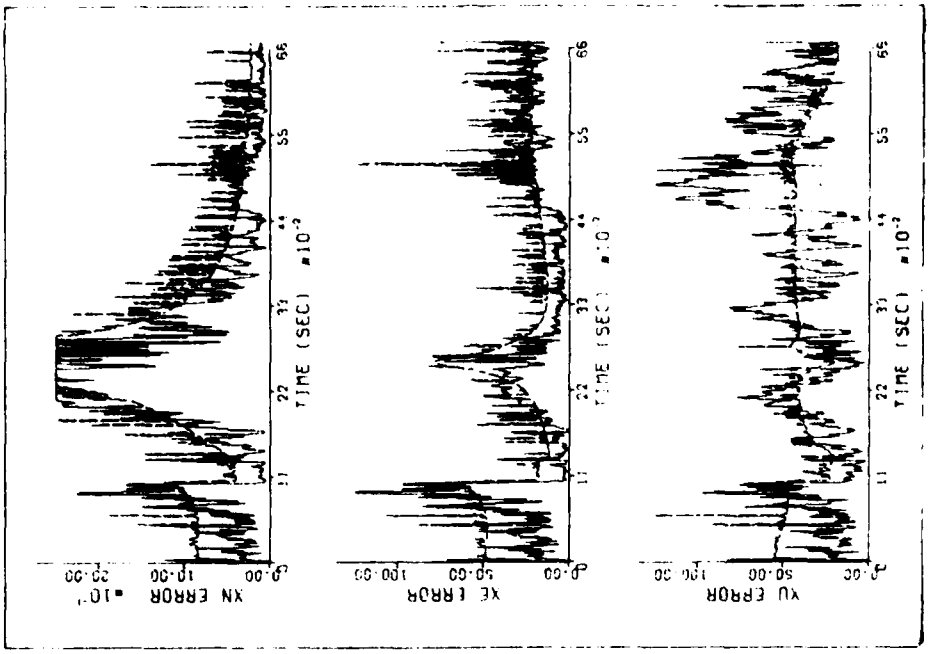

Figure 6.4 Case No. 8 Performance (q_B = 18. ft^2/sec^5, β = 0)

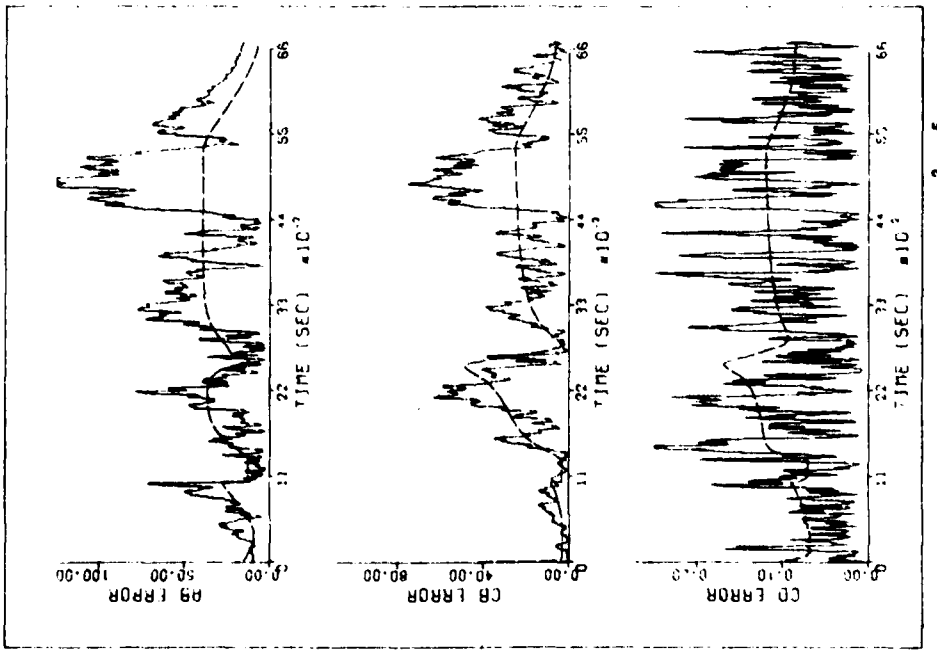

Figure 6.3 Case No. 7 Performance (q_B = .18 ft^2/sec^5, β = 0) (Continued)

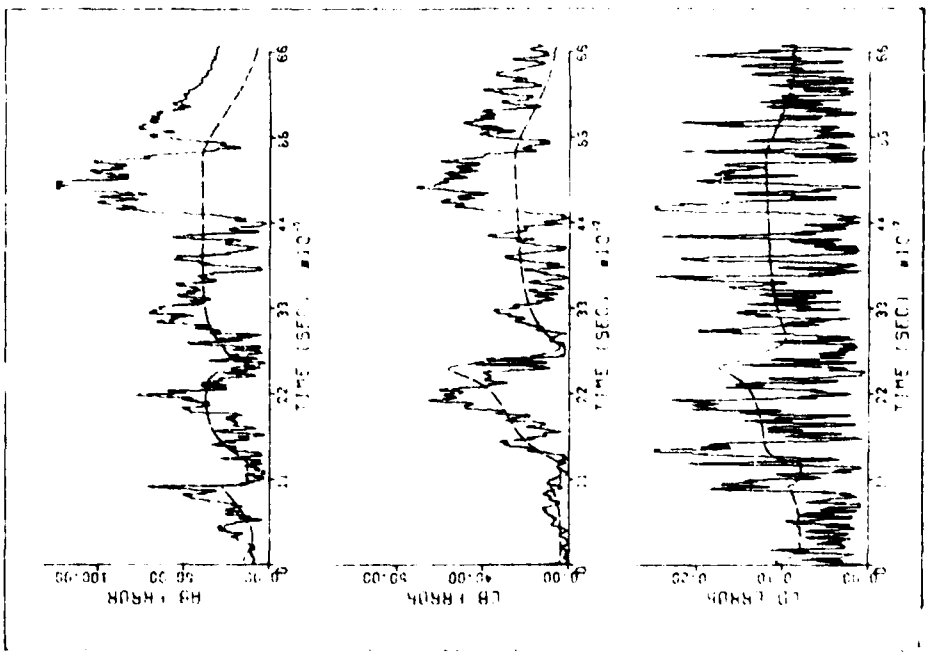

Figure 6.4 Case No. 8 Performance (q_a = 18. m^2/sec^5, β = 0) (Continued)

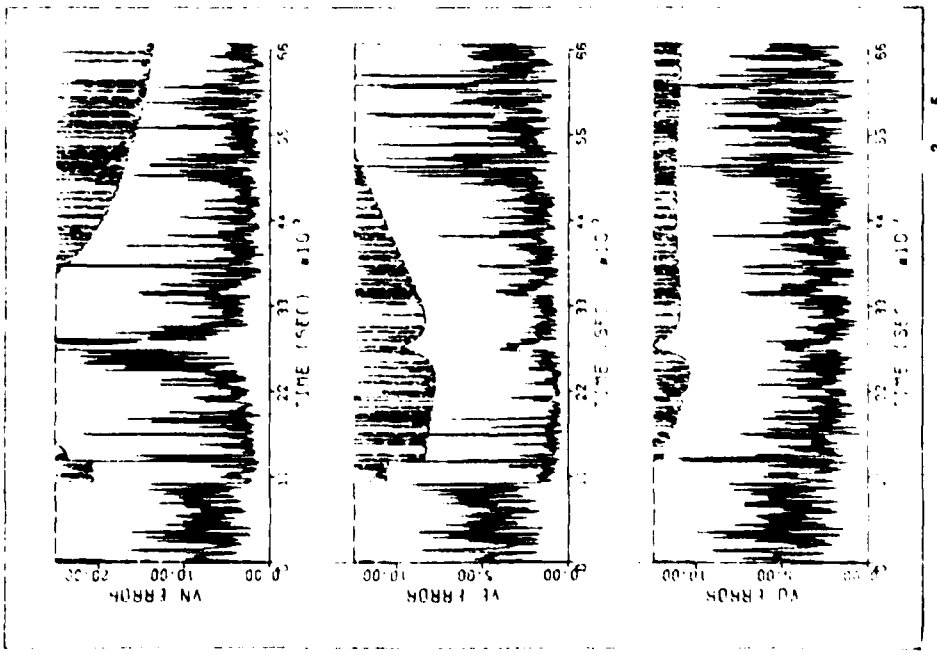

Figure 6.4 Case No. 8 Performance (q_a = 18. m^2/sec^5, β = 0) (Continued)

6.4 Estimation of Inverse Correlation Time

As is evident by an analysis of Tables 5.4 through 5.8 and 6.1 through 6.7, the ability of the filter covariance matrix to bound the errors varies with the process noise covariance. Large values of noise magnitude make the covariance matrix conservative; small values of noise magnitude result in overly optimistic covariances. In addition, the position covariance performance is not necessarily consistent with the performance of the velocity covariance.

The correlation time assumed by the navigation filter will affect the propagation of the covariance matrix by changing the state transition matrix and by changing the amount of discrete process noise added to the covariance matrix. Figure 6.5 depicts the elements of the discrete process noise matrix for unity spectral level noise and a sampling interval of 1.25 seconds. Note that the rates of change of the elements are not identical. For example, an increase in correlation time from one second to 20 seconds changes the discrete position noise covariance by a factor of 1.81, the discrete velocity noise covariance by a factor of 2.20, and the discrete acceleration noise covariance by a factor of 2.56. Estimation of correlation time would, hopefully, result in more consistent covariance performance and lower errors.

6.4.1 Development of the Beta-estimator. The structure of the exponentially correlated acceleration model was based on assumed statistics for random acceleration. By assigning an exponential structure to the acceleration itself and assuming that the acceleration noise

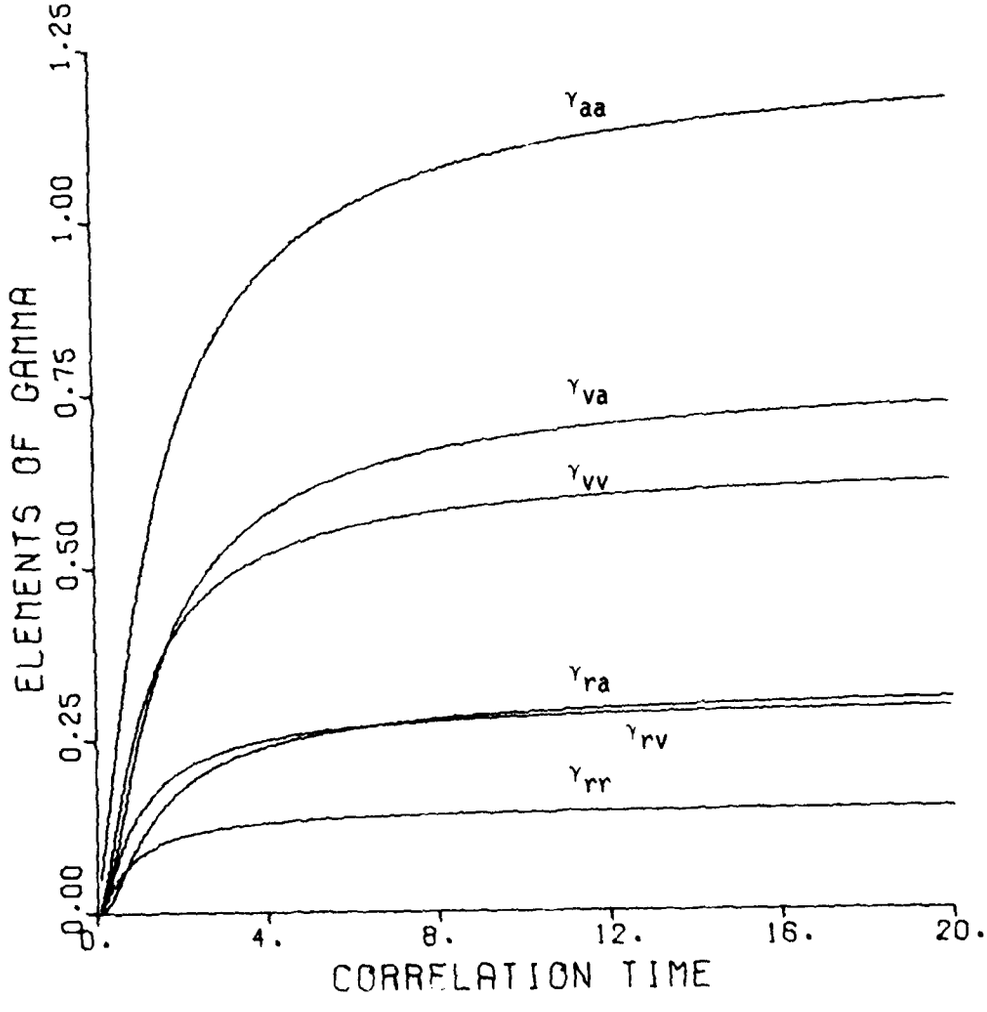

Figure 6.5 Process Noise Matrix Elements for Exponentially Correlated Random Acceleration Model (q_a = 1, Δt = 1.25)

is uncorrelated, a model can be developed that will permit estimation of inverse correlation time.

Assume the following system model:

$$\begin{aligned} \dot{r} &= v, \quad r(t_o) = r_o \\ \dot{v} &= a, \quad v(t_o) = v_o \\ \dot{a} &= -\beta a + u_a, \quad a(t_o) = a_o \\ \dot{\beta} &= u_\beta, \quad \beta(t_o) = {}_o \end{aligned} \tag{6.3}$$

where:

$$E[u_a] = 0, \quad E[u_a(t)u_a(\tau)] = q_a\delta(t-\tau) \tag{6.4}$$

$$E[u_\beta] = 0, \quad E[u_\beta(t)u_\beta(\tau)] = q_\beta\delta(t-\tau) \tag{6.5}$$

The parameters of Eq. 6.3 can be separated into a nominal state and a perturbation state in accordance with:

$$\begin{aligned} r &= \bar{r} + \delta r \\ v &= \bar{v} + \delta v \\ a &= \bar{a} + \delta a \\ \beta &= \bar{\beta} + \delta\beta \end{aligned} \tag{6.6}$$

The differential equations can be partitioned into a set of non-linear equations to be used for time propagation of the estimate in the extended sequential filter;

$$
\begin{aligned}
\dot{\bar{r}} &= \bar{v}, \quad \bar{r}(t_k) = \hat{r}_k \\
\dot{\bar{v}} &= \bar{a}, \quad \bar{v}(t_k) = \hat{v}_k \\
\dot{\bar{a}} &= -\bar{\beta}\bar{a}, \quad \bar{a}(t_k) = \hat{a}_k \\
\dot{\bar{\beta}} &= 0, \quad \bar{\beta}(t_k) = \hat{\beta}_k
\end{aligned}
\tag{6.7}
$$

and a set of linear differential equations which describe the deviation in the state from the solution to Eqs. 6.7

$$
\begin{aligned}
\delta\dot{r} &= \delta v, \quad \delta r(t_k) = 0 \\
\delta\dot{v} &= \delta a, \quad \delta v(t_k) = 0 \\
\delta\dot{a} &= -\bar{\beta}\delta a - \bar{a}\delta\beta + u_a, \quad \delta a(t_k) = 0 \\
\delta\dot{\beta} &= u_\beta, \quad \delta\beta(t_k) = 0
\end{aligned}
\tag{6.8}
$$

where: u_a and u_β have the statistics of Eqs. 6.4 and 6.5.

The solution to the non-linear time-propagation equations, Eqs. 6.7, is not the mean solution of Eqs. 5.7, 5.8 and 5.14. Since the acceleration itself is assumed to have exponential behavior, the solution to Eqs. 6.7 is given by

$$
\begin{aligned}
\bar{r}(t) &= \hat{r}_k + \hat{v}_k(t-t_k) + \phi_{ra}(\hat{\beta}_k)\,\hat{a}_k \\
\bar{v}(t) &= \hat{v}_k + \phi_{va}(\hat{\beta}_k)\hat{a}_k \\
\bar{a}(t) &= \phi_{aa}(\hat{\beta}_k)\hat{a}_k
\end{aligned}
\tag{6.9}
$$

where: $\phi_{ra}(\hat{\beta}_k)$, $\phi_{va}(\hat{\beta}_k)$, and $\phi_{aa}(\hat{\beta}_k)$ are defined in Eqs. 5.41.

The state transition matrix and the discrete process noise matrix can be analytically determined using Eqs. 4.63. and 4.69. The matrix A is determined from Eqs. 6.8.

$$\begin{bmatrix} \dot{\delta r} \\ \dot{\delta v} \\ \dot{\delta a} \\ \dot{\delta \beta} \end{bmatrix} = \begin{bmatrix} 0 & 1 & 0 & 0 \\ 0 & 0 & 1 & 0 \\ 0 & 0 & -\bar{\beta} & -\bar{a} \\ 0 & 0 & 0 & 0 \end{bmatrix} \begin{bmatrix} \delta r \\ \delta v \\ \delta a \\ \delta \beta \end{bmatrix} + \begin{bmatrix} 0 \\ 0 \\ u_a \\ u_\beta \end{bmatrix} \tag{6.10}$$

$$\dot{\underline{\delta x}} = A\underline{\delta x} + B\underline{u}$$

Solving Eq. 4.63 yields the state transition matrix

$$\Phi(t_{k+1}, t_k) = \begin{bmatrix} 1 & \Delta t & \phi_{ra}(\beta_k) & a_k\phi_{r\beta}(\beta_k) \\ 0 & 1 & \phi_{va}(\beta_k) & a_k\phi_{v\beta}(\beta_k) \\ 0 & 0 & \phi_{aa}(\beta_k) & a_k\phi_{a\beta}(\beta_k) \\ 0 & 0 & 0 & 1 \end{bmatrix} \tag{6.11}$$

where: ϕ_{ra}, ϕ_{va}, and ϕ_{aa} are defined in Eqs. 5.41.;

$$\phi_{r\beta}(\beta) = [\exp(-\beta\Delta t) - (\beta\Delta t)^2/2 + \beta\Delta t - 1]/\beta^3 \tag{6.11a}$$

$$\phi_{v\beta}(\phi) = [-\exp(-\beta\Delta t) - \beta\Delta t + 1]/\beta^2 \tag{6.11b}$$

$$\phi_{a\beta}(\beta) = [\exp(-\beta\Delta t) - 1]/\beta \tag{6.11c}$$

$$\Delta t = t_{k+1} - t_k$$

Equation 4.69 yields the discrete process noise matrix Γ.

$$\Gamma(t_{k+1}) = \begin{bmatrix} \Gamma_{1,1} & \Gamma_{1,2} & \Gamma_{1,3} & \Gamma_{1,4} \\ \Gamma_{1,2} & \Gamma_{2,2} & \Gamma_{2,3} & \Gamma_{2,4} \\ \Gamma_{1,3} & \Gamma_{2,3} & \Gamma_{3,3} & \Gamma_{3,4} \\ \Gamma_{1,4} & \Gamma_{2,4} & \Gamma_{3,4} & \Gamma_{4,4} \end{bmatrix} \tag{6.12}$$

where:

$$\Gamma_{1,1} = q_a \gamma_{rr}(\beta_k) + q_\beta a_k^2 \gamma'_{rr}(\beta_k)$$

$$\Gamma_{1,2} = q_a \gamma_{rv}(\beta_k) + q_\beta a_k^2 \gamma'_{rv}(\beta_k)$$

$$\Gamma_{1,3} = q_a \gamma_{ra}(\beta_k) + q_\beta a_k^2 \gamma'_{ra}(\beta_k)$$

$$\Gamma_{1,4} = q_\beta a_k \gamma'_{r\beta}(\beta_k)$$

$$\Gamma_{2,2} = q_a \gamma_{vv}(\beta_k) + q_\beta a_k^2 \gamma'_{vv}(\beta_k)$$

$$\Gamma_{2,3} = q_a \gamma_{va}(\beta_k) + q_\beta a_k^2 \gamma'_{va}(\beta_k)$$

$$\Gamma_{2,4} = q_\beta a_k \gamma'_{v\beta}(\beta_k)$$

$$\Gamma_{3,3} = q_a \gamma_{aa}(\beta_k) + q_\beta a_k^2 \gamma'_{aa}(\beta_k)$$

$$\Gamma_{3,4} = q_\beta a_k \gamma'_{a\beta}(\beta_k)$$

$$\Gamma_{4,4} = q_\beta \gamma_{\beta\beta}(\beta_k)$$

$$\gamma'_{rr}(\beta) = [-\exp(-2\beta\Delta t)/2 + ((\beta\Delta t)^2+2)\exp(-\beta\Delta t)$$

$$+ (\beta\Delta t)^5/20 - (\beta\Delta t)^4/4 + 2(\beta\Delta t)^3/3$$

$$- (\beta\Delta t)^2 + \beta\Delta t - 3/2] / \beta^7$$

$$= \Delta t^7(1/252 - \beta\Delta t/576 + 13(\beta\Delta t)^2/25920$$

$$- (\beta\Delta t)^3/8640 + 19(\beta\Delta t)^4/831600 - \ldots] \qquad (6.13a)$$

$$\gamma'_{rv}(\beta) = [\exp(-2\beta\Delta t)/2 + [-(\beta\Delta t)^2/2+\beta\Delta t-1]\exp(-\beta\Delta t)$$

$$+ (\beta\Delta t)^4/8 - (\beta\Delta t)^3/2 + (\beta\Delta t)^2 - \beta\Delta t + 1/2]/\beta^6$$

$$= \Delta t^6[1/72 - \beta\Delta t/144 + 13(\beta\Delta t)^2/5760$$

$$- (\beta\Delta t)^3/1728 + 19(\beta\Delta t)^4/151200$$

$$- 29(\beta\Delta t)^5/1209600 + \ldots] \qquad (6.13b)$$

$$\gamma'_{ra}(\beta) = [-\exp(-2\beta\Delta t)/2 + [(\beta\Delta t)^2+2]\exp(-\beta\Delta t)$$

$$+ (\beta\Delta t)^3/6 - (\beta\Delta t)^2/2 + \beta\Delta t - 3/2] / \beta^5$$

$$= \Delta t^5[1/30 - \beta\Delta t/48 + 41(\beta\Delta t)^2/5040$$

$$- 7(\beta\Delta t)^3/2880 + 109(\beta\Delta t)^4/181440$$

$$- 31(\beta\Delta t)^5/241920 + \ldots] \qquad (6.13c)$$

$$\gamma'_{r\beta}(\beta) = -[\exp(-\beta\Delta t) + (\beta\Delta t)^3/6 - (\beta\Delta t)^2/2$$

$$+ \beta\Delta t - 1]/\beta^4$$

$$= -\Delta t^4[1/24 - \beta\Delta t/120 + (\beta\Delta t)^2/720 - (\beta\Delta t)^3/5040$$

$$+ (\beta\Delta t)^4/40320 - (\beta\Delta t)^5/362880 + \ldots] \qquad (6.13d)$$

$$\gamma'_{vv}(\beta) = (-\exp(-2\beta\Delta t)/2 - 2\beta\Delta t \exp(-\beta\Delta t) + (\beta\Delta t)^3/3$$

$$- (\beta\Delta t)^2 + \beta\Delta t + 1/2]$$

$$= \Delta t^5[1/20 - \beta\Delta t/36 + 5(\beta\Delta t)^2/504$$

$$- (\beta\Delta t)^3/360 + 17(\beta\Delta t)^4/25920 - 41(\beta\Delta t)^5/302400] \qquad (6.13e)$$

$$\gamma'_{va}(\beta) = [\exp(-2\beta\Delta t)/2 + (\beta\Delta t-1)\exp(-\beta\Delta t)$$

$$+ (\beta\Delta t)^2/2 - \beta\Delta t + 1/2]/\beta^4$$

$$= \Delta t^4[1/8 - \beta\Delta t/12 + 5(\beta\Delta t)^2/144 - (\beta\Delta t)^3/90$$

$$+ 17(\beta\Delta t)^4/5760 - 41\ (\beta\Delta t)^5/60480$$

$$+ 167(\beta\Delta t)^6/1209600 - 23(\beta\Delta t)^7/907200 + \ldots] \qquad (6.13f)$$

$$\gamma'_{v\beta}(\beta) = -[\exp(-\beta\Delta t) + (\beta\Delta t)^2/2 - \beta\Delta t + 1]/\beta^3$$

$$= -\Delta t^3[1/6 - \beta\Delta t/24 + (\beta\Delta t)^2/120 + (\beta\Delta t)^3/720$$

$$- (\beta\Delta t)^4/5040 + (\beta\Delta t)^5/40320 - (\beta\Delta t)^6/362880 + \ldots] \quad (6.13g)$$

$$\gamma'_{aa}(\beta) = [-\exp(-2\beta\Delta t)/2 + 2\exp(-\beta\Delta t) + \beta\Delta t - 3/2]/\ ^2$$

$$= \Delta t^3[1/3 - \beta\Delta t/4 + 7(\beta\Delta t)^2/60 - (\beta\Delta t)^3/24$$

$$+ 31(\beta\Delta t)^4/2520 - (\beta\Delta t)^5/320 + 127(\beta\Delta t)^6/181440$$

$$- 17(\beta\Delta t)^7/120960 + \ldots] \quad (6.13h)$$

$$\gamma'_{a\beta}(\beta) = -[\exp(-\beta\Delta t) + \beta\Delta t - 1]/\beta^2$$

$$= -\Delta t^2(1/2 - \beta\Delta t/6 + (\beta\Delta t)^2/24 - (\beta\Delta t)^3/120$$

$$+ (\beta\Delta t)^4/720 - (\beta\Delta t)^5/5040 + (\beta\Delta t)^6/40320$$

$$- (\beta\Delta t)^7/362880 + \ldots) \quad (6.13i)$$

$$\gamma_{\beta\beta} = q_\beta \Delta t \qquad (6.13j)$$

and the remaining γ functions are defined in Eqs. 5.42.

6.4.2 Results of the Beta-estimator. The β-estimator was tested in the same manner as previous algorithm tests. The first ten minutes of flight were used to evaluate the behavior of the β-estimator with varying process noise in the β terms. Following this analysis, full flight tests were made using selected parameters. The tests used the initial parameters of the four exponentially correlated acceleration models which were used to obtain Tables 5.6 through 5.9. Also, an initial correlation time of infinity and a spectral level acceleration noise of 1.8 m^2/sec^5 were tested. The initial conditions associated with this latter case will be referred to as the "Case 7.5" initial conditions. The standard deviation of all inverse correlation times was initially assumed to be $1. \times 10^{-3}$ sec^{-1} for all cases. For each set of initial conditions, the process noise term for the inverse correlation time was varied from 10^{-2} sec^{-3} to 10^{-8} sec^{-3} and was identical for all directions. The results are given in Table 6.8.

As the β-process noise increased, the filter sensitivity increased and the performance parameters generally improved. For those cases where the spectral level of the acceleration noise was low and β-process noise was high, the filter diverged. Filters with high spectral level acceleration noise appeared to be more stable. A value of β-process noise equal to 10^{-4} sec^{-3} seemed to perform well in all

Table 6.8 Initial Evaluation of Beta-Estimation Algorithm

	β-Process Noise (sec^{-3})				
	12-state	10^{-8}	10^{-6}	10^{-4}	10^{-2}
q_a = .225 m^2/sec^5, β(0) = 1/20 sec^{-1}					
RSS POS ERR	58.66	60.73	57.14	53.76	
RSS VEL ERR	9.18	8.80	8.17	6.35	
MAX POS ERR	149.36	147.81	147.15	127.73	
MAX VEL ERR	30.58	30.22	30.19	30.32	Filter
POS ERR/SIG	1.04	1.08	1.00	.98	Diverged
VEL ERR/SIG	1.00	.96	.86	.73	
FIN POS ERR	50.01	50.14	50.67	47.78	
FIN VEL ERR	4.11	3.39	4.34	4.07	
q_a = .375 m^2/sec^5, β(0) = 1 sec^{-1}					
RSS POS ERR	298.96	295.10	253.57	62.34	
RSS VEL ERR	34.57	33.82	30.59	9.89	
MAX POS ERR	758.56	733.42	577.57	239.61	
MAX VEL ERR	74.39	73.25	72.85	35.83	Filter
POS ERR/SIG	7.18	7.08	6.01	1.59	Diverged
VEL ERR/SIG	13.24	12.94	10.86	2.09	
FIN POS ERR	22.79	40.20	32.83	28.74	
FIN VEL ERR	4.19	.75	.98	2.08	
q_a = .01875 m^2/sec^5, β(0) = 1/20 sec^{-1}					
RSS POS ERR	91.25	85.24	69.10	56.29	
RSS VEL ERR	16.16	13.63	11.32	11.00	
MAX POS ERR	258.69	251.28	241.14	184.40	
MAX VEL ERR	41.88	40.60	38.67	145.17	Filter
POS ERR/SIG	1.98	1.85	1.48	1.35	Diverged
VEL ERR/SIG	3.70	3.09	2.42	3.35	
FIN POS ERR	25.66	24.11	23.80	18.89	
FIN VEL ERR	1.46	1.45	1.50	.53	

Table 6.8 Initial Evaluation of Beta-Estimation Algorithm (Continued)

	β-Process Noise (sec^{-3})				
	12-state	10^{-8}	10^{-6}	10^{-4}	10^{-2}
q_a = 4.5 m^2/sec^5, β(0) = 1 sec^{-1}					
RSS POS ERR	107.12	109.70	108.44	67.85	56.63
RSS VEL ERR	19.18	19.02	18.85	12.79	7.41
MAX POS ERR	300.99	294.88	289.49	187.75	147.19
MAX VEL ERR	43.44	42.12	41.48	41.32	47.91
POS ERR/SIG	2.06	2.11	2.08	1.18	.96
VEL ERR/SIG	2.83	2.80	2.76	1.21	.56
FIN POS ERR	42.63	55.92	56.18	69.66	62.93
FIN VEL ERR	1.12	3.47	3.54	7.05	5.15
q_a = 1.8 m^2/sec^5, β(0) = 0					
RSS POS ERR	55.80		55.87	54.94	53.90
RSS VEL ERR	8.67		8.61	7.98	7.02
MAX POS ERR	139.95		139.99	139.82	140.98
MAX VEL ERR	28.73	Not	28.69	26.77	35.79E
POS ERR/SIG	.72	Tested	.72	.73	.89
VEL ERR/SIG	.42		.42	.41	.48
FIN POS ERR	80.52		80.28	77.69	53.33
FIN VEL ERR	11.51		11.37	10.12	3.52

600-second tests. Accordingly, full flight tests were made using the initial conditions of Cases 1 through 4 and 7.5 and using a β-process noise equal to 10^{-4} sec^{-3}. The full flight results are summarized in Tables 6.9 through 6.13 and are shown in Figures 6.6 through 6.10.

If the β-estimator did not diverge, the results were generally better than the corresponding 12-state filter. The β-estimator, however, was unstable. This is especially evident by Cases 9 and 11 where the filter performed well during the takeoff and departure flight phases then continued to perform slightly better than the 12-state filter through the cruise portion of flight. After the turn at 5230 seconds, however, the filter diverged. The impact of the turn at 5230 seconds is sharply evident in Case 10.

Based on the 600-second tests, reducing the β-process noise may eliminate this divergence. Reduction of β-process noise, however, also tends to inactivate the estimation of inverse correlation time so that the β-estimator algorithm reduces to the basic 12-state case.

6.5 Summary of Non-Adaptive Modifications

The assumption that the random acceleration is uncorrelated reduces the dimension of the aircraft state by eliminating the acceleration components. This assumption also reduces the capability of the navigation algorithm to predict aircraft position and velocity since the assumed acceleration is zero.* The results of the uncorrelated random

*It may be possible to use the estimated position and velocity of the aircraft to compute acceleration by a deterministic formula. The time propagation of the aircraft state can then be accomplished using an acceleration dead-reckoning formula.

Table 6.9 Case No. 9 Performance (q_a = .225 m^2/sec^5, $\beta(0)$ = 1/20 sec^{-1}, q_β = .0001 sec^{-3}) (Continued)

	Flight Phase Final Times (sec)					
	598.75	1013.75	1295.00	2760.00	5100.00	6687.50
RSS POS ERR	53.76	139.76	19.04	234.69	100.10	
RSS VEL ERR	6.35	2.13	.44	1.66	1.00	
MAX POS ERR	127.73	228.43	129.01	857.58	300.95	Filter Diverged
MAX VEL ERR	30.32	4.51	1.42	8.12	6.87	
POS ERR/SIG	.98	1.77	1.05	.86	1.14	
VEL ERR/SIG	.73	.35	.14	.31	.27	

Table 6.10 Case No. 10 Performance (q_a = .375 m^2/sec^5, $\beta(0)$ = 1 sec^{-1}, q_β = .0001 sec^{-3})

	Flight Phase Final Times (sec)					
	598.75	1013.75	1295.00	2760.00	5100.00	6687.50
RSS POS ERR	56.29	133.80	20.18	195.81	100.47	
RSS VEL ERR	11.00	1.20	.35	1.12	.53	
MAX POS ERR	184.40	223.73	675.09	675.09	224.50	
MAX VEL ERR	145.17	1.90	5.42	5.42	.53	Filter Diverged
POS ERR/SIG	1.35	1.82	.81	.81	1.22	
VEL ERR/SIG	3.31	.70	.49	.49	.42	

Table 6.11 Case No. 11 Performance (q_a = .01875 m^2/sec^5, $\beta(0)$ = 1/20 sec^{-1}, q_β = .0001 sec^{-3})

	Flight Phase Final Times (sec)					
	598.75	1013.75	1295.00	2760.00	5100.00	6687.50
RSS POS ERR	72.34	124.44	16.61	238.55	99.81	62.24
RSS VEL ERR	9.89	1.92	.58	1.76	1.14	39.52
MAX POS ERR	239.61	215.26	110.73	863.78	317.39	949.22
MAX VEL ERR	35.83	3.88	1.66	8.79	8.24	998.89
POS ERR/SIG	1.59	1.59	.89	.86	1.13	1.83
VEL ERR/SIG	2.09	.39	.17	.27	.28	3.17

Table 6.12 Case No. 12 Performance (q_a = 4.5 m^2/sec^5, $\beta(0)$ = 1 sec^{-1}, q_β = .0001 sec^{-3}) *(Continued)*

	Flight Phase Final Times (sec)					
	598.75	1013.75	1295.00	2760.00	5100.00	6687.50
RSS POS ERR	67.85	144.78	17.75	242.85	99.97	56.97
RSS VEL ERR	12.79	4.39	1.28	3.36	2.64	3.04
MAX POS ERR	187.75	246.43	119.27	853.68	419.48	67.02
MAX VEL ERR	41.32	11.32	5.39	19.82	19.51	28.17
POS ERR/SIG	1.18	1.62	.60	.81	1.01	1.52
VEL ERR/SIG	1.21	.46	.12	.19	.25	.29

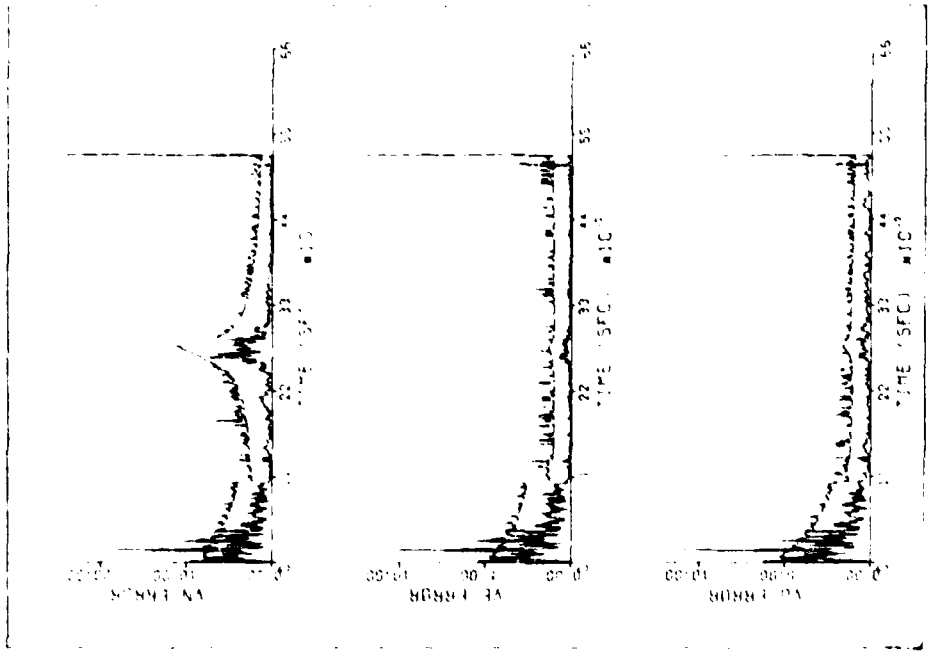

Figure 6.6 Case No. 9 Performance (q_β = .225 m^2/sec^5, $\beta(0)$ = 1/20 sec^{-1}, q_β = .0001 sec^{-3})

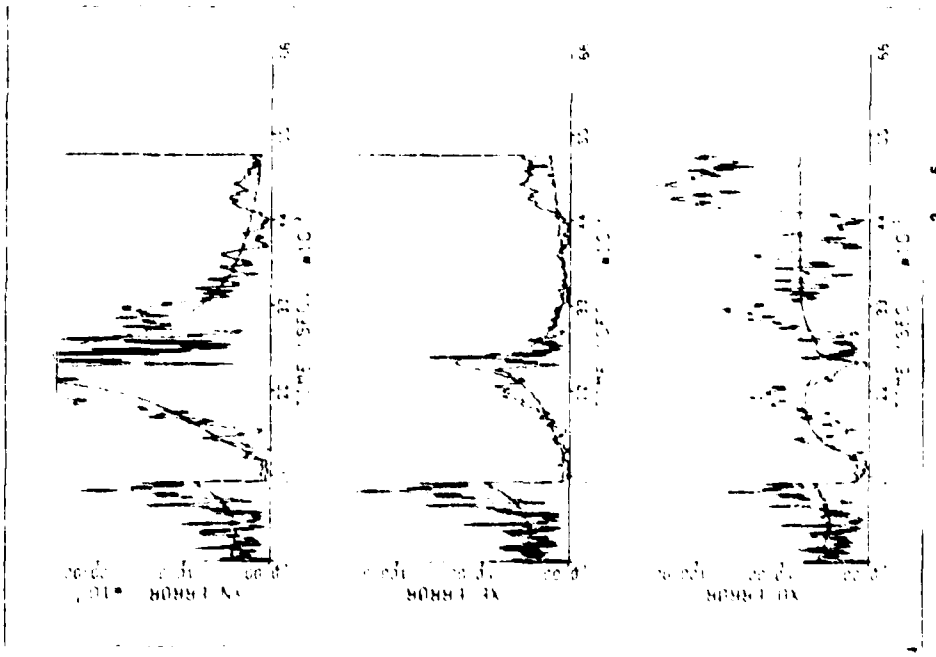

Figure 6.6 Case No. 9 Performance (q_β = .225 m^2/sec^5, $\beta(0)$ = 1/20 sec^{-1}, q_β = .0001 sec^{-3}) (Continued)

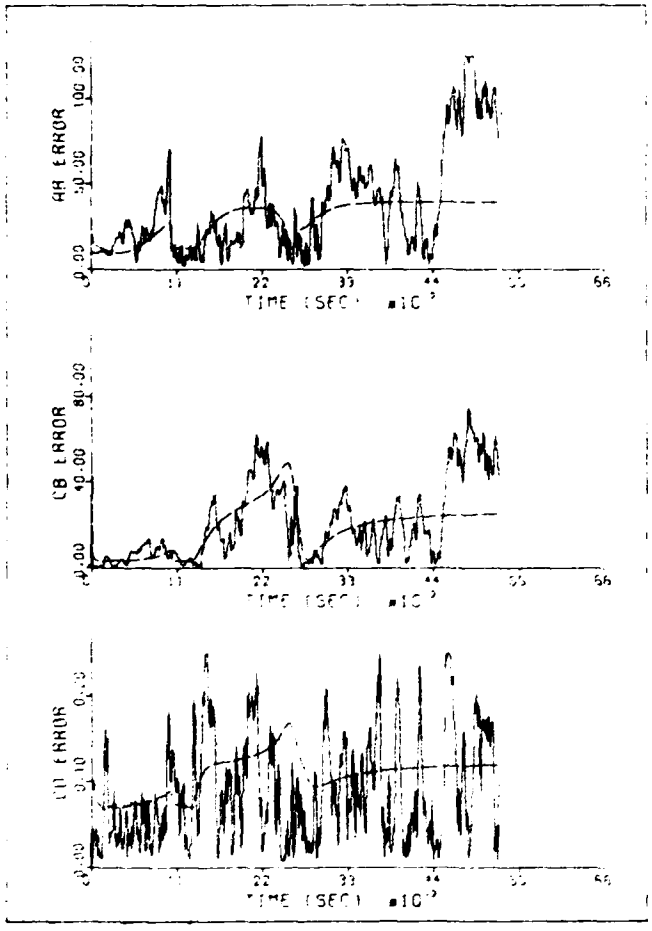

Figure 6.6 Case No. 9 Performance (q_a = .225 m^2/sec^5, $\beta(0)$ = 1/20 sec^{-1}, q_β = .0001 sec^{-3}) (Continued)

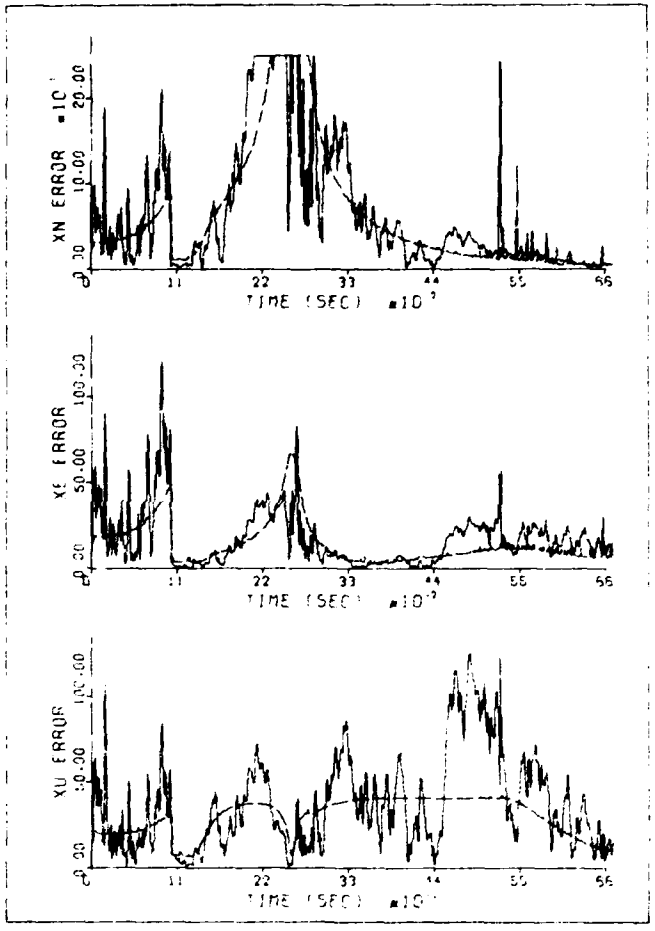

Figure 6.7 Case No. 10 Performance (q_a = .375 m^2/sec^5, $\beta(0)$ = 1 sec^{-1}, q_β = .0001 sec^{-3})

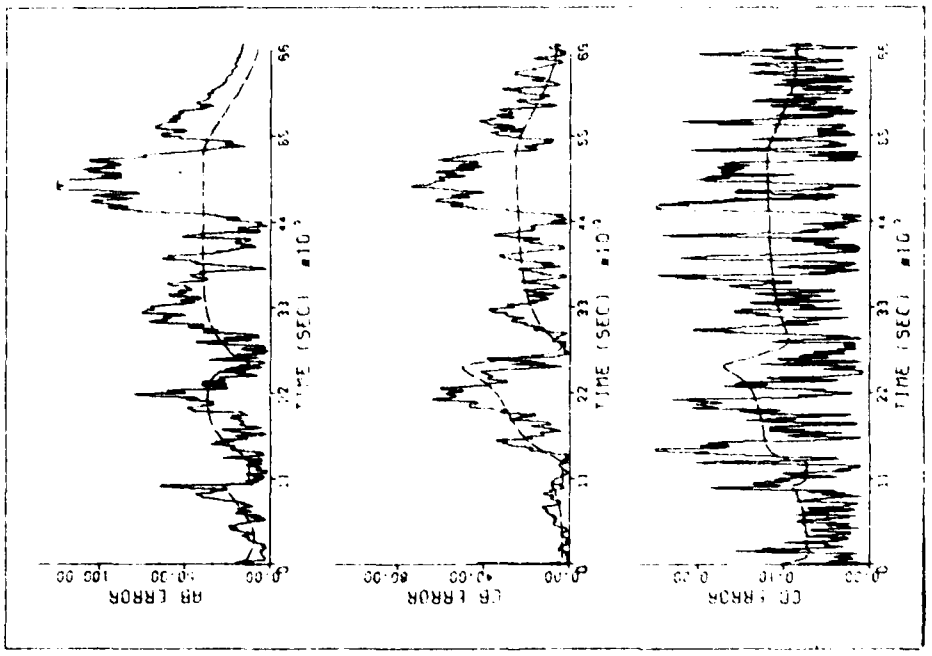

Figure 6.7 Case No. 10 Performance (q_a = .375 m^2/sec^5, $\beta(0)$ = 1 sec^{-1}, q_β = .0001 sec^{-3}) (Continued)

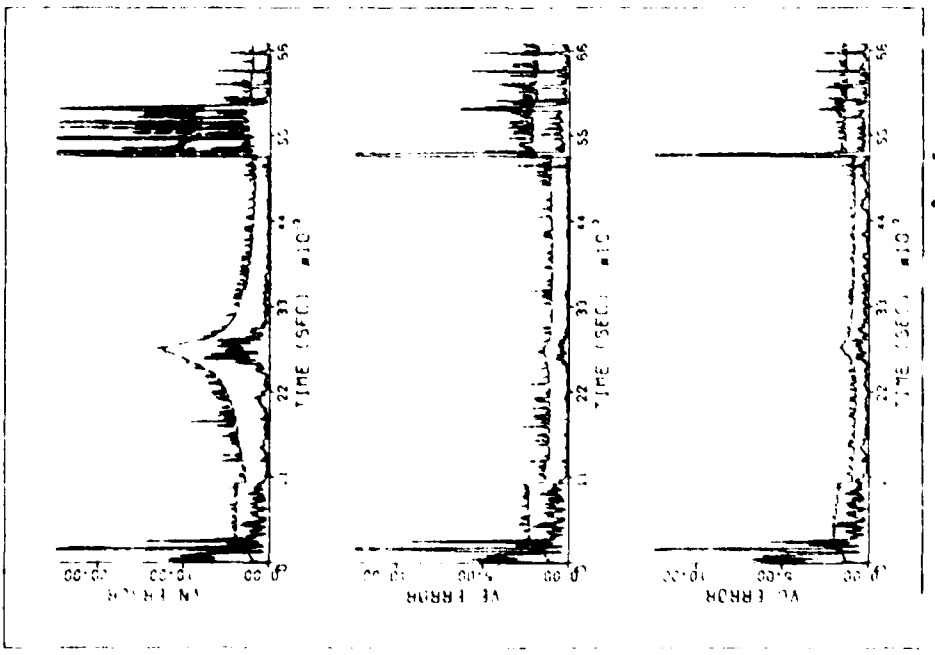

Figure 6.7 Case No. 10 Performance (q_a = .375 m^2/sec^5, $\beta(0)$ = 1 sec^{-1}, q_β = .0001 sec^{-3}) (Continued)

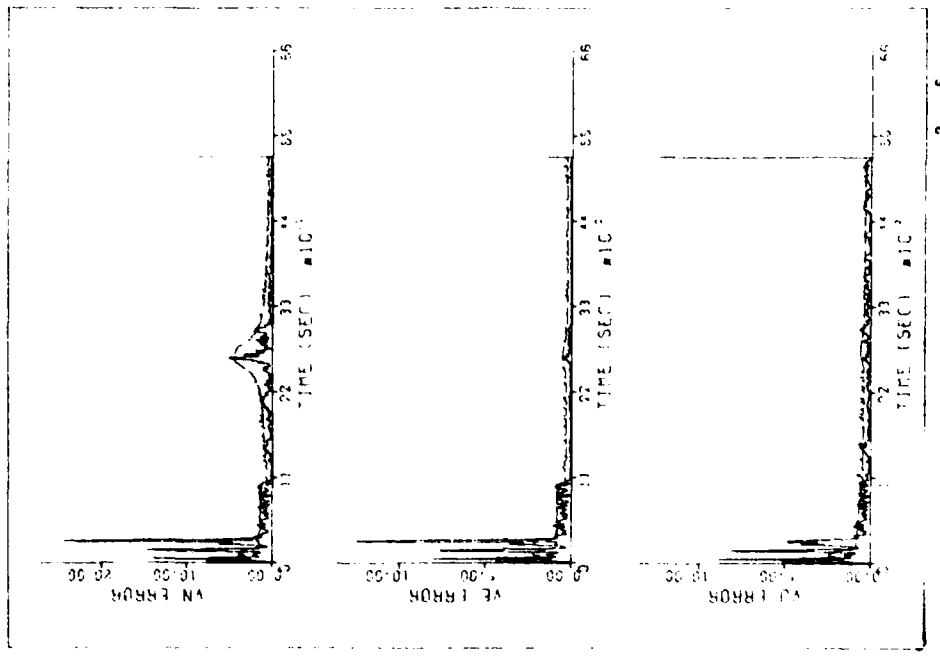

Figure 6.8 Case No. 11 Performance (q_β = .01875 m^2/sec^5, $\beta(0)$ = 1/20 sec^{-1}, q_β = .0001 sec^{-3}) (Continued)

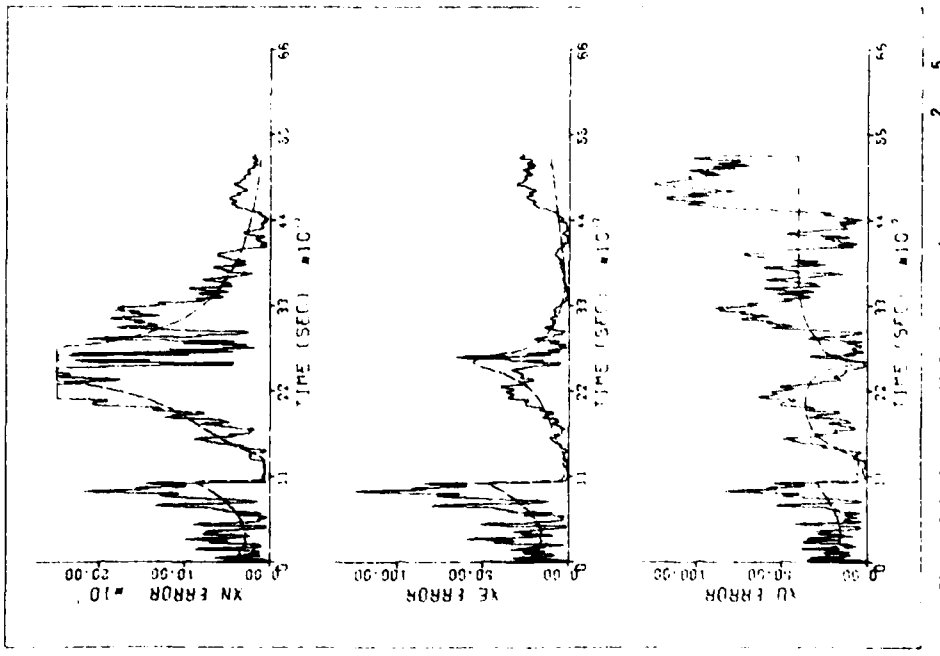

Figure 6.8 Case No. 11 Performance (q_β = .01875 m^2/sec^5, $\beta(0)$ = 1/20 sec^{-1}, q_β = .0001 sec^{-3})

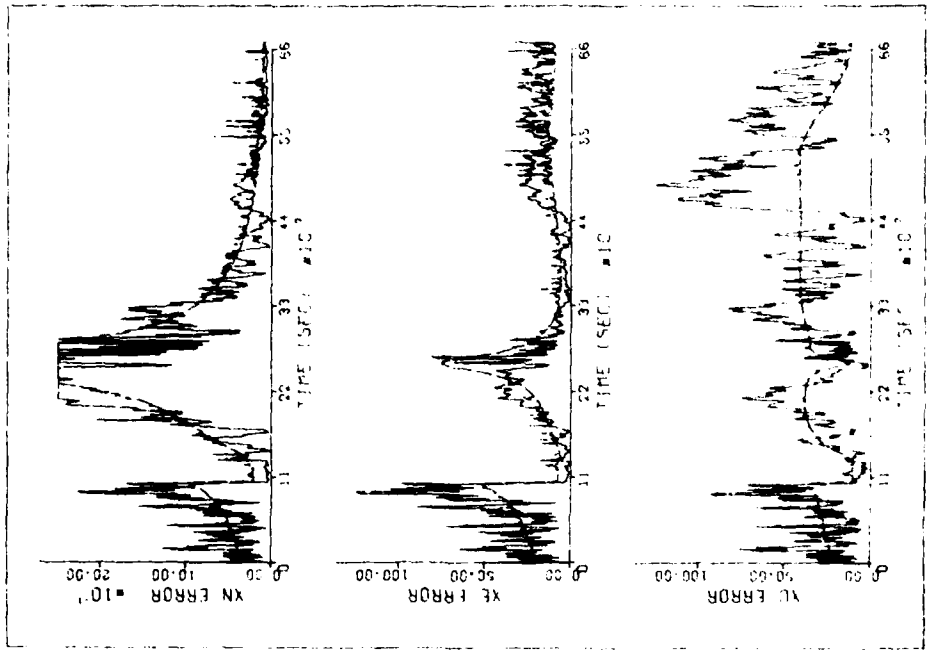

Figure 6.9 Case No. 12 Performance (q_β = 4.5 m^2/sec^5, $\beta(0)$ = 1 sec^{-1}, q_β = .0001 sec^{-3})

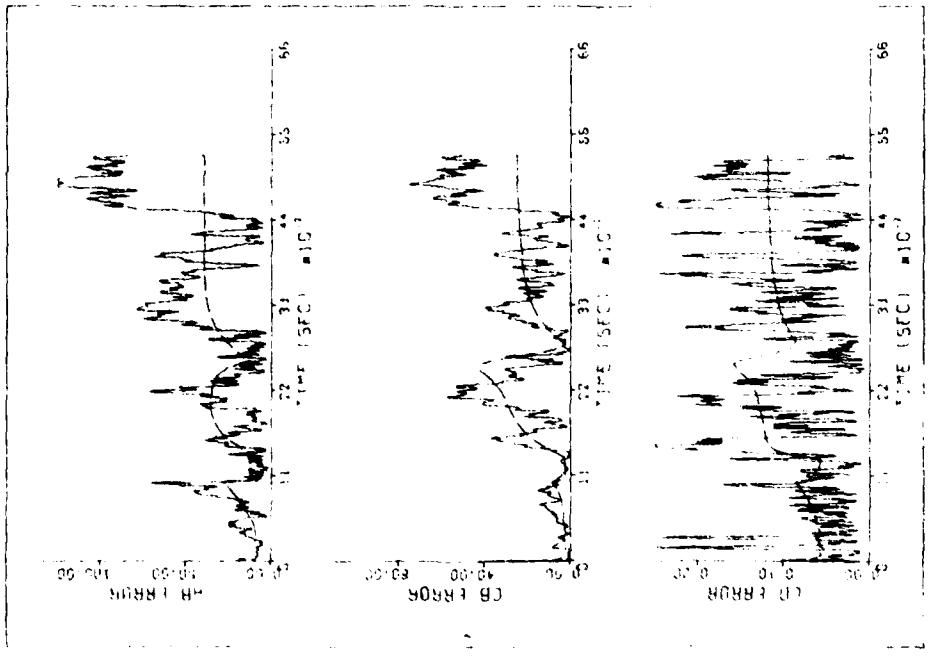

Figure 6.8 Case No. 11 Performance (q_β = .01875 m^2/sec^5, $\beta(0)$ = 1/20 sec^{-1}, q_β = .0001 sec^{-3}) (Continued)

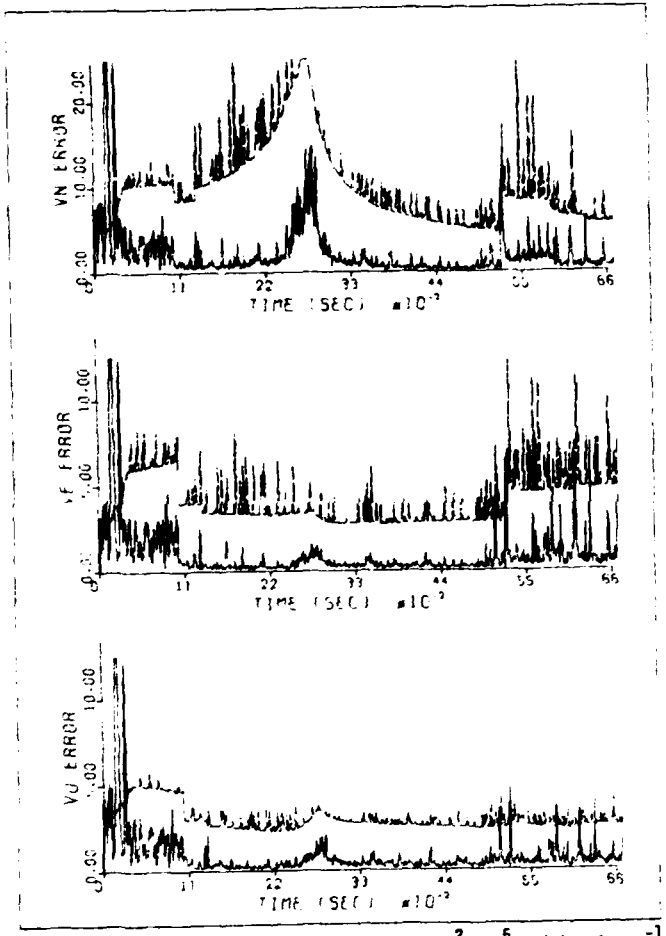

Figure 6.9 Case No. 12 Performance (q_a = 4.5 m^2/sec^5, $\beta(0)$ = 1 sec^{-1}, q_β = .0001 sec^{-3}) (Continued)

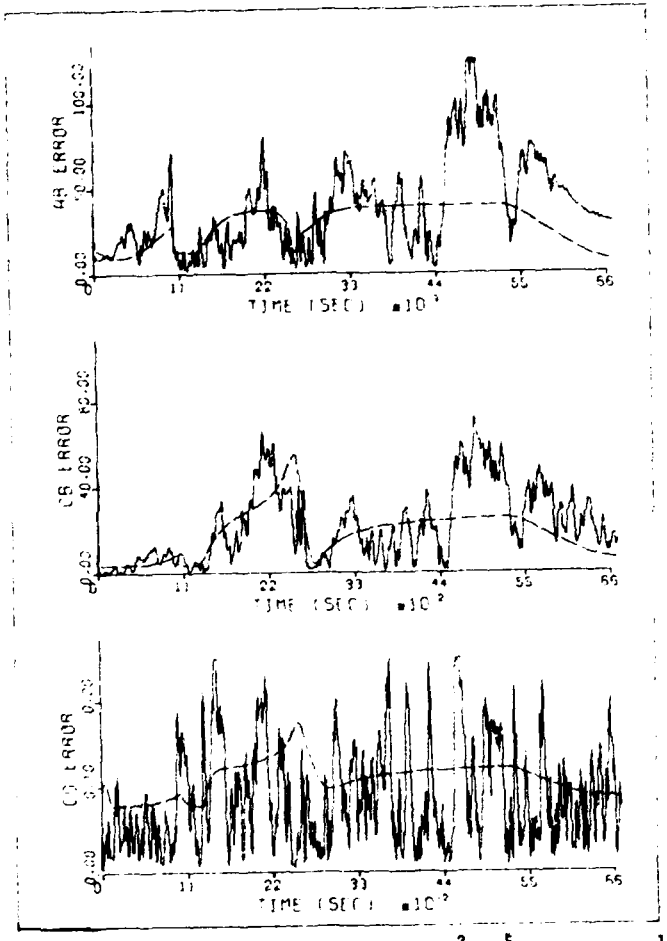

Figure 6.9 Case No. 12 Performance (q_a = 4.5 m^2/sec^5, $\beta(0)$ = 1 sec^{-1}, q_β = .0001 sec^{-3}) (Continued)

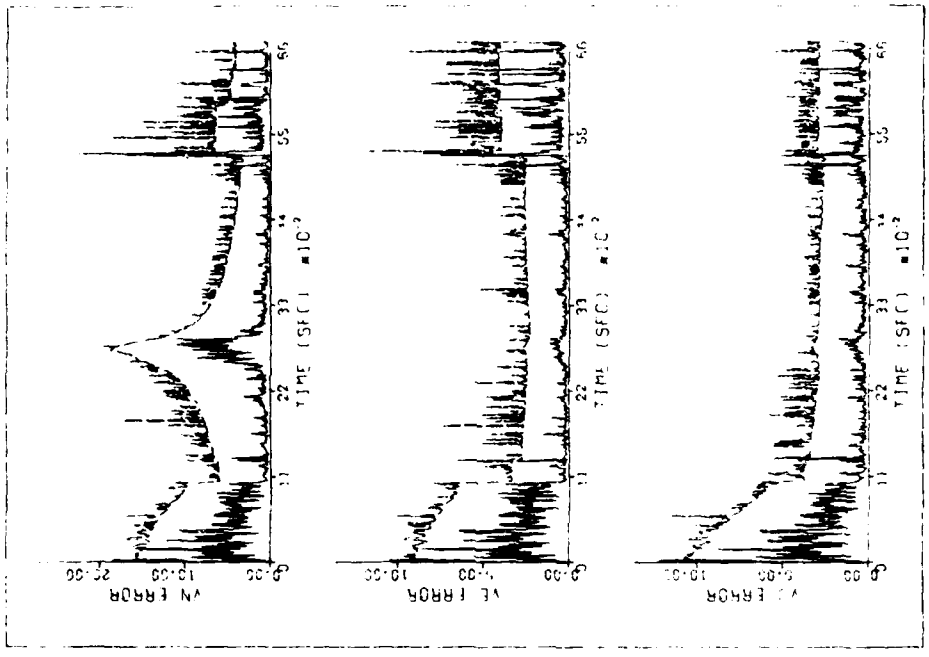

Figure 6.10 Case No. 13 Performance (q_a = 1.8 m^2/sec^5, $\beta(0)$ = 0, q_β = .0001 sec^{-3}) (Continued)

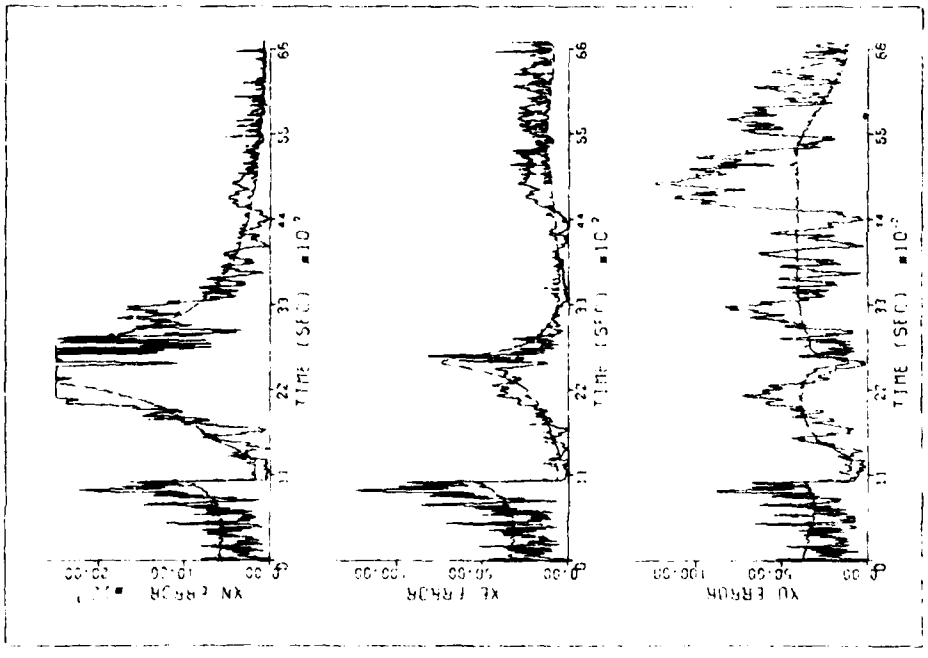

Figure 6.10 Case No. 13 Performance (q_a = 1.8 m^2/sec^5, $\beta(0)$ = 0, q_β = .0001 sec^{-3})

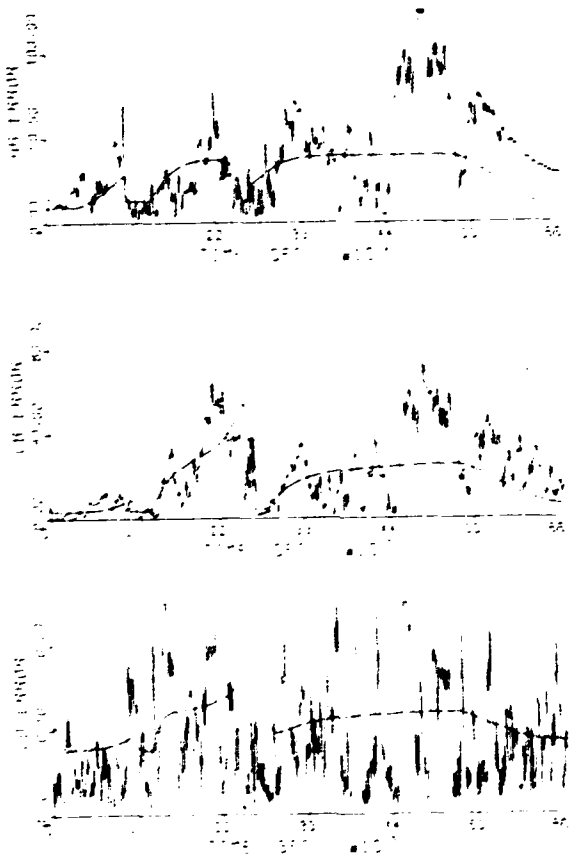

Figure 6.10 Case No. 13 Performance (q_θ = 1.8 m^2/sec^5, $\theta(0)$ = 0, q_ε = .0001 sec^{-3}) (Continued)

Table 6.13 Case No. 13 Performance (q_a = 1.8 m^2/sec^5, $\beta(0)$ = 0, q_β = .0001 sec^{-3})

	Flight Phase Final Times (sec)					
	598.75	1013.75	1295.00	2760.00	5100.00	6687.50
RSS POS ERR	54.94	142.62	18.07	241.07	99.31	56.75
RSS VEL ERR	7.98	5.11	1.04	2.55	2.03	3.45
MAX POS ERR	139.82	233.12	121.35	855.51	386.69	109.21D
MAX VEL ERR	26.77	11.69	3.90D	12.69	13.57	39.56
POS ERR/SIG	.73	1.57	.68	.82	1.05	1.56
VEL ERR/SIG	.41	.34	.12	.21	.25	.38

acceleration model, however, were competitive with the exponentially correlated acceleration models of Chapter 5. If computer time and/or storage are critical, the numerical results indicate that implementation of the uncorrelated random acceleration model will not result in a severe loss of accuracy. Testing of the exponentially correlated random acceleration model with an assumption of infinite correlation time demonstrated that this model also can be competitive with models using correlation times from one to fifty seconds.

Given the "competitive" performance of the uncorrelated random acceleration model and the infinite correlation time model, one might question the implementation of the more complex algorithm of Chapter 5. Following are some justifications for use of correlation times from one to fifty seconds.

1. The uncorrelated random acceleration model and the infinite correlation time random acceleration model simply appear to be less complex because they have reduced the numbers of parameters from the two associated with finite correlation time exponentially correlated random acceleration models (q_a and β) to one (q_v for the uncorrelated model and q_a for the infinite correlation time model). In reality, the simpler models have given up flexibility by losing one degree of freedom.

2. Intuitively, aircraft acceleration is not uncorrelated nor does it have an infinite correlation time.

3. It can be shown that for $\beta = \infty$, (uncorrelated random acceleration) and for $\beta = 0$ (infinite correlation time), the steady-state a posteriori position covariance vanishes. This behavior was also pointed out by Singer [68]. Accordingly, the steady-state filter gains are determined by the discrete process noise matrix Γ.

In an attempt to improve the performance of the exponentially correlated random acceleration algorithm, the filter state vector was expanded to include the inverse correlation times for the three aircraft directions. To accomplish this, the filter model was changed from a nominal constant acceleration assumption to a nominal exponential acceleration assumption. The resulting algorithm was unstable. The instability is probably due to the attempt by the algorithm to fit jumps in acceleration with exponential curves. The correlation time of the

estimated exponential acceleration resulted in adverse behavior of the covariance matrix propagation which, in turn, yielded catastrophic estimation results. This is apparent in the large increases in both covariance matrix and estimation errors shown in Figures 6.6 and 6.8.

An exponentially correlated random acceleration model depends on the parameters q_a, spectral level acceleration noise magnitude, and β, the inverse correlation time. Since estimation of inverse correlation time failed to produce improved algorithm performance without a loss in reliability, one is naturally led to consider the estimation of q_a. The technique chosen to accomplish estimation of q_a requires a modification to the Kalman filter operation. Accordingly, the Q-estimation algorithm will be classified an adaptive modification* and will be discussed in the following chapter.

---

*In this study, "non-adaptive" algorithms use the measurement residuals only to update the estimate of the state. (See Par. 4.6.) In the "adaptive" algorithms of this study, the measurement residuals will be also used to indicate non-optimal filter performance so that the algorithms can modify the filter operation.

CHAPTER 7

ADAPTIVE MODIFICATION OF FILTER STATISTICS

7.1 The Meaning and Uses of Measurement Residuals

If a Kalman filter is operating satisfactorily, then the covariance matrix will bound the errors in the estimated state. Without knowledge of the true state, however, the user cannot calculate the errors in the estimate. Therefore, he cannot determine whether the covariance matrix is correct for a given application. The covariance of the observation residual, however, is a natural product of the estimation process. Since the user calculates the residual as part of the filter operation, he can compare the statistical properties of the residuals with the statistics as predicted by the filter. If the predicted covariance matches the actual statistical behavior, then it can be assumed that the filter is operating properly.*

In its normal mode of operation, the Kalman filter uses the residual only to correct the a priori estimate of the state. The a priori state error covariance matrix, the measurement noise covariance matrix, and other filter parameters are assumed to be correct. Adaptive methods

*It must be emphasized that small observation residuals are not a guarantee that the error in the estimate is small. An ill-conditioned system may have small residuals, but large errors in the estimate.

seek to modify the filter gains either directly or by changing the values of the covariance matrices that are used in the gain computation. Adaptive methods generally consist of a performance index, which is a quantitive indicator of filter behavior, and a gain modification scheme, which is the specific technique used to modify the filter parameters. Frequently, the performance index is calculated using a sample variance of the residuals and the covariance of the residuals as determined from the a priori statistics. The gain modification scheme can be based on the formulation of the performance index or it can be an intuitively developed method.

The goal of any adaptive method is to permit a filter with incorrect a priori statistics to function satisfactorily. In systems with stationary statistics, successful adaptive methods can provide the user with better knowledge of the statistics in addition to providing an improved estimate of the state. If the statistics are not stationary but vary slowly with respect to the sampling interval, then adaptive methods may still improve the statistics assumed by the filter. For systems with rapidly changing statistics, the sample variance of the residuals, used to calculate the performance index, can be of questionable value since a sample variance is computed either using a number of past residuals, thereby including residuals from a time when the statistics were different from the current statistics, or by using a very limited number of residuals (for example, only the current residual) and is, therefore, of poor statistical significance. Unfortunately, it is for the case of rapidly changing statistics that an adaptive method

may be a requirement to maintain accuracy in the estimate and confidence in the covariance.

The statistical parameters for an exponentially correlated random acceleration model of an aircraft in cruising flight include typically a short correlation time and a low maneuver variance. The parameters for a maneuvering aircraft consist typically of large correlation times and large maneuver variances. The regimes of flight are not distinct and may be characterized by any combination of correlation times and maneuver variances within physical limits. More critical than the wide range of values for aircraft model parameters is the rapidity with which the aircraft may change from one flight regime to another.

In Chapter 5, the exponentially correlated random acceleration model was tested assuming stationary statistics for the aircraft model. As would be expected, no single set of parameters was "best" for all performance indicators. For this study, adaptive methods were derived, implemented, and tested in an attempt to find a filter which was competitive with the best performance indicators combined from the non-adaptive filter tests. To accomplish this, the intital conditions of Cases 1 through 4 and 7.5 were used with adaptive methods in the hopes of improving the poor performance areas of each filter without incurring a severe degradation in the good performance indicators of the non-adaptive filter.

Four adaptive methods were tested and the performance was evaluated using the simulated New York-to-Chicago flight. The four

algorithms studied are:

1. The Q-estimator in which the residual is used in a secondary filter to sequentially estimate elements of the process noise matrix.

2. Adaptive age-weighting in which the residual is used to directly scale the a priori covariance matrix.

3. Adaptive process noise weighting in which the residual is used to alter the a priori covariance matrix by applying a scale factor to the discrete process noise matrix.

4. An adaptive algorithm using a performance index developed by Aidala and Davis [78]. The performance index is used in an intuitively developed scheme to alter the amount of process noise added during the time propagation of the covariance matrix.

7.2 Estimation of the Spectral Level Process Noise Magnitude

7.2.1 Development of the Q-estimator. The results obtained using the Beta-estimation algorithm indicate a limited ability to match widely varying noise conditions. A filter that estimates the magnitude of the spectral level noise will now be examined. The development is similar to Tapley and Hagar [79] and Hagar [77:Par. 3.6]. Basically, the Q-estimator is the application of a Kalman filter to the estimation of the elements of the spectral level process noise matrix Q. Assuming scalar measurements, the extended sequential algorithm is implemented with the following definitions:

$\underline{q}_k$ is a vector composed of the elements of the matrix $B(t_k)Q(t_k)B^T(t_k)$ (see Eqs. 4.11 and 4.69);

r_k is the measurement residual;

$\bar{S}_k$ is the *a priori* q-covariance matrix* defined by

$$\bar{S}_k = E[(\bar{\underline{q}}_k - \underline{q}_k)\,(\bar{\underline{q}}_k - \underline{q}_k)^T \,|r_{k-1}];$$

S_k is the *a posteriori* q-covariance matrix defined by

$$S_k = E[(\hat{\underline{q}}_k - \underline{q}_k)(\hat{\underline{q}}_k - q_k)^T \,|r_k];$$

W_k is the discrete q-process noise matrix;

J_k is the q-observation-state matrix;

Δ_k is the q-observation residual. This will be defined to be $r_k^2 - E[r_k^2]$ and will be shown to be equal to $J_k\underline{\delta q}_k$ assuming $\underline{q} = \bar{\underline{q}} + \delta q$; and

T_k is the q-measurement noise term.

---

*The prefix "q-" will be used to distinguish the parameters of the filter which is used to estimate $\underline{q}$ from the parameters used in the filter which estimates the aircraft and measurement states.

The sequential Q-estimator algorithm is given as follows:

1. Propagate the state $\underline{q}$ and its covariance assuming an identity state transition matrix.

$$\bar{\underline{q}}_k = \hat{\underline{q}}_{k-1}$$

$$\bar{S}_k = S_{k-1} + W_k$$

2. Compute the gain.

$$M_k = \bar{S}_k J_k^T (J_k \bar{S}_k J_k^T + T_k)^{-1}$$

3. Determine the q-observation residual.

$$\Delta_k = r_k^2 - (H_k \bar{P}_k H_k^T + R_k)$$

4. Estimate the q-corrections.

$$\hat{\underline{\delta q}} = M_k \Delta_k$$

5. Update the q-covariance matrix.

$$S_k = (I - M_k J_k) \bar{S}_k$$

6. Rectify the spectral noise terms.

$$\hat{\underline{q}}_k = \bar{\underline{q}}_k + \hat{\underline{\delta q}}_k$$

At this point, the elements of $\hat{\underline{q}}_k$ are stored in the spectral noise matrix and the Kalman filter equations are used to obtain a navigation fix.

The primary difficulty in the Q-estimation algorithm is the development of the q-observation-state relationship J. Since the q-observation is defined to be the square of the measurement residuals, then the q-observation residual is the difference between the square of the measurement residual and the expected value of the square of the measurement residual. In other words, the q-observation residual is the difference between the single-sample variance of the residuals and the predicted variance of the residuals. Using the linear equations, the predicted residual is given by

$$\bar{r}_k = y_k - H_k \bar{x}_k \tag{7.1}$$

The a priori state vector is predicted using

$$\bar{x}_k = \phi(t_k, t_{k-1}) \hat{x}_{k-1} \tag{7.2}$$

The scalar measurement is assumed to be (see Eq. 4.52)

$$y_k = H_k x_k + \varepsilon_k \tag{7.3}$$

The actual state is assumed to propagate as

$$x_k = \phi(t_k, t_{k-1}) x_{k-1} + u_k \tag{7.4}$$

where: u_k represents the discrete process noise contribution.

Substituting Eqs. 7.2 through 7.4 into Eq. 7.1 provides an expression for the predicted residual $\bar{r}_k$.

$$\bar{r}_k = H_k\Phi(t_k,t_{k-1})(\underline{x}_{k-1} - \hat{\underline{x}}_{k-1}) + H_k\underline{u}_k + \varepsilon_k \qquad (7.5)$$

Applying the expected value operator to the inner product of the predicted residual yields

$$E[\bar{r}_k\bar{r}_k^T] = E[\bar{r}_k^2] = H_k\Phi(t_k,t_{k-1})P(t_{k-1})\Phi^T(t_k,t_{k-1})H_k^T + H_k\Gamma(t_k)H_k^T + R_k \qquad (7.6)$$

where: $\Gamma(t_k)$ is the discrete process noise matrix and contains the elements of the spectral level noise matrix $Q(t_k)$ as evaluated using Eq. 4.89.

The q-observation-state matrix J can be obtained from Eq. 7.6 by expanding $H_k\Gamma(t_k)H_k^T$ in terms of the elements of the spectral level noise matrix. Equation 5.22 becomes

$$E[\bar{r}_k^2] = H_k\Phi(t_k,t_{k-1})P(t_{k-1})\Phi^T(t_k,t_{k-1})H_k^T + J_k\underline{q}_k + R_k \qquad (7.7)$$

The term $H_k\Gamma(t_k)H_k^T$ has been replaced by the product of the vector composed of the elements of the spectral level noise matrix and the matrix J_k. The q-observation-state relationship is contained in the elements of J_k. The determination of J will be discussed later. Hagar [79:101] has shown that the replacement is valid for scalar measurements.

The square of the true residual is assumed to be

$$r_k^2 = H_k\Phi(t_k,t_{k-1})P(t_{k-1})\Phi(t_k,t_{k-1})H_k^T + J_k(\bar{q}_k + \delta\underline{q}_k) + R_k \qquad (7.8)$$

The q-measurement residual is then

$$\Delta_k = r_k^2 - E[\bar{r}_k^2] = J_k \underline{\delta q}_k \tag{7.9}$$

If only the diagonal elements of the spectral level process noise matrix are to be estimated using only pseudo-range, pseudo-range-rate, and altimeter measurements, then the resulting expressions for the basic twelve-state filter are

$$\underline{q}^T = [Q_{1,1}, Q_{2,2}, \ldots, Q_{12,12}] \tag{7.10}$$

$$J = [J_1, J_2, \ldots, J_{12}] \tag{7.11}$$

where:

$$J_1 = H_1^2 \Delta t$$

$$J_2 = H_2^2 \Delta t$$

$$J_3 = H_3^2 \Delta t$$

$$J_4 = H_1^2 \Delta t^3/3 + H_1 H_4 \Delta t^2 + H_4^2 \Delta t$$

$$J_5 = H_2^2 \Delta t^3/3 + H_2 H_5 \Delta t^2 + H_5^2 \Delta t$$

$$J_6 = H_3^2 \Delta t^3/3 + H_3 H_6 \Delta t^2 + H_6^2 \Delta t$$

$$J_7 = H_1^2 \gamma_{rr}(\beta_N) + 2H_1 H_4 \gamma_{rv}(\beta_N) + H_4^2 \gamma_{vv}(\beta_N)$$

$$J_8 = H_2^2 \gamma_{rr}(\beta_E) + 2H_2 H_5 \gamma_{rv}(\beta_E) + H_5^2 \gamma_{vv}(\beta_E)$$

$$J_9 = H_3^2\gamma_{rr}(\beta_D) + 2H_3H_6\gamma_{rv}(\beta_D) + H_6^2\gamma_{vv}(\beta_D)$$

$$J_{10} = H_{10}^2\gamma_{aa}(\beta_{alt})$$

$$J_{11} = H_{11}^2\Delta t$$

$$J_{12} = H_{11}^2\gamma_{vv}(\beta_{clk}) + 2H_{11}H_{12}\gamma_{va}(\beta_{clk}) + H_{12}^2\gamma_{aa}(\beta_{clk}); \text{ and}$$

the γ terms are defined in Eq. 5.42.

Estimation of the diagonal elements only has the following advantages compared to estimation of the entire spectral noise matrix:

1. The size of the Q-estimator state is limited to the same size as the navigation algorithm state. Including a 9x9 Q-matrix for the aircraft states and a 2x2 Q-matrix for the clock states would increase the q-estimator state to 49 terms.

2. Positive-definiteness of the Q-matrix can be assured by insuring that all the elements of $\hat{q}$ are positive.

3. The results are easily implemented into the basic filter mechanization where an analytical solution for the discrete process noise matrix is used.

The q-process noise matrix W_k and the q-measurement noise T_k remain to be specified. For the test runs, the q-process noise matrix was a diagonal matrix with constant values. The measurement noise term

T_k was computed as follows:

$$T_o = \Delta_o^2$$
$$T_k = 0.9\, T_{k-1} + \Delta_k^2 \qquad (7.11)$$

This simple method maintains a finite positive value for the q-measurement noise term without the requirement to maintain a table of residuals.

Systems with inertia cannot experience instantaneous changes in position and velocity. Uncorrelated random process noise for such systems cannot, therefore, appear as position and velocity terms. Accordingly $Q_{1,1}$,$Q_{2,2}$, and $Q_{3,3}$ should be identically zero. Physically non-realizable process noise can be included, however, if their appearance can be justified as approximations to physically justifiable noise. In fact, the spectral level process noise (white noise) used in the development of the exponentially correlated random acceleration model is not physically realizable. Also, if it can be shown that the inclusion of a physically non-realizable noise improves the performance of a filter, then arguments against their appearance may become superfluous.

7.2.2 Results of Q-Estimator Tests. The 600-second tests of the Q-estimator are summarized in Table 7.1. For these tests, the acceleration process noise terms and the measurement bias process noise terms were estimated. The q-process noise terms for the acceleration, identified as W_a, were identical for all acceleration components. The

Table 7.1 Initial Evaluation of Process Noise Estimation Algorithm

	W_a Process Noise (m^4/sec^{11})					
	.00	.01	.10	1.00	10.00	100.00
q_a = .225 m^2/sec^5, β = 1/20 sec^{-1}						
RSS POS ERR	58.66	58.90	58.60	56.52	62.81	60.43
RSS VEL ERR	9.18	9.16	8.96	6.88	9.01	10.40
MAX POS ERR	149.36	149.30	148.75	136.65	204.77	156.79
MAX VEL ERR	30.58	30.56	30.37	29.94	33.73	34.82
POS ERR/SIG	1.04	1.08	1.10	1.20	1.32	1.15
VEL ERR/SIG	1.00	1.00	1.03	1.07	1.35	1.08
FIN POS ERR	50.01	52.52	38.62	15.61	34.75	37.18
FIN VEL ERR	4.11	4.09	.87	.45	1.06	2.35
q_a = .375 m^2/sec^5, β = 1 sec^{-1}						
RSS POS ERR	298.96	297.81	297.44	293.83	266.05	221.49
RSS VEL ERR	34.57	34.47	34.44	34.22	32.62	32.72
MAX POS ERR	758.56	753.76	752.73	742.72	668.98	475.31
MAX VEL ERR	74.39	74.08	74.02	73.42	69.60	72.64
POS ERR/SIG	7.18	7.63	7.62	7.51	6.71	5.29
VEL ERR/SIG	13.24	13.23	13.21	13.01	11.69	8.53
FIN POS ERR	22.79	33.77	33.64	33.10	62.63	357.01
FIN VEL ERR	4.19	4.14	4.14	4.17	7.56	26.93
q_a = .01875 m^2/sec^5, β = 1/20 sec^{-1}						
RSS POS ERR	91.25	90.60	85.35	68.08	56.64	53.87
RSS VEL ERR	16.16	15.96	14.21	10.31	8.35	7.85
MAX POS ERR	258.69	256.66	229.88	158.98	192.30	201.93
MAX VEL ERR	41.88	41.36	34.48	27.63	33.33	36.57
POS ERR/SIG	1.98	2.07	1.99	1.54	1.26	1.11
VEL ERR/SIG	3.70	3.69	3.40	2.13	1.48	1.07
FIN POS ERR	25.66	27.66	92.88	90.54	30.87	34.17
FIN VEL ERR	1.46	1.26	5.49	5.01	1.02	2.32

Table 7.1 Initial Evaluation of Process Noise Estimation Algorithm (Continued)

	W_a Process Noise (m^4/sec^{11})					
	.00	.01	.10	1.00	10.00	100.00
$q_a = 4.5\ m^2/sec^5$, $\beta = 1\ sec^{-1}$						
RSS POS ERR	107.12	107.04	107.04	107.02	106.46	167.17
RSS VEL ERR	19.18	19.15	19.15	19.11	18.54	29.46
MAX POS ERR	300.99	300.72	300.71	300.57	297.52	482.87
MAX VEL ERR	43.44	43.43	43.43	43.35	42.18	83.83
POS ERR/SIG	2.06	2.14	2.14	2.15	2.94	3.63
VEL ERR/SIG	2.83	2.82	2.83	2.83	2.94	5.54
FIN POS ERR	42.03	44.02	43.93	43.07	15.94	69.01
FIN VEL ERR	1.12	1.16	1.15	1.08	5.58	15.39
$q_a = 1.8\ m^2/sec^5$, $\beta = 0$						
RSS POS ERR	55.80	56.01	56.00	55.87	54.95	119.60
RSS VEL ERR	8.67	8.67	8.66	8.56	6.76	22.61
MAX POS ERR	139.95	140.59	140.56	140.25	124.13	399.38
MAX VEL ERR	28.73	28.73	28.72	28.61	27.08	66.56
POS ERR/SIG	.72	.74	.74	.75	.92	2.22
VEL ERR/SIG	.42	.42	.42	.42	.49	2.10
FIN POS ERR	80.52	82.82	82.57	79.23	38.83	48.53
FIN VEL ERR	11.51	11.57	11.50	10.58	1.35	3.21

q-process noise terms for the measurement bias states were: 10^{-3} m^4/sec^3 for the altimeter bias; 10^{-5} m^4/sec^3 for the clock bias; and 10^{-6} m^4/sec^7 for the clock drift. The q-process noise terms for the measurement bias states were not varied in the test summarized in Table 7.1. Since the altimeter process noise was to be estimated, the non-stationary term used in the basic twelve-state filter was eliminated. It was anticipated that the Q-estimator would determine the proper value of process noise for the altimeter bias state. The process noise estimates were restricted to values greater than 10^{-14} in all cases.

The results of the Table 7.1 tests indicate that the Q-estimator is capable of improving the performance of the filter compared to the performance of the corresponding non-adaptive filter. The performance changes became more pronounced as the q-process noise is increased but the algorithm did not appear to have the instability of the Beta-estimator.

The Case 1 and Case 7.5 initial conditions were selected for full flight tests with q-process noise in the acceleration components equal to 1 m^4/sec^{11} and 10 m^4/sec^{11} respectively and with the q-process noise for the measurement bias states that were used in the Table 7.1 tests. Case 14, using the initial conditions of Case 1, is summarized in Table 7.2 and Figure 7.1. Case 15, using the initial conditions of Case 7.5, is summarized in Table 7.3 and Figure 7.2.

Table 7.2 Case No. 14 Performance ($q_a(0) = .225\ m^2/sec^5$, $\beta = 1/20\ sec^{-1}$, $W_a = 1\ m^4/sec^{11}$)

	Flight Phase Final Times (sec)					
	598.75	1013.75	1295.00	2760.00	5100.00	6687.50
RSS POS ERR	56.92	136.67	25.41	155.54	209.87	1123.74
RSS VEL ERR	6.88	1.16	.43	1.38	1.19	8.78
MAX POS ERR	136.65	220.43	123.52	426.45	498.78D	1308.55
MAX VEL ERR	29.94	1.82	2.26D	8.91	10.03	137.36
POS ERR/SIG	1.20	4.23	2.77	2.98	6.96	67.38
VEL ERR/SIG	1.07	1.21	.46	.38	.40	2.12

Table 7.3 Case No. 15 Performance ($q_a(0) = 1.8\ m^2/sec^5$, $\beta = 0$, $W_a = 10\ m^4/sec^{11}$)

	Flight Phase Final Times (sec)					
	598.75	1013.75	1295.00	2760.00	5100.00	6687.50
RSS POS ERR	54.95	141.30	27.37	147.25	185.13	1007.69
RSS VEL ERR	6.76	1.73	1.06	2.94	2.97	6.27
MAX POS ERR	124.13	229.34	128.93	504.26	603.97	1200.32
MAX VEL ERR	27.08	3.91D	7.52D	25.51	30.89	110.09
POS ERR/SIG	.92	3.73	2.41	2.30	4.34	52.22
VEL ERR/SIG	.49	.65	.41	.25	.37	1.01

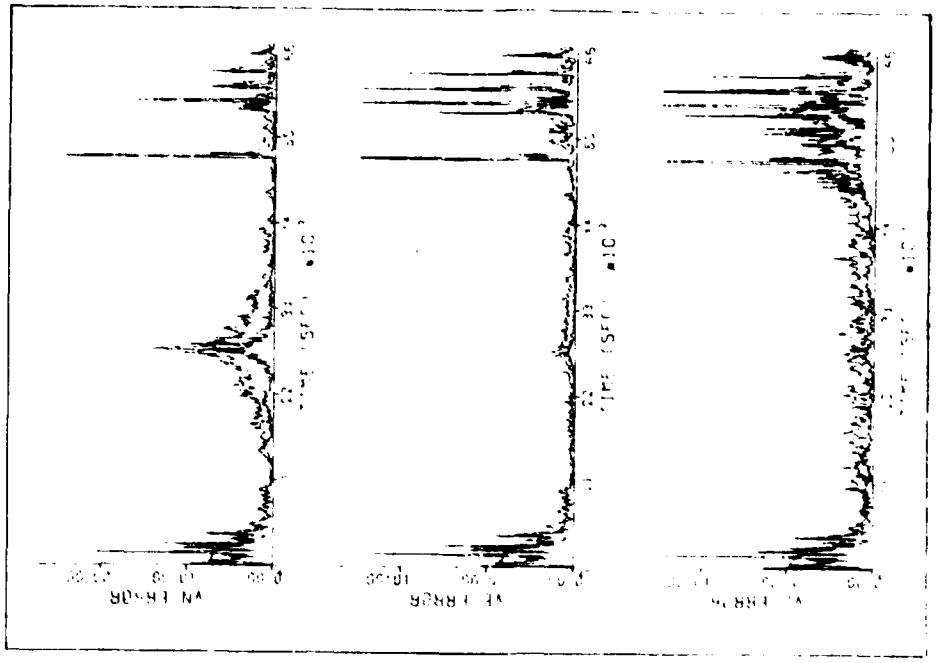

Figure 7.1 Case No. 14 Performance ($q_a(0) = .225\ m^2/sec^5$, $\beta = 1/20\ sec^{-1}$, $W_a = 1\ m^4/sec^{11}$) (Continued)

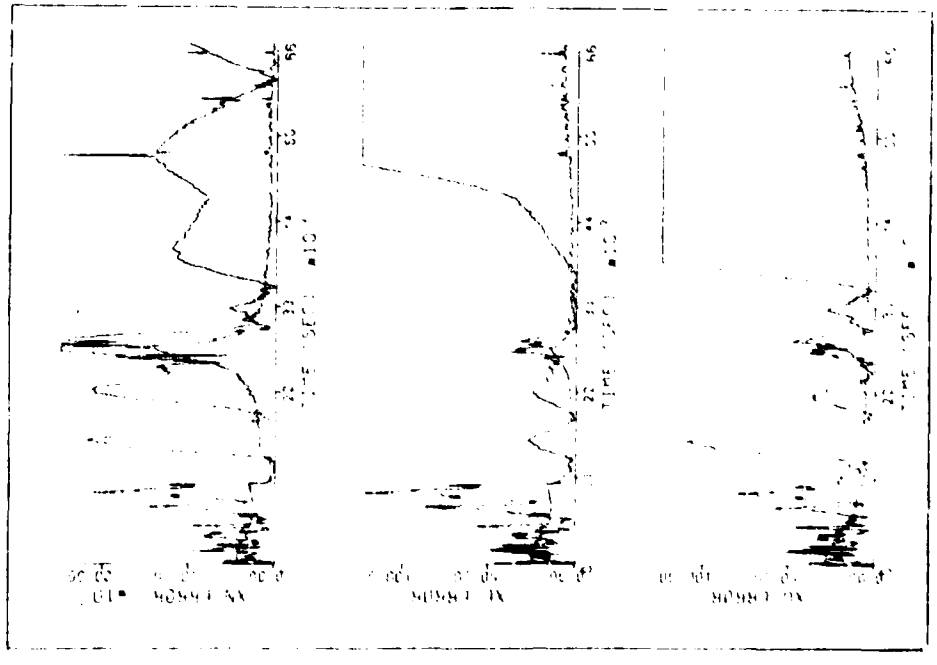

Figure 7.1 Case No. 14 Performance ($q_a(0) = .225\ m^2/sec^5$, $\beta = 1/20\ sec^{-1}$, $W_a = 1\ m^4/sec^{11}$)

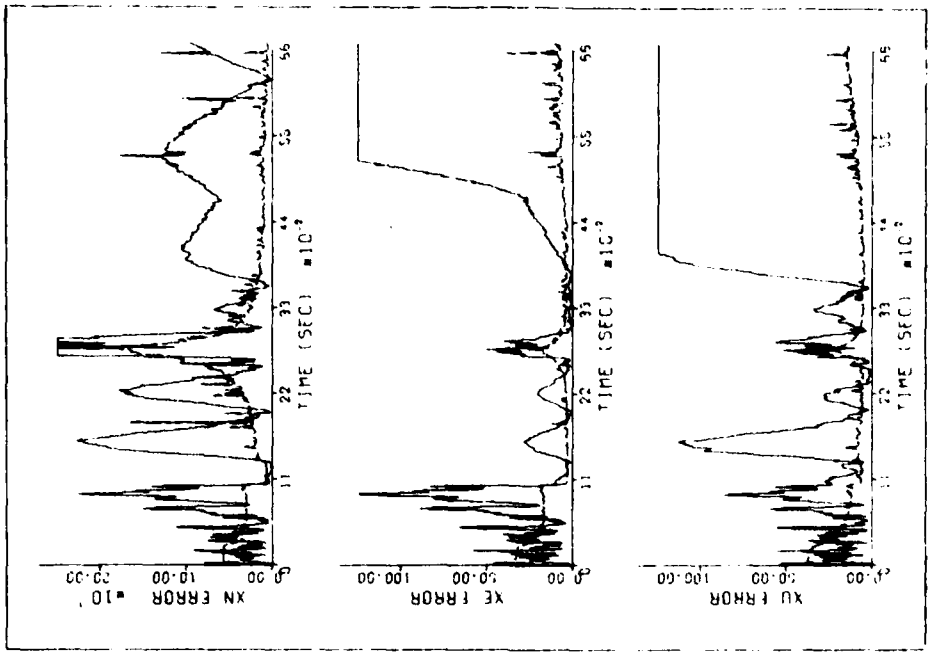

Figure 7.2 Case No. 15 Performance ($q_a(0) = 1.8\ m^2/sec^5$, $\beta = 0$, $M_a = 10\ m^4/sec^{11}$)

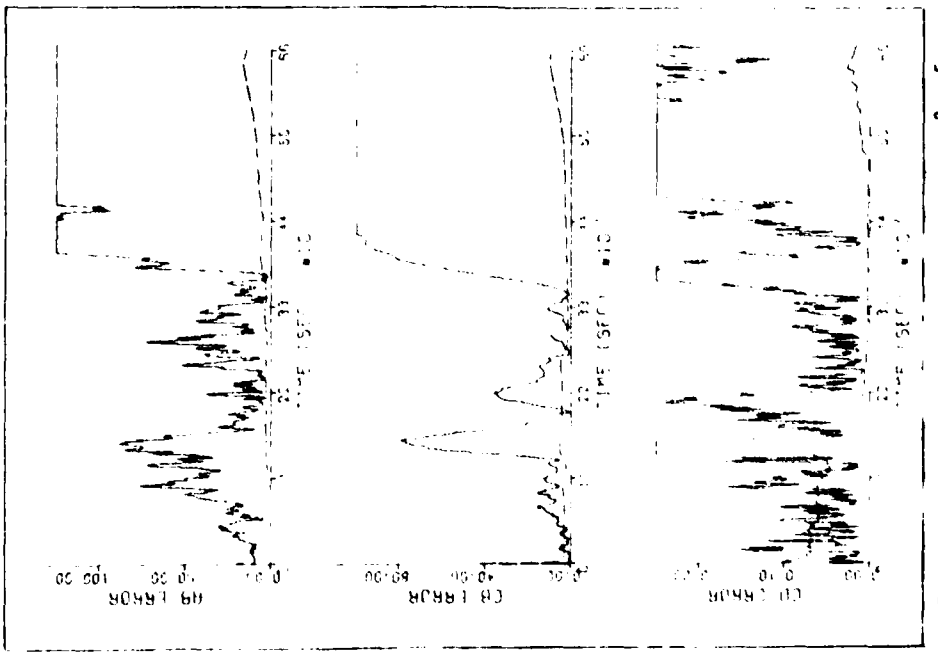

Figure 7.1 Case No. 14 Performance ($q_a(0) = .225\ m^2/sec^5$, $\beta = 1/20\ sec^{-1}$, $M_a = 1\ m^4/sec^{11}$) (Continued)

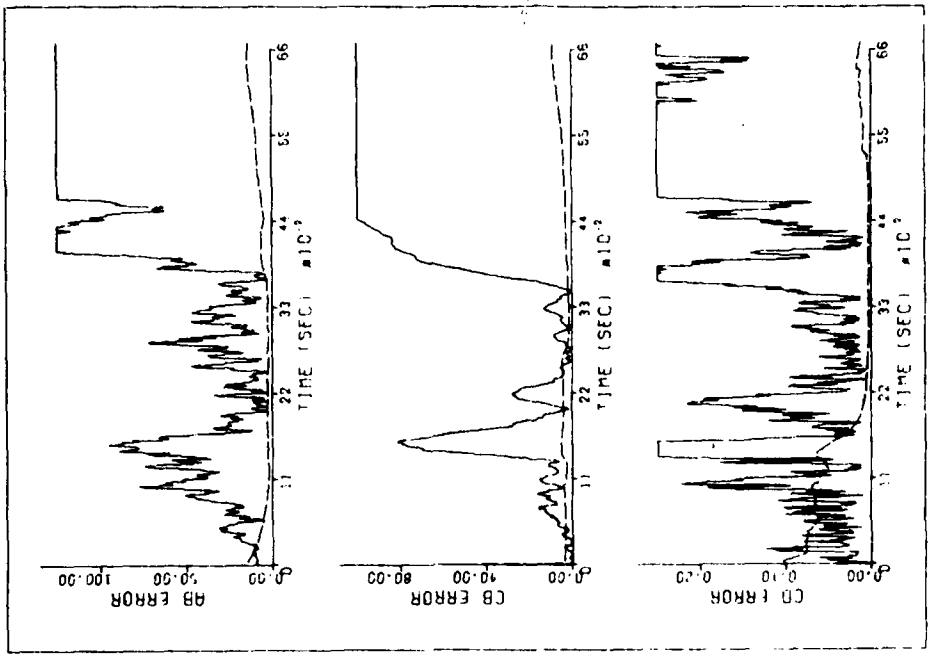

Figure 7.2 Case No. 15 Performance ($q_g(0) = 1.8\ m^2/sec^5$, $\beta = 0$, $H_g = 10\ m^4/sec^{11}$) (Continued)

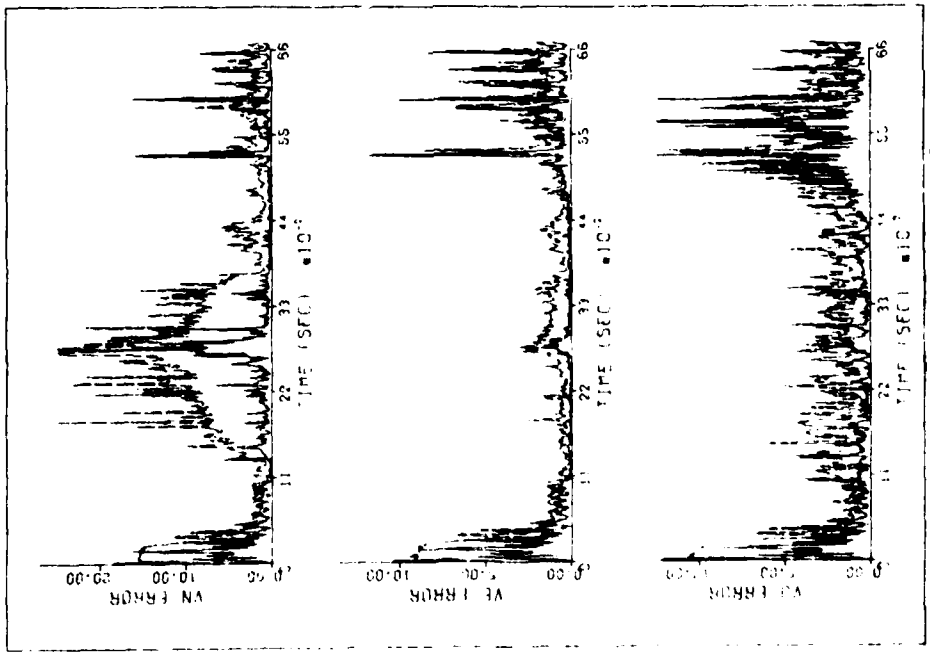

Figure 7.2 Case No. 15 Performance ($q_g(0) = 1.8\ m^2/sec^5$, $\beta = 0$, $H_g = 10\ m^4/sec^{11}$) (Continued)

The predicted process noise terms were generally optimistic. This is evident from the standard deviation curves of Figures 7.1 and 7.2. The gains became small and the filter had difficulty following the aircraft position. Errors became unacceptably large later in flight. In addition, the q-estimator was not determining the proper altimeter process noise.

A test was made using the Case 1 initial conditions in which the altimeter bias q-process noise was increased to 10^{-1} m^4/sec^3. This test used the acceleration state q-process noise of 1 m^4/sec^{11} as in Case 15. The results are given in Table 7.4 and are shown in Figure 7.3. Although there is some improvement, the final flight phase RSS position error was still greater than one kilometer. The altimeter bias q-process noise was increased further but the filter performance did not improve.

Table 7.4 Case No. 16 Performance ($q_a(0) = .225$ m^2/sec^5, $\beta = 1/20$ sec^{-1}, $W_a = 1$ m^4/sec^{11})

	Flight Phase Final Times (sec)					
	598.75	1013.75	1295.00	2760.00	5100.00	6687.50
RSS POS ERR	56.53	157.16	23.73	150.72	174.39	1065.25
RSS VEL ERR	6.88	1.12	.35	1.71	1.05	3.78
MAX POS ERR	136.64	246.86	157.89	398.25	479.55	1218.16D
MAX VEL ERR	29.94	1.82	1.38D	11.04	9.47	36.83
POS ERR/SIG	1.19	3.74	2.40	1.35	5.12	50.91
VEL ERR/SIG	1.08	1.16	.50	.48	.36	1.29

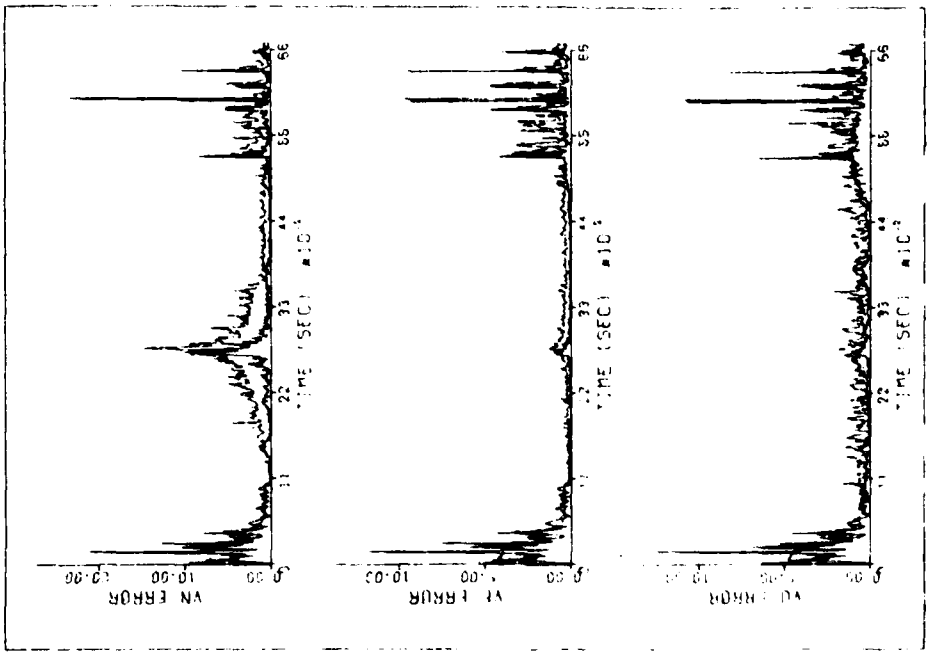

Figure 7.3 Case No. 16 Performance ($q_a(0) = .225\ m^2/sec^5$, $\beta = 1/20\ sec^{-1}$, $H_a = 1\ m^4/sec^{11}$) (Continued)

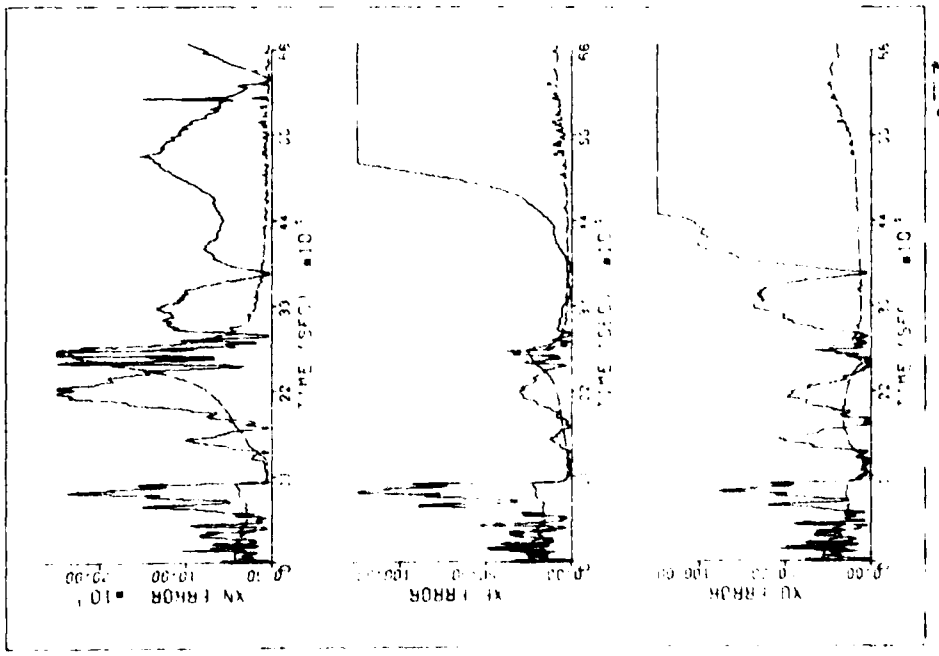

Figure 7.3 Case No. 16 Performance ($q_a(0) = .225\ m^2/sec^5$, $\beta = 1/20\ sec^{-1}$, $H_a = 1\ m^4/sec^{11}$)

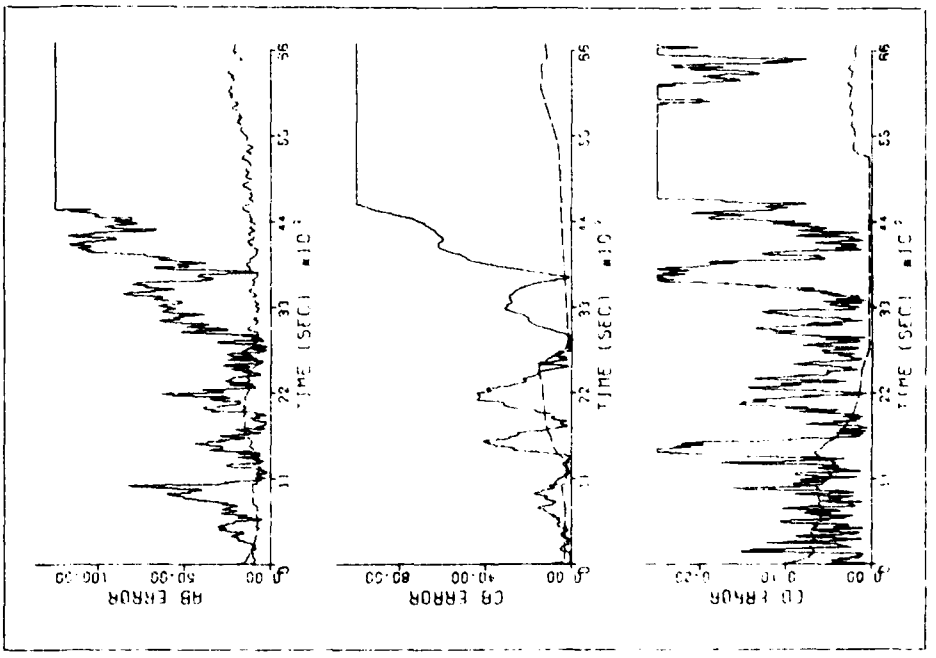

Figure 7.3 Case No. 16 Performance ($q_a(0) = .225\ m^2/sec^5$, $\beta = 1/20\ sec^{-1}$, $M_a = 1\ m^4/sec^{11}$) (Continued)

The Q-estimator was then modified so that only the acceleration process noise terms were estimated. Spot checks of 600-second tests were made to determine the validity of Table 7.1 for the reduced state Q-estimator. The revised Q-estimator resulted in better performance than the corresponding Table 7.1 tests but the relative behavior of the revised filters was similar to the behavior shown in Table 7.1. The revised Q-estimator was tested for the entire flight using the Case 1, Case 3, and Case 7.5 initial conditions with acceleration q-process noise equal to 1 m^4/sec^{11}, 10 m^4/sec^{11} respectively. The results, identified as Cases 17, 18, and 19 are given in Tables 7.5 through 7.7 and in Figures 7.4 through 7.6. In general, the revised Q-estimator performance is similar to the performance of the 12-state filter with some improvement early in flight and some degradation later in flgiht.

Table 7.5 Case No. 17 Performance ($q_a(0)$ = .225 m^2/sec^5, β = 1/20 sec^{-1}, W = 1 m^4/sec^{11})

	Flight Phase Final Times (sec)					
	598.75	1013.75	1295.00	2760.00	5100.00	6687.50
RSS POS ERR	56.18	142.75	21.24	208.25	102.21	55.42
RSS VEL ERR	6.88	.52	.33	1.93	1.00	3.57
MAX POS ERR	136.66	223.29	140.59	842.82	229. 53	110.99D
MAX VEL ERR	29.94	1.90	1.44	8.69	8.85	26.75D
POS ERR/SIG	1.14	1.98	1.48	.82	1.22	1.78
VEL ERR/SIG	1.08	1.08	.53	.49	.33	1.02

Table 7.6 Case No. 18 Performance ($q_a(0) = .01875\ m^2/sec^5$, $\beta = 1/20\ sec^{-1}$, $W = 10\ m^4/sec^{11}$)

	Flight Phase Final Times (sec)					
	598.75	1013.75	1295.00	2760.00	5100.00	6687.50
RSS POS ERR	56.59	143.35	20.83	235.26	104.62	62.26
RSS VEL ERR	8.34	1.58	.46	2.20	1.64	3.26
MAX POS ERR	192.29	233.12	142.56	925.12	283.80	114.75D
MAX VEL ERR	33.33	2.75D	2.10D	10.82	13.34	34.18
POS ERR/SIG	1.19	1.94	1.35	.87	1.17	1.93
VEL ERR/SIG	1.48	.73	.26	.23	.21	.64

Table 7.7 Case No. 19 Performance ($q_a(0) = 1.8\ m^2/sec^5$, $\beta = 0$, $W = 10\ m^4/sec^{11}$)

	Flight Phase Final Times (sec)					
	598.75	1013.75	1295.00	2760.00	5100.00	6687.50
RSS POS ERR	54.66	152.54	22.20	234.54	105.32	62.14
RSS VEL ERR	6.76	1.66	.50	2.47	2.04	3.13
MAX POS ERR	123.40	240.82	152.45	921.55	272.93	115.45D
MAX VEL ERR	27.08	3.63D	2.14D	13.80	17.07	33.97
POS ERR/SIG	.89	2.04	1.44	.87	1.17	1.90
VEL ERR/SIG	.49	.61	.26	.23	.23	.57

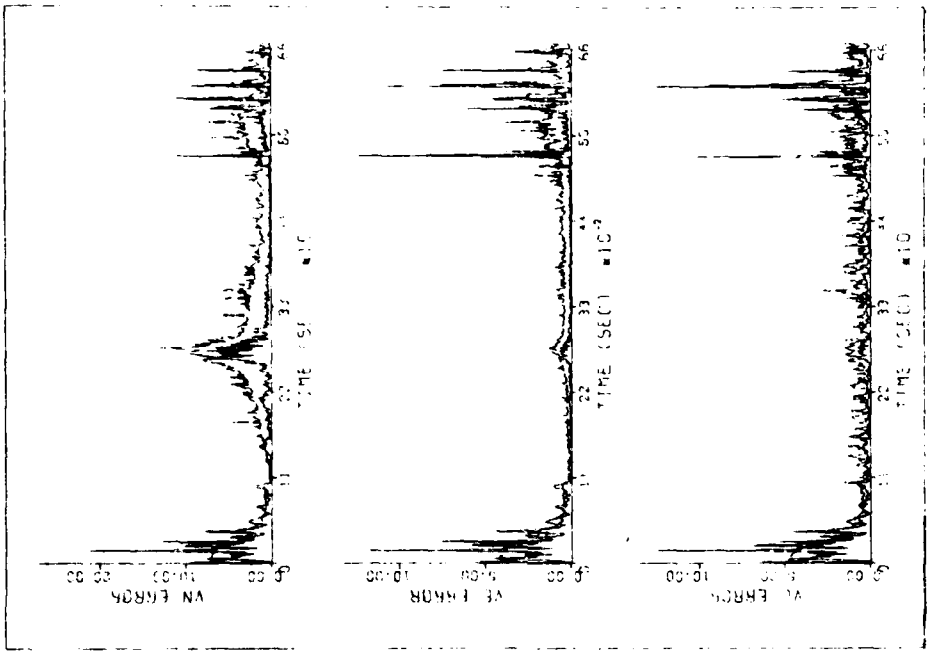

Figure 7.4 Case No. 17 Performance ($q_a(0) = .225\ m^2/sec^5$, $\beta = 1/20\ sec^{-1}$, $W = 1\ m^4/sec^{11}$) (Continued)

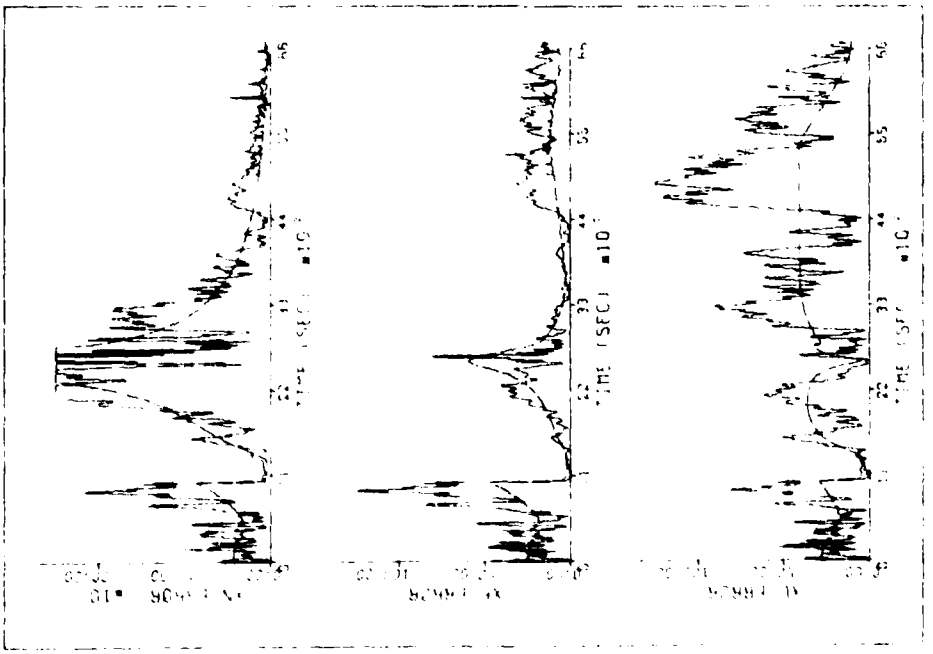

Figure 7.4 Case No. 17 Performance ($q_a(0) = .225\ m^2/sec^5$, $\beta = 1/20\ sec^{-1}$, $W = 1\ m^4/sec^{11}$)

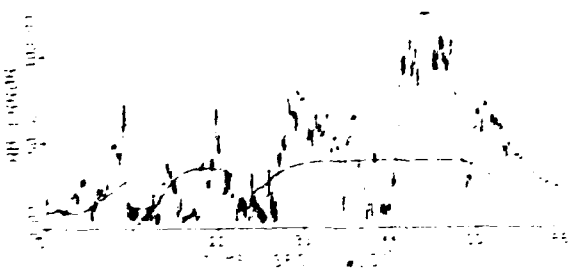

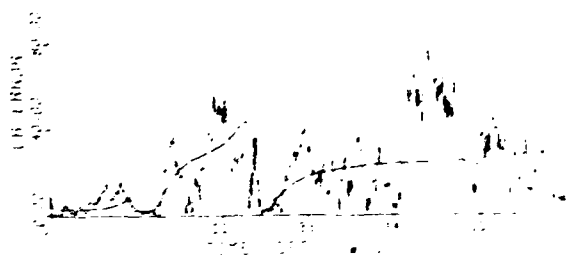

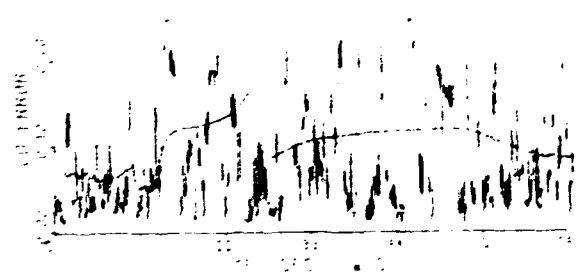

Figure 7.4 Case No. 17 Performance ($q_a(0)$ = .225 m^2/sec^5, ε = 1/20 sec^{-1}, W = 1 m^4/sec^{11}) (Continued)

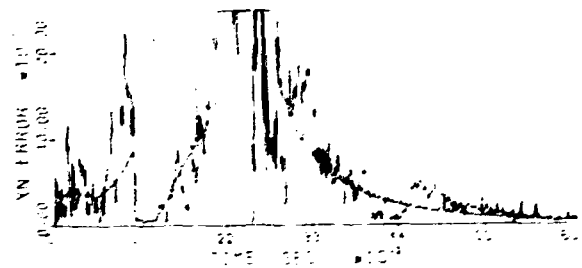

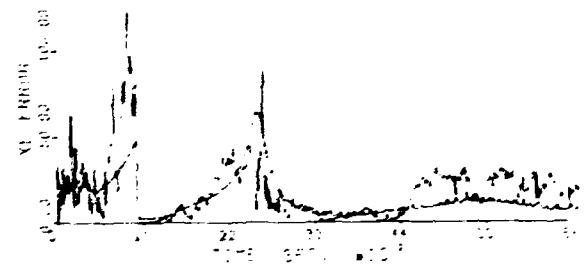

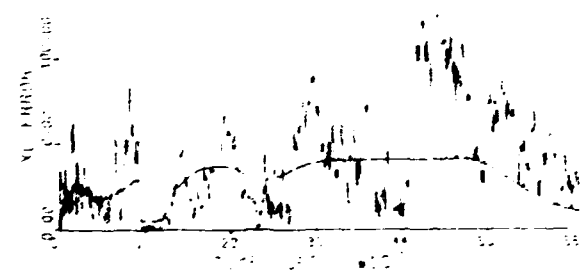

Figure 7.5 Case No. 18 Performance ($q_a(0)$ = .01875 m^2/sec^5, ε = 1/20 sec^{-1}, W = 10 m^4/sec^{11})

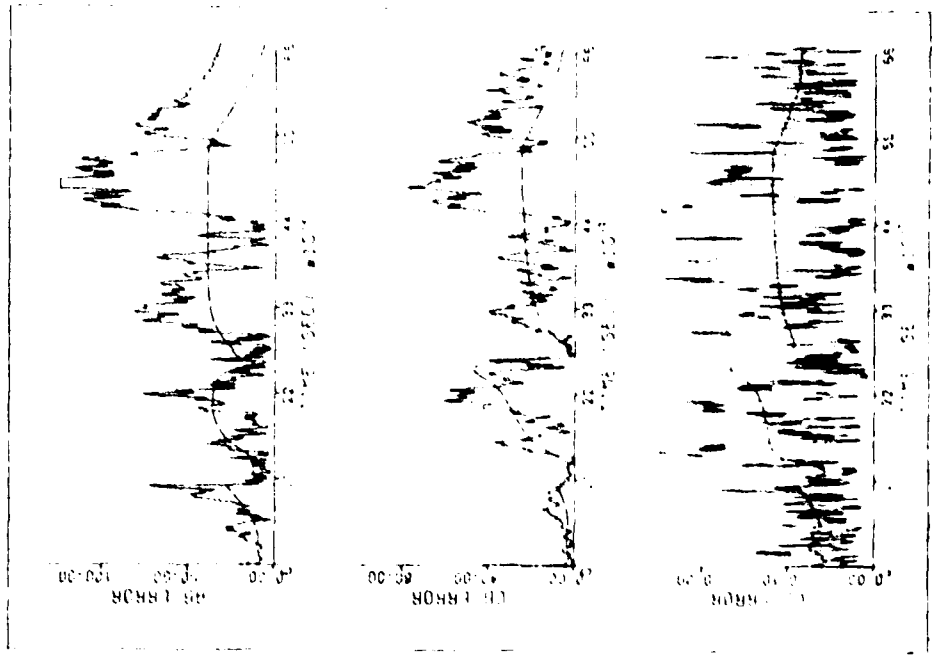

Figure 7.5 Case No. 18 Performance ($q_s(0) = .01875\ m^2/sec^5$, $\beta = 1/20\ sec^{-1}$, $M = 10\ m^4/sec^{11}$) (Continued)

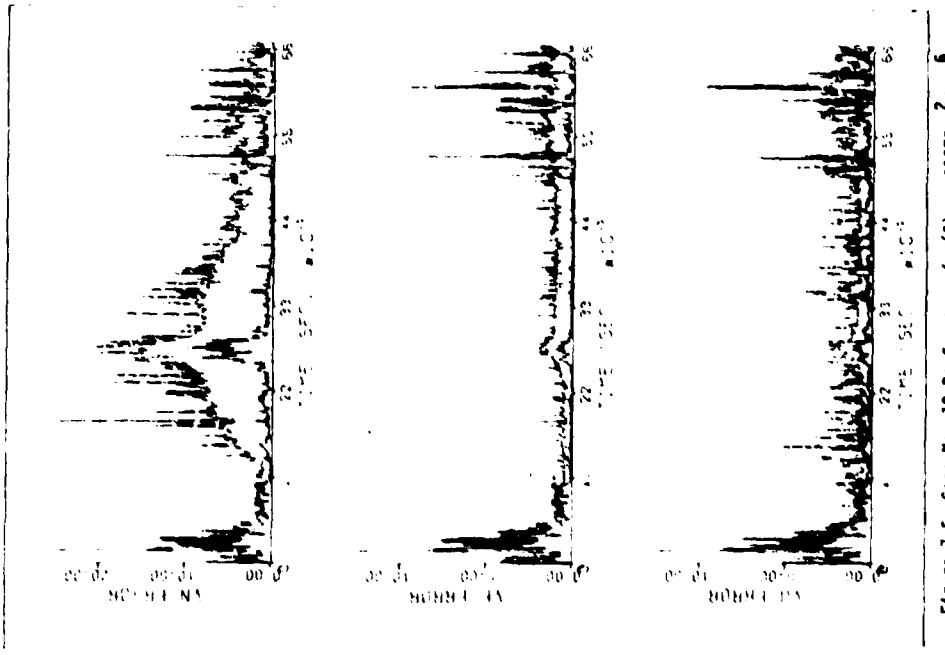

Figure 7.5 Case No. 18 Performance ($q_s(0) = .01875\ m^2/sec^5$, $\beta = 1/20\ sec^{-1}$, $M = 10\ m^4/sec^{11}$) (Continued)

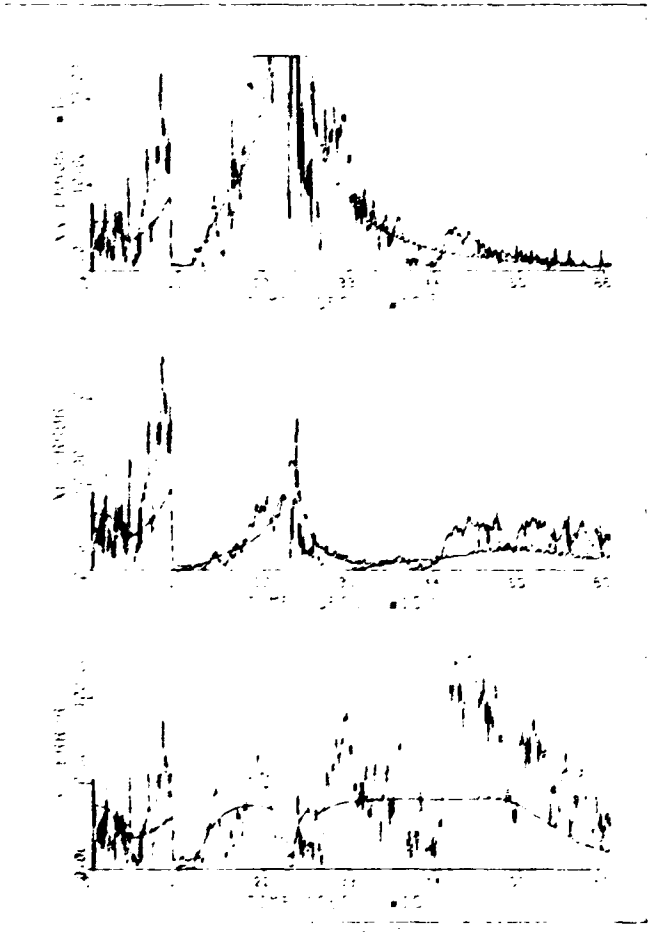

Figure 7.6 Case No. 19 Performance ($q_a(0) = 1.8\ m^2/sec^5$, $\beta = 0$, $W = 10\ m^4/sec^{11}$)

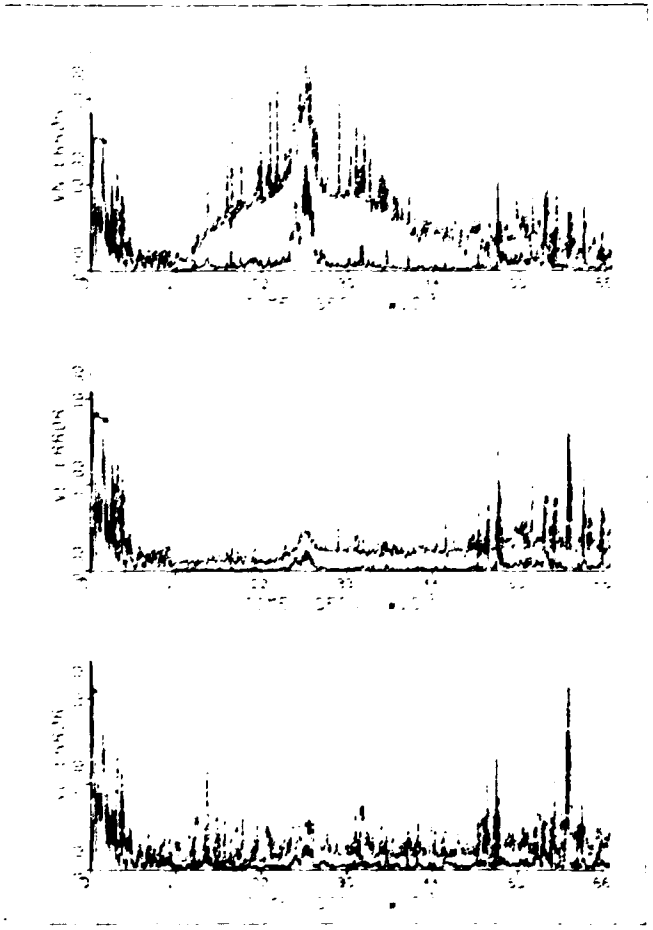

Figure 7.6 Case No. 19 Performance ($q_a(0) = 1.8\ m^2/sec^5$, $\beta = 0$, $W = 10\ m^4/sec^{11}$) (Continued)

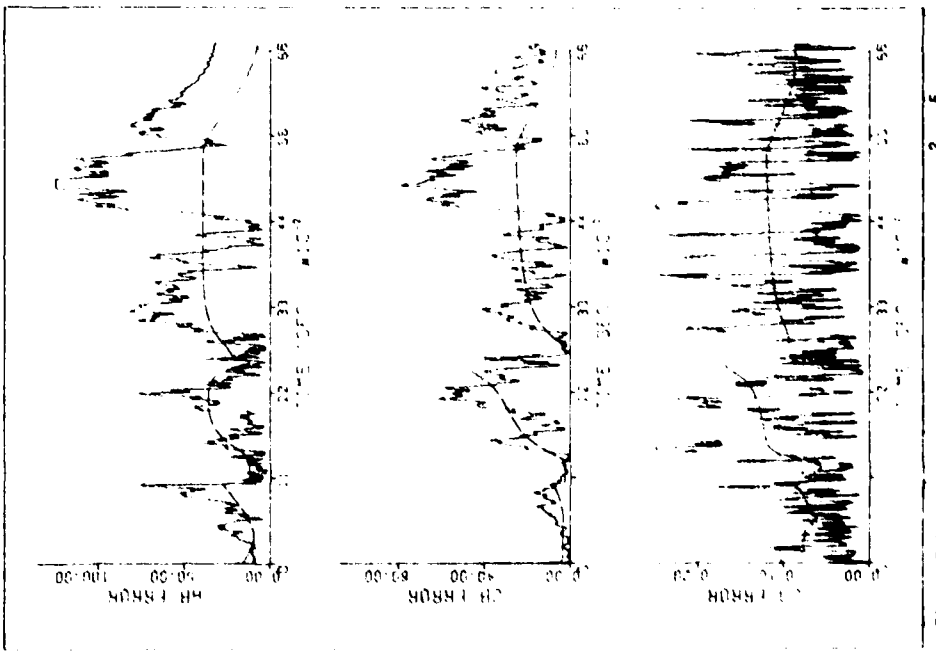

Figure 7.6 Case No. 19 Performance ($q_s(0) = 1.8\ m^2/sec^5$, $\beta = 0$, $M = 10\ m^4/sec^{11}$) (Continued)

7.3 Adaptive Age-Weighting

7.3.1 Development of the adaptive age-weighting algorithm.

Tarn and Zaborszky [80] pointed out that, within the constraints of the modeled noise statistics, the Kalman filter assumes that observations taken at a time in the past contribute the same amount of information as current observations. They developed a simple technique to downgrade the influence of past measurements by modifying the measurement noise statistics. Using their modification, the linear observation expressions are assumed to have the form

$$\begin{aligned} \underline{y}(t_k) &= H(t_k)\underline{x}(t_k) + \underline{\varepsilon}_k \\ E[\underline{\varepsilon}_k] &= 0 \\ E[\underline{\varepsilon}_k \underline{\varepsilon}_j^T] &= s^{k-j} R_j \delta_{jk} \end{aligned} \tag{7.12}$$

where: $s \geq 1$;

t_k is current time; and

t_j is a time in the past.

The result can be expressed as a modification to the time update covariance equation

$$\bar{P}' = \Phi(t_k, t_{k-1})\, sP(t_{k-1})\, \Phi^T(t_k, t_{k-1}) + \Gamma(t_k) \tag{7.13}$$

The expression for $\bar{P}$ that results from Eq. 7.13 is used then in place

of $\bar{P}$ in the remaining equations of the sequential filter.

Fagin [81] developed a similar technique based on a recursive least squares derivation. Hagar [77:48] showed that Fagin's exponential weighting factor is related to Tarn and Zaborszky's factor as follows:

$$s = \exp[(t_k - t_j) / \tau] \tag{7.14}$$

where: τ is an arbitrary factor.

Age-weighting can be applied as a non-adaptive technique by choosing a constant s or τ. Hagar [77:79-80], however, suggested the use of the predicted covariance of the residual to determine the factor s. The following technique is a modification to Hagar's suggestion and is identical to the covariance double update of Heck [82:191-196].

If γ_k is an estimate of the variance of the residuals, then the estimate of the residual variance is set equal to the predicted residual variance as in Eq. 6.22 except that $\bar{P}'$ is used to designate the covariance matrix that will satisfy the equality.

$$\gamma_k = H_k \bar{P}' H_k^T + R_k \tag{7.15}$$

If $\bar{P}'_k$ is related to $\bar{P}_k$ by

$$\bar{P}'_k = s\bar{P}_k \tag{7.16}$$

then Eq. 7.15 can be solved for the scalar s where the measurement is assumed to be a scalar.

$$s = \frac{\gamma_k - P_k}{H_k \bar{P}_k H_k^T} \tag{7.17}$$

The navigation filter then modifies the a priori covariance matrix in accordance with Eq. 7.16. Note that this technique differs from that of Tarn and Zaborszky's result, Eq. 7.13, in that the factor s is assumed to apply to the discrete process noise matrix Γ as well as to the previous a posteriori covariance matrix.

Since the covariance matrix must be positive definite, s must be positive. In fact, to satisfy the restriction on values of s from Tarn and Zaborszky's algorithm and from Fagin's exponential from, s must be greater than or equal to unity. Heck [82:194] suggested implementing a maximum value for s of 1.2. A similar algorithm suggested by Lear [83] would also limit s to a maximum of 1.2.

The calculation of γ_k remains to be discussed. Hagar suggested using the mean of the square of the latest N residuals. This has the advantage of smoothing large fluctuations caused by measurement noise. If N is too large, however, the adaptive parameter may be slow to recognize aircraft turns. The situation is further complicated for GPS users because, if three satellites are visible and the user has an altimeter implemented, then the user has a sequence of seven independent and statistically different measurements. Also, the assumed measurement noise variance R is not necessarily stationary though it may vary slowly. To eliminate the requirement that arrays of residuals

be maintained for each measurement type, the adaptive age-weighting algorithm tested in this study used only the square of the current measurement residual as its estimate of the residual variance. The upper limit on the weighting factor should prevent disastrous modifications based on large measurement noises. If, however, a measurement source fails and continually provides large residuals, then the continued application of the factor may cause difficulties.

The adaptive age-weighting algorithm was implemented in two modes. In the first mode, the age-weighting factor was calculated and applied for all measurements. In the second mode, the factor was not calculated for the range-rate measurements. The philosophy behind the second method is made apparent by examining Eq. 7.14. Since the pseudo-range measurement and the pseudo-range-rate measurement are time-tagged with the same time, the age-weighting factor for the covariance matrix should be unity.

7.3.2 Results of adaptive age-weighting tests. Both adaptive age-weighting algorithms were tested using various combinations of correlation time and spectral level noise magnitude. Poor filter performance resulted in all tests with little or no improvement over the corresponding non-adaptive filters. Analysis of the results indicated that the method may be more suited as a covariance maintenance technique for applications where the covariance matrix would otherwise vanish or become very small. The exponentially correlated random acceleration model has no requirement for such a covariance maintenance scheme.

7.4 Adaptive Process Noise Weighting

7.4.1 Development of the adaptive process noise weighting algorithm.

The a priori covariance matrix $\bar{P}$ defines a region of uncertainty about the a priori state estimate. A portion of the region is due to uncertainty in the initial conditions. This region is accounted for by the $\Phi P \Phi^T$ term in Eq. 4.69. The rest of the region of uncertainty is due to process noise that may occur during the time interval of the covariance propagation. If the previous a posteriori covariance matrix P is correct and if the system dynamics as represented by Φ are reasonable, then it can be assumed that the $\Phi P \Phi^T$ term is reasonably accurate. It can be argued then that any deviation of the true state beyond the region of uncertainty as defined by $\bar{P}$ is due to an error in the process noise matrix Γ. Similarly, if the true state remains in a region about the predicted state that is smaller than that specified by $\bar{P}$, then it can be argued that the filter process noise matrix is too large.* These assumptions form the basis for the adaptive process noise weighting algorithm.

Assume that the desired a priori covariance matrix is given by

$$\bar{P}'(t_k) = \Phi(t_k,t_{k-1})P(t_{k-1})\Phi^T(t_k,t_{k-1}) + s\Gamma(t_k) \quad (7.18)$$

---

*The assumed statistics must be considered before deciding that the state is "in" or "out" of its region of uncertainty.

Substituting Eq. 7.18 into Eq. 7.15 yields

$$s = \frac{\gamma_k - H_k\Phi(t_k,t_{k-1})P(t_{k-1})\Phi^T(t_k,t_{k-1})H_k^T - R_k}{H_k\Gamma H_k^T} \qquad (7.19)$$

The adaptive process noise weighting algorithm is implemented by calculating the factor s using Eq. 7.19 and then calculating the a priori covariance matrix using Eq. 7.18. The filter equations then use the modified a priori covariance matrix for the calculation of the gain and for the covariance matrix measurement update. Since process noise is not added between the processing of the pseudo-range measurement and the processsing of the pseudo-range-rate measurement, process noise weighting was not accomplished when the pseudo-range-rate measurements were processed.

For this technique, the factor s must be greater than or equal to zero. A value of s between zero and unity effectively lowers the process noise added to the propagated covariance matrix. To prevent difficulties caused by large measurement noises, a maximum value of s was specified.

7.4.2 Results of adaptive process noise weighting. The adaptive process noise weighting algorithm was tested using various values of correlation time, spectral level process noise, and maximum allowable weighting factors. For those filters which assumed high maneuver variance, the performance was generally worse than the performance of the corresponding non-adaptive filter in all phases of flight. When the

maneuver variance was decreased, the adaptive process noise weighting algorithm improved the performance of the takeoff and departure flight phases but resulted in worse performance during cruise, approach, and landing.

7.5 The Aidala-Davis Performance Index

7.5.1 Disadvantages of previous performance indices. The performance indices used in the adaptive age-weighting and adaptive process noise weighting algorithms have three major disadvantages. First, they can be calculated only for scalar measurements. Second, they use a single-sample variance to estimate the variance of the residuals. And, third, the value of the index can be strongly influenced by the type of measurement. The first two disadvantages also apply to the Q-estimator. A performance index developed by Aidala and Davis [78] eliminates these disadvantages.

7.5.2 Derivation of the index. Aidala and Davis [78] derived the sequential filter equations utilizing the classical method of least squares with a somewhat unorthodox performance index. Following is an outline of their derivation.

Assume a system defined by the linear difference equation

$$\underline{x}_{k+1} = \Phi_{k+1,k}\underline{x}_k + B_k\underline{w}_k \tag{7.20}$$

where: $\underline{x}_k$ is a p-dimensional state vector;

$\Phi_{k+1,k}$ is the state transition matrix;

B_k is the state noise matrix; and

$\underline{w}_k$ is the process noise vector.

The observations are defined by

$$\underline{y}_k = H_k \underline{x}_k + \underline{\varepsilon}_k \tag{7.21}$$

where: $\underline{y}_k$ is an m-dimensional measurement vector;

H_k is the observation-state matrix; and

$\underline{v}_k$ is the observation noise vector.

The statistics of Eqs. 7.20 and 7.21 are as follows:

$$E[\underline{x}_0] = \bar{\underline{x}}_0 \tag{7.22a}$$

$$E[(\underline{x}_0 - \bar{\underline{x}}_0)(\underline{x}_0 - \bar{\underline{x}}_0)^T] = \bar{P}_0 \tag{7.22b}$$

$$E[\underline{w}_k] = \bar{\underline{w}}_0 \tag{7.23a}$$

$$E[\underline{w}_j - \bar{\underline{w}}_j)(\underline{w}_k - \bar{w}_k)^T] = Q_k \delta_{jk} \tag{7.23b}$$

$$E[\underline{\varepsilon}_k] = 0 \tag{7.24a}$$

$$E[\underline{\varepsilon}_j \underline{\varepsilon}_k] = R_k \delta_{jk} \tag{7.24b}$$

$$E[(\underline{x}_0 - \bar{\underline{x}}_0)(\underline{w}_0 - \bar{\underline{w}}_0)^T] = 0 \tag{7.25a}$$

$$E[(\underline{x}_0 - \bar{\underline{x}}_0)\underline{\varepsilon}_k^T] = 0, \quad \text{for all } k \tag{7.25b}$$

$$E[(\underline{w}_j - \bar{\underline{w}}_j)\underline{\varepsilon}_k^T] = 0, \quad \text{for all } j \text{ and } k \tag{7.25c}$$

where: δ_{jk} is the Kronecker delta;

$\bar{\underline{x}}_i$ is the *a priori* estimate of the state $\underline{x}_i$; and

$\bar{\underline{w}}_i$ is the *a priori* estimate of the noise $\underline{w}_i$;

Note that in the definition of the system given above, reference is made to an estimate of the process noise vector $\underline{w}_i$. The filter equations to be derived, however, are oriented toward the estimation of the state $\underline{x}_i$.

The following constraint will be placed on the estimates:

$$\hat{\underline{x}}_{k+1|n} = \Phi_{k+1,k}\hat{\underline{x}}_{k|n} + B_k\hat{\underline{w}}_{k|n} \tag{7.26}$$

where: $\underline{x}_{k+1|n}$ is the optimal estimate of $\underline{x}_{k+1}$ based on n m-dimensional observations;

$\underline{w}_{k+1|n}$ is the optimal estimate of $\underline{w}_{k+1}$ based on n m-dimensional observations.

Equation 7.26 ensures that the estimates satisfy the system equations. The following equivalences should be noted:

$$\hat{\underline{x}}_{k|o} = \bar{\underline{x}}_k$$

$$\hat{\underline{w}}_{k|o} = \bar{\underline{w}}_k$$

$$B_k Q_k B_k^T = \Gamma_k$$

where: Γ_k is the discrete process noise matrix discussed in Par. 4.5.

Using the system defined by Eqs. 7.20 through 7.26, Aidala and Davis defined a performance index as follows:

$$J_n = 1/2\,(\hat{\underline{x}}_{o|n} - \overline{\underline{x}}_o)^T \overline{P}^{-1} (\hat{\underline{x}}_{o|n} - \overline{\underline{x}}_o) + 1/2 \sum_{\ell=0}^{n-1} (\hat{\underline{w}}_{\ell|n} - \overline{\underline{w}}_\ell)^T Q_\ell^{-1} (\hat{\underline{w}}_{\ell|n} - \overline{\underline{w}}_\ell) \quad w + 1/2 \sum_{\ell=0}^{n} (\underline{y}_\ell - H_\ell \hat{\underline{x}}_{\ell|n})^T R_\ell^{-1} (\underline{y}_\ell - H_\ell \hat{\underline{x}}_{\ell|n}) \quad (7.27)$$

The first term on the right hand side of Eq. 7.27 is a measure of the error in the a priori estimate of the initial conditions normalized (weighted) by the a priori covariance matrix for the estimate of the intital conditions. The second term on the right hand side of Eq. 7.27 is a measure of the system noise normalized by the process noise covariance matrix. The last term is a weighted least squares term to account for data-fit errors. The performance index is thus a quantitative measure of the estimation process with a good intuitive basis.

The solution to Eq. 7.20 is given by

$$\underline{x}_k = \Phi_{k,o}\underline{x}_o + \sum_{j=0}^{k-1} \Phi_{k,j+1} B_j \underline{w}_j \;, \; k = 1,2,\ldots \quad (7.28)$$

Equation 7.28 is the discrete analogue to Eq. 4.62. If Eq. 7.26 is to constrain the estimates, then Eq. 7.28 can be applied also to the optimal estimates.

$$\hat{\underline{x}}_{k|n} = \Phi_{k,o}\hat{\underline{x}}_{o|n} + \sum_{j=0}^{k-1} \Phi_{k,j+1}B_j\hat{\underline{w}}_{j|n}, \quad k = 1,2,\ldots \quad (7.29)$$

Aidala and Davis proceed to develop filter equations by minimizing J_n under the constraints imposed by Eq. 7.26. The independent vectors in Eq. 7.27 are the a posteriori estimate of the initial state, $\hat{\underline{x}}_{o|n}$ and the a posteriori estimate of the process noise $\hat{\underline{w}}_{j|n}$, $j=0,1,\ldots,n-1$. Aidala and Davis minimize J_n by taking the partial derivatives of Eq. 7.27 with respect to $\hat{\underline{x}}_{o|n}$ and $\hat{\underline{w}}_{j|n}$ $j=0,1,\ldots,n-1$, and setting the partials equal to zero. By analyzing the effect of an additional measurement on the optimal estimate, the sequential filter equations are derived. For convenience, the sequential filter equations, using the above notation, are summarized as follows:

$$\bar{\underline{x}}_{k+1|k} = \Phi_{k+1,k}\hat{\underline{x}}_{k|k} + B_k\bar{\underline{w}}_{k|o} \quad (7.30a)$$

$$\bar{P}_{k+1} = \Phi_{k+1,k}P_k\Phi_{k+1,k}^T + \Gamma_k \quad (7.30b)$$

$$K_{k+1} = \bar{P}_{k+1}H_{k+1}(H_{k+1}\bar{P}_{k+1}H_{k+1}^T + R_{k+1})^{-1} \quad (7.30c)$$

$$\hat{\underline{x}}_{k+1|k+1} = \bar{\underline{x}}_{k+1|k} + K_{k+1}(\underline{y}_{k+1} - H_{k+1}\bar{\underline{x}}_{k+1|k}) \quad (7.30d)$$

$$P_{k+1} = (1 - K_{k+1}H_{k+1})\bar{P}_{k+1} \quad (7.30e)$$

A measurement residual is defined by

$$\underline{z}_k = \underline{y}_k - H_k \underline{x}_{k|k-1} \tag{7.31}$$

Aidala and Davis, after considerable algebra, show that the performance index of Eq. 7.27 can be written in terms of the residuals.

$$J_n = 1/2 \sum_{\ell=1}^{n} \underline{z}_\ell^T (H_\ell \bar{P}_\ell H_\ell^T + R_\ell)^{-1} \underline{z}_\ell \tag{7.32}$$

Note that the bracketed term in Eq. 7.32 is (see Eq. 6.22)

$$E[\underline{z}_\ell^T \underline{z}_\ell] = H_\ell \bar{P}_\ell H_\ell^T + R_\ell \text{ , for all } \ell. \tag{7.33}$$

The performance index is a random variable and, as such, its statistical properties can be examined. It can be shown that

$$E[\underline{z}_\ell^T (H_\ell \bar{P}_\ell H_\ell^T + R_\ell)^{-1} \underline{z}_\ell] = m, \text{ for all } \ell. \tag{7.34}$$

where: m is the dimension of the measurement vector.

The mean and covariance of J_n are given by

$$E[J_n] = mn/2 \tag{7.35}$$

$$E[(J_n - E[J_n])^2] = mn/2 \tag{7.36}$$

where: J_n is Chi-Square distributed [90:178] if all statistics are Gaussian.

As the number of measurements gets large, adaptive decisions, based on a performance index as evaluated by Eq. 7.32, are difficult. To eliminate this difficulty, Aidala and Davis introduced a modified performance index.

$$L_n = 1/2 \sum_{\ell=1}^{n} \gamma^{n-1} [\underline{z}_\ell^T (H_\ell \bar{P}_\ell H_\ell^T + R_\ell)^{-1} \underline{z}_\ell - m] \tag{7.37}$$

where: $0 \leq \gamma \leq 1$.

The mean and covariance of the modified performance index are bounded.

$$E[L_n] = 0 \tag{7.38a}$$

$$E[L_n^2] = \frac{m}{2} \frac{1 - \gamma^{2n}}{1 - \gamma^2} \tag{7.38b}$$

$$\lim_{n \to \infty} E[L_n^2] = \frac{m}{2(1 - \gamma^2)} \tag{7.38c}$$

The modified index can be expressed in a recursive form as follows:

$$L_{n+1} = \gamma L_n + 1/2[\underline{z}_{n+1}^T (H_{n+1} \bar{P}_{n+1} H_{n+1}^T + R_{n+1})^{-1} \underline{z}_{n+1} - m] \tag{7.39}$$

7.5.3 Implementation of the Aidala-Davis index. The performance index of Eq. 7.39 should be a good quantitative measure of system performance. The difficulty is in the selection of the memory factor γ and the development of a gain modification scheme. In tests implementing the performance index, only the aircraft portion of the process

noise matrix was modified based on the value of the performance index. This approach was selected under the assumption that aircraft maneuvers were the primary source of errors in the state estimate.

After calculating L_k using Eq. 7.39, the a priori covariance matrix was modified as follows:

$$\bar{P}'_k = \bar{P}_k + S(L_k)\, \Gamma_{ac} \tag{7.42}$$

where: Γ_{ac} represents the aircraft state portion of the discrete process noise matrix, Γ_k; and
$S(L_k)$ is a factor based on the performance index, L_k.

Prior to describing the functional form of $S(L_k)$ chosen for the numerical example considered in this investigation, the behavior of L_k must be examined beyond the determination of mean and variance. Of importance is the fact that the performance index has an absolute lower limit, i.e., if all residuals are zero, the performance index has a finite lower bound. To demonstrate this behavior, set the residuals in Eq. 7.39 equal to zero giving

$$L'_{k+1} = \gamma L'_k - m/2 \tag{7.43}$$

The solution to the difference equation of Eq. 7.43 can be obtained by using z-tranform theory [84:384-393]. The z-transform of L'_{k+1} is given by

$$Z[L'_{k+1}] = \gamma Z[L'_k] + Z[-m/2]$$

$$= zZ[L'_k] - zL_o + Z[-m/2] \qquad (7.44)$$

Solving Eq. 7.44 for the z-transform of L'_k yields

$$Z[L'_k] = \frac{z}{z-\gamma} L_o - \frac{1}{z-\gamma} \frac{z}{z-1} (m/2) \qquad (7.45)$$

where: $z/(z-1)$ is the z-transform of unity.

Expanding Eq. 7.45 by partial fractions

$$Z[L'_k] = \frac{z}{z-\gamma} L_o + \frac{m}{2} \frac{1}{1-\gamma} \frac{z}{z-\gamma} - \frac{m}{2} \frac{1}{1-\gamma} \frac{z}{z-1} \qquad (7.46)$$

Taking the inverse transform leads to

$$L'_k = \gamma^k L_o + \left(\frac{m}{2(1-\gamma)}\right) - \frac{m}{2(1-\gamma)} \qquad (7.47)$$

which, in the limit as $k \to \infty$, yields

$$L_{min} = \lim_{k \to \infty} L'_k = -\frac{m}{2(1-\gamma)} \qquad (7.48)$$

The results of Eq. 7.48 could have been obtained by applying the Final Value Theorem for z-transforms [84:390-391].

The calculation of $S(L_k)$ in Eq. 7.42 must consider the limiting behavior of the index. In the algorithms tested, the calculations used to determine $S(L_k)$ are summarized as follows:

$$S(L_k) = \begin{cases} S'(L_k) - 1 & \text{for pseudo-range and altimeter measurements} \\ S'(L_k) & \text{for pseudo-range-rate measurements} \end{cases} \tag{7.49}$$

$$S'(L_k) = \begin{cases} \exp(C_1 L_k) & \text{if } L_k \leq L_{max} \quad (7.50a) \\ S'_{max} & \text{if } L_k \geq L_{max} \quad (7.50b) \end{cases}$$

$$C_1 = \frac{\ln(S'_{min})}{L_{min}} \tag{7.51}$$

$$L_{max} = \frac{\ln(S'_{max})}{C_1} \tag{7.52}$$

If the index memory factor γ is small, then the Chi-Square distribution of L_k can cause large magnification of the performance index by causing small absolute values of L_{min}. This can be disastrous when the performance index increases because of aircraft turns.

Implementation of Eq. 7.49a allows for the reduction of process noise if the performance index is below its mean value. Since process noise is not added normally when the pseudo-range-rate measurement is processed, Eq. 7.49b is implemented to insure that the covariance matrix does not become non-positive definite.

When the performance index equals its minimum values, the factor takes on the value of S'_{min}. The primary purpose of S'_{min} is to scale the effect of the performance index L_k on the factor $S'(L_k)$. The factor $C_1 L_k$ is a function of S'_{min} and the number of standard

deviations that L_k departs from the mean. For large values of γ the modified performance index effectively includes more terms in the summation. Since the Chi-Square distribution approaches a normal distribution as the number of terms increases, the statistical behavior of $C_1 L_k$ is approximately Gaussian for large γ. For small γ, however, the performance index may have poorly behaved statistics. For $\gamma=0$, a single residual determines the gain modification.

The implementation method described above was intuitively developed. Many other possibilities exist, for example, on/off process noise depending on the value of the performance index or a linear function of the performance index. Each method would have to be analyzed using specific parameters. The method described was applied to an ADR filter using the initial conditions of Cases 1 through 4 and 7.5.

7.5.4 Results of the Aidala-Davis Index Implementation. The algorithm implementing the Aidala-Davis index was tested using the initial conditions of Cases 1 through 4 and 7.5 for the first 600 seconds of flight. The performance of the filter using the initial conditions of Cases 1, 4, and 7.5 was considerably worse than the corresponding non-adaptive filter. This is similar to the adaptive process noise weighting results for the high noise cases except that the magnification inherent in the exponential function magnified the errors. The Case 2 and Case 3 initial conditions, however, did result in better navigation results for the initial tests. Table 7.8 lists the performance indicators of the Aidala-Davis index implementation for Case 2 and Case 3

Table 7.8 Initial Results of the Aidala-Davis Index Filter

	non-adaptive	Memory Factor (γ)					
		0.	.40	.50	.60	.707	.90
$q_a = .375\ m^2/sec^5$, $\beta = 1\ sec^{-1}$, $.1 \leq S'(L_k) \leq 1000.$							
RSS POS ERR	298.96	70.91	70.08	73.21	70.89	79.43	90.58
RSS VEL ERR	34.57	11.41	12.92	14.01	14.01	14.17	15.49
MAX POS ERR	758.56	203.27	194.61	196.51	190.56	202.14	274.87
MAX VEL ERR	74.39	28.11	37.97D	33.53	40.27E	32.63	38.31
POS ERR/SIG	7.18	1.14	1.21	1.21	1.32	1.46	1.80
VEL ERR/SIG	13.24	.71	.95	.93	1.22	1.12	1.61
FIN POS ERR	22.79	53.76	21.96	67.61	13.24	27.06	30.15
FIN VEL ERR	4.29	1.78	1.76	5.79	1.03	1.52	2.30
$q_a = .01875\ m^2/sec^5$, $\beta = 1/20\ sec^{-1}$, $.1 \leq S'(L_k) \leq 1000.$							
RSS POS ERR	91.25	50.88	51.50	49.29	52.41	55.87	57.67
RSS VEL ERR	16.16	7.55	7.25	7.11	7.90	9.42	9.70
MAX POS ERR	258.69	149.02	137.23	138.07	143.84	152.11	128.98
MAX VEL ERR	41.88	28.81	29.27	29.40	28.77	37.19	28.72
POS ERR/SIG	1.98	.93	.98	.94	1.01	1.10	1.11
VEL ERR/SIG	3.70	.67	.72	.71	.79	1.00	.91
FIN POS ERR	24.94	22.11	19.39	18.42	18.09	18.39	18.64
FIN VEL ERR	1.44	1.08	.98	.95	.93	.90	.87

initial conditions and for various values of the Aidala-Davis index weight γ.

The initial tests showed a marked improvement over the non-adaptive cases in all parameters except the Case 2 initial condition final position error. Full flight tests were accomplished with a memory factor γ equal to $\sqrt{.5}$. Using the Case 2 initial conditions, the full flight test diverged. The maximum value of the process noise weight $S'(L_k)$ was reduced to 10. The filter, designated as Case 20, did not diverge during the flight but did have unacceptable performance. Table 7.9 and Figure 7.7 summarize the Case 20 results.

Case 21 was a full flight test using the Case 3 initial conditions and a maximum process noise weight equal to 1000. The results of Case 21 are given in Table 7.10 and are shown in Figure 7.8. Many adaptive filters which recognize aircraft turns quickly are also sensitive to measurement noise or turbulence. When sensitivity is reduced, sluggish response to a maneuvering aircraft is usually the result. The Case 21 conditions, however, improved the performance of the navigation filter during the takeoff and landing phases of flight without severely degrading the filter performance during cruise. Case 21 appears to have the ability to steer a safe course between this Scylla and Charybdis of the navigation filter.

Table 7.9 Case No. 20 Performance (q_a = .375 m^2/sec^5, β = 1 sec^{-1}, γ = .707, .1 $\leq$ S'(L_k) $\leq$ 10)

	Flight Phase Final Times (sec)					
	598.75	1013.75	1295.00	2760.00	5100.00	6687.50
RSS POS ERR	109.23	128.57	149.49	1626.93	2082.81	1554.10
RSS VEL ERR	18.90	1.70	k3.52	6.59	7.92	3.61
MAX POS ERR	271.33	242 32	971.91E	29149.	3866.80D	1532.68
MAX VEL ERR	40.18	5.51D	63.67	90.20	181.08E	24.45
POS ERR/SIG	2.38	1.73	8.33	5.08	35.96	57.86
VEL ERR/SIG	4.13	.74	5.14	2.36	3.19	1.64

Table 7.10 Case No.21 Performance (q_a = .01875 m^2/sec^5, β = 1/20 sec^{-1}, γ = .707, .1 $\leq$ S'(L_k) $\leq$ 1000)

	Flight Phase Final Times (sec)					
	598.75	1013.75	1295.00	2760.00	5100.00	6687.50
RSS POS ERR	55.87	142.76	24.48	176.40	102.81	39.76
RSS VEL ERR	9.42	1.39	.29	1.57	.73	3.98
MAX POS ERR	152.11	231.08	159.69	716.15	202.33	98.69D
MAX VEL ERR	37.19	2.59	1.46D	7.60	4.82	31.65
POS ERR/SIG	1.10	1.95	1.77	.77	1.29	1.23
VEL ERR/SIG	1.00	.69	.41	.62	.55	.74

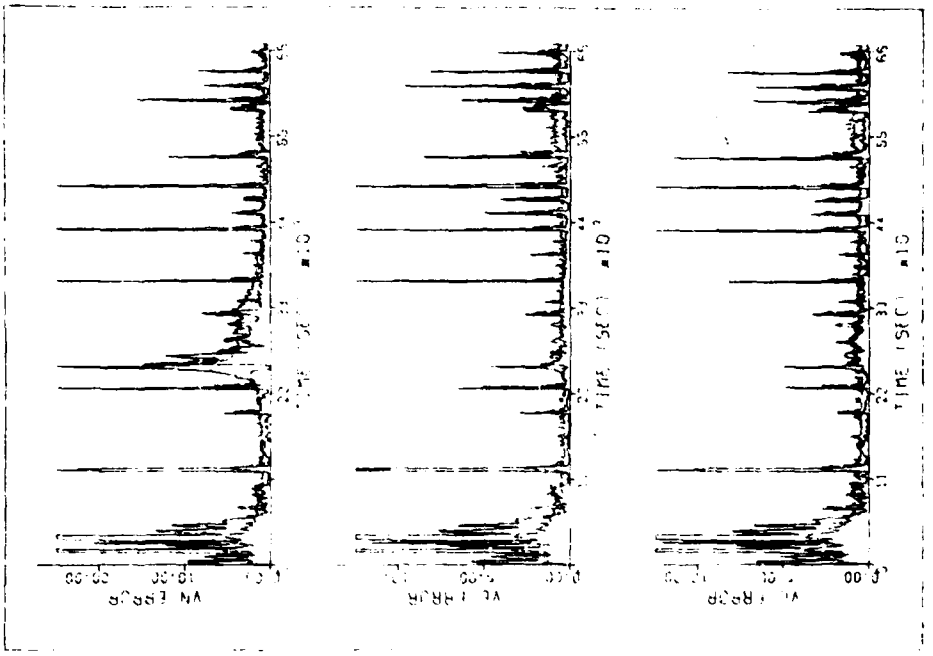

Figure 7.7 Case No. 20 Performance (q_a = .375 m^2/sec^5, β = 1 sec^{-1}, γ = .707, .1 ≤ $S'(L_k)$ ≤ 10.) (Continued)

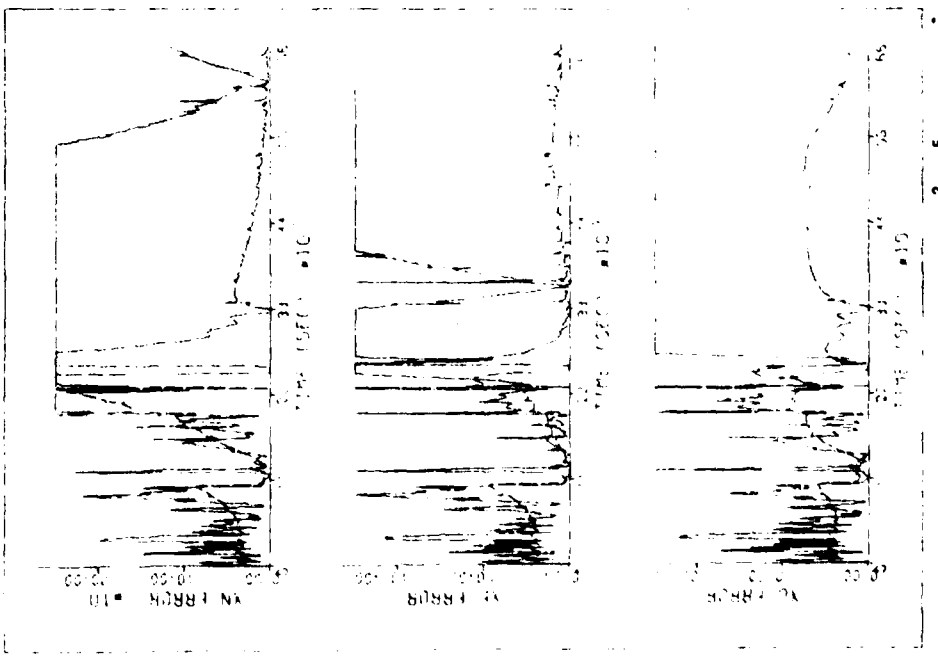

Figure 7.7 Case No. 20 Performance (q_a = .375 m^2/sec^5, β = 1 sec^{-1}, γ = .707, .1 ≤ $S'(L_k)$ ≤ 10.)

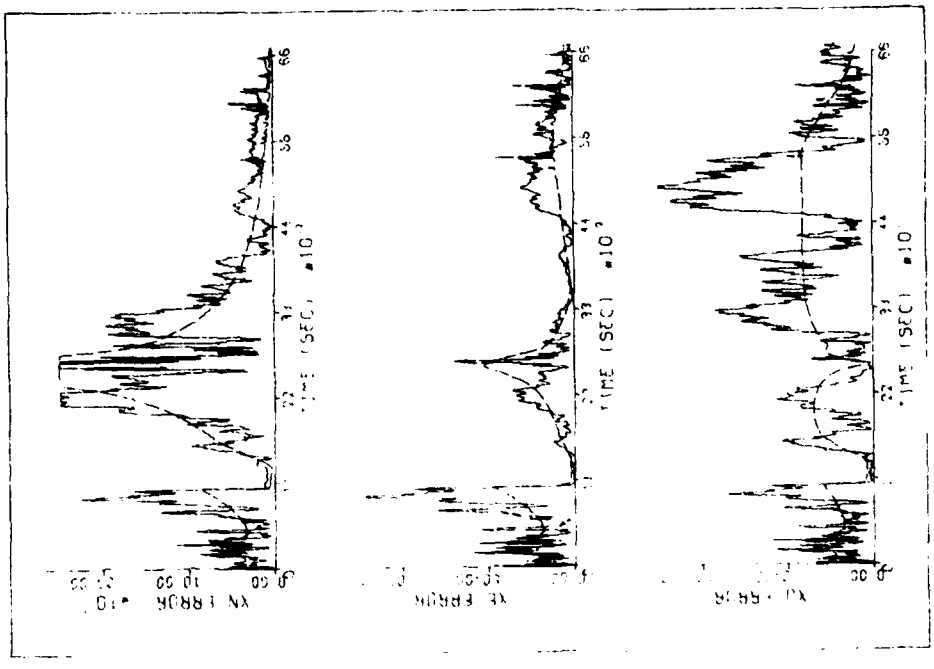

Figure 7.8 Case No. 21 Performance (q_a = .01875 m^2/sec^5, β = 1/20 sec^{-1}, γ = .707, .1 ≤ $S'(L_k)$ ≤ 1000.)

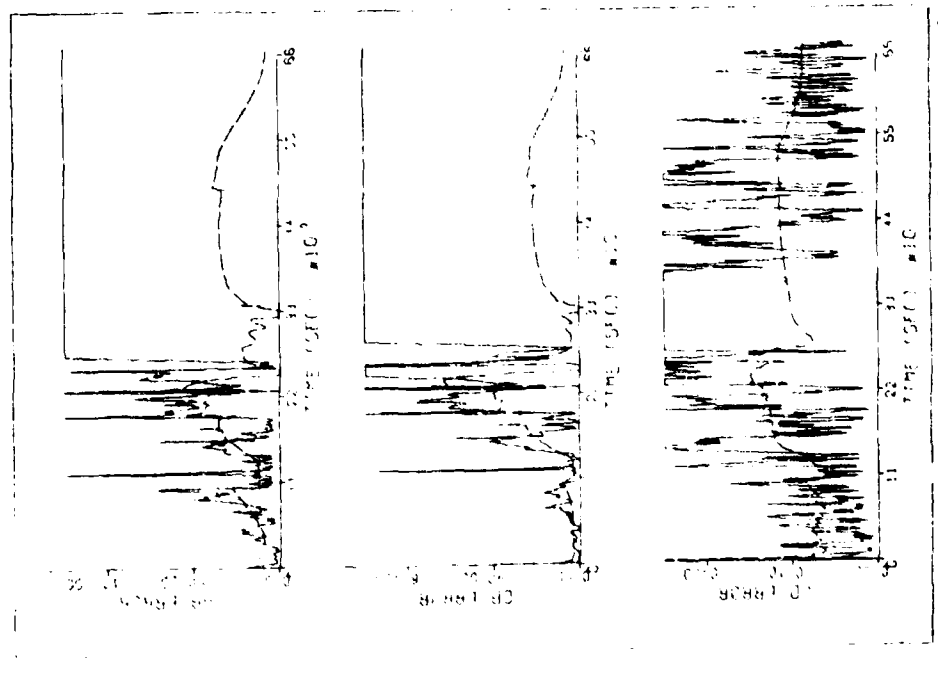

Figure 7.7 Case No. 20 Performance (q_a = .375 m^2/sec^5, β = 1 sec^{-1}, γ = .707, .1 ≤ $S'(L_k)$ ≤ 10.) (Continued)

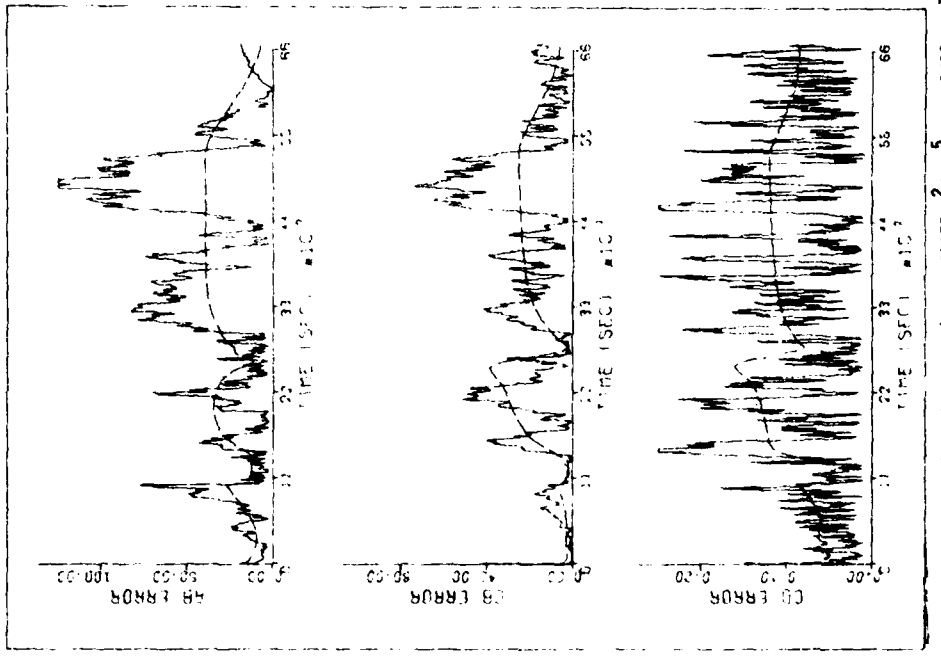

Figure 7.8 Case No. 21 Performance (q_a = .01875 m^2/sec^5, β = 1/20 sec^{-1}, γ = .707, .1 ≤ $S'(L_k)$ ≤ 1000.) (Continued)

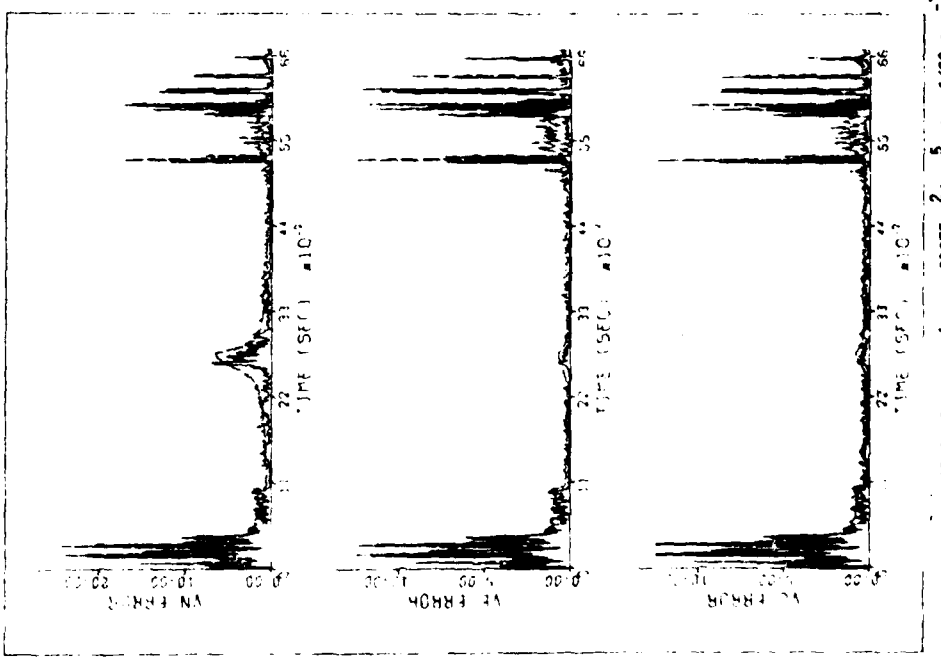

Figure 7.8 Case No. 21 Performance (q_a = .01875 m^2/sec^5, β = 1/20 sec^{-1}, γ = .707, .1 ≤ $S'(L_k)$ ≤ 1000.) (Continued)

CHAPTER 8

SUMMARY, CONCLUSIONS, AND RECOMMENDATIONS

8.1 Summary

The sequential estimation techniques investigated in this study provide "optimal" estimates if the filter has an accurate representation of the system dynamics. With respect to the aircraft, this requires that either the acceleration is known *a priori* and is included in the filter algorithm, or that an accurate model for the acceleration is available and that the unknown parameters for the model are included in the filter state vector. Because of the inherent character of aircraft trajectories, *a priori* knowledge of aircraft acceleration is unavailable and no computationally tractable model exists which will precisely model the acceleration. Also, because of the lack of a true aircraft model, the goal of an "optimal" estimate should be replaced with the requirement for a "satisfactory" model. A satisfactory model is one which is easily implemented and which will result in accurate and reliable filter performance. The continuous coverage by the Global Positioning System (GPS) satellites and the short prediction time intervals will allow approximate models to be used successfully by the navigation filter.

Successful evaluation of navigation algorithms for accuracy and reliability required two fundamental efforts. The first effort was the design and verification of a simulation computer program to realistically represent a user trajectory and the corresponding satellite

observations. The second major effort involved the derivation, implementation, and evaluation of the various navigation algorithms. The results of these efforts, as presented in this dissertation, are summarized in the following.

8.1.1 The simulation program. To design the simulation computer program, it was necessary to understand the major elements of the GPS, its concepts, and its environment. The primary functional segments of the GPS include the Control System Segment, which is responsible for ephemeris generation and satellite data maintenance; the Space System Segment, which consists of the navigation satellites; and the User System Segment, which includes the hardware and software necessary to provide a navigation fix.

The specific models and methods used to simulate motion of the GPS satellites, the satellite navigation signals, and a typical user were described. The simulation program is coded in modular form to allow flexibility in the choice of system models, navigation algorithms, and user trajectories. The resulting computer simulation is a valuable tool which can be used to provide a realistic simulation for navigation algorithm studies. As adopted for use in this dissertation, the accuracy of the simulation is sufficient for initial algorithm investigations. Because of its inherent flexibility, the program can be upgraded by incorporating more exact models of the GPS and the user equipment. The information in Chapters 2 and 3 of this dissertation and the references cited can be used to guide a programmer in his selection of alternate simulation models.

8.1.2 Navigation studies. The sequential equations for the linear, minimum variance filter were derived. The requirement for accurate covariance matrix propagation was discussed and a new technique to aid in the numerical integration of the covariance matrix differential equation was developed. The sequential filter equations served as a framework for the development of several navigation algorithms.

Four aircraft models were investigated. The velocity dead-reckoning model maintained finite filter gains because of the inclusion of process noise in the differential equation of velocity. Such process noise is representative of uncorrelated random accelerations. In order to be competitive with other algorithms, the process noise assumed by the filter must be large. Otherwise, the filter gains will be inadequate to track an aircraft maneuver. The assumption of large uncorrelated random acceleration is not only intuitively displeasing but also degrades filter performance during the cruise portion of flight.

A second aircraft model was based on the assumption that the acceleration is an exponentially correlated random variable. Over the prediction interval, acceleration is assumed to be a constant equal to the last estimated value. The model can be referred to as an acceleration dead-reckoning model. Because of the effects of the correlation time parameter, this model permits the maintenance of reasonable filter gains with low magnitudes for the spectral level acceleration process noise. The numerical results established that the exponentially correlated random acceleration model could maintain track during aircraft

maneuvers and could also improve the cruise phase performance as compared to the velocity-dead-reckoning model. Much of the improvement in filter performance may be due to the estimation of acceleration whereas acceleration is not estimated in the velocity-dead-reckoning model.

A third aircraft model is a minor variation of the exponentially correlated random acceleration model. With infinite correlation time, the acceleration is characterized as a random walk. This model is a limiting case of the exponentially correlated random acceleration model and provided numerical results similar to the results seen for correlation times of twenty seconds and longer.

The fourth aircraft model, the Beta-estimator, was based on the assumption that the acceleration has an exponential character. This model requires the estimation of correlation time and thus increases the size of the filter state vector, the required computer storage, and the required computer run time. The model also, unfortunately, adds an instability to the algorithm because of the difficulty in matching exponential functions to rapid acceleration changes during aircraft turns. Since the correlation time associated with the assumed exponential acceleration affects the covariance matrix propagation, the entire filter operation is subjected to erratic behavior associated with the state of the aircraft.

Adaptive techniques were tested in an attempt to improve the performance of the exponentially correlated random acceleration models. Three basic adaptive methods were tested. The first method, the

Q-estimator, employed a secondary filter to estimate the spectral level process noise magnitude. When applied to the estimation of acceleration noise magnitude only, the performance of this filter was slightly improved compared to the non-adaptive results. This method, however, significantly increases program complexity.

The second adaptive method used a single-sample variance of the residuals to scale the a priori covariance matrix (adaptive age-weighting) or to scale the process noise matrix (adaptive process noise weighting). The former method was unstable, probably because of the size of the covariance matrix elements; the latter method did not improve performance during maneuvers without degrading performance during cruise.

The third adaptive method was based on a performance index with a direct relationship to the loss function of the sequential filter equations. This method has the capability to consider vector measurements, to effectively use a multi-sample variance of the residuals, and to combine different measurement sources. The numerical results showed that the filter could perform as an adaptive filter should, i.e., filter gains were increased during maneuvers and were decreased during cruise.

8.2 Conclusions

Based on the numerical tests, it can be concluded that an aircraft model which assumes the acceleration to be exponentially correlated will provide an accurate navigation fix with little danger

of filter divergence. In addition, the Aidala-Davis performance index can be incorporated into the algorithm easily and will enhance the performance of the filter.

Based on the total effort expended in this investigation, the following additional conclusions are offered:

1. The influence of geometry on filter performance is pervasive. In fact, those algorithms which had covariance behavior that severely distorted the geometrical predictions, generally performed poorly.

2. Satellite clock errors are critical. Because the satellite clock errors will appear as biases over short time intervals, the navigation filter will move the estimated user position to minimize the residuals. Locations of the satellites and the signs of the clock errors can cause large position errors without a large measurement residual to indicate difficulties.

3. The Phase II configuration is inadequate for terminal area navigation. If, in the simulated flight, the aircraft had to land at T = 45 minutes, he would be landing with an extremely poor geometrical configuration. Considering effects of maneuvers, the errors could easily exceed one kilometer.

4. Numerical tests, which were performed in the early stages of this research, showed that an altimeter is a valuable additional sensor. Also, if the altimeter errors are significantly worse than that of the adopted model, then an ill-conditioning between the altitude estimate and the altimeter bias estimate can occur.

5. Adaptive methods which cause significant changes to the covariance matrix, can result in unstable performance if the covariance matrix is not small.

8.3 Recommendations

Based on the overall efforts of this investigation, the following recommendations can be made with regard to navigation algorithm selection:

1. The algorithm should estimate acceleration.

2. The algorithm should have reasonable steady-state gains when tested with a constant satellite-user geometry. Algorithms which allow the covariance matrix to vanish or to become unrealistically small are not acceptable.

3. Any schemes to modify filter performance based on detecting maneuvers should operate via the process noise matrix. With a realistic covariance matrix, modification of the a priori covariance matrix (as in the adaptive age-weighting method) or modification of the covariance matrix propagation (as results from the Beta-estimator) can lead to disastrous results.

The aircraft model based on exponentially correlated random acceleration can be combined with the Aidala-Davis performance index and a covariance modification scheme similar to that tested in Chapter 7 to provide an algorithm which meets the criteria of the above recommendations. Assuming adequate computer storage and time, this

algorithm can be easily implemented on an on-board computer for GPS user navigation.

8.4 Future Efforts

Future efforts should be directed toward a sensitivity analysis of the recommended algorithm. In particular, the following modifications should be made to the simulation program for further tests of the algorithm:

1. A more accurate GPS hardware/software representation should be incorporated. Because this study was initiated early in the development of the GPS program, certain elements of the hardware/software had not yet been specified. As more precise knowledge of the computer/receiver interface and the downlink data message is made available, the information should be incorporated into the simulation.

2. The algorithm should be tested with less accurate user clocks. The clock simulation adopted for the tests is equivalent to a good quartz crystal clock. Clock accuracy on the order of the timing used in on-board computers should be considered.

3. The adopted receiver accuracy is between that associated with the Precision code and that associated with the Clear/Acquisition code. Sensitivity to this error source should be investigated.

4. A rate gyro should be investigated as an additional sensor.

5. Tests should be made with larger wind gusts.

6. Other flight profiles, such as an over-the-pole flight and a North-South trajectory, should be included to verify the results.

In addition to further testing of the recommended algorithm, the algorithm itself could be modified to provide additional insight. For example,

1. The aircraft model could be reduced to the velocity dead-reckoning model. Additional analysis of this model is required if a user has inadequate computer capability for the recommended algorithm.

2. A simpler covariance modification scheme could be used with the Aidala-Davis performance index.

3. Parameter sensitivity analyses should be reaccomplished for the algorithm using selected realizations of the scenario. Such an effort is required to verify the sensitivity analyses contained in this report.

Prior to actual on-board testing of an algorithm, all available information should be examined and the appropriate modifications made to the simulation computer program. The recommended algorithm should then be evaluated using the techniques of this dissertation. It is expected that the recommended algorithm will perform satisfactorily in the ground simulation and in the on-board tests.

APPENDIX A

COORDINATE SYSTEMS

One of the characteristics of the Global Positioning System is its use of a worldwide common coordinate grid. The navigation signals and the downlink data will, after processing, locate a user at a specific point in a coordinate system common to users worldwide. The relationships between the GPS coordinate system and other systems can be used to transform the navigation output to coordinates in a desired system.

Coordinate systems are defined by specifying an orgin, the direction of the positive third-(z-) axis, the fundamental (xy-) plane which is perpendicular to the positive third-axis, and the direction of the first-axis which is in the fundamental plane. The second-(y-) axis will always be defined to complete a right-handed coordinate system. In the simulation and test programs, the common grid is assumed to be the geocentric earth-fixed (GEF) system. The origin of the GEF system is the center of the Earth (the geocenter). The positive third-axis is assumed to be aligned with the Earth's angular velocity vector. The GEF system is simulated as an "earth-fixed" system by assuming that polar motion is negligible. The fundamental plane is the equatorial plane, and the first-axis is aligned with the Greenwich meridian.

Satellite state propagation is accomplished by taking the Keplerian elements at an epoch and determining the satellite

position and inertial velocity in the orbital plane. The orientation of the orbital plane is assumed to be fixed in an inertial coordinate system. For the simulation and test programs, the geocentric inertial (GI) system is defined to be the inertial system. The origin of the GI system is at the geocenter. The positive third-axis is aligned with the Earth's angular velocity vector. The first-axis is assumed to be aligned with the GEF first-axis (Greenwich meridian) at T = 0. In the simulation and test programs, precession and nutation have not been modeled. The orientation of the GI system is therefore the mean orientation for the entire test flight. It should be noted that corrections for polar motion, precession, and nutation will be accopplished by the Control System Segment. User processing of the downlink satellite ephemeris data will result in satellite positions in an earth-fixed system. The effects of precession, nutation, and polar motion will not effect a user over the one-hour applicability of the ephemeris information. Figure A.1 shows the relationship between the GI system and the GEF system.

Figure A.1 also shows an additional rotation about the Earth's angular velocity vector equal to the user's longitude. It is convenient to describe the North-East-Down (NED) directions by examining the meridional section of the reference ellopsoid at the user's longitude (Fig. A.2).

The origin of the Topocentric North-East-Down (TNED) system is the user's location. The user's subpoint is the point on the reference ellipsoid nearest the user. The vector from the user to the user's

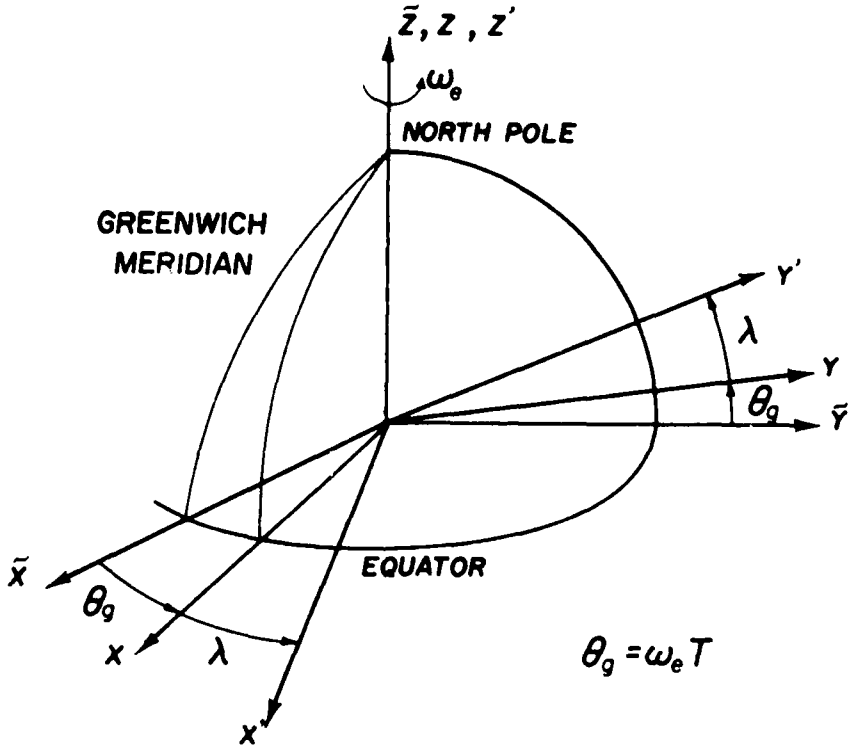

FIG. A.I. RELATIONSHIP BETWEEN GEOCENTRIC SYSTEMS

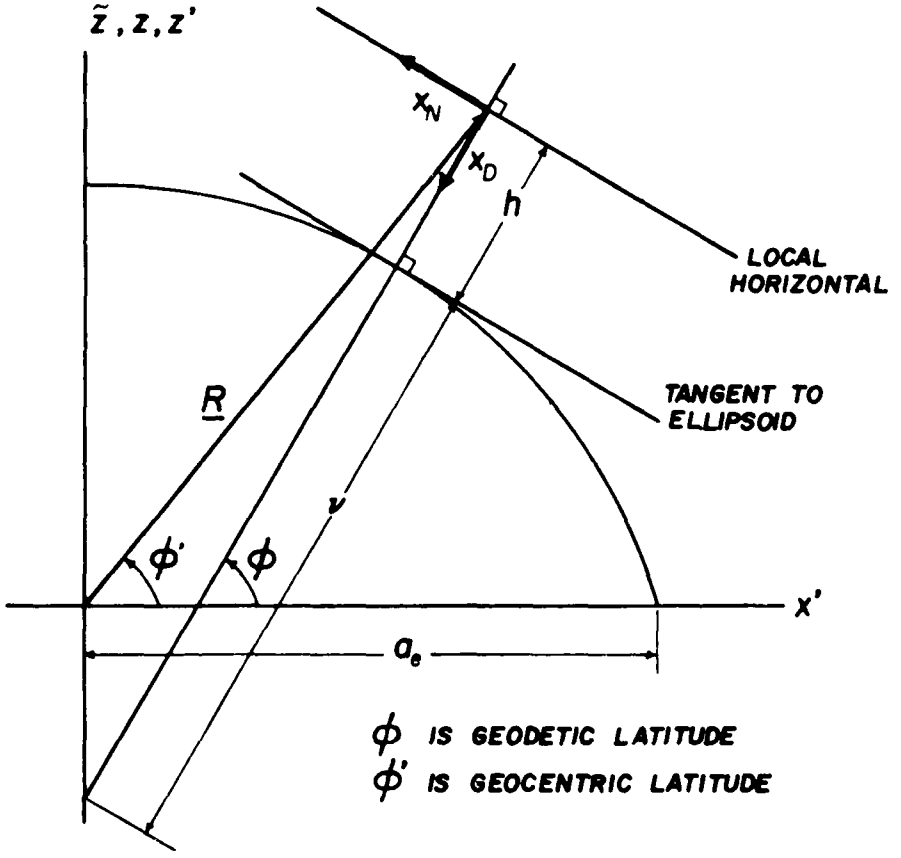

FIG. A.2. DEFINITION OF TOPOCENTRIC-NORTH-EAST-DOWN SYSTEM

subpoint is the direction a plumb bob would point if the ellipsoidal Earth were homogeneous. This direction is called the local vertical. The third-axis of the TNED system is along the local vertical, pointing toward the center of the Earth. The third-axis does not point directly at the geocenter unless the user is on the equator or at one of the poles. The fundamental plane of the TNED system is the local horizontal which is defined as the plane perpendicular to the local vertical at the user's location. The local horizontal is parallel to the plane which is tangent to the ellipsoid at the user's subpoint. The first-axis of the TNED system is along the intersection of the local horizontal plane and the plane of the user's meridian. The first-axis is positive toward the North pole. The second-axis points East, completing the right-handed coordinate system.

If a column matrix is defined to consist of the basis vectors of a coordinate system and a second column matrix consists of the components of a vector along the basis vectors, then a vector can be defined as the inner product of the matrix of components and the matrix of basis vectors. For example, if the basis vectors of the GI coordinate system are $\underline{I}$, $\underline{J}$, and $\underline{K}$, then the satellite position vector, which has components $\dot{X}$, $\dot{Y}$, and $\dot{Z}$ along $\underline{I}$, $\underline{J}$, and $\underline{K}$, can be written

$$\underline{R}_S = \dot{X}\underline{I} + \dot{Y}\underline{J} + \dot{Z}\underline{K} \qquad (A.1)$$

or as the inner product

$$\underline{R}_S = [\tilde{X}, \tilde{Y}, \tilde{Z},] \begin{bmatrix} \tilde{\underline{I}} \\ \tilde{\underline{J}} \\ \tilde{\underline{K}} \end{bmatrix} = \tilde{R}_S^T \tilde{B} \tag{A.2}$$

where: $$\tilde{R}_S^T = [\tilde{X}, \tilde{Y}, \tilde{Z}]; \text{ and} \tag{A.3}$$

$$\tilde{B}^T = [\tilde{\underline{I}}, \tilde{\underline{J}}, \tilde{\underline{K}}]. \tag{A.4}$$

If the basis vectors for the GEF coordinate system are $\underline{i}$, $\underline{j}$, and $\underline{k}$, then the satellite position vector can also be written

$$\underline{R}_S = X\underline{i} + Y\underline{j} + Z\underline{k} = [X, Y, Z] \begin{bmatrix} \underline{i} \\ \underline{j} \\ \underline{k} \end{bmatrix} = R_S^T B \tag{A.5}$$

where: $$R_S^T = [X, Y, Z]; \tag{A.6}$$

$$B^T = [\underline{i}, \underline{j}, \underline{k}]. \tag{A.7}$$

The relationship between the GI components of $\underline{R}_S$ and the GEF components of $\underline{R}_S$ is given by

$$R_S = \begin{bmatrix} X \\ Y \\ Z \end{bmatrix} = \begin{bmatrix} \cos \omega_e T & \sin \omega_e T & 0 \\ -\sin \omega_e T & \cos \omega_e T & 0 \\ 0 & 0 & 1 \end{bmatrix} \begin{bmatrix} \tilde{X} \\ \tilde{Y} \\ \tilde{Z} \end{bmatrix} \tag{A.8}$$

$$R_S = [\omega_e T]_3 \tilde{R}_S$$

The matrix representing a rotation of $\omega_e T$ degrees about the third coordinate axis is expressed as $[\omega_e T]_3$. Similar rotation matrices can be defined for rotations about the first and second coordinate axes.

$$[\alpha]_1 = \begin{bmatrix} 1 & 0 & 0 \\ 0 & \cos\alpha & \sin\alpha \\ 0 & -\sin\alpha & \cos\alpha \end{bmatrix} \tag{A.9}$$

$$[\alpha] = \begin{bmatrix} \cos\alpha & 0 & -\sin\alpha \\ 0 & 1 & 0 \\ \sin\alpha & 0 & \cos\alpha \end{bmatrix} \tag{A.10}$$

Complex rotations can be expressed as a product of rotation matrices. For more information on the properties of rotation matrices see Eisenman [85].

The components of the satellite position and inertial velocity vectors are first computed in the GI coordinate system and rotated to the GEF coordinate system as follows:

$$R_S = [\omega_e T]_3 \tilde{R}_S \tag{A.11}$$

$$V_S^{(I)} = [\omega_e T]_3 \tilde{V}_S^{(I)} \tag{A.12}$$

The user's location can be specified by the three parameters: geodetic latitude ϕ, longitude λ, and altitude above the reference ellipsoid h. Unless otherwise specified, altitude will imply altitude above the reference ellipsoid and latitude will imply geodetic latitude.

The routine TOP2GEF, as used in the computer programs, solves for the GEF components of user position and relative velocity. The input to TOP2GEF is user location expressed as latitude, longitude, and altitude and the user's relative velocity expressed as velocity North v_N, velocity East v_E, and velocity down v_D. The components of the relative velocity vector $\underline{v}$ are rotated into the GEF system using

$$V = [-\lambda]_3[\phi + \pi/2]_2 \, v \tag{A.13}$$

where: $$v^T = [v_N, v_E, v_D]. \tag{A.14}$$

The user's position vector $\underline{R}$ is calculated using

$$\underline{R} = x\underline{i} + y\underline{j} + z\underline{k} = R^T B \tag{A.15}$$

$$\nu = a_e \left[1 - e^2 \sin^2\phi\right]^{-1/2} \tag{A.16}$$

$$\begin{aligned} x &= (\nu + h)\cos\phi \ \cos\lambda \\ y &= (\nu + h)\cos\phi \ \sin\lambda \\ z &= (\nu\,(1-e^2) + h)\sin\phi \end{aligned} \tag{A.17}$$

where: a_e is the semi-major axis of the reference ellipsoid;

e is the eccentricity of the ellipsoid; and

$$R^T = [x, y, z]. \tag{A.18}$$

It is frequently necessary to determine the latitude, longitude, and altitude of a point whose components are given in the TNED system.

$$\Delta\underline{r} = \Delta x_N \underline{i}_N + \Delta x_E \underline{j}_E + \Delta x_D \underline{k}_D = \Delta r^T b \tag{A.19}$$

where:

$$\Delta r^T = [\Delta x_N, \Delta x_E, \Delta x_D]; \text{ and} \tag{A.20}$$

$$b^T = [\underline{i}_N, \underline{j}_E, \underline{k}_D]. \tag{A.21}$$

Latitude, longitude, and altitude can be obtained by first rotating Δr into the GEF system, then adding the result to the GEF components of the user position vector.

$$R + \Delta R = R + [-\lambda]_3 [\phi + \pi/2]_2 \Delta r \tag{A.22}$$

The result of Eq. A.22 is then used to solve for latitude, longitude and altitude. Unfortunately, there is no closed expression for geodetic latitude on the reference ellipsoid as a function of the GEF components. A recursive algorithm must be used.

If the vector $\Delta\underline{r}$ is small, the latitude, longitude, and altitude can be approximated by

$$\phi + \Delta\phi \cong \phi + \partial\phi/\partial\underline{r}|_{\underline{R}}\ \Delta r \tag{A.23}$$

$$\lambda + \Delta\lambda \cong \lambda + \partial\lambda/\partial\underline{r}|_{\underline{R}}\ \Delta\underline{r} \tag{A.24}$$

$$h + \Delta h \cong h + \partial h/\partial\underline{r}|_{\underline{R}}\ \Delta\underline{r} \tag{A.25}$$

The partial derivatives in Eqs. A.23 through A.25 are approximated as follows:

$$\frac{\partial\phi}{\partial x_n} = \frac{\partial x/\partial x_N}{\partial x/\partial\phi} \tag{A.26}$$

$$\frac{\partial\lambda}{\partial x_E} = \frac{\partial x/\partial x_E}{\partial x/\partial\lambda} \tag{A.27}$$

$$\frac{\partial h}{\partial x_D} = -1 \tag{A.28}$$

The terms $\partial x/\partial x_N$ and $\partial x/\partial x_E$ are evaluated from the rotation equation

$$\Delta R = \begin{bmatrix}\Delta x\\ \Delta y\\ \Delta z\end{bmatrix} = [-\lambda]_3[\phi+\pi/2]_2 \begin{bmatrix}\Delta x_n\\ \Delta x_E\\ \Delta x_D\end{bmatrix} \tag{A.29}$$

yielding

$$\partial x/\partial x_N = -\sin\phi\cos\lambda \tag{A.30}$$

$$\partial x/\partial x_E = -\sin\lambda \tag{A.31}$$

Differentiating Eqs. A.17 yields the following results:

$$\partial x/\partial \phi = -[a_e(1-e^2)(1-e^2\sin^2\phi)^{-3/2}+h] \sin \phi \cos \lambda \quad (A.32)$$

$$\partial x/\partial \lambda = -[a_e(1-e^2\sin^2\phi)^{-1/2}+h] \cos \phi \sin \lambda \quad (A.33)$$

Equations A.26 and A.27 can now be evaluated. The results are stored in the parameters R_{20} and R_{21}.

$$R_{20} = (\partial\phi/\partial x_N|_{\underline{R}})^{-1} = a_e(1-e^2)(1-e^2\sin^2\phi)^{-3/2} + h \quad (A.34)$$

$$R_{21} = (\partial\lambda/\partial x_E\ \underline{R})^{-1} = [a_e(1-e^2\sin^2\phi)^{-1/2}+h] \cos \phi \quad (A.35)$$

To first order, the latitude, longitude, and altitude of the point $(\underline{R} + \Delta\underline{R})$ are

$$\phi + \Delta\phi = \phi + \Delta x_N/R_{20} \quad (A.36)$$

$$\lambda + \Delta\lambda = \lambda + \Delta x_E/R_{21} \quad (A.37)$$

$$h + \Delta h = h - \Delta x_D \quad (A.38)$$

On a spherical earth, Eqs. A.34 and A.35 reduce to

$$R_{20} = a_e + h \quad (A.39)$$

$$R_{21} = (a_e + h) \cos \phi \quad (A.40)$$

APPENDIX B

THE GENERATION OF RANDOM NUMBERS

Uniformly Distributed Numbers

Three types of random number distributions were required in the simulation and testing programs: independent random numbers with uniform distribution; independent random numbers with Gaussian distribution; and random numbers with exponential correlation. The computer system used in the numerical tests was a Control Data Corp. CDC-6600, UT-2D operating system. The computer system has a random number generator called RANF which is a "multiplicative congruential" generator. Details of the exact methods used in RANF and the implications of the method are available in [86:Par. 13.9]. To satisfy the noise-generation requirements of the simulation program adopted in this study, RANF is used to provide independent random numbers with uniform distribution between zero and one. The mean and variance of RANF are given by:

$$E[RANF] = 1/2 \tag{B.1}$$

$$E[RANF^2] = 1/12 \tag{B.2}$$

Gaussian Distribution

The Central Limit Theorem states that the summation of independent random variables with a common distribution approaches the Gaussian or normal distribution as the number of samples gets large

[87:229]. Using this theorem, a random variable which is defined as follows:

$$x = \sum_{i=1}^{12} (RANF_i - 1/2) \tag{B.3}$$

will be assumed to have Gaussian distribution. The mean and variance of x are given by

$$E[x] = 0 \tag{B.4}$$

$$E[(x - E[x])^2] = 1 \tag{B.5}$$

The random variable of Eq. B.3 provides a good approximation to the Gaussian distribution between plus/minus six standard deviations. Hamming [55:309-323] discusses generation of uniform distributions and Gaussian distribution in more detail.

Exponentially Correlated Random Numbers

The third type of random variable that is required must have exponential correlation. Kochenburger [71:Chap.9] discussed the simulation of an exponentially correlated random process by attempting to match the power spectral density of the process. Lear [89] analyzed, in detail, the behavior of an exponentially correlated random sequence. Lear's method was incorporated into the simulation and test programs. The random numbers were generated using the following equation:

$$w_k = w_{k-1}\exp(-(t_k - t_{k-1})/\tau + \sigma\sqrt{1 - \exp(-2(t_k - t_{k-1})/\tau)}\ x \tag{B.6}$$

where: τ is the desired correlation time;

$t_{k-1} \leq t_k$; and

x is calculated using Eq. B.3.

The mean, variance, and covariance kernel of Eq. B.6 are given by:

$$E[w_k] = E[w_{k-1}] = \cdots = E[w_1] = w_0 \quad (B.7)$$

$$E[w_k^2] = \sigma^2 \quad (B.8)$$

$$E[w_j w_k] = \sigma^2 \exp(-(t_k - t_j)/\tau), \quad t_j \leq t_k \quad (B.9)$$

Repeatability and Independence

By saving the contents of the random number generator RANF between time steps for each noise source, the random numbers generated identical results for all computer tests. Also, by choosing starting values for RANF that were sufficiently separated in the period of RANF, independence of the various noise sources was assured.

APPENDIX C

THE MEASUREMENT PARTIALS

Expressions for psuedo-range, pseudo-range-rate, and altimeter measurements can be separated into three parts: a part which is determined by the positions and velocities of the satellite and the user; a part which is a function of variables to be estimated by the filter other than the user's position and velocity; and any remaining terms. The only remaining term which was evaluated by the tested user algorithms was an atmospheric delay in the pseudo-range measurement. In addition to user position and velocity, the variables to be estimated include user clock bias, user clock drift, and altimeter bias. Each of these terms can be considered to be an unknown measurement bias. Values estimated for each term may actually contain contributions from sources other than those suggested by their names. For example, unaccounted equipment delay in the user electronics will affect the estimation of the "user clock bias."

The expressions for the observations as required in Eq. 4.80 are given by:

$$G_\rho(\underline{X},T) = \rho + a_1 + \delta_{atm} \tag{C.1}$$

$$G_{\dot\rho}(\underline{X},T) = \dot\rho + a_2 \tag{C.2}$$

$$G_h(\underline{X},T) = h + \delta_h \tag{C.3}$$

where: ρ is the line-of-sight range between the user and the satellite;

$\dot{\rho}$ is the range-rate between the user and the satellite;

a_1 and a_2 are user clock bias and user clock drift expressed in units of distance and velocity by multiplying the time values by the vacuum speed of light;

δ_{atm} is the atmospheric delay expressed in units of distance;

h is the altitude of the user above the reference ellipsoid; and

δ_h is the altimeter bias.

If a_1, a_2, and δ_h are to be estimated, then the following partial derivatives are required:

$$\frac{\partial G_\rho}{\partial a_1} = 1 \; ; \; \frac{\partial G_{\dot{\rho}}}{\partial a_2} = 1 \; ; \; \frac{\partial G_h}{\partial \delta_h} = 1 \qquad \text{(C.5)}$$

For the altimeter measurement, one more partial is required.

$$\frac{\partial G_h}{\partial x_D} = -1 \qquad \text{(C.6)}$$

The altimeter observation-state matrix for the basic twelve-state filter is

$$H_h = [0\ 0\ -1 \vdots 0\ 0\ 0 \vdots 0\ 0\ 0 \vdots 1\ 0\ 0] \qquad (C.7)$$

The partial derivatives for the range and range rate can be derived as follows. From Par. 3.6.1, the range is computed by the following relation

$$\rho = [(X-x)^2 + (Y-y)^2 + (Z-z)^2]^{1/2} \qquad (C.8)$$

where: X, Y, and Z are the Geocentric - Earth - Fixed components of the satellite position vector, $R_S^T = [X,Y,Z]$; and

x,y, and z are the GEF components of the user position vector, $R^T = [x,y,z]$.

Taking the partial derivative of Eq. C.8 with respect to the user GEF position coordinate yields:

$$\frac{\partial\rho}{\partial x} = \frac{-(X - x)}{\rho}\ ;\ \frac{\partial\rho}{\partial y} = \frac{-(Y - y)}{\rho}\ ;\ \frac{\partial\rho}{\partial z} = \frac{-(Z - z)}{\rho} \qquad (C.9)$$

Equations C.9 contain the three GEF components of the unit vector directed from the satellite to the user. Defining $\underline{l}_{ui}$ as the unit vector from the user to the satellite, the partial derivative of the range with respect to the GEF components of the user's position vector is given by:

$$\frac{\partial \rho}{\partial R} = \left[\frac{\partial \rho}{\partial x}, \frac{\partial \rho}{\partial y}, \frac{\partial \rho}{\partial z}\right] = -l^{T}_{ui_{GEF}} \qquad (C.10)$$

where: $l_{ui_{GEF}}$ is a column matrix of the GEF components of the vector $\underline{l}_{ui}$.

The desired state vector, however, is oriented along the North-East-Down directions. Using the chain rule, the partial derivatives with respect to the user's position in a Geocentric-North-East-Down (GNED) coordinate system are:

$$\frac{\partial \rho}{\partial x_N} = \frac{\partial \rho}{\partial x}\frac{\partial x}{\partial x_N} + \frac{\partial \rho}{\partial y}\frac{\partial y}{\partial x_N} + \frac{\partial \rho}{\partial z}\frac{\partial z}{\partial x_N}$$

$$\frac{\partial \rho}{\partial x_E} = \frac{\partial \rho}{\partial x}\frac{\partial x}{\partial x_E} + \frac{\partial \rho}{\partial y}\frac{\partial y}{\partial x_E} + \frac{\partial \rho}{\partial z}\frac{\partial z}{\partial x_E} \qquad (C.11)$$

$$\frac{\partial \rho}{\partial x_D} = \frac{\partial \rho}{\partial x}\frac{\partial x}{\partial x_D} + \frac{\partial \rho}{\partial y}\frac{\partial y}{\partial x_D} + \frac{\partial \rho}{\partial z}\frac{\partial z}{\partial x_D}$$

Equation C.11 can be written in matrix form:

$$\begin{bmatrix} \frac{\partial \rho}{\partial x_N} \\ \frac{\partial \rho}{\partial x_E} \\ \frac{\partial \rho}{\partial x_D} \end{bmatrix} = \begin{bmatrix} \frac{\partial x}{\partial x_N} & \frac{\partial y}{\partial x_N} & \frac{\partial z}{\partial x_N} \\ \frac{\partial x}{\partial x_E} & \frac{\partial y}{\partial x_E} & \frac{\partial z}{\partial x_E} \\ \frac{\partial x}{\partial x_D} & \frac{\partial y}{\partial x_D} & \frac{\partial z}{\partial x_D} \end{bmatrix} \begin{bmatrix} \frac{\partial \rho}{\partial x} \\ \frac{\partial \rho}{\partial y} \\ \frac{\partial \rho}{\partial z} \end{bmatrix} \tag{C.12}$$

The coordinate transformation from the GNED directions to the GEF was given in Appendix A.

$$R = [-\lambda]_3[\phi + \pi/2]_2 \; R_{GNED} \tag{C.13}$$

where: λ is longitude;

ϕ is geodetic latitude; and

$[\cdot]_2$ and $[\cdot]_3$ represent standard rotation matrices.

The matrix in Eq. C.12 corresponds to the inverse of the rotation matrices in Eq. C.13. The partials given by Eq. C.9 can be computed using the GEF components then rotated to obtain the partials with respect to the GNED components, i.e.,

$$\frac{\partial \rho}{\partial R_{GNED}} = [-\phi-\pi/2]_2[\lambda]_3 \frac{\partial \rho}{\partial R} \qquad (C.14)$$

Equation C.10 implies that the partial of the range with respect to user position vector components in any frame is equal to the components of the unit vector in that frame. With this fact, Eq. C.14 can be used to rotate the components of the unit vector to the orientation of any desired coordinate system.

A programming simplification can be obtained with the above analysis. The range vector from the user to the satellite, expressed in Topocentric-North-East-Down (TNED) components, is given by:

$$\underline{\rho} = [\rho \cos el \cos az, \rho \cos el \sin az, -\rho \sin el]b \qquad (C.15)$$

where: b is a matrix consisting of the basis vectors of the TNED coordinate system. (See App. A.)

The unit vector along the range vector is

$$\underline{1}_{ui} = [\cos el \cos az, \cos el \sin az, -\sin el]b$$

$$= 1^T_{ui} b \qquad (C.16)$$

The components of unit vectors aligned in specific directions are equal regardless of their origin. Therefore,

$$1_{ui_{TNED}} = 1_{ui_{GNED}} \qquad (C.17)$$

Since elevation and azimuth are normally obtained as part of the satellite ephemeris operation, the partial derivative can be obtained using Eq. C.16 without any reference to rotation matrices.

The range-rate is given by Eq. 3.38.

$$\dot{\rho} = \frac{[(X-x)(V_X-v_x+\omega_e y)+(Y-y)(V_Y-v_y-\omega_e x)+(Z-z)(V_Z-v_z)]}{[(X-x)^2 + (Y-y)^2 + (Z-z)^2]^{1/2}} \quad (3.38)$$

where: V_X, V_Y, and V_Z are the GEF components of the satellite inertial velocity vector, $V_S = [V_X, V_Y, V_Z]$ (See Eq. A.12)

v_x, v_y, and v_z are the GEF components of the user's relative velocity vector, $V = [v_x, v_y, v_z]$ (See Eq. A.14)

ω_e is the rotation rate of the Earth; and the denominator in Eq. 3.38 is the range.

It can be verified from Eq. 3.38 that

$$\frac{\partial \dot{\rho}}{\partial V} = -1_{ui_{GEF}} \quad (C.18)$$

Therefore, Eq. C.16 can be used to evaluate the partial derivative of range rate with respect to the TNED components of the user's relative velocity vector.

To evaluate the partials of range-rate with respect to the GNED position, the chain rule is used to obtain

$$\begin{bmatrix} \frac{\partial \rho}{\partial x_N} \\ \frac{\partial \dot{\rho}}{\partial x_E} \\ \frac{\partial \dot{\rho}}{\partial x_D} \end{bmatrix} = [-\phi-\pi/2]_2[\lambda]_3 \begin{bmatrix} \frac{\partial \dot{\rho}}{\partial x} \\ \frac{\partial \dot{\rho}}{\partial y} \\ \frac{\partial \dot{\rho}}{\partial z} \end{bmatrix} + \begin{bmatrix} \frac{\partial v_x}{\partial x_N} & \frac{\partial v_x}{\partial x_N} & \frac{\partial v_z}{\partial x_N} \\ \frac{\partial v_x}{\partial x_E} & \frac{\partial v_y}{\partial x_E} & \frac{\partial v_z}{\partial x_E} \\ \frac{\partial v_x}{\partial x_D} & \frac{\partial v_y}{\partial x_D} & \frac{\partial v_z}{\partial x_D} \end{bmatrix} \begin{bmatrix} \frac{\partial \dot{\rho}}{\partial v_x} \\ \frac{\partial \dot{\rho}}{\partial v_y} \\ \frac{\partial \dot{\rho}}{\partial v_z} \end{bmatrix} \quad \text{(C. 19)}$$

The magnitude of the range-rate seen by a suer is affected by his position on the earth. The first term on the right hand side of Eq. C.19 accounts for this effect. A change in user position also changes the orientation of a user's relative velocity vector in the GEF frame. The second term on the right hand side of Eq. C.19 accounts for this effect.

The two vectors in Eq. C.19 are evaluated directly from Eq. 3.38.

$$\begin{aligned} \frac{\partial \dot{\rho}}{\partial x} &= [v_x - V_X - \omega_e Y + \dot{\rho}(X - x)/\rho]/\rho \\ \frac{\partial \dot{\rho}}{\partial y} &= [v_y - V_Y + \omega_e Y + \dot{\rho}(Y - y)/\rho]/\rho \\ \frac{\partial \dot{\rho}}{\partial z} &= [v_z - V_Z + \dot{\rho}(Z - z)/\rho]/\rho \end{aligned} \quad \text{(C.20)}$$

$$\frac{\partial \dot{\rho}}{\partial v_x} = \frac{-(X-x)}{\rho} ; \frac{\partial \dot{\rho}}{\partial v_y} = \frac{-(Y-y)}{\rho} ; \frac{\partial \dot{\rho}}{\partial v_z} = \frac{-(Z-z)}{\rho} \quad \text{(C.21)}$$

The remaining matrix in Eq. C.19 will be identified as D. The D matrix will not be zero since Eq. C.13 also applies to the rotation of the velocity components, i.e.,

$$V = [-\lambda]_3 [\phi + \pi/2]_2 V_{GNED} \tag{C.22}$$

A change in user position changes the latitude and longitude of the user and will therefore change the values of the GEF components of the user's relative velocity.

Geodetic latitude cannot be expressed as a closed form function of the cartesian coordinates for an eccentric Earth. Intuitive arguments will be used in the following analysis to derive the partial derivatives.

Note that the elements of V in Eq. C.22 have no dependence on altitude or, equivalently, x_D. Therefore, the third row of the matrix D is zero. Also, from the definition of geodetic latitude and longitude on the reference ellipsoid, a movement in the North-South direction has no effect on longitude and movement in the East-West direction has no effect on latitude. After expanding the elements of D using the chain rule and after considering these remarks, the matrix D is given by

$$D = \begin{bmatrix} \frac{\partial v_x}{\partial \phi}\frac{\partial \phi}{\partial x_N} & \frac{\partial v_y}{\partial \phi}\frac{\partial \phi}{\partial x_N} & \frac{\partial v_z}{\partial \phi}\frac{\partial \phi}{\partial x_N} \\ \frac{\partial v_x}{\partial \lambda}\frac{\partial \lambda}{\partial x_E} & \frac{\partial v_y}{\partial \lambda}\frac{\partial \lambda}{\partial x_E} & 0 \\ 0 & 0 & 0 \end{bmatrix} \tag{C.23}$$

From Eqs. A.34 and A.35

$$\frac{\partial \phi}{\partial x_N} = [a_e(1-e^2)(1-e^2\sin\phi)^{-3/2} + h]^{-1} \quad (C.24)$$

$$\frac{\partial \lambda}{\partial x_E} = [(a_e(1-e^2\sin^2\phi)^{-1/2} + h)\cos\phi]^{-1} \quad (C.25)$$

The rotation matrices used in Eq. C.22 can be expanded as follows:

$$[-\phi-\pi/2]_2[\lambda]_3 = \begin{bmatrix} -\sin\phi\cos\lambda & -\sin\phi\sin\lambda & \cos\phi \\ -\sin\lambda & \cos\lambda & 0 \\ -\cos\phi\cos\lambda & -\cos\phi\sin\lambda & -\sin\phi \end{bmatrix} \quad (C.26)$$

The remaining terms of D are obtained by substituting Eq. C.26 into Eq. C.22 and taking the appropriate partials.

$$\frac{\partial v_x}{\partial \phi} = (-v_N\cos\phi + v_d\sin\phi)\cos\lambda \quad (C.27)$$

$$\frac{\partial v_y}{\partial \phi} = (-v_N\cos\phi + v_d\sin\phi)\sin\lambda \quad (C.28)$$

$$\frac{\partial v_z}{\partial \phi} = -v_N\sin\phi - v_D\cos\phi \quad (C.29)$$

$$\frac{\partial v_x}{\partial \lambda} = (v_N\sin\phi + v_D\cos\phi)\sin\lambda - v_E\cos\lambda \quad (C.30)$$

$$\frac{\partial v_y}{\partial \lambda} = -(v_N\sin\phi + v_D\cos\phi)\cos\lambda - v_E\sin\lambda \quad (C.31)$$

It was previously shown that the components of unit vectors aligned in specific directions are equal regardless of the origin. Similarly, the components of the user's relative velocity vector, aligned in specific directions, will not change as the origin of the coordinate system is changed. Accordingly, the partial derivatives which were

derived with respect to the GNED components of the user's relative velocity vector are identical to the partial derivatives with respect to the TNED components.

Summarizing the results:

$$\frac{\partial \rho}{\partial r} = \underbrace{[-\phi-\pi/2]_2[\lambda]_3}_{\text{Eq. C.26}} \underbrace{\frac{\partial \rho}{\partial R}}_{\text{Eq. C.9}} \qquad \text{(C.32)}$$

$$\frac{\partial \dot{\rho}}{\partial r} = \underbrace{[-\phi-\pi/2]_2[\lambda]_3}_{\text{Eq. C. 26}} \underbrace{\frac{\partial \dot{\rho}}{\partial R}}_{\text{Eq. C.20}} + \underbrace{D \frac{\partial \dot{\rho}}{\partial V}}_{\text{Eq. C.21}} \qquad \text{(C.33)}$$

$$\frac{\partial \dot{\rho}}{\partial v} = \underbrace{[-\phi-\pi/2]_2[\lambda]_3}_{\text{Eq. C.26}} \underbrace{\frac{\partial \dot{\rho}}{\partial V}}_{\text{Eq. C.21}} \qquad \text{(C.34)}$$

where: The D matrix is evaluated using Eq. C.23 through C.31; and

r and v are column matrices of the TNED components of the user's position and relative velocity vectors.

Equations C.32 and C.34 can be replaced by Eq. C.16.

$$\frac{\partial \rho}{\partial r} = \frac{\partial \dot{\rho}}{\partial v} = [-\cos el \cos az, -\cos el \sin az, \sin el] \qquad \text{(C.35)}$$

The observation-state matrices for the pseudo-range and pseudo-range-rate measurements are:

$$H_\rho = [-1_{ui_{TNED}} \vdots 0\ 0\ 0 \vdots 0\ 0\ 0 \vdots 0\ 1\ 0] \qquad (C.36)$$

$$H_{\dot\rho} = [\ \partial\dot\rho/\partial r \vdots -1_{ui_{TNED}} \vdots 0\ 0\ 0 \vdots 0\ 0\ 1] \qquad (C.37)$$

BIBLIOGRAPHY

1. Pinsent, John. Greek Mythology. Paul Hamlyn, London, 1969.

2. Kline, Morris. Mathematical Thought from Ancient to Modern Times. Oxford University Press, New York, 1972.

3. Taylor, E.G.R. The Haven-Finding Art. Hollis and Carter, London, 1956.

4. Frenkel, G., et al. Radio Navigation Study, Volume I. Prepared for the Office of Telecommunications Policy, Executive Office of the President, by Computer Sciences Corp., Falls Church, VA., AD A010114, February, 1975.

5. Guier, W.H. and G.C. Weiffenbach. "A Satellite Doppler Navigation System." Proc. IRE, v. 48, pp. 507-516, April, 1960.

6. Smith, Douglas and William Criss. "GPS Navstar Global Positioning System." Astronautics and Aeronautics, April, 1976, pp. 26-32.

7. Wiener, Norbert. Extrapolation, Interpolation, and Smoothing of Stationary Time Series. The M.I.T. Press, Massachusettes Institute of Technology, Cambridge, MA, 1949.

8. Kalman, R.E. "A New Approach to Linear Filtering and Prediction Problems." Journal of Basic Engineering, pp. 35-45, March, 1960.

9. Kalman, R.E. and R.S. Bucy. "New Results in Linear Filtering and Prediction Theory." Journal of Basic Engineering, pp. 95-108, March, 1961.

10. Fehlner, L.F. Precision Aircraft Navigation Based on Loran-C and Digital Altimetry. John Hopkins Univ., Applied Physics Lab. Technical Memorandum TG 1184, Silver Spring, MD, AD 740894, January, 1972.

11. Naval Postgraduate School Group Thesis Project 0910. The Preliminary Design of a Long Range Navigation System for Tactical Aircraft. Naval Postgraduate School, Monterey, CA, AD 881748, December, 1970.

12. Ehrlich, Eugene. "The Role of Time-Frequency in Satellite Position Determination Systems." Proc. IEEE, v. 60, n. 5, pp. 564-571, May, 1972.

13. Easton, Roger L. "The Role of Time/Frequency in Navy Navigation Satellites." Proc. IEEE, v. 60, no. 5, pp. 557-563, May 1972.

14. Rueger, Lauren J. "Transit Navigation Satellite." Pro. Precise Time and Time Interval (PTTI) Strategic Planning Meeting, Vol. I, sponsored by U. S. Naval Observatory, December 10-11, 1970, Washington, D.C., AD 881014, pp. 84-107.

15. McCaskill, Thomas B. and James A. Buisson. NTS-1 (Timation III) Quartz- and Rubidium-Oscillator Frequency-Stability Results. Naval Research Lab. Report 7932, Washington, D.C. AD A019156, December, 1975.

16. Van Dierendonck, A.J., et al. "The Approach to Satellite Ephemeris Determination for the NAVSTAR Global Positioning System." presented at 31st Annual Meeting of Institute of Navigation, Washington, D.C., 24-26 June, 1975.

17. Rockwell International Corp., Space Division. "Space Vehicle Nav Subsystem and NTS PRN Navigation Assembly/User System Segment and Monitor Station." Rockwell International Corp. Drawing No. MH08-00002-400, rev. E, Downey, CA, September, 1975.

18. Bogen, A.H. Geometric Performance of the Global Positioning System. AF Report SAMSO-TR-74-169, Aerospace Corp. Report TR-0074(4461-02)-2, El Segundo, CA., June, 1974.

19. Barnes, James A. "Atomic Timekeeping and the Statistics of Precision Signal Generators." Proc. IEEE, v. 54, n. 2, pp. 207-220, February, 1966.

20. Bartholomew, C.A. Quartz Crystal Oscillator Development for Timation. Naval Research Lab. Report 7478, Washington, D.C., AD 906077, October, 1972.

21. Hellwig, Helmut. "Atomic Frequency Standards: A Survey." Proc. 28th Annual Symposium on Frequency Control, U.S. Army Electronics Command, Fort Monmouth, NJ, pp. 315-339 (1974). Copies available from Electronics Industries Association, 2001 Eye St., NW, Washington, D.C., 20006.

22. Kartaschoff, Peter and James A. Barnes, "Standard Time and Frequency Generation." Proc. IEEE, v. 60, n. 5, pp. 493-501, May, 1972.

23. Barnes, James A., et al. "Characterization of Frequency Stability." IEEE Trans. Instrumentation and Measurement, v. IM-20, n. 2, pp. 105-120, May, 1971.

24. Gray, James E. and David W. Allan. "A Method for Estimating the Frequency Stability of an Individual Oscillator." Proc. 28th Annual Symposium on Frequency Control, U.S. Army Electronics Command, Fort Monmouth, NJ, pp. 243-246 (1974). Copies available from Electronics Industries Association, 2001 Eye St., NW, Washington, D.C., 20006.

25. Allan, David W. "Statistics of Atomic Frequency Standards." Proc. IEEE, v. 54, n. 2, pp. 221-230, February, 1966.

26. Lindsey, William C. and James L. Lewis. Modeling, Characterization and Measurement of Oscillator Frequency Instability. Naval Research Lab. Report NRL-1.1351, LinCom Corp., Pasadena, CA, AD 785862, June, 1974.

27. Allan, David W. "The Measurement of Frequency and Frequency Stability of Precision Oscillators." Proc. Sixth Ann. Precise Time and Time Interval (PTTI) Planning Meeting, held at the U.S. Naval Research Lab., December 3-5, 1974, Goddard Space Flight Center Report X-814-75-117, Greenbelt, MD., pp. 109-131.

28. System Segment Specification for the Space Vehicle System Segment of the NAVSTAR Global Positioning System Phase I. Air Force Spec. SS-SVS-101A, June 20, 1974.

29. Nichols, Stephen A. and Joseph White. "Satellite Application of a Rubidium Frequency Standard." Proc. 28th Annual Symposium on Frequency Control, U.S. Army Electronics Command, Fort Monmouth, NJ, pp. 401-405, (1974), Copies available from Electronics Industries Association, 2001 Eye St., NW, Washington, D.C., 20006.

30. Taylor, R.J. "Satellite to Ground Timing Experiments." Proc. 28th Annual Symposium on Frequency Control, U.S. Army Electronics Command, Fort Monmouth, NJ, pp. 384-388, (1974), Copies available from Electronics Industries Association, 2001 Eye St., NW, Washington, D.C., 20006.

31. Hewlett-Packard Co. Frequency and Time Standards. Hewlett-Packard Application Note 52, Palo Alto, CA., November, 1965.

32. Winkler, Gernot M.R. "Path Delay, Its Variations, and Some Implications for the Field Use of Precise Frequency Standards." Proc. IEEE, v. 60, n. 5, pp. 522-529, May, 1972.

33. Frequency and Time Systems, Inc. Cesium-Atomic Beam Oscillator Technology for Navigation Satellites. Frequency and Time Systems, Inc. Report F6174, Danvers, MA, January, 1975.

34. Cretcher, C.K. and R.H. Huddlestone. Relativistic Considerations for the Global Positioning System. Aerospace Corp. Report TOR-0074(4461-01)-9, El Segundo, CA, March, 1974.

35. Ristenbatt, M.P. "Pseudo-Random Binary Coded Waveforms." in Raymond S. Berkowitz (ed.). Modern Radar; Analysis, Evaluation, and System Design, John Wiley & Sons, New York, 1965, pp. 274-313.

36. Gold, Robert. "Optimal Binary Sequences for Spread Spectrum Multiplexing." IEEE Trans. Info. Theory, October, 1967, pp. 619-621.

37. Cahn, C.R. et al. Timation Modulation Study. Magnovox Research Labs. Report R-4439, Torrance, CA, AD 902855, August, 1972.

38. General Dynamics Electronics Div. Global Positioning System Control/User Segments, Vol III, User Segment Description, Performance, Error Budgets, and RF Link Budgets. AF Report SAMSO-TR-74-182, Vol. 3, General Dynamics Electronics Div., San Diego, CA, AD 921525, June, 1974.

39. Wand, Ronald H. Ionospheric Limitations on Radar Accuracy at L-Band. Mass. Inst. of Tech. Lincoln Lab. Tech. Note 1975-28, Lexington, MA, AD A013731, May, 1975.

40. Rao, N. Narayana, Maurice Y. Youakim, and Kung C. Yeh. Feasibility Study of Correcting for the Excess Time Delay of Transionospheric Navigational Ranging Signals. AF Report SAMSO-TR-71-163, Dept. of Elect. Eng. Report UILU-ENG-71-2548, Univ. of Illinois, Urbana, IL, AD 729797, July, 1971.

41. Bent, Rodney B., Sigrid K. Llewellyn, and Margaret K. Walloch. Description and Evaluation of the Bent Ionospheric Model, Vol. 1. AF Report SAMSO-TR-72-239, DBA Systems Inc., Melbourne, FL, AD 753081, October, 1972.

42. Pisacane, Vincent L., Michael M. Feen, and Martins Sturmanis. Prediction Techniques for the Effect of the Ionosphere on Pseudo-Ranging from Synchronous Altitude Satellites. AF Report SAMSO-TR-72-22, Applied Physics Lab Report APL/JHU TG-1197, Johns Hopkins Univ., Silver Springs, MD, AD 749486, August, 1972.

43. Rohde, Frederick W. The Propagation of Very Short Radio Waves Through the Ionosphere and the Investigation of Ionospheric Models. U.S. Army Topographic Labs. Research Note ETL-RN-74-1, Fort Belvoir, VA, August, 1973.

44. Melbourne, W.G., et al. Constants and Related Information for Astrodynamic Calculations. Jet Propulsion Lab. Tech. Report 32-1306, Pasadena, CA, July, 1968.

45. Pisacane, Vincent L. and Michael M. Feen. Propagation Effects at Radio Frequencies on Satellite Navigation Systems. Applied Physics Lab. Report TG 1243, Johns Hopkins Univ., Silver Spring, MD, AD 784378, May, 1974.

46. Hopfield, H.S. "Tropospheric Effect on Electromagnetically Measured Range: Prediction from Surface Weather Data." Radio Science, v. 6, n. 3, pp. 357-367, 1971.

47. Bean, B.R., B.A. Cahoon, and G.D. Thayer. CRPL Standard Atmospheric Radio Refractive Index Sample. National Bureau of Standards Tech. Note 44, 1960.

48. Altschuler, Edward E. Corrections for Tropospheric Range Error. Air Force Cambridge Research Lab. Report AFCRL-71-0419, L.G. Hanscom Field, Bedford, MA, AD 731170, July, 1971.

49. Altschuler, Edward E. and Paul M. Kalagher. Tropospheric Range Error Corrections for the NAVSTAR System. Air Force Cambridge Research Lab. Report ARCRL-TR-74-0198, L.G. Hanscom Field, Bedford, MA, AD 786928, April, 1974.

50. System Specification for the NAVSTAR Global Positioning System, Phase I. Air Force Spec. SS-GPS-101B, 15 August, 1974.

51. Duiven, Edward M. and A. Richard LeSchack. Global Positioning System Development and Analysis. The Analytic Science Corp. Report TR-428-2, Reading, MA, December, 1974.

52. Fedchin, S.S. Aircraft Navigation. Translated from "Transport" Press, Moscow, 1966. NASA Tech. Translation TT F-524, Washington, D.C., February, 1969.

53. Meditch, James S. Clock Error Models for Simulation and Estimation. Aerospace Corp. Report TOR-0076(6474-01)-2, El Segundo, CA, July, 1975.

54. Boeing Commercial Airplane Co. ATS-5 Multipath/Ranging/Digital Data L-Band Experimental Program Summary. Federal Aviation Agency Report FAA-RD-73-57, Boeing Report D6-60176, Seattle, WA, AD 783581, April, 1973.

55. Hamming, Richard W. Introduction to Applied Numerical Analysis. McGraw-Hill Book Co., New York, 1971.

56. Lear, William. Baro Altimetry and Associated Error Models for the Space Shuttle. TRW Systems Group Report 27054-6004-TU-00, Redondo Beach, CA, November, 1974.

57. Meditch, J.S. Stochastic Optimal Linear Estimation and Control. McGraw Hill Book Co., New York, 1969.

58. du Plessis, Roger M. "Poor Man's Explanation of Kalman Filtering or How I Stopped Worrying and Learned to Love Matrix Inversion." unpublished report, North American Aviation Inc., Autonetics Div., Anaheim, CA, June, 1967.

59. Burke, J.J. Understanding Kalman Filtering and its Application in Real-Time Tracking Systems. AF Report ESD-TR-72-312, Mitre Corp. Report MTR-2417, Bedford, MA, AD 715485, July, 1975.

60. Jazwinski, Andrew H. Stochastic Processes and Filtering Theory. Academic Press, New York, 1970.

61. Gelb, Arthur (ed.). Applied Optimal Estimation. The M.I.T. Press, Massachusetts Institute of Technology, Cambridge, MA, 1974.

62. Leondes, Cornelius T. (ed.). Theory and Application of Kalman Filtering. NATO AGARDograph 139, London, AD 704306, February, 1970.

63. Liebelt, Paul B. An Introduction to Optimal Estimation. Addison-Wesley, Reading, MA, 1967.

64. Tapley, B.D. Statistical Orbit Determination Theory." in B.D. Tapley and V. Szebehely (eds.). Recent Advances in Dynamical Astronomy. D. Reidel Publishing Co., Dondrecht, Holland, 1972, pp. 396-425.

65. Sorenson, H.W. and A.R. Stubberud. "Linear Estimation Theory." in Cornelius T. Leondes (ed.). Theory and Applications of Kalman Filtering. NATO AGARDograph 139, London, AD 704306, February, 1970, pp. 1-42.

66. Nishimura, T. "Modeling Errors in Kalman Filters." in Cornelius T. Leondes (ed.). Theory and Applications of Kalman Filtering. NATA AGARDograph 139, London, AD 704306, February, 1970, pp. 87-103.

67. Brock, Larry D. and George T. Schmidt. "General Questions on Kalman Filtering in Navigation System." in Cornelius T. Leondes (ed.). Theory and Applications of Kalman Filtering. NATO AGARDograph 139, London, AD 704306, February, 1970, pp. 205-230.

68. Singer, Robert A. "Estimating Optimal Tracking Filter Performance for Manned Maneuvering Targets." IEEE Trans. on Aerospace and Electronic Systems, v. AES-6, n. 4, pp. 473-483, July, 1970.

69. Bucy, Richard S. and Peter D. Joseph. Filtering for Stochestic Processes with Applications and Guidance. Interscience Publishers, New York, 1968.

70. Schwartz, Mischa. Information Transmission, Modulation, and Noise. McGraw-Hill, New York, 1959.

71. Kochenburger, Ralph J. Computer Simulation of Dynamic Systems. Prentice-Hall, Englewood Cliffs, NJ.

72. Laning, J. Halcombe and Richard H. Battin. Random Processes in Automatic Control. McGraw-Hill Book Co., New York, 1956.

73. Cole, Allen E., Air Force Cambridge Research Laboratory, 16 May 1974 letter to Mr. Fred Bower, Aerospace Corp., Subject: Variation in Height of 300 mb. Pressure Surface.

74. Hampton, R.L.T. and James R. Cooke. "Unsupervised Tracking of Maneuvering Vehicles." IEEE Trans. on Aerospace and Electronic Systems, v. AES-9, n. ?, pp. 197-207, March, 1973.

75. Kanyuck, A.J. "Transient Response of Tracking Filters with Randomly-Interrupted Data." IEEE Trans. on Aerospace and Electronic Systems, v. AES-6, n. 3, pp. 313-323, May, 1970.

76. Asher, Robert B. and David H. Watjen. "Kalman Filtering for Precision Pointing and Tracking Applications." Proc. of the Symposium on Air Force Applications of Modern Control Theory, 9-11 July 1974, Wright-Patterson AFB, OH, Air Force Report No. ARL 74-1060, pp. 49-73.

77. Hagar, Hamilton, Jr. Model Error Compensation Techniques for Linear Filtering. PhD. Dissertation, published as Applied Mechanics Research Lab. Report AMRL 1055, The University of Texas at Austin, Austin, TX, August, 1973.

78. Aidala, Vincent J. and John S. Davis. The Utilization of Data Measurement Residuals for Adaptive Kalman Filtering. Naval Underwater Systems Center Report No. TR 4502, Newport Laboratory, Newport, RI, AD 776218, February, 1974.

79. Hagar, H. and B.D. Tapley. "Sequential Filter for Estimating State Noise Covariances." Proc. Fourth Symposium on Nonlinear Estimation Theory and its Applications, pp. 98-101, San Diego, CA, September 10-12, 1973, copies available from Western Periodicals Co., North Hollywood, CA.

80. Tarn, Tzyh Jong and John Zaborszky. "A Practical Nondiverging Filter." AIAA Journal, v. 8, n. 6, pp. 1127-1133, June, 1970.

81. Fagin, S.T. "Recursive Linear Regression Theory, Optimal Filter Theory, and Error Analysis of Optimal Systems." IEEE Intern. Conv. Record, v. 12, pp. 216-240, 1964.

82. Heck, Michael T. Estimation and Prediction of the Orbiting Space Shuttle in the Presence of Random Propulsion Venting. Ph.D. Dissertation, published as Applied Mechanics Research Lab. Report No. AMRL 1069, The University of Texas at Austin, Austin, TX, May, 1975.

83. Lear, William M. The Multi-Phase Navigation Program for the Space Shuttle Orbiter. NASA Johnson Space Center Internal Note No. 73-FM-132, Houston, TX, September, 1973.

84. Elgerd, Olle I. Control Systems Theory. McGraw Hill, New York, 1967.

85. Eisenman, Richard L. Matrix Vector Analysis. McGraw-Hill, New York, 1963.

86. User's Manual. Computation Center, The University of Texas at Austin, Austin, TX, December, 1974.

87. Feller, William. An Introduction to Probability Theory and Its Applications, Volume 1. John Wiley & Sons, New York. 1957.

88. Fehlberg, Erwin. Some Experimental Results Concerning the Error Propagation in Runge-Kutta Type Integration Formulas, NASA Tech. Report TR R-352, Marshall Space Flight Center, AL, October, 1970.

89. Lear, William M. Discussion of an Discrete, Exponentially-Correlated, Random Variable and Variations Thereof. TRW Report 20029-6024-TU-00, Redondo Beach, CA, October, 1973.

90. Mulholland, H. and C. R. Jones. Fundamentals of Statistics. Butterworth's, London, 1968.